Aerodynamic Characteristics of a Vertical Axis Vane Type Wind Turbine

Faizul Mohammad Kamal

MASTER OF SCIENCE IN MECHANICAL ENGINEERING

DEPARTMENT OF MECHANICAL ENGINEERING
BANGLADESH UNIVERSITY OF ENGINEERING AND TECHNOLOGY,
DHAKA-1000, BANGLADESH

April 2008

Aerodynamic Characteristics of a Vertical Axis Vane Type Wind Turbine

by

Faizul Mohammad Kamal

A Thesis
Submitted to the Department of Mechanical Engineering in partial fulfillment of the requirements for the degree
of
MASTER OF SCIENCE IN MECHANICAL ENGINEERING

DEPARTMENT OF MECHANICAL ENGINEERING
BANGLADESH UNIVERSITY OF ENGINEERING AND TECHNOLOGY,
DHAKA-1000, BANGLADESH
April 2008

RECOMMENDATION OF THE BOARD OF EXAMINERS

The Board of Examiners hereby recommends to the Department of Mechanical Engineering, Bangladesh University of Engineering and Technology, Dhaka, the acceptance of the thesis titled "**Aerodynamic Characteristics of a Vertical Axis Vane Type Wind Turbine**", submitted by **Faizul Mohammad Kamal**, Roll No: 040510008P, Session: April 2005, in partial fulfillment of the requirements for the degree of Master of Science in Mechanical Engineering on April 30, 2008.

1.	Dr. Md. Quamrul Islam Professor Department of Mechanical Engineering BUET, Dhaka-1000	(Supervisor)	Chairman
2.	Dr. Abu Rayhan Md. Ali Professor & Head Department of Mechanical Engineering BUET, Dhaka-1000	(Ex-Officio)	Member
3.	Dr. Dipak Kanti Das Professor Department of Mechanical Engineering BUET, Dhaka-1000		Member
4.	Dr. Amalesh Chandra Mandal Professor Department of Mechanical Engineering BUET, Dhaka-1000		Member
5.	Dr. A. K. M. Iqbal Hussain Professor Energy and Environmental Centre Islamic University of Technology (IUT) Board Bazar, Gazipur		Member (External)

CERTIFICATE OF RESEARCH

This is to certify that the work presented in this thesis is an outcome of the investigation carried out by the author under the supervision of Dr. Md. Quamrul Islam, Professor, Department of Mechanical Engineering, Bangladesh University of Engineering and Technology (BUET), Dhaka.

DR. MD. QUAMRUL ISLAM
Supervisor

FAIZUL MOHAMMAD KAMAL
Author

ACKNOWLEDGEMENT

I wish to express my sincerest gratitude and indebtedness to Dr. Md. Quamrul Islam for his guidance and supervision throughout the entire period of the experimental investigation. His encouragement and invaluable suggestions are gratefully acknowledged.

I am also grateful to Professor Dr. Abu Rayhan Md. Ali, Head of the Department of Mechanical Engineering for his encouragement in completing this work in time.

Sincere thanks are offered to Superintendent and Chief Instructors and technicians of Machine Shop, Carpentry Shop, Welding and Sheet Metal Shop, BUET for their co-operation in fabricating and assembling different parts and components of the experimental set-up. Thanks are also due to Lab Instructors and technicians of Fluid Mechanics Laboratory of Mechanical Engineering Department for their co-operation at different stages of the work.

Lastly, I would like to thank my father, mother, younger brother and wife for their inspiration to complete this work in proper time.

ABSTRACT

This research work has been carried out to study the aerodynamic characteristics and to analyze the effect on an equally spaced vertical axis four, five and six bladed vane type rotor. The aerodynamic characteristics i.e. torque coefficient, drag coefficient etc. of vertical axis vane type rotor have been studied in this present research work by measuring the pressure distribution on the blade surfaces at various rotor angles. The experiments have been carried out at a Reynolds number of 1.65×10^5 in a uniform flow jet produced by an open circuit wind tunnel.

The pressure measurements have been made at 8 tapping points on each blade of the vane rotors. Pressure on the convex and concave surfaces have been measured for every 10° interval of rotor angle up to 360° angle of rotation. The data obtained experimentally has presented in terms of non-dimensional coefficients. To calculate drag force and torque in non-dimensional form, computer based software has been used and the output have been subsequently plotted and analyzed. Aerodynamic characteristics on individual and group of four, five, six blades have also been determined in the present work.

A quasi-steady approach has been applied for studying the dynamic performance of the rotor at different rotor angle using the static drag and torque coefficients. Power coefficient versus tip speed ratio curve for four, five and six bladed vane type rotor has also been drawn. Power coefficient versus tip speed ratio of the present measurement and the previous researcher's works has plotted on the same graph for comparison. This method results in a reasonable agreement with the previous measurement.

CONTENTS

LIST OF FIGURES

LIST OF SYMBOLS

C_p	Power Coefficient, $2(P-Pa)/\rho U_o^3$
C_{pe}	Pressure coefficient for concave surface of the blade
C_{px}	Pressure coefficient for convex surface of the blade
C_n	Drag coefficient in the normal direction of the blade
C_t	Drag coefficient in the transverse direction of the blade
C_q	Static torque coefficient for a single blade
C_Q	Total static torque coefficient
d	Diameter of the blade
D	Diameter of the rotor
H	Height of the rotor
F_n	Normal force acting on a blade
F_t	Tangential force acting on a blade
P	Pressure on blade
Pa	Atmospheric pressure
R_e	Reynolds number, U_oD/ ν
S	Ratio between distance of two blades and diameter of a blade
a	Distance between the two blades
T	Static torque on blade
U_o	Free stream velocity
V_r	Relative velocity
V_w	Component of relative velocity along U_o

Greek Symbols:

α	Rotor angle
Φ	Angle of pressure tappings
λ	Tip speed ratio, $D\omega/2U_0$
ω	Angular speed of the rotor
ν	Kinematics viscosity of air
ΔP	Difference of pressure between concave and convex surfaces of a blade

CHAPTER 1

INTRODUCTION

Chapter-1

INTRODUCTION

1.1 General

Over the centuries mankind have been using various types of energy, like oil, hydro, coal, natural gas, nuclear etc. as fuel for different activities all around the world. Among these conventional fuel, only hydro is renewable in nature and the other sources are found to be major causes of air pollution and greenhouse effect. Replacement of the conventional fuel with renewable energy source can be made by wind energy, solar (photovoltaic) systems, solar thermal systems, biomass energy (wood and other plant fuel), geothermal energy, fuel cell, municipal waste etc. The cost of many of these technologies has come down considerably in recent years, particularly wind energy, which is now competitive with conventional power sources in regions with strong winds.

The science of exploitation of wind energy is an old concept. Over the years people are extracting wind energy in various ways. One of the means for converting the wind energy to a more useful form is through the use of windmills. Recently, due to the fuel crisis, this branch of engineering is gaining more popularity. Wind energy has become very lucrative now-a-days due to its reliability. According to World Wind Energy Association (WWEA), 73,904 MW capacity wind turbine has been installed worldwide, in which Europe and US have installed 62,991 MW, Asia have 8,675 MW and Other 2,238 MW. According to projection by World Wind Energy Association (WWEA), wind turbine installation in the world through the end of 2010 will be 160 GW.

There are various types of windmills. The most common one is the horizontal axis wind turbine. Another type is the vertical axis wind turbine. The primary attraction of the vertical axis wind turbine is the simplicity of its manufacture compared to that of horizontal axis wind turbine. Among the different vertical axis wind turbines, the Savonius Type Wind Turbine is a slow running wind machine and has relatively lower efficiency. Still it is being used in the developing countries because of its simple design, easy and cheap technology for construction and good starting torque characteristics at low wind speed [1, 2, 3]. It is independent of wind direction for generation of power and also works even at low speed. Rigorous studies on the performance characteristics of the Savonius rotor are found in the literature and these enable the identification of an optimum geometrical configuration for practical design [4, 5, 6, 7, 8].

1.2 Wind as a Source of Energy

For a long time people have been extracting energy mainly from the fossil fuel in almost all the countries. In some of the countries, they are also utilizing uranium fuel, which is a source of nuclear energy. With the rising demand of energy and for many other reasons, prices of these fuels are increasing day by day. So the scientists and engineers are trying to find the alternate sources of energy to exploit them at the cheapest rate. Wind energy is a kind of energy source that will never be finished. It is available almost all the times, in all the places and in large quantities all over the world. Again, fossil and uranium fuel will be completely depleted someday. Moreover, these are not available in all the countries. Besides these, every nation is interested to be self-dependent; they do not like to rely on imported fuel that requires huge amount of foreign currency. On the other hand, to date no effective method has been developed to and utilizes the solar energy. As a result in different parts of the world, scientists are taking keen interest to develop efficient and economic devices to collect energy from the wind. In the recent times, the utilization of wind power is on the rise in many developed, as well as, in many under developed countries.

1.3 Global Wind Energy Utilization Scenario

Wind energy technology continues to be the most dynamic energy source and wind is clearly emerging as the currently the most promising energy solution to replace the most common yet undesirable fossil fuel.

In 1997, wind turbines installed all around the world generated about 13 trillion watt-hour of energy, the installed capacity being 7,500 MW. Wind energy continued its dynamic growth worldwide in the recent year. About 14,900 MW were added in the past year summing up to a global installed capacity of 73,904 MW by the end of December 2006. The added capacity equals a growth rate of 25%, after 24% in 2005. Based on the accelerated development, WWEA has revised its prediction for 2010 and now expects about 160,000 MW to be installed by the end of 2010.

According to WWEA, Europe will continue to dominate worldwide installations over the next 10 years, erecting 14,310 MW of additional wind capacity, or nearly half of the 73,904 MW projected for the world. European countries particularly Germany, Spain, Denmark, Italy and the United Kingdom have very strong and consistent domestic market support in place for at least several years. While those supports are being reduced in many markets, the European wind industry now has enough momentum and investment that has rapid growth, which is expected to continue into the indefinite future. According to American Wind Energy Association (AWEA), total installed U.S. wind energy capacity was 12,634 MW as of June 30, 2007.

1.4 Aim of the Present Work

Both aerodynamic and structural works on the vertical-axis Savonius wind turbine have been done in many parts of the world. Islam et al. [12] investigated the aerodynamic forces acting on a stationary S-shaped rotor and made an attempt to predict the dynamic performance from these forces. Islam et al. [1] analyzed the performance of S-shaped rotor by placing a flat plate in front of the retreating blade. F. Diaz et al. [4] analyzed the Drag and lift coefficient of Savonius wind machine in order to obtain quantitative information about the Savonius rotor. Islam et al [12] investigated Aerodynamic characteristics of a stationary two bladed Savonius rotor. However, little attention has been given on the static and dynamic characteristics when the number of blade of the Savonius rotor is increased. The present research work consists of finding static drag coefficients at the normal and tangential direction of the chord, static torque coefficient for individual blade $C_{q,}$ total static torque coefficient C_Q at a fixed Reynolds number for four/five/six bladed Vertical Axis Vane type rotor at different angle of rotation ranging from $\alpha=0°$ to 360° by measuring the surface pressures of blades. The quasi-steady approach applied to the analysis of a Darrieus rotor has been finally considered for predicting the performance of the Vertical Axis Vane type rotors.

Objectives with Specific Aims and Possible Outcomes:

Present research work has been performed to predict the effect of increasing the number of blades by developing a vertical axis equally spaced four/five/six bladed vane type rotor. The study has the following objectives:

1. To study the effects of the four/five/six blades of the Vertical Axis Vane Type rotor on aerodynamic characteristics i.e. torque coefficient, drag coefficient etc. Determination of the location of separation point with the increase of rotor angle at various Reynolds number will also be included.

2. To determine the drag coefficient and torque coefficient from the measurement of the pressure difference between the convex and concave surface of the blades.

3. Finally, a comparison will be made between the present dynamic predictions (for four/five/six bladed Vertical Axis Vane Type rotor) with other works of Vertical Axis Wind Turbines in terms of power coefficient for different tip speed ratios.

1.5 Scope of the Thesis

The study covers only the experimental investigation although some important computer programming has been done for useful purposes and analysis.

The prime objective of the investigation was to observe the effects and aerodynamic characteristics of a vertical axis wind turbine having four/five/six semi-circular blades in place of two/three bladed system of similar shape and to compare the results.

The present research programme covers only the experimental investigation of pressure distribution over the blade surfaces of the vertical axis vane type rotor both on the convex and concave surfaces for different angles of rotation, α ranging from 0° to 360° for every 10° interval. The several phases of the entire investigation are described in this thesis.

Chapter 2 provides the brief description of the findings of several researchers in the field of flow over different types of Savonius rotor, Darrieus rotor and S-shaped rotor with different conditions. Notable contributions were mainly made by E.H. Lysen, H.G. Bos, E.H. Cordes, J. Park, R. D. Littler, M.D. Huda, M.A.Selim, M.Q. Islam, A.K.M.S. Islam, A.C. Mandal, M.M. Razzaque, J. Gavvalda, J. Massons, F. Diz, T.K. Aldoss, M.A. Koth, T.Ogawa and H. Yoshida. Besides these, findings of several other researchers are also included in this chapter.

In the chapter 3 mainly an account of the experimental arrangement and procedure adopted for the investigation are presented. It includes the description of the wind tunnel, the constructional details of the test section and the four/five/six semi-cylindrical bladed vane rotor that are used for the study. This chapter includes the experimental procedure of the research work. The experiment was conducted in the wind tunnel for two-dimensional uniform cross flow keeping the velocity and turbulence intensity constant.

Chapter 4 presents the derivation technique of different non-dimensional parameters both for static and dynamic aerodynamic characteristics. The equations of coefficient of pressure, normal and tangential drag, individual torque, and total static torque are derived briefly in this chapter. Derivation of equations for the prediction of power coefficient from the static drag coefficient for different tip speed ratios are also provided in this chapter. Velocity diagrams for different bladed vane type rotor with different tip speed ratio are also included.

Chapter 5 contains the analysis concerning the results and discussions of the present experimental results that are illustrated in the graphical form. This chapter provides discussions of the results of experimental investigation conducted for the wind tunnel flow over the four, five and six bladed vane rotor. The results of the pressure distribution over the convex and concave surfaces of each blade at different angle of rotation are analyzed first. Nature of the drag and static torque characteristics are also analyzed in this chapter. In some cases the existing experimental results of different researchers are compared with the present one.

Finally, the conclusions, which are drawn from the present investigations of flow over the four, five and six bladed vane rotor, are given in the chapter 6. The scope of extension and development of the present study is also included in this chapter.

CHAPTER 2

REVIEW OF LITERATURE

Chapter-2

REVIEW OF LITERATURE

2.1 Introduction

Arising from the increasing practical importance of wind turbine aerodynamics, there have been, over the past few decades, an enormous increase in research works concerning laboratory simulations, full-scale measurements and more recently, numerical calculations and theoretical predications for flows over a wide variety of Savonius rotors. Researches in different countries have contributed greatly to the knowledge of analytical prediction methods of wind turbines, but the major part of the reported works is of fundamental nature involving the flow over horizontal axis wind turbine and vertical axis Darrieus rotor. Most of the researchers have conducted research works on either two/three semi cylindrical bladed Savonius rotor or S-shaped rotor with various flow parameters. A brief description of some of the papers related to the present work is given in this chapter.

2.2 Historical Background

From the ancient period people have been working on various classes of wind contrivances to extract energy from the wind. Works on windmills have probably been started from 2000 B.C. The period from the ancient time up to the end of the 19th century may be categorized as the ancient development period while that from the end of 19th century up to date may be termed as the modern development period.

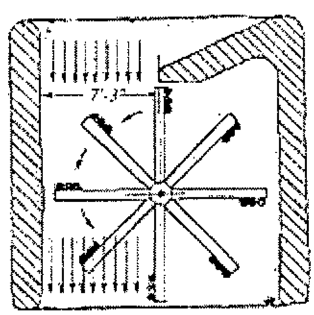

Figure 2.1: Persian windmill of vertical-axis type

In the ancient development period, in the middle of 7th century, Persian vertical-axis windmill circa (Figure 2.1) was constructed which was used to grind grain. That kind of windmill was working up to about 12th century, when simultaneously in France and England Dutch type of windmills were made whose purpose were to grind grain and pump water. These windmills were of horizontal-axis types. Up to the end of 19th century people were working with these classes of windmills only.

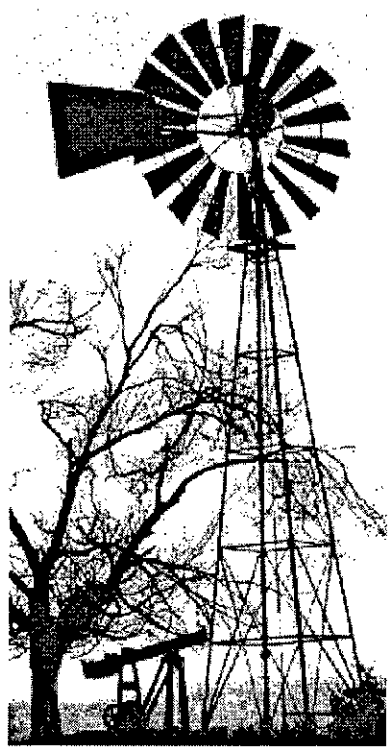

Fig 2.2: Windmill for water pumping

At the end of 19th century, the first modern windmill of horizontal-axis type with multi-blade was built in Denmark to produce electricity. It was the beginning of the modern development period. Starting from that time people in different countries especially in rural America has been constructing a large number of multi-bladed wind turbines for pumping water and generating electricity. Afterwards as a consequence of development works for several years, two or three bladed propeller type of windmills with airfoil shape blades were built in near about 1925. In 1931, 100 kW Russian horizontal-axis wind turbine was constructed while in 1934; the large 1250 kW Smith-Putnam horizontal-axis wind turbine was built.

Modern development period have really begun with the development of horizontal-axis wind turbines. In 1924 Finnish Engineer S.J. Savonius constructed the first Savonius rotor of vertical-axis type (Figure 2.3) and he conceived the idea from the

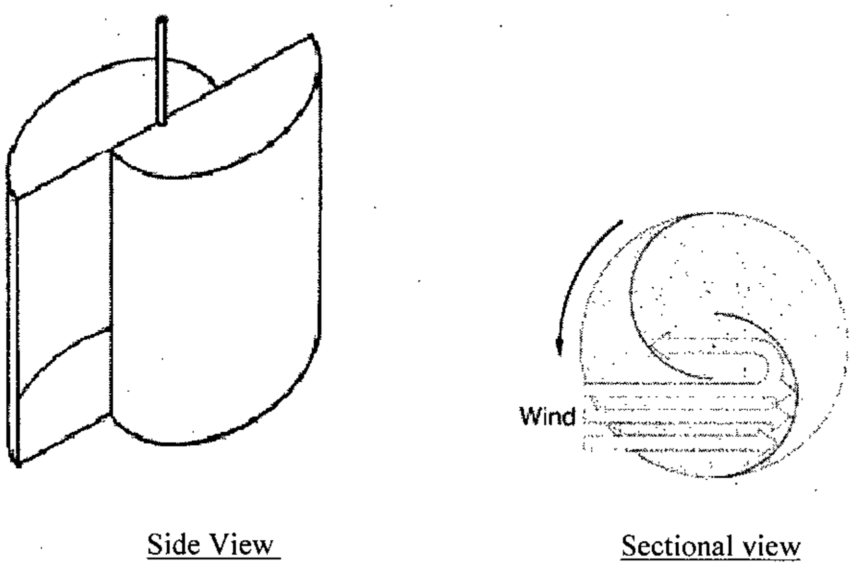

Figure 2.3: Savonius rotor

Flattener's Rotor. In 1925 G. J. M. Darrieus of France, proposed for United State patent a new type of wind turbine designed for the generation of power. The patent issued in 1931 as number 1,835,018 was for a "turbine having its rotating shaft transverse to the flow of the current". The straight-bladed configuration was also covered in the original Darrieus patent. This kind of wind machine is called Darrieus turbine (Figure 2.4) after the name of G. J. M. Darrieus.

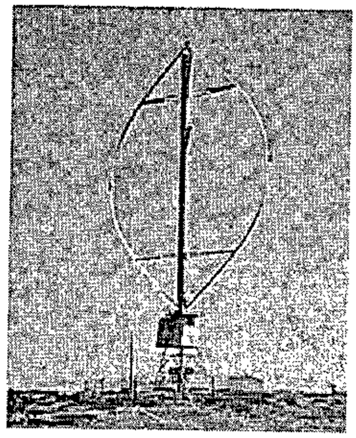

Figure 2.4: Darrieus wind turbine

Since the beginning of the twentieth century, researchers in the various part of the world had been giving much effort in the development works of the wind turbines but from about the middle of this century, it began to loose its momentum for further development. In about 1970's people took renewed interest in this field. Especially in 1973 with oil embargo, people were thinking regarding the alternate sources of energy. As a result in many developed and underdeveloped countries, a lot of new projects concerning the development of wind turbines have been taken.

Only during the last decade in the different countries enormous attention has been paid in the field of performance prediction method applicable to wind turbines. As an outcome, a number of analytical prediction methods have been developed. Works have also been extended to both the static and dynamic analyses of wind turbines. Different type of design methods has been worked out in many places. Still there exists no good and reasonable analytical performance prediction method especially for a high solidity Darrieus wind turbine.

2.3 Literature Concerning S-Shaped Savonius Rotor

Islam et al. [1] investigated the aerodynamic forces acting on a stationary S-shaped rotor and made an attempt to predict the dynamic performance from these forces. The work was done by measuring the pressure distribution over the surface of the blades. The measurements were carried out in a uniform flow jet produced by an open circuit wind tunnel and at a constant wind speed of 8.9 m/s, which corresponds, to a Reynolds ($R_e = \rho UoD/\mu$) of $1.1x10^5$. The results indicate that flow separates over the front and back surfaces of the blades and the point of separation depends on the rotor angle. The pressure difference was observed between the two surfaces of each blade, which in turn, gives drag coefficients. The drag and hence, the torque of each blade varies with rotor angle and becomes maximum at $\alpha = 45°$ for the advancing blade and at $\alpha = 105°$ for the returning blade. The net torque is maximum at $\alpha = 45°$ and becomes negative in the range of rotor angle between 135° to 165°.

Islam et al. [5] analyzed the performance of S-shaped rotor by placing a flat plate in front of the returning blade. They found that the power coefficient of an S-rotor is dependent on the Reynolds number and the value of Cp (power coefficient) is increased with Reynolds number (in the range of the Reynolds number studied). Maximum 20% of power coefficient can be increased by using the deflecting plate which occurs at a deflecting angle of 35° for b = 0.5D, where b = distance between plate and rotor center and D = diameter of the rotor.

Bowden, G.J. and McAleese, S.A [13] made some measurements on the Queensland optimum S-shaped rotor to examine the properties of isolated and coupled S-shaped rotor. In particular it is shown that the efficiency of the turbine is around 18%, which is lower than the figure of 23% given by earlier workers. In the experimental setup the UNSW open jet air-stream, diameter 0.76 m, was used to produce wind speeds in the range 0 to 30 m/s. The turbulence ($\sqrt{u^2}/V_\alpha$) in the jet stream was low. Wind flow measurement was investigated using 'tell-tales' (light pieces of cotton attached to a probe) and a stroboscope. In this way, it was possible to detect the direction of the airflow relative to the angular position of the rotor blades. Many photographs were taken and later used to construct a visual airflow pattern around the rotor. The linearized hot-wire anemometer, on the other hand, enabled measurements to be made of velocity magnitudes and fluctuations to an upper frequency limit of 5 kHz. It cannot however be used to measure direction. The hot-wire anemometer linearizer was based on a design due to the Institute of Sound and Vibration Research (ISVR), Southampton University, U.K. In general, a storage oscilloscope was used to record the data, particularly from the more structured turbulent regions. However, measurements of turbulence intensity were also made by connecting an rms voltmeter to the output of the hot-wire linearizer. The results of this research were subsequently used to suggest that some form of active coupling between Savonius rotors might be possible. In particular, it has been shown that if two counter-rotating rotor are placed side by side, a natural phase locking occurs between the two turbines.

2.4 Literature Concerning Vertical Axis Darrieus Wind Turbine

The most simple prediction method for the calculation of the performance characteristics of a Darrieus wind turbine is the single stream tube model. It has been introduced first by Dr. Templin [14] in 1974. In this model the whole turbine is assumed to be enclosed within the single stream tube. Dr. Templin first incorporated the concept of the windmill actuator disc theories into the analytical model of a Darrieus wind turbine. In the actuator disc theory the induced velocity (rotor axial flow velocity) is assumed to be constant through the "disc" and is obtained by equating the stream-wise drag with the change in axial momentum. In the assumption of Templin, the actuator disc is considered as the surface of the imaginary body of revolution. It is assumed that the flow velocity is constant although the upstream and the downstream faces of the swept volume. This theory presented by Templin is the first approach to permit numerical design calculations for a vertical-axis Darrieus wind turbine.

An analytical method using single stream tube model is presented by Noll and Ham [15] for the performance prediction of a vertical-axis wind turbine with straight blades, which are cyclically pitched. They added the effect of strut drag, turbulent wake state and dynamic stall to their analytical method.

An improvement to the above method is the multiple stream tube model introduced by Wilson and Lissaman [16]. In this model the swept volume of the turbine is divided into a series of adjacent, aerodynamically independent stream tube. Blade element and momentum theories are then employed for each stream tube. In their method, they consider the flow as inviscid and incompressible for the calculation of the induced velocity through the stream tube. As a result, there appears only the lift force in the calculation of induced velocity. Wilson et al considered the theoretical lift for their calculation. This induced velocity varies over the frontal disc area both in the vertical and the horizontal directions. Atmospheric wind shear can be included in the multiple stream tube models. Multiple stream tube model is still inadequate in its description of the flow field. Wilson's model can be applied only for a fast running lightly loaded wind turbine.

Strickland [17] in his paper presents a multiple stream tube model for a vertical axis Darrieus turbine. He finds the induced velocity by equating the blade element forces (including airfoil drag) and the change in the momentum along each stream tube. The basic difference between Wilson's and Strickland's model is that Wilson used the lift force (theoretical) only in the calculation of induced velocity while Strickland added the effect of drag force as well for the similar calculation. Wilson's model gives first convergence while Strickland's model gives slow convergence.

An improved version of multiple streamtube method is presented by Read and Sharpe [18] for vertical-axis Darrieus wind turbines. In their model, the parallel streamtube concept is dispensed with and expansion of the streamtube is included. It is strictly applicable to low solidity lightly loaded wind turbines with large aspect ratio. It can predict the instantaneous aerodynamic blade forces and the induced velocities better than that by the conventional multiple streamtube model. But prediction of overall power coefficients cannot be made with reasonable accuracy. It usually gives lower power than that obtained experimentally.

In their paper, Paraschivoiu and Delcalaux [19], presented improvements in the double multiple streamtube model. They considered the induced velocity variation as a function of the azimuthal angle for each streamtube. They have added a new formulation for an approximate Troposkien shape by considering the effect of gravitational field and a semi-empirical dynamic stall model.

Paraschivoiu, Fraunie and Beguier [20] introduce in their paper the expansion effects of the streamtube through the rotor and these are included with the double multiple model. With the measured and the predicted data they observe that streamtube expansion effects are relatively significant at high tip speed ratios.

Fanacci and Walters [21] presented a two-dimensional vortex model applicable to a straight-bladed wind turbine. In their analysis they consider the angle of attack very small thereby eliminating the stall effect.

Holme [22] presents a vortex model for a fast running vertical-axis wind turbine having a large number of straight, very narrow blades and a high height-diameter ratio (in order to make a two dimensional flow assumption). The analysis is valid for lightly loaded wind turbines only.

Wilson [23] also introduces a two-dimensional vortex analysis to predict the performance of a giromill. In his method he does not take into account the stall effect, because the angle of attack is assumed to be small.

2.5 Literature Concerning Two Semi-cylindrical Bladed Savonius Rotor

F. Diaz et al [4] analyzed the drag and lift coefficient of Savonius wind machine, in order to obtain quantitative information about the aerodynamic performance of the Savonius rotor. The experiments were carried out in a low turbulence open jet of 30x50 cm section outlet, which provides an air speed adjustable between 0 and 30 m/s. The results of this work showed that for e/d=1/6, at which the rotor generates the optimum power, the drag and lift coefficients are little dependent on the operating conditions (Reynolds number, tip speed ratio λ) if λ is near the optimum value $\lambda \approx 1$. There are three findings of this work: (a) the maximum efficiency of the Savonius rotor, it terms of power coefficient, takes place for $\lambda \approx 1$, and that c_d decreases sharply when λ increases or decreases from this value, (b) for a given Reynolds number, as the tip speed ratio increases from zero, the drag values are maintained practically constant, $C_D \approx 1.5$ in the interval ranging from $\lambda = 0$ to $\lambda = 1.25$. The most interesting zone for power extraction is located near $\lambda \approx 1$, where C_D shows minimal values. For tip speed ratios greater than 1.25, the drag coefficient increases, (c) in a wide interval around $\lambda = 1$ (the most important region of operation of the Savonius rotor) the lift coefficient remains practically constant at $C_L \approx 0.5$.

Sawada, T., Nakamura, M. and Kamada, S., [24] experimentally studied the mechanism of rotation of Savonius rotor which have two semi-cylindrical blades. The force acting on a blade is measured in a water tank while a rotor is at rest condition and also while it is rotating. A flow around the rotor is observed by using aluminum powder floating on the water surface. The researchers concluded that (a) when the rotor is at rest, the rotor with overlap ratio 0.21 produces a positive torque at any attitude angle, (b) the lift around α = 240°~330° contributes a lot to the torque occurring when the rotor is rotated. Although the Savonius rotor is classified as a resistance type, the lift produce a torque in a pretty wide range of angles relative to the flow, (c) when the rotor is related, the effect of the pressure recovery by the flow through the overlap portion on the lift is little for the rotor with overlap ratio 0.21. For the rotor of a/d=0.51, the existence of a flow through the center of the rotor contributes to the production of a negative torque opposing the clockwise rotation.

Taha K. Aldos and Khalid M. Obeidat [25] analyzed the performance of two Savonius rotor running side by side at different separations using the discrete vortex method. Two configurations were considered. The torque and power coefficients were computed and compared with the available experimental results presented by Aldoss and Najjar in an earlier paper.

R.D. Littler et al [26] made comparative tests of the Savonius rotor at constant Reynolds number. They suggested that a plain S-rotor might be good as or better than the conventional Savonius rotor with an inter-vane gap. A single S-rotor gives a Cp>0.15 (0.225 uncorrected wind-tunnel value), although duplex rotors have given Cp> 0.18 (0.32 uncorrected value). Comparative particle flow visualization studies within these rotors (Savonius rotor with conventional gap, S-rotor with no gap) and a rotor with separated vanes ('negative' gap) in a water-channel suggest the importance of attached flow round the convex surfaces of the vanes, the doubtful value of the conventional gap, and the importance of vane shape.

Sivasegaram, S. and Sivapalan, S. [27] made an experiment in improving the sectional geometry of slow-running vertical-axis wind rotors of the Savonius type has resulted in considerable improvement in rotor performance. They suggested that further improvement in power output from a rotor of given overall dimension demands the use of power augmenting systems. The influence of important design parameters of the augmenting system and that of wind direction has been determined. They showed that an eighty percent increase in power output could be achieved using a pair of vanes of moderate size.

Islam et al [12] investigated Aerodynamic characteristics of a Stationary Savonius rotor of two semi-cylindrical blades. The tests were carried out in a uniform flow jet produced by an open circuit wind tunnel. The exit of the wind tunnel consists of a square section nozzle with side length of 500m. The rotor was placed at the jet axis and 750 mm downstream of the nozzle exit. This study was carried out at a constant wind speed of $U_0 = 13.3$ m/s i.e., at Reynolds number, $R_e = 2 \times 10^5$. The results of this work showed that flow separates over the convex surface of the blades and the separation point moves towards the leading and trailing edges of the advancing and returning blades respectively as the rotor angle increases from 0° to 90°. Beyond α = 90°, flow separates over the convex surface of the returning blade only. They also found that the difference in pressure on the convex and concave surfaces produces drag coefficients, C_n and C_t in the normal and tangential directions of the chord. Drag coefficients, C_n and C_t are a function of rotor angle and their resultant reaches maximum value at α = 120° and minimum value at α = 0°.

CHAPTER 3

DERIVATION TECHNIQUE OF NON-DIMENSIONAL PARAMETERS

Chapter-3

DERIVATION TECHNIQUE OF NON-DIMENSIONAL PARAMETERS

3.1 Introduction

The local surface pressures on the blade surfaces of the rotor were measured relative to the free upstream static pressure prevailing in the test section of the wind tunnel. The data obtained experimentally are presented in terms of non-dimensional coefficients. The equations of coefficient of pressure, normal and tangential drag, individual torque, and total static torque are derived briefly in this chapter. Derivation of equations for the prediction of power coefficient from the static drag coefficient for different tip speed ratios are also provided in this chapter.

3.2 Derivation of Static Aerodynamic Characteristics

Static aerodynamic characteristics are derived in three steps:

Step 1: Using raw data from experiment pressure coefficient both for concave and convex surfaces of blades are calculated for angle of rotation ranging from 0° to 80° for four bladed rotor, from 0° to 60° for five bladed rotor and from 0° to 50° for six bladed rotor because after these rotational angle (α) the system would repeat.

Step 2: Using the pressure difference between concave and convex surfaces of blades of the Vertical Axis Vane Type rotor, the drag coefficients in normal and tangential directions were calculated.

Step 3: Using the drag coefficient in the normal direction the torque coefficient for a single blade and the total static torque coefficient produced on the rotor shaft were also calculated.

3.2.1 Pressure Co-efficient, C_p

In the experiment, the pressure measurements were made at 8 tapping points on each blade for the angle of rotation (α) of every 10° interval ranging from 0° to 360° both on the convex and concave surfaces. Using these raw data pressure coefficient on convex surfaces (C_{px}) of four/five/six blades and pressure coefficient on concave surfaces (C_{pe}) of four/five/six blades were calculated using the following expression of pressure coefficient.

Pressure coefficient is defined as

$$C_p = \frac{P - P_o}{\frac{1}{2}\rho U_o^2} \qquad (3.1)$$

Where, $P - P_0$ = Difference between blade and atmospheric pressure in Pascal

ρ = Density of air = 1.2 kg/m^3

U_0 = Free stream velocity, 13 m/s

These calculations were performed up to 80° angle of rotation (α) for four bladed Vane rotors. After that angle of rotation, the system will be repetitive. At 90° angle of rotation, the second blade takes the position of the first blade, third blade takes the position of the second blade and the fourth blade takes the position of the third blade respectively. The calculated values of C_{px} and C_{pe} were plotted against pressure tapping points on the same graph for analysis. The procedure of the calculations for five /six bladed rotor is also same as four bladed Vane rotor.

3.2.2 Drag Co-efficient, C_p

At a particular rotor angle, α the rotor blades experience forces (per unit span length) due to pressure difference between the concave surface and convex surface and these forces can be resolved into two components, F_n and F_t. Since the blade surfaces are circular, F_n and F_t pass through the centre of the semicircle. The positive direction of F_n and F_t are shown in Figure 4.7.

The drag coefficients in normal and tangential directions can be written as follows:

$$C_n = \frac{F_n}{\frac{1}{2}\rho U_o^2 d}$$

$$C_t = \frac{F_t}{\frac{1}{2}\rho U_o^2 d} \tag{3.2}$$

To obtain the drag coefficients in the normal and tangential direction of the chord, the values of F_n and F_t must be known beforehand. The values of the forces F_n and F_t are obtained by integrating the pressure for blades as follows:

$$F_n = \int F_n = \int_0^{\pi} \Delta p \frac{d}{2} \cos\phi d\phi = \sum_{i=1}^{8} \Delta p \frac{d}{2} \cos\phi_i \Delta\phi_i \tag{3.3}$$

and similarly,

$$F_t = \sum_{i=1}^{8} \Delta p_i \frac{d}{2} \sin\phi_i \Delta\phi_i$$

Where Δp_i is the difference in pressure on the concave and convex surfaces at a particular pressure tapping, i.

Force F_n is responsible for producing a torque on the shaft of the rotor and this torque can be expressed for a blade as

Torque on a blade,

$$T = F_n \times \frac{d-a}{2}$$

$$= F_n \times \frac{d}{2}\left(1-\frac{a}{d}\right)$$

$$= F_n \times \frac{d}{2} \times (1-s) \qquad (3.4)$$

3.2.3 Torque Co-efficient

Equation (3.4) can be reduced to get the torque coefficient for a single blade at a particular rotor angle as

$$C_q(\alpha) = \frac{F_n}{\frac{1}{2}\rho U_0^2 d} \times \frac{(d-a)}{2} \times \frac{2}{(2d-a)}$$

$$= C_n(\alpha) \times \frac{d-a}{2d-a}$$

$$= C_n(\alpha) \times \frac{d(1-\frac{a}{d})}{d(2-\frac{a}{d})}$$

$$C_q(\alpha) = C_n(\alpha)\frac{(1-s)}{(2-s)} \qquad (3.5)$$

The total static torque coefficient produced on the rotor shaft by the four blades can be expressed as follows:

$$C_Q = \frac{(F_{n1}+F_{n2}+F_{n3}+F_{n4})}{\frac{1}{2}\rho U_0^2 D} \times \frac{\frac{(d-a)}{2}}{\frac{(2d-a)}{2}}$$

$$= \frac{F_{n1}+F_{n2}+F_{n3}+F_{n4}}{\frac{1}{2}\rho U_0^2 d} \times \frac{d-a}{(2d-a)} \times \frac{d}{D}$$

$$= \left[\frac{F_n(\alpha)}{\frac{1}{2}\rho U_0^2 d} + \frac{F_n(\alpha+90^0)}{\frac{1}{2}\rho U_0^2 d} + \frac{F_n(\alpha+180^0)}{\frac{1}{2}\rho U_0^2 d} + \frac{F_n(\alpha+270^0)}{\frac{1}{2}\rho U_0^2 d}\right] \times \frac{d(1-a/d)}{d(2d-a/d)} \times \frac{1}{D}$$

$$= \left[C_n(\alpha)+C_n(\alpha+90^0)+C_n(\alpha+180^0)+C_n(\alpha+270^0)\right] \times \frac{(1-s)}{(2-s)} \times \frac{1}{\frac{(2d-a)}{d}}$$

$$= \left[C_n(\alpha)+C_n(\alpha+90^0)+C_n(\alpha+180^0)+C_n(\alpha+270^0)\right] \times \frac{(1-s)}{(2-s)} \times \frac{1}{(2-s)}$$

$$= \left[C_n(\alpha)+C_n(\alpha+90^0)+C_n(\alpha+180^0)+C_n(\alpha+270^0)\right] \times \frac{(1-s)}{(2-s)^2}$$

$$C_Q(\alpha) = \left[C_n(\alpha)+C_n(\alpha+90^0)+C_n(\alpha+180^0)+C_n(\alpha+270^0)\right] \times \frac{(1-s)}{(2-s)^2} \qquad (3.6)$$

Where, C_n (α), C_n (α + 90°), C_n (α + 180°) and C_n (α + 270°) refer to the drag coefficients of the first, second, third and fourth blade respectively at rotor angle α.

Similarly, the total static torque coefficient produced on the rotor shaft by the five blades can be expressed as follows:

$$C_Q(\alpha)=\begin{bmatrix}C_n(\alpha)+C_n(\alpha+72^0)+C_n(\alpha+144^0)+C_n(\alpha+216^0)\\+C_n(\alpha+288^0)\end{bmatrix}\times\frac{(1-s)}{(2-s)^2} \qquad (3.7)$$

And the total static torque coefficient produced on the rotor shaft by the six blades can be expressed as follows:

$$C_Q(\alpha)=\begin{bmatrix}C_n(\alpha)+C_n(\alpha+60^0)+C_n(\alpha+120^0)+C_n(\alpha+180^0)\\+C_n(\alpha+240^0)+C_n(\alpha+300^0)\end{bmatrix}\times\frac{(1-s)}{(2-s)^2} \qquad (3.8)$$

3.2.4 Numerical Prediction

A computer programme was performed using C++ programming language software to calculate forces experienced by the rotor blades, drag coefficients and torque coefficients using equations (3.2) to (3.6).

In the first programme two components of force experienced by the individual tapping points on each blades are calculated by using the equation (3.3) and also torque T was calculated by using equation (3.4). The programme output gives 36 sets of 8 data for F_n, F_t and T.

In the second programme, integration performed using the output of the first programme to calculate the total forces F_n, F_t and total torque T acting on individual blades and shafts respectively. The programme output gives three types of 36 number integrated values. In the same programme using the integrated values of forces and torques, two types of drag coefficients and torque coefficients were calculated with the help of equations (3.2) and (3.5). The programme output gives 36 numbers of normal drag coefficients, tangential drag coefficients and torque coefficients for every individual blade at 36 positions ranging from 0° to 350° angle of rotation of every 10° interval.

In the third programme, combined effects of four blades on the normal and tangential drag coefficients were performed. The total static torque coefficient produced on the rotor shafts were also calculated in the same programme with the help of equation (3.6).

All these programme output of drag coefficients and torque coefficients are plotted against angle of rotation for analysis.

3.3 Prediction of Dynamic Characteristics

This topic includes the prediction of power coefficient by drawing the velocity triangles for different rotor angles at different tip speed ratios of four/five/six bladed Vane rotor.

3.3.1 Prediction of Power Co-efficient

The quasi-steady approach applied to the analysis of Darrieus rotor has been considered for the prediction of performance of the four/five/six bladed Vane rotor. The static drag coefficient obtained experimentally at a blade angle α, has been used in conjunction with the relative velocity V_r corresponding to a tip speed ratio λ to evaluate the forces acting on the blade. The power coefficient has been estimated by averaging the work done over a cycle.

3.3.1.a Velocity Triangles

Six sets of velocity triangles are drawn for six different tip speed ratios (λ) i.e. 0.5, 0.8, 0.9, 1.1, 1.2 and 1.5 respectively. In each set 9 number of velocity triangles diagrams are drawn for 4 bladed Vane rotor for angle of rotation (α) ranging from 0° to 80° from which typical diagrams are shown in Figures 3.1 to 3.6. Two sets of velocity triangles of five and six bladed rotor are drawn for tip speed ratio (λ) of 0.5.

Velocity triangles diagrams are drawn on the basis of the following calculations:

Diameter of the blade,

$$d = 65 \text{ mm} = 0.065 \text{ m}$$

$$r = 32.5 \text{ mm} = 0.0325 \text{ m}$$

Distance between the two blades,

$$a = 75 \text{ mm}$$

Ratio between distance of two blades and diameter of a blade,

$$S = \frac{a}{d} = \frac{75}{65} = 1.153$$

Diameter of the Rotor,

$$D = 2\,d + a = 200 \text{ mm}$$

$$R = 100 \text{ mm} = 0.1\text{m}$$

$$U_0 = 13 \text{ m/s}$$

At Tip Speed Ratio, λ = 0.5

$$\lambda = 0.5 = \frac{R\omega}{U_0}$$

$$\omega = \frac{0.5 \times U_0}{R} = \frac{0.5 \times 13}{0.1} = 63.41 \text{ rad/s}$$

$$r\omega = 0.0325 \times 63.14 = 2.06 \text{ m/s}$$

At Tip Speed Ratio, λ = 0.8

$$\lambda = 0.8 = \frac{R\omega}{U_0}$$

$$\omega = \frac{0.8 \times U_0}{R} = \frac{0.8 \times 13}{0.1} = 101.46 \text{ rad/s}$$

$r\omega = 0.0325 \times 101.46 = 3.29$ m/s

At Tip Speed Ratio, $\lambda = 0.9$

$$\lambda = 0.9 = \frac{R\omega}{U_0}$$

$$\omega = \frac{0.9 \times U_0}{R} = \frac{0.9 \times 13}{0.1} = 114.14 \text{ rad/s}$$

$r\omega = 0.0325 \times 114.14 = 3.7$ m/s

At Tip Speed Ratio, $\lambda = 1.1$

$$\lambda = 1.1 = \frac{R\omega}{U_0}$$

$$\omega = \frac{1.1 \times U_0}{R} = \frac{1.1 \times 13}{0.1} = 139.51 \text{ rad/s}$$

$r\omega = 0.0325 \times 139.51 = 4.53$ m/s

At Tip Speed Ratio, $\lambda = 1.2$

$$\lambda = 1.2 = \frac{R\omega}{U_0}$$

$$\omega = \frac{1.2 \times U_0}{R} = \frac{1.2 \times 13}{0.1} = 152.19 \text{ rad/s}$$

$r\,\omega = 0.0325 \times 152.19 = 4.94$ m/s

At Tip Speed Ratio, $\lambda = 1.5$

$$\lambda = 1.5 = \frac{R\omega}{U_0}$$

$$\omega = \frac{1.5 \times U_0}{R} = \frac{1.5 \times 13}{0.1} = 190.24 \text{ rad/s}$$

$r\,\omega = 0.0325 \times 190.24 = 6.18$ m/s

3.3.1.b Power Co-efficient, C_p

The following equations have been used to estimate the power coefficient at a blade angle, α.

$$C_n'(\alpha) = C_n(\alpha) \times (V_{w1}/U_0)^2 \tag{3.9}$$

$$C_n'(90+\alpha) = C_n(90+\alpha) \times (V_{w2}/U_0)^2 \tag{3.10}$$

$$C_n'(180+\alpha) = C_n(180+\alpha) \times (V_{w3}/U_0)^2 \tag{3.11}$$

$$C_n'(270+\alpha) = C_n(270+\alpha) \times (V_{w3}/U_0)^2 \tag{3.12}$$

Torque coefficient at α,

$$C_Q'(\alpha) = [C_n'(\alpha) + C_n'(90+\alpha) + C_n'(180+\alpha) + C_n'(270+\alpha)] \frac{1-s}{(2-s)^2} \tag{3.13}$$

$$C_p(\alpha) = C_Q'(\alpha).\lambda \tag{3.14}$$

3.3.2 Numerical Prediction

A computer programme was performed to calculate the power coefficient (C_p) using the value of the component of relative velocity V_w along U_o and static normal drag coefficient C_n (α) for different tip speed ratio λ with the help of equations (3.9) to (3.14). The programme output gives different sets of dynamic torque coefficients and power coefficient and finally average value of power coefficient Cp_{ave}.

Power coefficient vs. tip speed ratio of the present prediction and the previous researcher's prediction were plotted on the same graph for analysis.

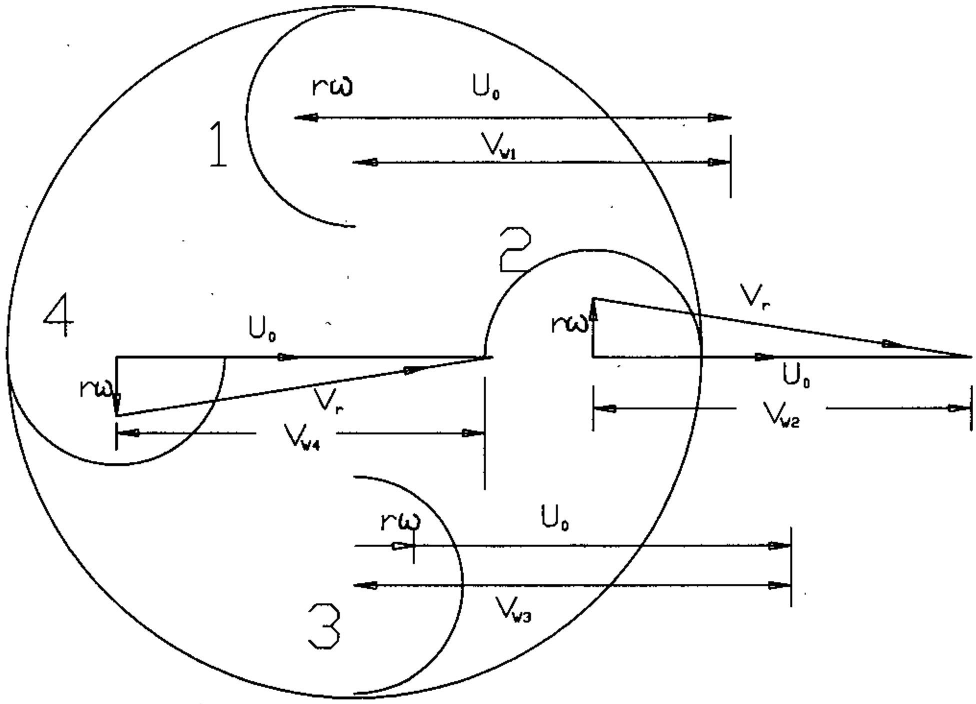

(i): At α = 0°

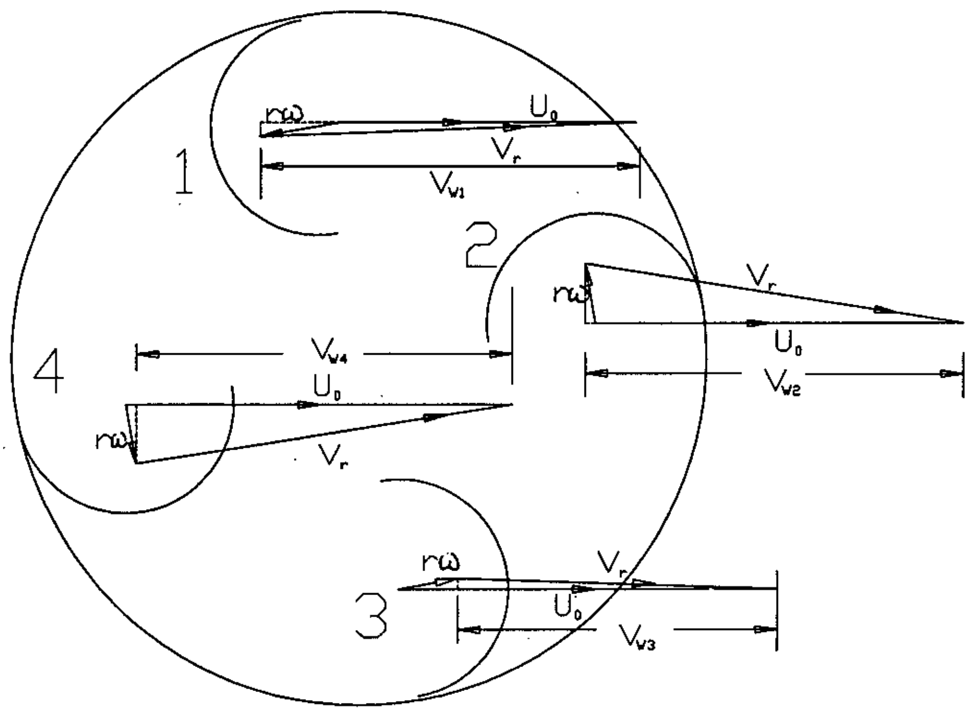

(ii): At α = 10°

Figure 3.1: Velocity triangles combining the effect of free stream velocity and blade rotation at λ = 0.5 (for 4 bladed vertical axis vane type rotor).

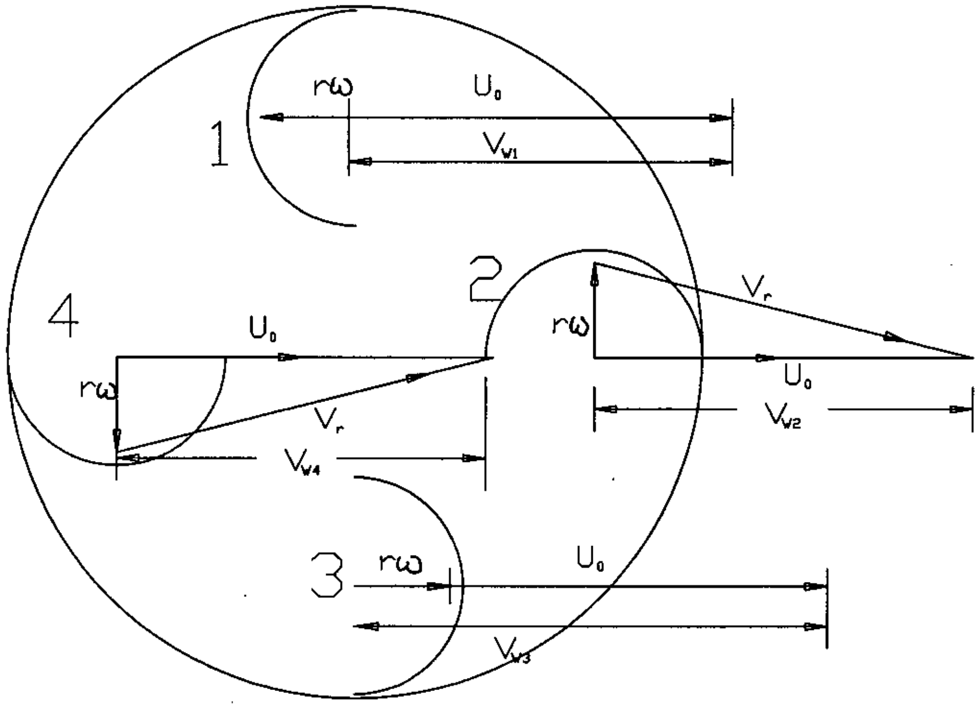

(i): At α = 0°

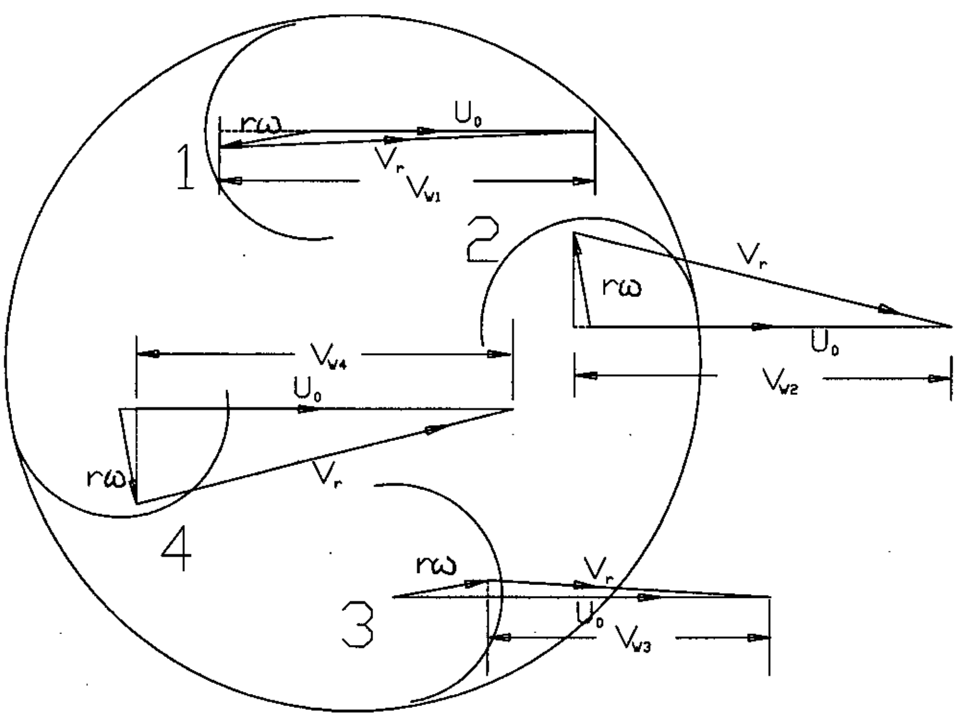

(ii): At α = 10°

Figure 3.2: Velocity triangles combining the effect of free stream velocity and blade rotation at λ = 0.8 (for 4 bladed vertical axis vane type rotor).

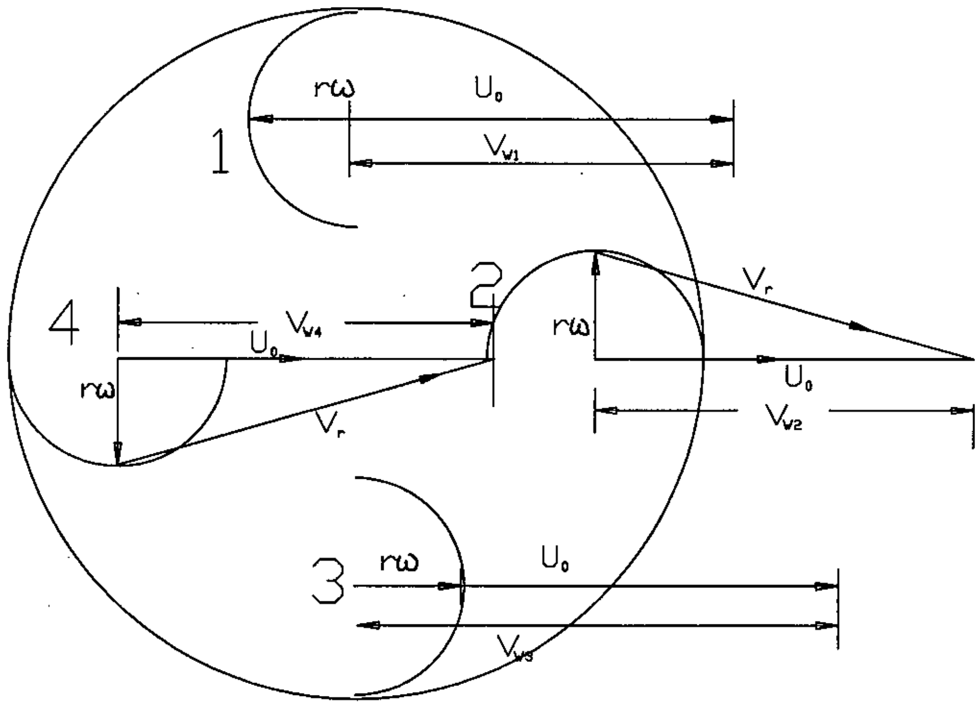

(i): At α = 0°

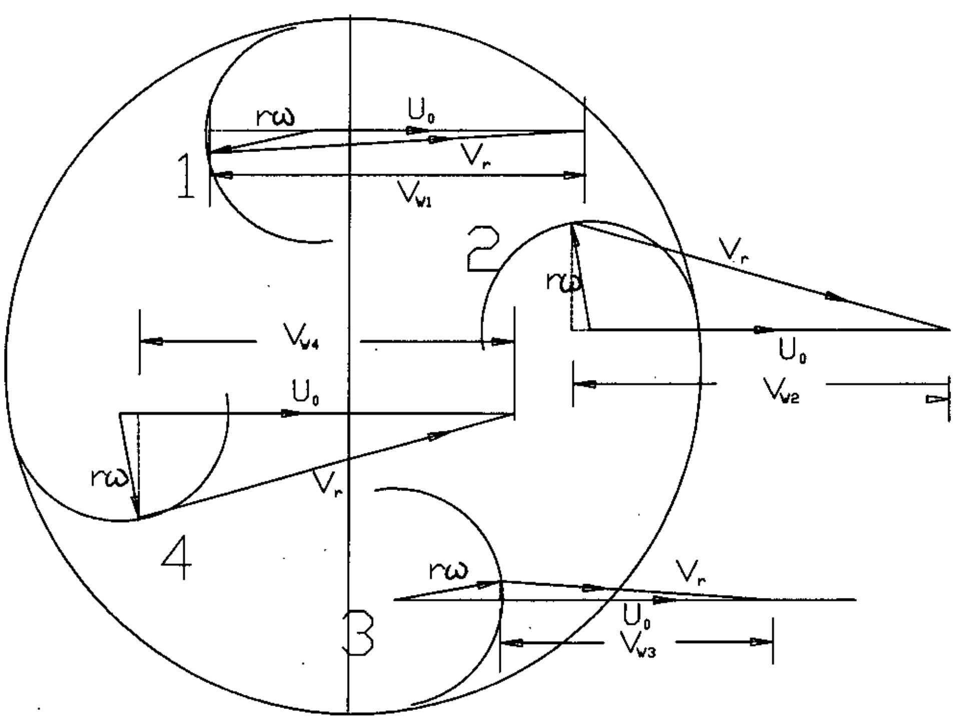

(ii): At α = 10°

Figure 3.3: Velocity triangles combining the effect of free stream velocity and blade rotation at λ = 0.9 (for 4 bladed vertical axis vane type rotor).

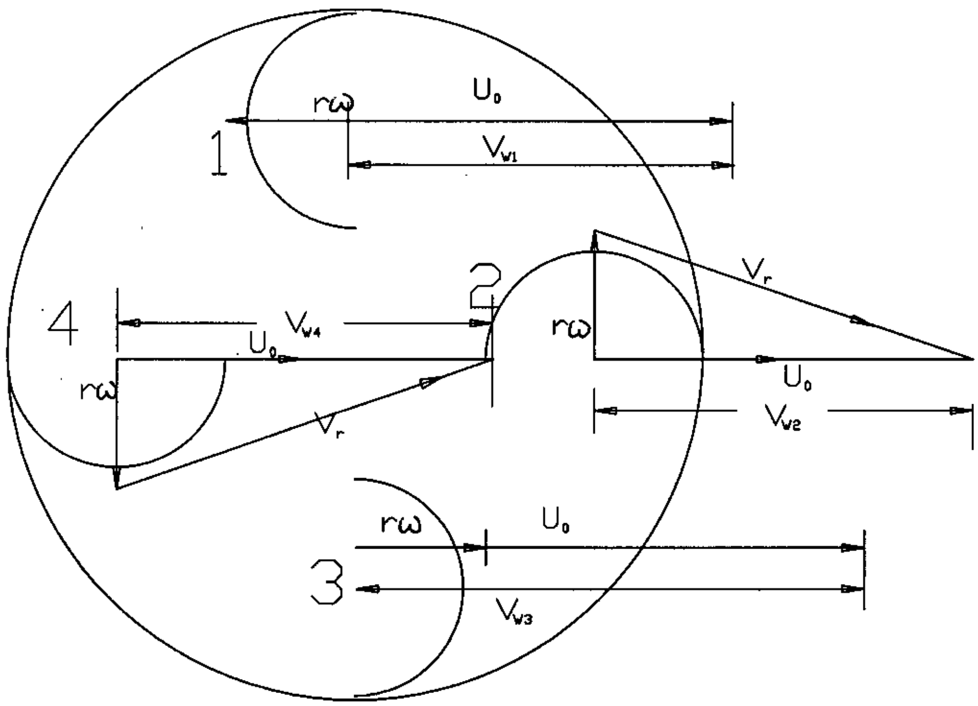

(i): At α = 0°

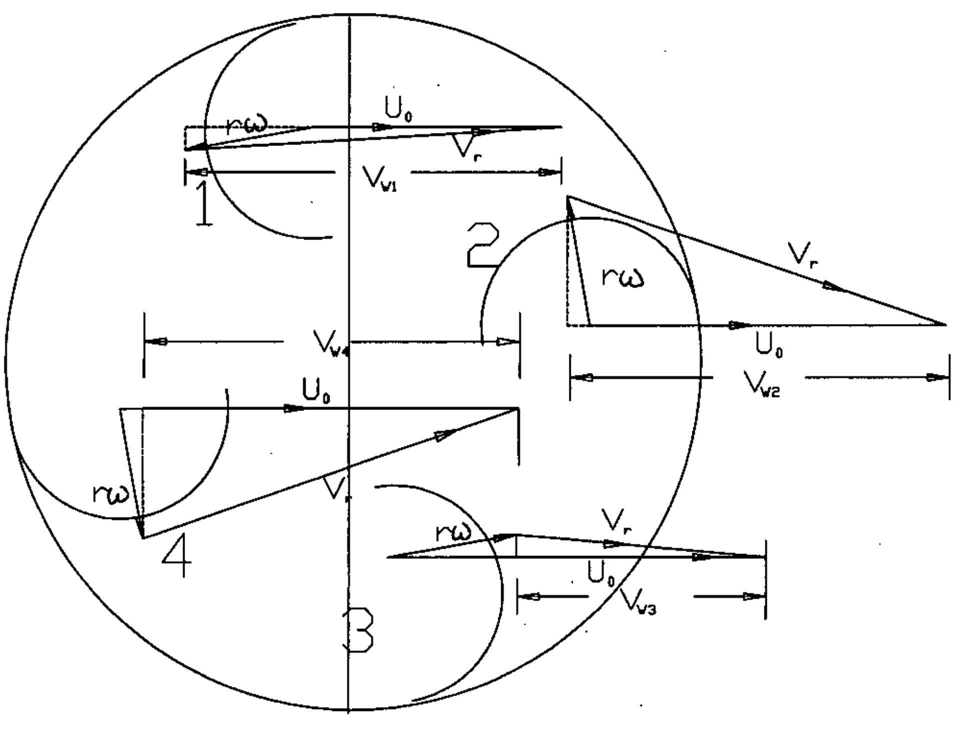

(ii): At α = 10°

Figure 3.4: Velocity triangles combining the effect of free stream velocity and blade rotation at λ = 1.1 (for 4 bladed vertical axis vane type rotor).

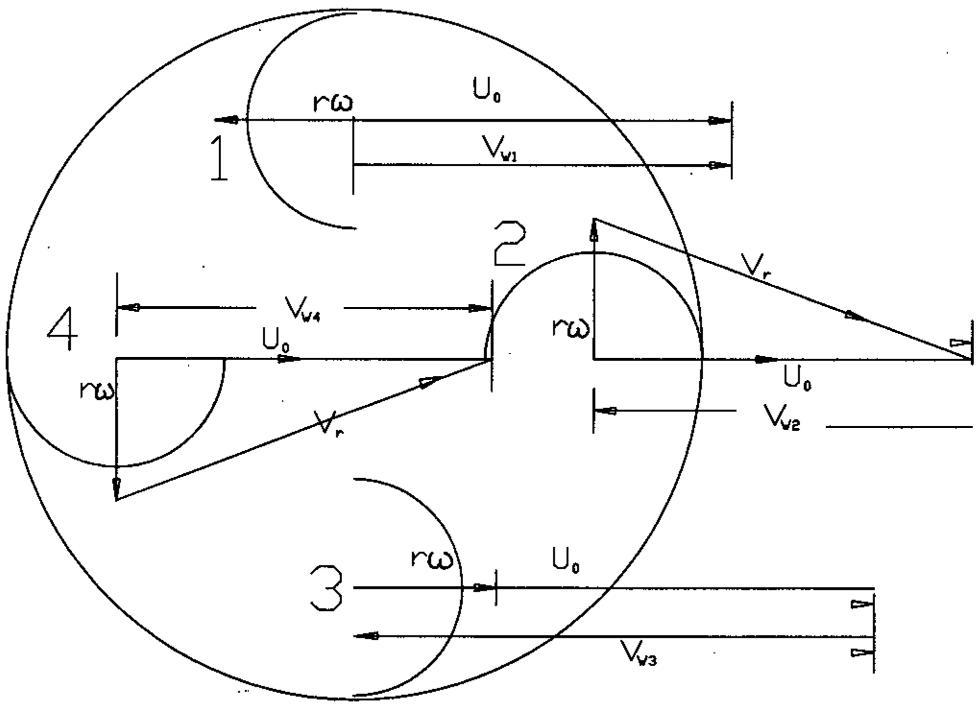

(i): At α = 0°

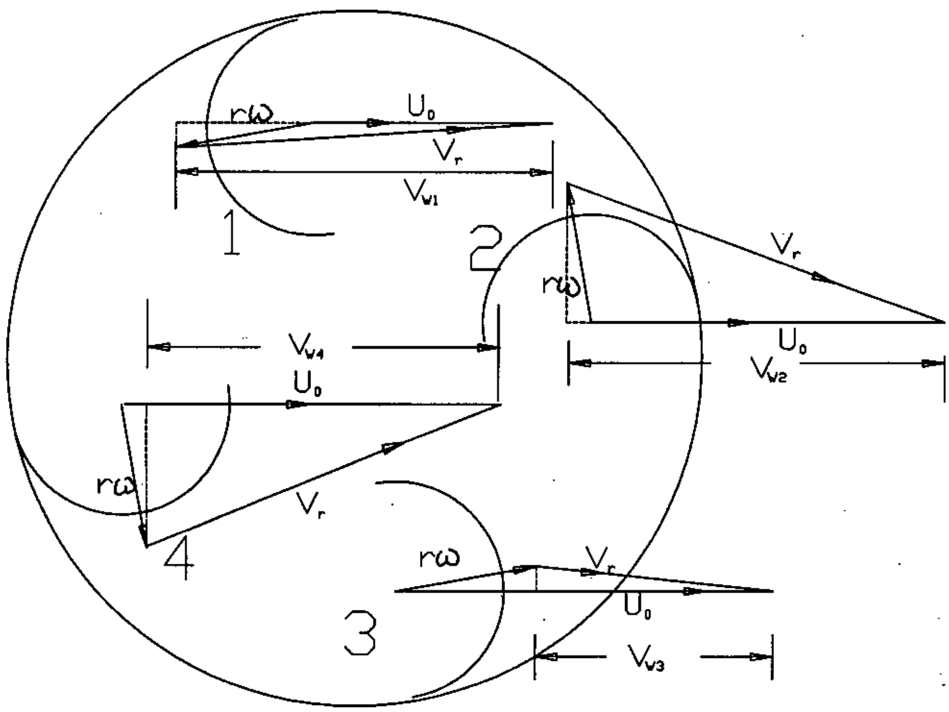

(ii): At α = 10°

Figure 3.5: Velocity triangles combining the effect of free stream velocity and blade rotation at λ = 1.2 (for 4 bladed vertical axis vane type rotor).

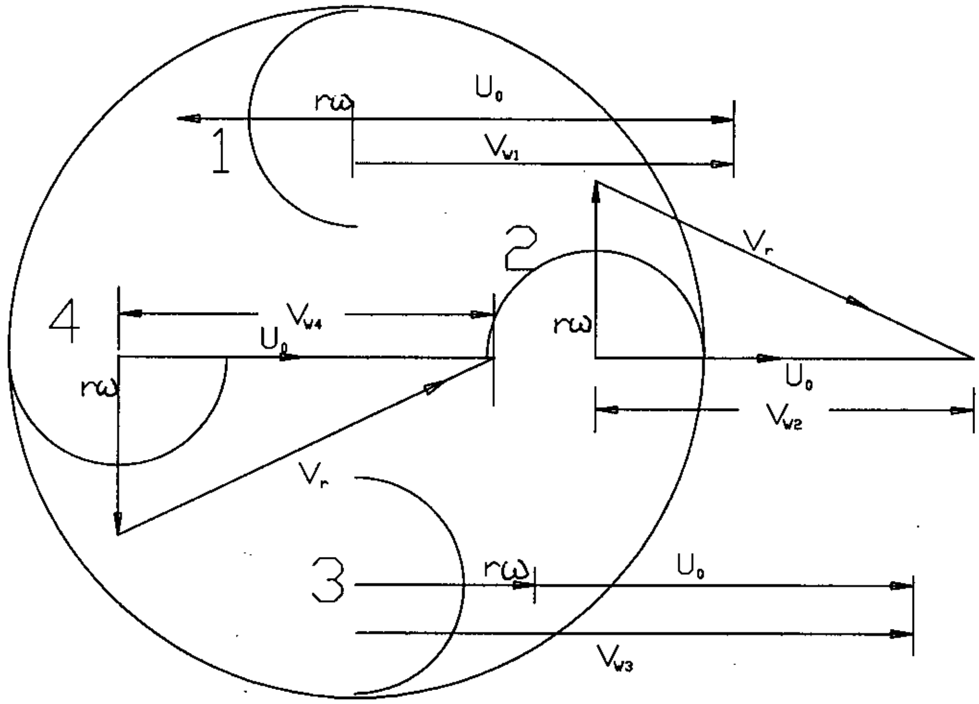

(i): At α = 0°

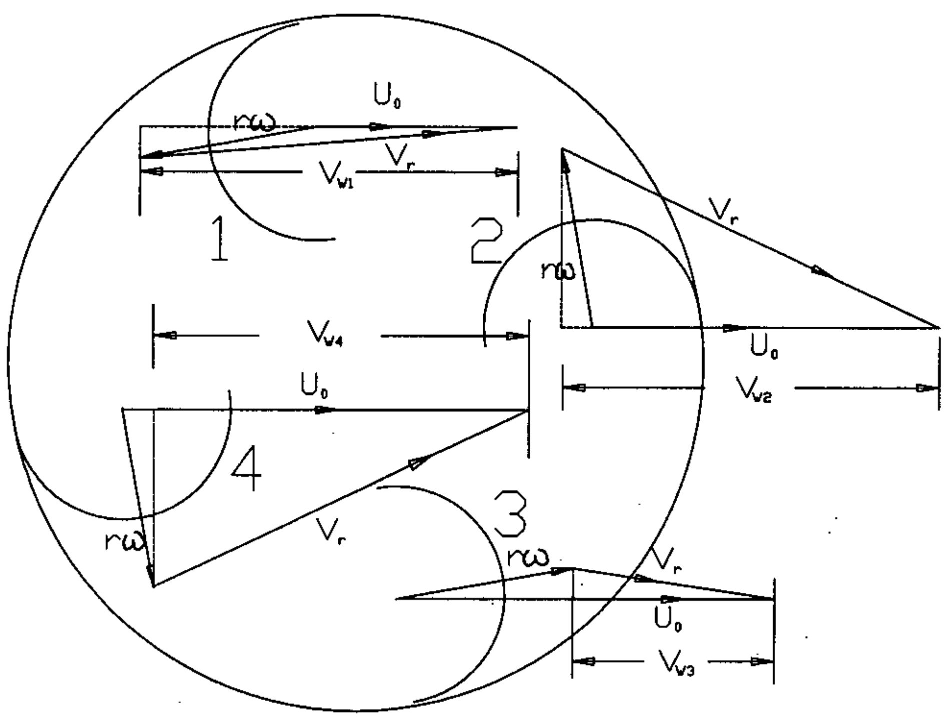

(ii): At α = 10°

Figure 3.6: Velocity triangles combining the effect of free stream velocity and blade rotation at λ = 1.5 (for 4 bladed vertical axis vane type rotor).

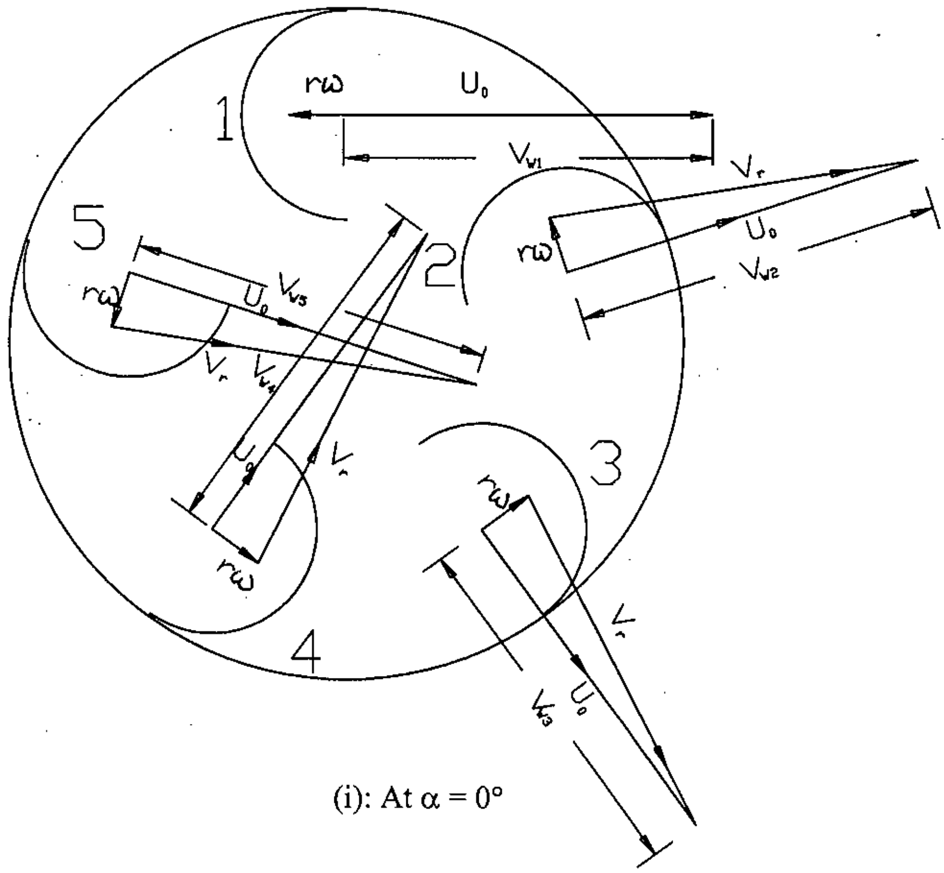

(i): At $\alpha = 0°$

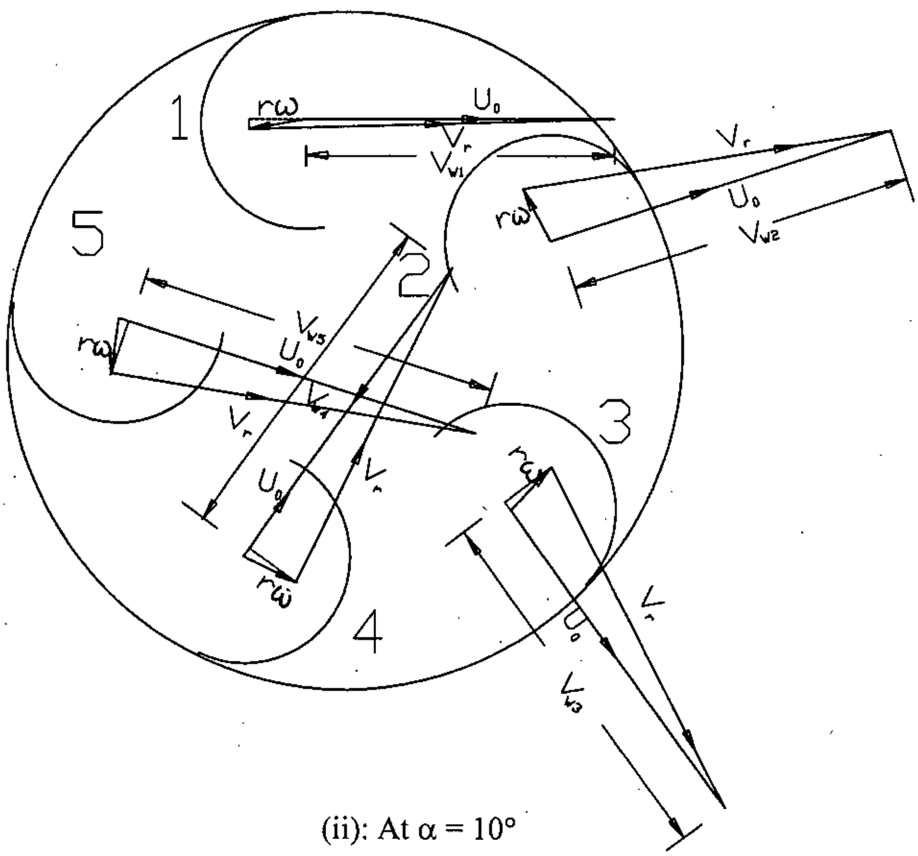

(ii): At $\alpha = 10°$

Figure 3.7: Velocity triangles combining the effect of free stream velocity and blade rotation at $\lambda = 0.5$ (for 5 bladed vertical axis vane type rotor).

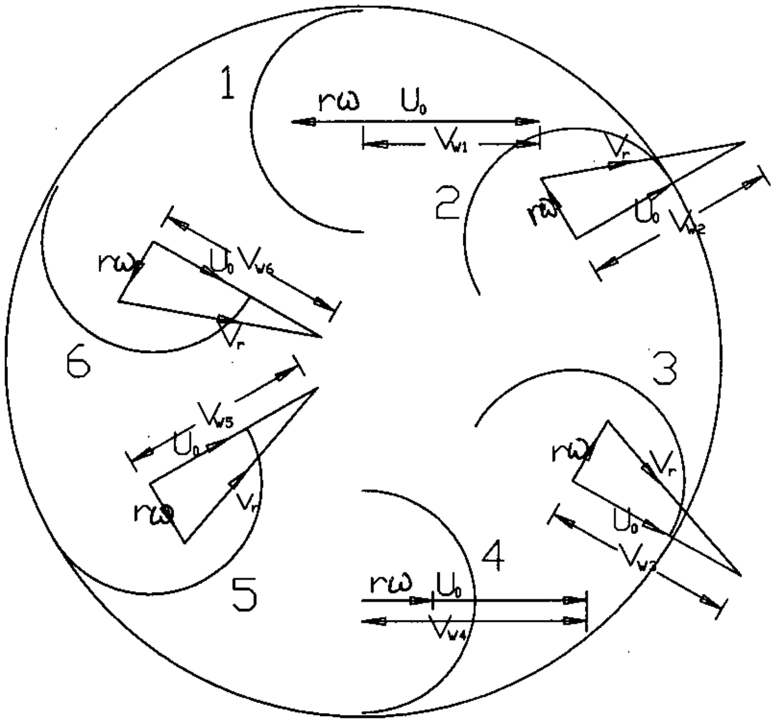

(i): At α = 0°

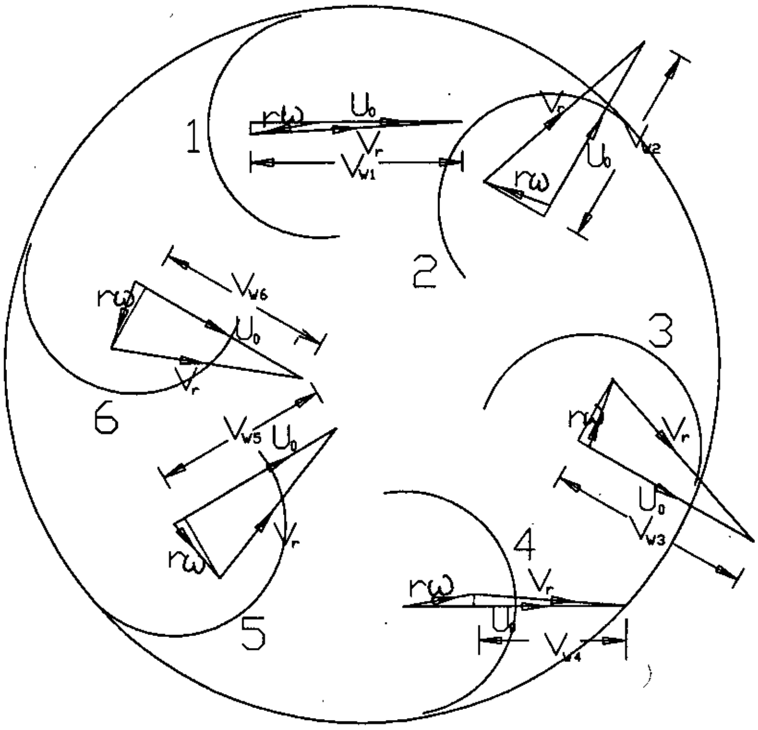

(ii): At α = 10°

Figure 3.8: Velocity triangles combining the effect of free stream velocity and blade rotation at λ = 0.5 (for 6 bladed vertical axis vane type rotor).

CHAPTER 4

EXPERIMENTAL SET-UP AND PROCEDURE

Chapter -4

EXPERIMENTAL SET-UP AND PROCEDURE

4.1 Introduction

The investigation on wind loading and aerodynamic effects on the four/five/six semi-cylindrical bladed Vertical Axis vane rotor has been conducted essentially with the help of a subsonic wind tunnel together with the experiment set-up of the Vane rotor and an inclined multi-manometer. Pressure distribution over the convex and concave surfaces of each blade of the vane rotor was measured with the help of the multi-manometer. The following sections describe in detail set-up of the experiment and techniques adopted for the investigation.

4.2 Specification of the Wind Tunnel

The experimental setup of the present investigation has been shown in the schematic diagram of Figure 4.1. An open circuit subsonic type wind tunnel was used to develop the required flow, and the rotor was positioned at the outlet section of the wind tunnel. The tunnel is 5.93 meter long with a test section of 460 x 480 mm cross-section. In order to smooth the flow, a honeycomb was fixed near the end of the wind tunnel. There is a bell-shaped converging duct at the entry. To generate the wind velocity, two axial flow fans are used, with each of the fans connected to a motor of 2.25 kilowatt capacity and 2900 rpm. There is a butterfly valve to control the wind speed. There is a silencer just after the butterfly valve as shown in the Figure 4.1 and 4.2.

The central longitudinal axis of the wind tunnel is always kept at a constant height of 990 mm from the floor. The axis of the model is also placed coinciding with the wind tunnel. The converging duct inlet is then merged into the wind tunnel so that air can enter smoothly into the tunnel and maintain uniform flow into the duct, keeping it free from any outside disturbances. The flow through the wind tunnel is induced by a two-

1. CONVERGING MOUTH ENTRY
2. PERSPEX SECTION
3. RECTANGULAR DIVERGING SECTION
4. FAN SECTION
5. BUTTER FLY SECTION
6. SILENCER WITH HONEYCOMB SECTION
7. DIVERGING SECTION
8. CONVERGING SECTION
9. RECTANGULAR SECTION
10. FLOW STRAIGHTNER SECTION
11. RECTANGULAR EXIT SECTION

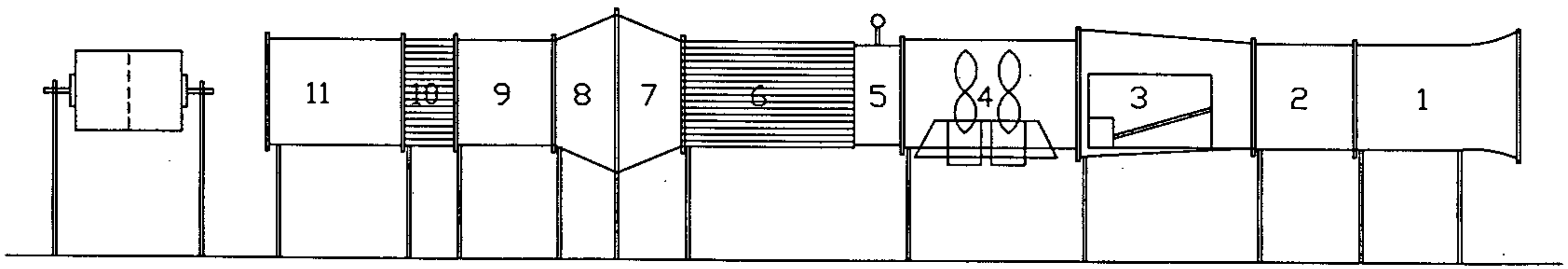

Figure 4.1: Schematic diagram of wind tunnel

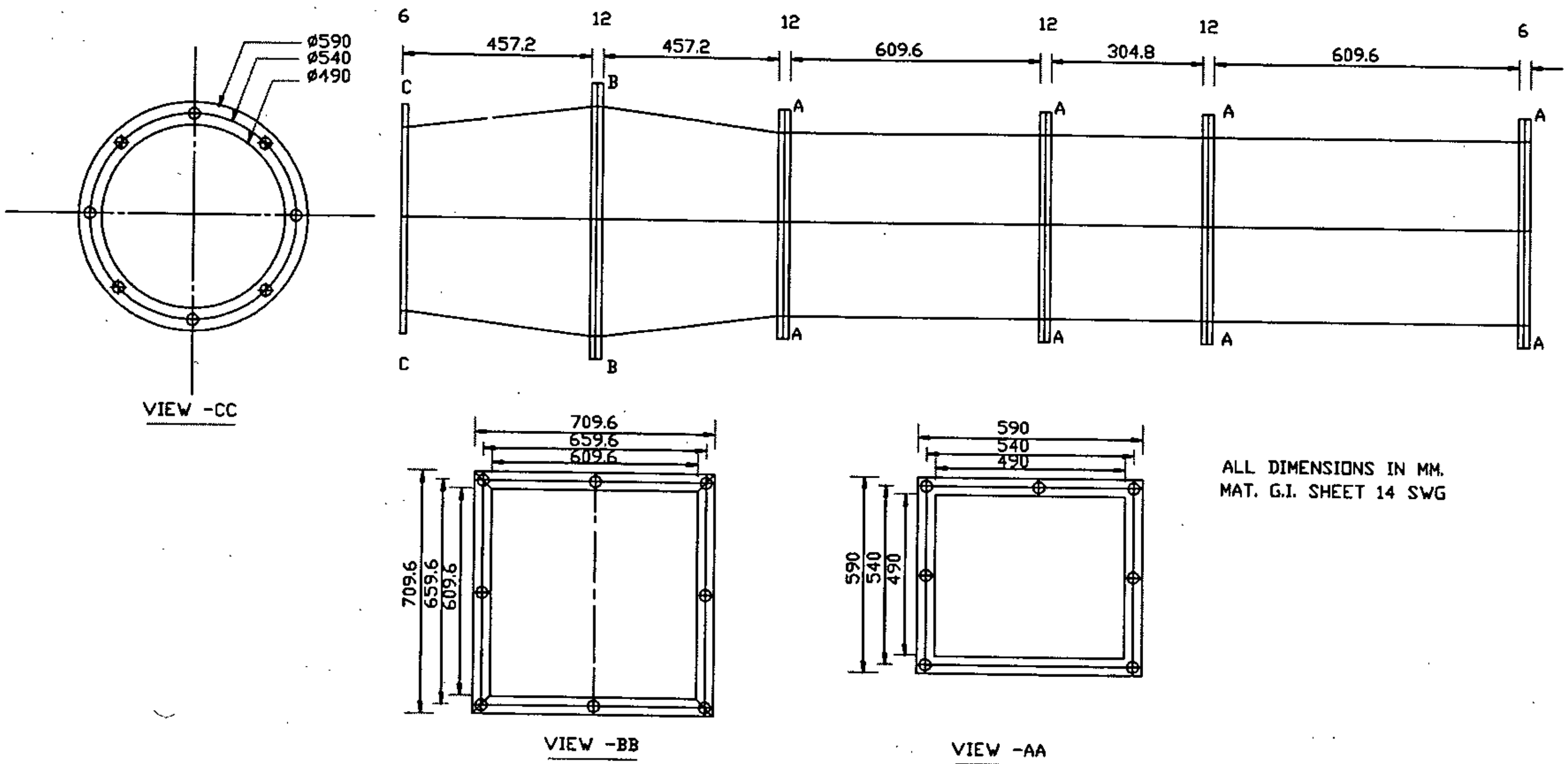

Figure 4.2: Modification part of the wind tunnel

stage rotating axial flow fan of 18.16 m^3/s capacity with a head of 152.4 mm of water and 1475 rpm.

A butterfly valve, which is used to control the flow, was actuated by a screw thread mechanism placed behind the fan. A silencer, which is incorporated with a honeycomb, is fitted at the end of the flow controlling section, which helps reduce the noise of the system. The diverging and converging section of the wind tunnel is 1550 mm long and made of 16 SWG black sheets. The angle of divergence and convergence is 7°, which has been done with a view to minimize expansion, contraction loss and reduce the possibility of flow separation.

A digital anemometer is used in each of these tests to measure the wind velocity. Results show that the flow velocity was maintained at approximately 13 m/s. In the tunnel test section, the measured velocity distribution was uniform almost throughout the upstream side of the model.

4.3 Constructional Detail of the Four/Five/Six Bladed Vane Type Rotor

The constructional details of the test section are shown in the Figures 4.3 (a), (b), (c) and Figure 4.4. Four Bladed Vane rotor was made up of four half cylinders (blade) of diameter, d = 65 mm and height, H = 340 mm. Five Bladed Vane rotor was made up of five half cylinders (blade) of diameter, d = 65 mm and height, H = 340 mm. Six Bladed Vane rotor was made up of six half cylinders (blade) of diameter, d = 65 mm and height, H = 340 mm. Rotor diameter, D is 200 mm. Optimum value of d/D ratio is taken 3. The cylinders were made of PVC material. The center-to-center distance of the blade is 137.5 mm. The whole rotor was fixed on an iron frame by using two side shafts and two ball bearings.

The pressure measurements were made at 8 pressure tappings on each blade. The tappings were made with copper tubes of 1.5 mm outer diameter and 10 mm length that were press fitted to the tapping holes. The tappings were located at the mid-plane of one side of each blade, so that pressure distribution at every 10° on the blade surface could be measured. The pressure tappings were connected to an inclined multi-manometer (manometric fluid was water and had an accuracy of ± 0.1 mm of water column) through 2 mm PVC tubes. The pressures were measured at every 10° interval of rotor angle (Figure 4.5), so that a detailed picture of the aerodynamic loading and torque characteristics could be obtained.

4.4 Experiment Procedure

The flow velocity in the test section was kept constant at 13 m/s. The Reynolds number based on the rotor diameter d = 200 mm was 1.65 x 10^5. The effect of temperature was considered in this experiment and the experiment was carried out at atmospheric temperature i.e. at T = 30°C where kinematics viscosity of air was ν =1.6 x 10^{-5} m^2/s.

Before measuring the pressure distribution, the mean velocity was measured in a vertical plane 100 cm downstream from the outlet of the wind tunnel (without placing the rotor) by means of a pitot static tube connected to an inclined manometer with kerosene as the manometric fluid.

The measured velocity distribution was uniform that can be seen from the Figure 4.6. One may also observe from the figure that, there is a velocity gradient within 3 cm from the tunnel surface, which is caused due to the surface friction of the tunnel.

The pressure distribution over the blade surfaces was measured step by step by using the multi-manometer. At first, the vane rotor with the frame was placed 100 cm down stream in front of the exit section of the tunnel on a table. One blade of the rotor was fixed parallel to the free stream velocity i.e. parallel to the horizontal, which was called the reference plane and from which plane angle of rotation was also measured. In the case of four bladed vane rotor, the first blade was at 0° angle of rotation, exposing the convex surface in front of free stream air, so the other three blades were at 90°, 180° and 270° angle of rotation respectively. The rotor was then made static by fixing one end of the shaft with the angle-fixing device. Power was supplied to the motor of the wind tunnel to start flow of the free stream air of uniform velocity over the blades of the rotor. Pressure on the convex surface of blades was measured at a particular rotor angle α, fixing the rotor at static condition. Gradually, pressure on the convex surfaces was measured in this process for every 10° interval of rotor angle up to 350° angle of rotation. The same steps were performed for the measurement of the pressure on the concave surfaces. As the first blade of the four bladed rotor took the position of the second, second blade took the position of the third and third blade took the position of the fourth blade, pressure distribution for four bladed vane rotor has been shown from 0° to 80° after which the distribution repeated itself.

Same procedure has been followed for five and six bladed vane type rotor. So pressure distribution for five bladed vane type rotor has been shown from 0° to 60° after which the distribution repeated itself. And pressure distribution for six bladed vane type rotor has been shown from 0° to 50° after which the distribution repeated itself.

At a particular rotor angle, α the rotor blades experience forces (per unit span length) due to the pressure difference between the concave surface and convex surface and these forces can be resolved into two components F_n and F_t. Since the blade surfaces are circular, F_n and F_t are shown in Figure 4.7.

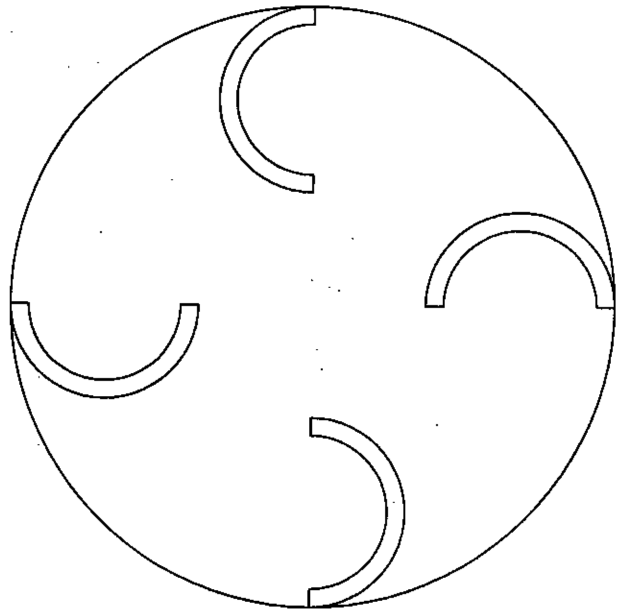

Figure 4.4(a): Sectional view of four bladed vertical axis vane type rotor.

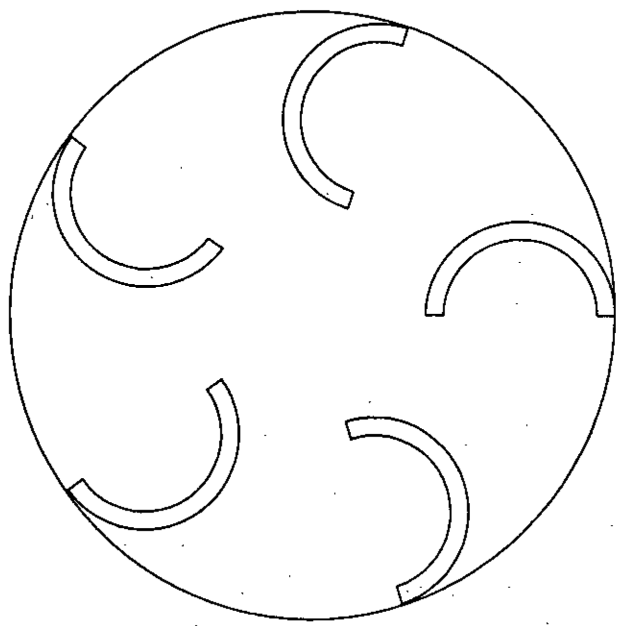

Figure 4.4(b): Sectional view of five bladed vertical axis vane type rotor.

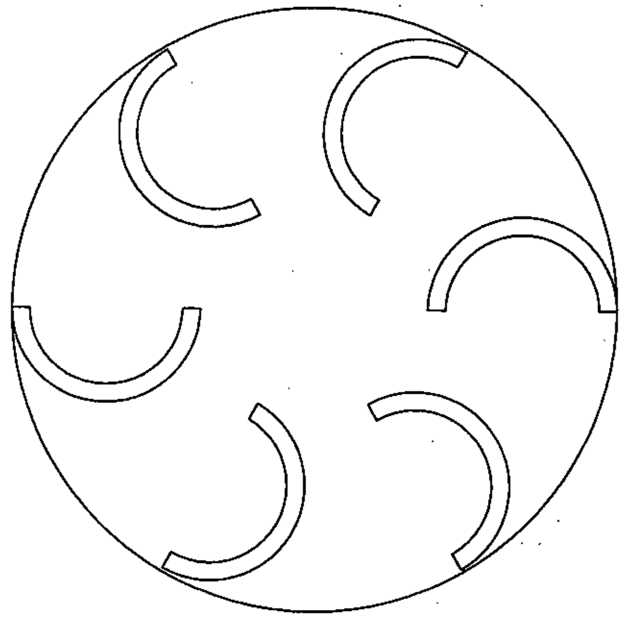

Figure 4.3(c): Sectional view of six bladed vertical axis vane type rotor.

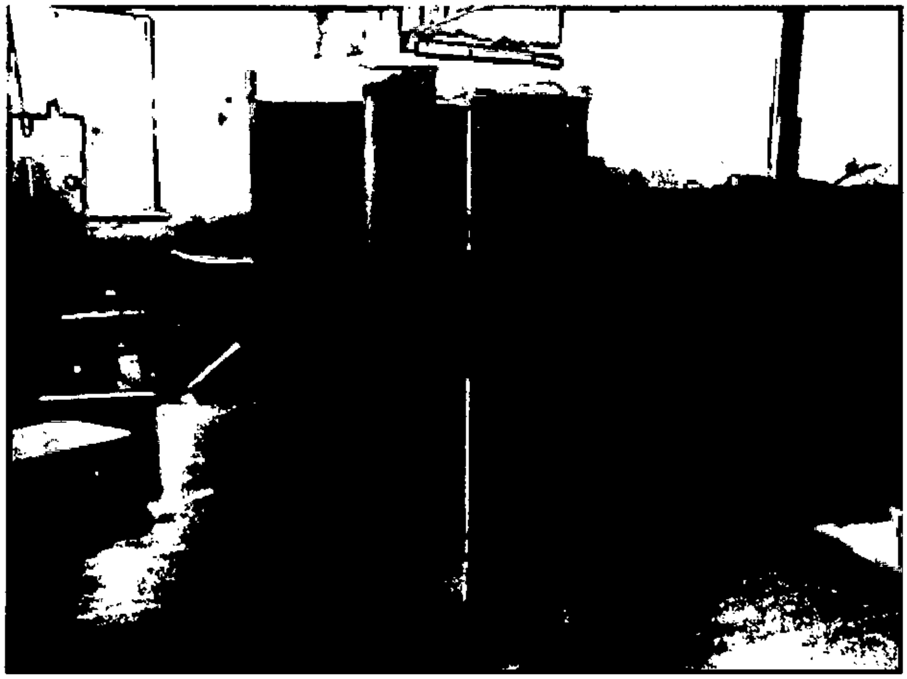

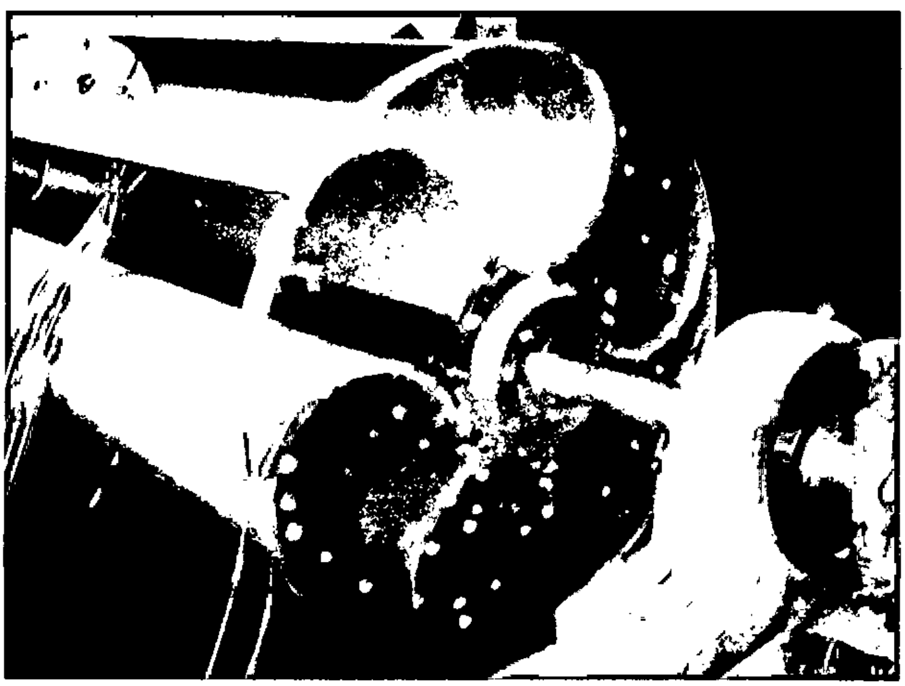

Figure 4.4: Constructional Details of the test section.

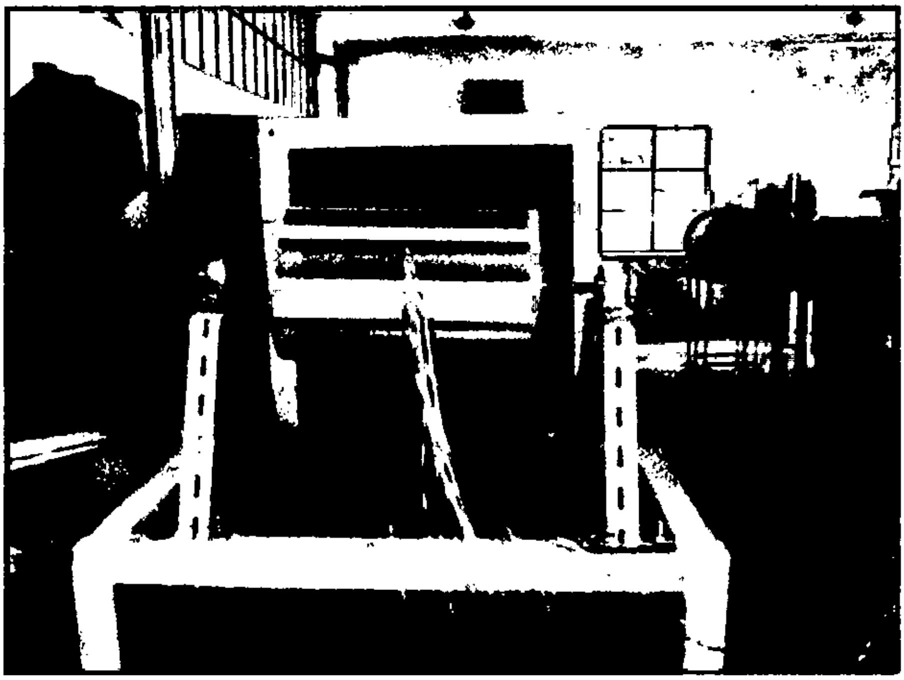

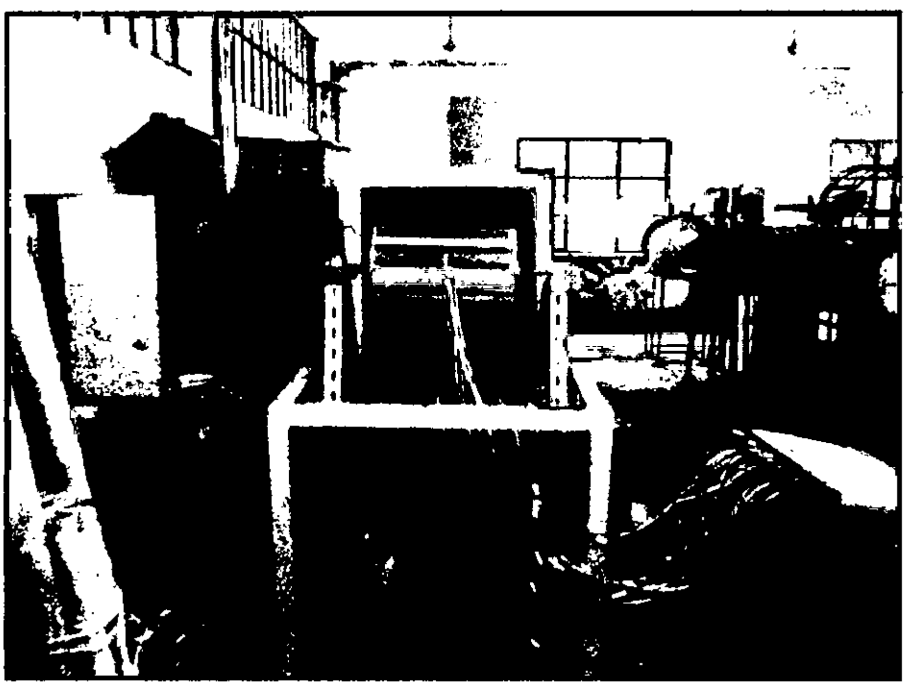

Figure 4.5: Set-up of the Experiment

DISTANCE VS. VELOCITY
(VELOCITY PROFILE)

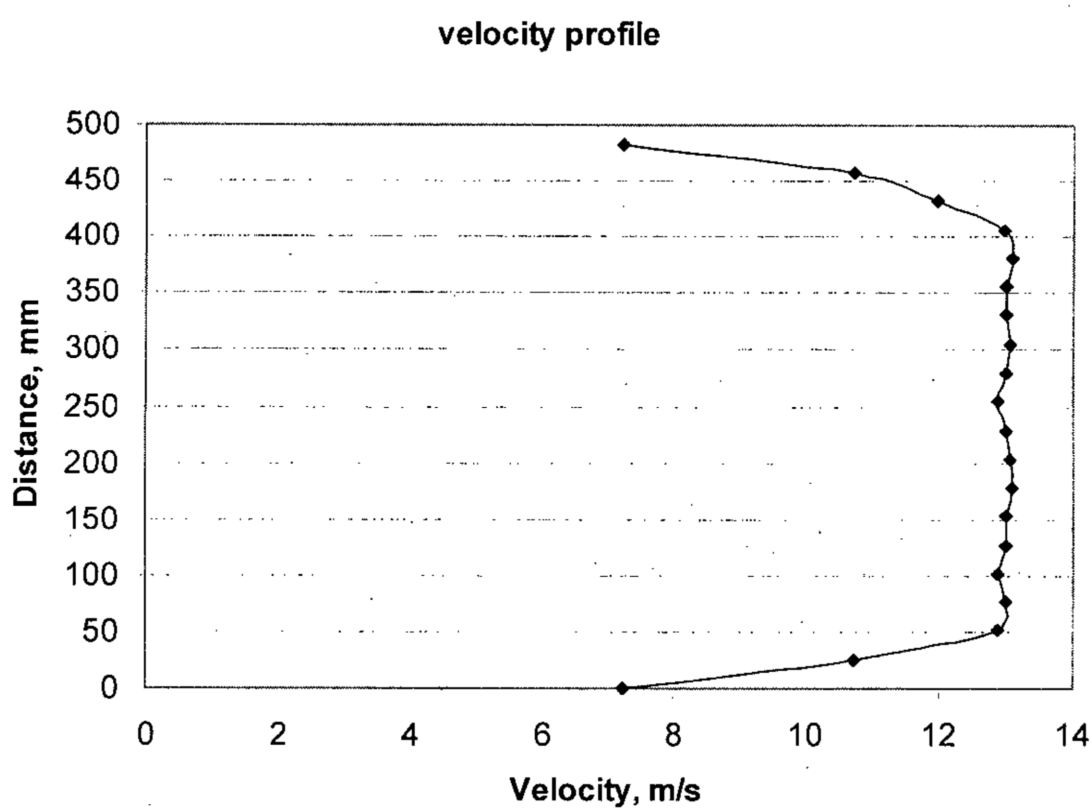

Figure 4.6: Velocity distribution in upstream side of test section.

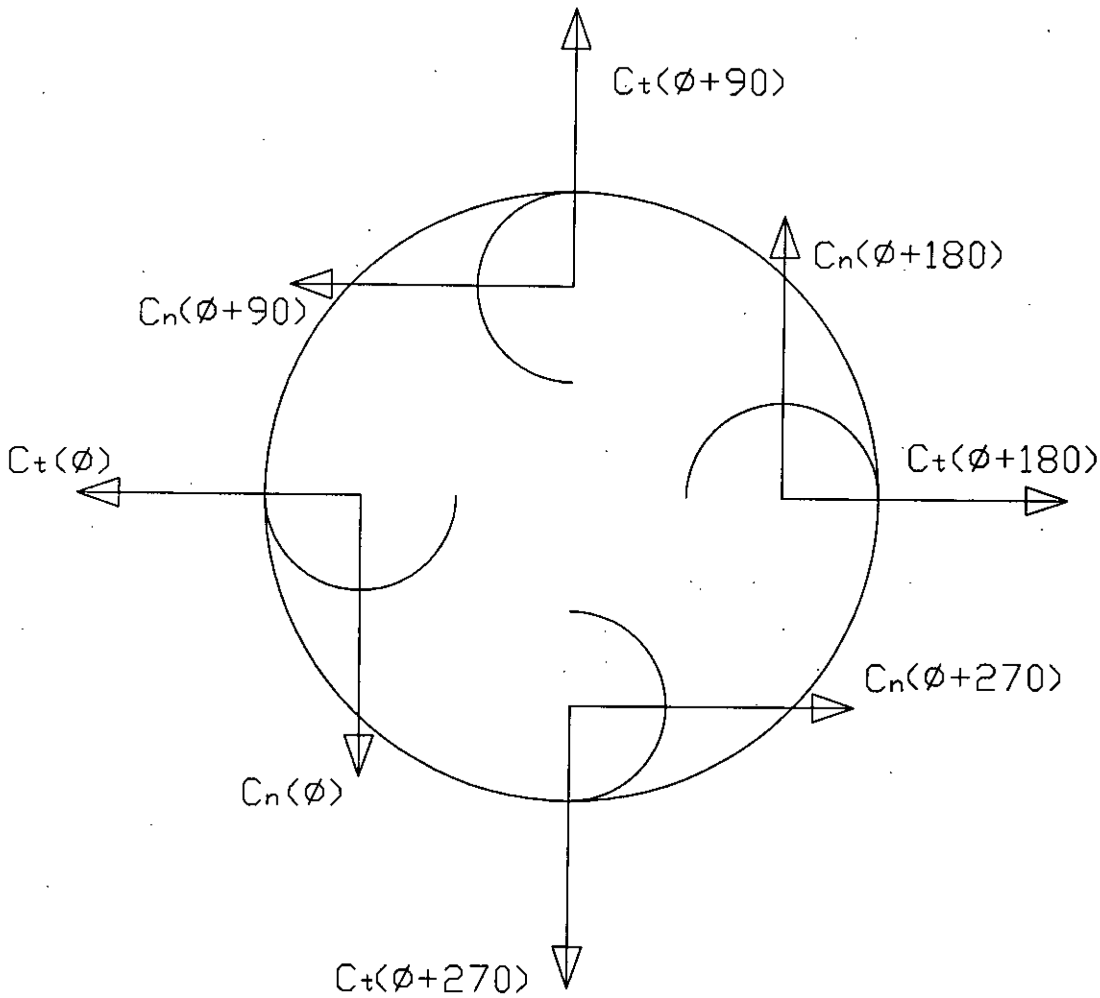

Figure 4.7(a): Forces acting on the blades (4 bladed vane type rotor).

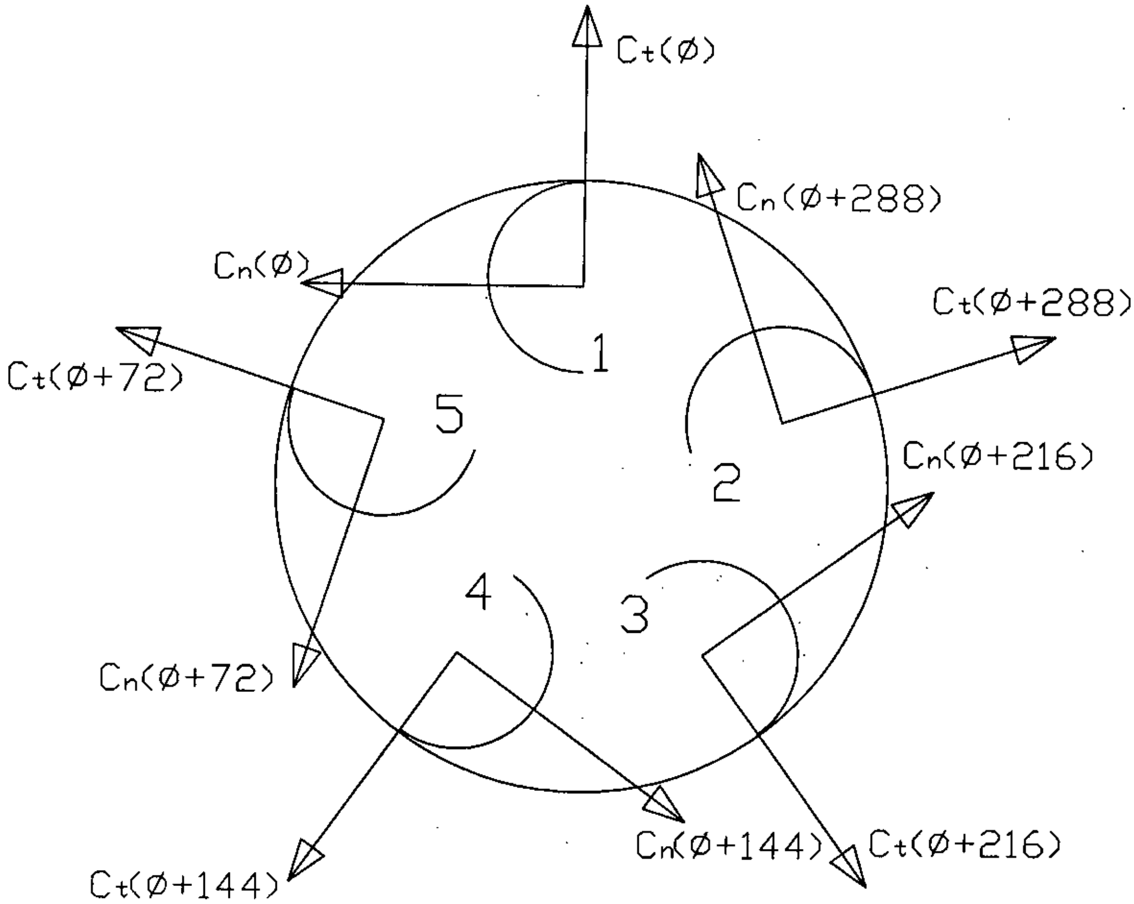

Figure 4.7(b): Forces acting on the blades (5 bladed vane type rotor).

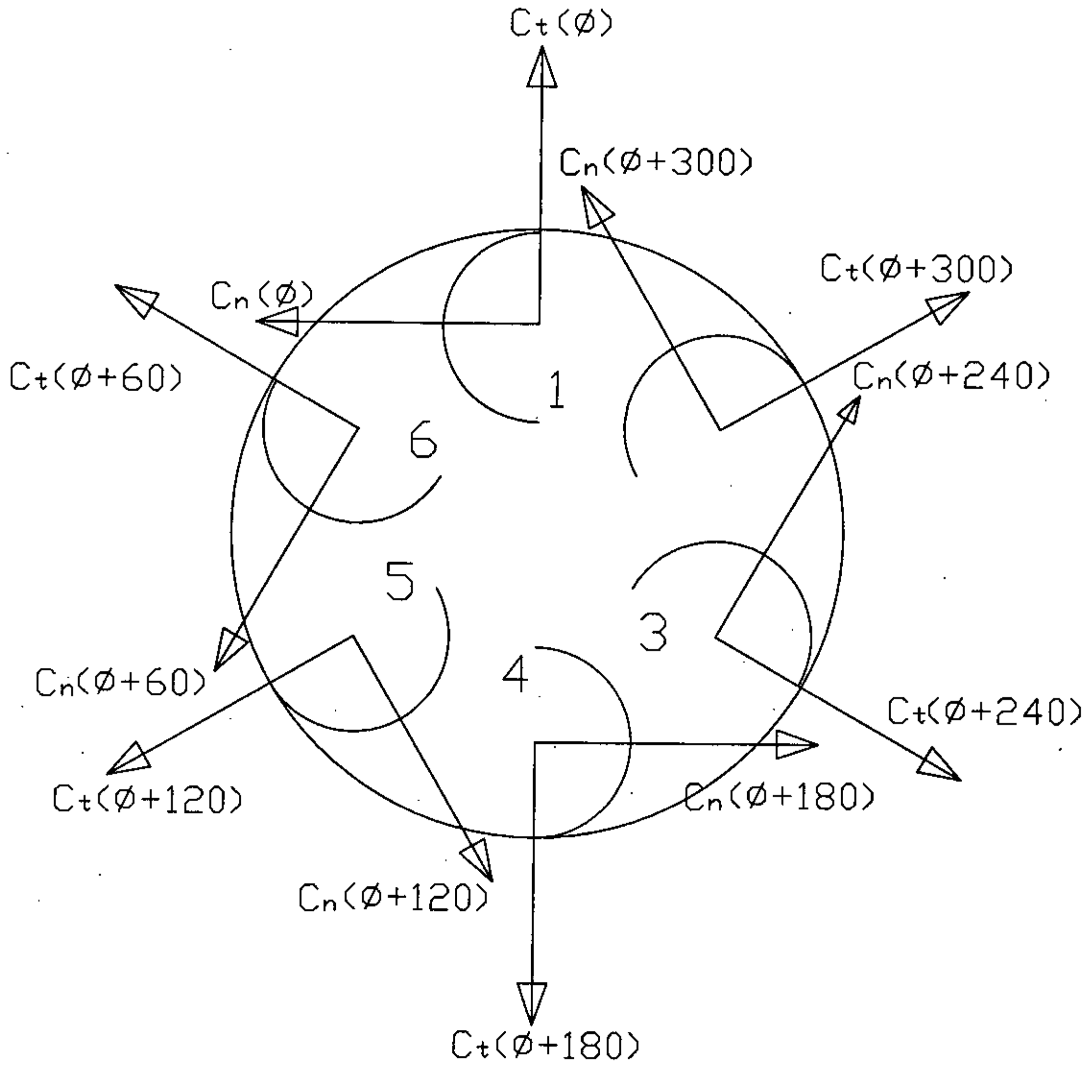

Figure 4.7(c): Forces acting on the blades (6 bladed vane type rotor).

CHAPTER 5

RESULTS AND DISCUSSIONS

Chapter-5

RESULTS AND DISCUSSIONS

5.1 Introduction

This chapter provides with the discussions of the results of experimental investigation conducted for the wind tunnel flow over the four, five and six bladed vane rotor. The results of the pressure distribution over the convex and concave surfaces of each blade at different angle of rotation are analyzed first. Nature of the drag and static torque characteristics are also analyzed in this chapter. In addition, comparative study of the existing research works and the present investigation in the prediction of dynamic characteristics are presented in this chapter.

5.2 Static Aerodynamic Characteristics

This topic includes the analysis of pressure distribution, normal drag coefficient (C_n), tangential drag coefficient (C_t), torque coefficient (C_q) and total static torque coefficient (C_Q).

5.2.1 Pressure Distribution

(a) Pressure Distribution for Four bladed Vertical Axis Vane Type Rotor:

The pressure distributions over the surfaces of the blades were measured at every 10° interval of rotor angle between $0^\circ \leq \alpha \leq 80^\circ$. The results are presented in Figure 5.1(a) to 5.1(i).

At rotor angle of $\alpha = 0^\circ$ (Figure 5.1(a)) as the flow accelerates over the leading edge of the convex surface of the first blade, the pressure slightly increases and then drastically reduces to negative direction from $\Phi_I = 90^\circ$ to $\Phi_I = 157^\circ$ and pressure remains negative. At $\Phi_I = 137.5^\circ$ the flow separates as caused by an adverse pressure gradient. In case of the second blade the pressure decreases up to $\Phi_2 = 112.5°$ and again it increases from $\Phi_2 = 112.5°$ to $\Phi_2 = 180°$. The flow separation occurs at $\Phi_1 = 112.5°$ by an adverse pressure gradient on the second blade of the convex surface. On the third blade the pressure coefficient, C_{px} decreases from positive to atmospheric pressure and remains almost constant through out the blade. For the fourth blade the pressure drastically decreases up to $\Phi_4 = 67.5°$ and between $\Phi_4 = 67.5°$ to $\Phi_4 = 180°$, it increases smoothly.

Considering the concave surface the pressure fluctuates on the first blade. It is noticed that the pressure slightly falls at $\Phi_1 = 135°$ and then again increases. However, the pressure remains positive on the first blade. The pressure slightly decreases up to $\Phi_2 = 112.5°$ on the second blade. Then it slightly increases from $\Phi_2 = 112.5°$ to $\Phi_2 = 135°$ and approximately remains constant from $\Phi_2 = 135°$ to $\Phi_2 = 180°$. Therefore at $\Phi_1 = 157°$ the flow separates as caused by pressure gradient. On the concave surface of the third blade pressure slightly decreases in negative value from $\Phi_3 = 0°$ to $\Phi_3 = 180°$. Pressure remains approximately constant positive value from $\Phi_4 = 0°$ to $\Phi_4 = 180°$ on the fourth blade. The pressure coefficient, C_{pe} is positive on the first and fourth blades. Whereas on the second and third blades, the pressure coefficient is negative.

At rotor angle of $\alpha = 10°$ (Figure 5.1(b)) pressure on the convex surface of the first blade increases from $\Phi_1 = 0°$ to $\Phi_1 = 67.5°$, after that pressure decreases to negative value. On the convex surface of the second blade pressure increases to positive value from $\Phi_2 = 0°$ to $\Phi_2 = 67.5°$ and then decreases up to $\Phi_2 = 112.5°$. It is found that the pressure again increases from $\Phi_2 = 112.5°$ to $\Phi_2 = 180°$. But on the third blade pressure decreases to negative value from $\Phi_3 = 0°$ to $\Phi_3 = 67.5°$ and increases to positive value in the middle portion of the blade. In case of the fourth blade pressure drastically decreases to negative value from $\Phi_4 = 0°$ to $\Phi_4 = 67.5°$ and then pressure increases from $\Phi_4 = 67.5°$ to $\Phi_4 = 180°$.

On the concave surface of the first blade pressure remains approximately constant in positive value from $\Phi_1 = 0°$ to $\Phi_1 = 112.5°$ and then decreases to $\Phi_1 = 135°$ and again increases. Whereas, on the second blade pressure remains approximately constant negative values from $\Phi_2 = 0^\circ$ to $\Phi_2 = 112.5^\circ$. Then it increases to positive value up to $\Phi_2 = 135^\circ$ and again decreases to negative value. It is seen that on the third blade pressure fluctuates slightly. But on the concave surface of the fourth blade pressure remains constant value from $\Phi_4 = 0^\circ$ to $\Phi_4 = 180^\circ$.

At rotor angle of $\alpha = 20^\circ$ (Figure 5.1(c)) pressure on the convex surface of the first blade increases from $\Phi_1 = 0^\circ$ to $\Phi_1 = 90^\circ$ and then decreases to negative value. On the second blade, pressure distribution over the convex surfaces shows the same characteristics as for $\alpha = 10^\circ$ with slightly different in the separation point. On the third blade pressure decreases from $\Phi_3 = 0^\circ$ to $\Phi_3 = 45^\circ$ and then increases to positive value from negative from $\Phi_3 = 45^\circ$ to $\Phi_3 = 180^\circ$. On the fourth blade, pressure distribution over the convex surfaces shows the same characteristics as for rotor angle $\alpha = 10^\circ$ with slightly different in the separation point.

Considering the concave surface of the first blade pressure fluctuates slightly in positive values from $\Phi_1 = 0^\circ$ to $\Phi_1 = 112.5^\circ$ and then decreases slightly from $\Phi_1 = 112.5^\circ$ to $\Phi_1 = 135^\circ$ and again increases. On the second blade pressure remains approximately constant in negative values from $\Phi_2 = 0^\circ$ to $\Phi_2 = 112.5^\circ$. Then it slightly increases to positive value from $\Phi_2 = 112.5^\circ$ to $\Phi_2 = 135^\circ$ and again decreases to negative value. On the third blade pressure decreases in the negative region from $\Phi_3 = 0^\circ$ to $\Phi_3 = 157.5^\circ$, then increases to positive direction up to $\Phi_3 = 180^\circ$. Considering the concave surface of the fourth blade pressure drastically increases from $\Phi_4 = 0^\circ$ to $\Phi_4 = 22.5^\circ$ and then remains almost constant value from $\Phi_4 = 22.5^\circ$ to $\Phi_4 = 180^\circ$.

At rotor angle of $\alpha = 30^\circ$ (Figure 5.1(d)) pressure on the convex surface of the first blade increases from $\Phi_1 = 0^\circ$ to $\Phi_1 = 90^\circ$ and then decreases smoothly to negative value. On the convex surface of the second blade pressure increases from $\Phi_2 = 0^\circ$ to $\Phi_2 = 67.5^\circ$, remains constant between $\Phi_2 = 67.5^\circ$ to $\Phi_2 = 157^\circ$ and then slightly decreases from $\Phi_2 = 157^\circ$ to $\Phi_2 = 180^\circ$. Finally, pressure becomes negative. On the third blade pressure increases to positive value from negative from $\Phi_3 = 0^\circ$ to $\Phi_3 = 67.5^\circ$ and then slightly decreases from $\Phi_3 = 67.5^\circ$ to $\Phi_3 = 112.5^\circ$. From $\Phi_3 = 112.5^\circ$, pressure again increases and becomes positive. On the fourth blade, pressure distribution over the convex surface shows the same characteristics as for rotor angle $\alpha = 20^\circ$ with slightly different in the separation point.

For the concave surface of the first blade pressure increases in positive values from $\Phi_1 = 0^\circ$ to $\Phi_1 = 90^\circ$ and then decreases up to $\Phi_1 = 180^\circ$. On the second blade, pressure distribution over the concave surfaces shows the same characteristics as for rotor angle $\alpha = 20^\circ$. On the third blade pressure remains constant from $\Phi_3 = 0^\circ$ to $\Phi_3 = 90^\circ$. Then it slightly increases to positive value to $\Phi_3 = 112.5^\circ$ and again decreases from $\Phi_2 = 112.5^\circ$ to $\Phi_3 = 135^\circ$. From $\Phi_3 = 135^\circ$ to $\Phi_3 = 180^\circ$, pressure remains constant. On the concave surface of the fourth blade pressure increases from $\Phi_4 = 0^\circ$ to $\Phi_4 = 45^\circ$ and decreases from $\Phi_4 = 45^\circ$ to $\Phi_4 = 67.5^\circ$. It again increases from $\Phi_4 = 67.5^\circ$ to $\Phi_4 = 112.5^\circ$ and then again pressure started decreasing.

At rotor angle $\alpha = 40^\circ$ (Figure 5.1(e)) pressure on the convex surface of the first blade increases from $\Phi_1 = 0^\circ$ to $\Phi_1 = 112.5^\circ$ and pressure decreases smoothly from $\Phi_1 = 112.5^\circ$ to $\Phi_1 = 180^\circ$ to negative value. On the second blade pressure increases from $\Phi_2 = 0^\circ$ to $\Phi_2 = 67.5^\circ$ and then slightly decreases up to $\Phi_2 = 90^\circ$. From $\Phi_2 = 90^\circ$ to $\Phi_2 = 157^\circ$, pressure again increases and decreases from $\Phi_2 = 157^\circ$ to negative value. On the third blade pressure increases to positive value from negative from $\Phi_3 = 0^\circ$ to $\Phi_3 = 45^\circ$ and then slightly decreases to $\Phi_3 = 90^\circ$. From $\Phi_3 = 90^\circ$, pressure again started increasing and becomes positive. On the fourth blade pressure drastically increases from $\Phi_4 = 0^\circ$ to $\Phi_4 = 45^\circ$ and decreases from $\Phi_4 = 45^\circ$ to $\Phi_4 = 67.5^\circ$ to approximately atmospheric value and then pressure coefficient C_{pe} remains constant at atmospheric level from $\Phi_4 = 67.5^\circ$ to $\Phi_4 = 180^\circ$.

On the concave surface of the first blade pressure increases from $\Phi_1 = 0^\circ$ to $\Phi_1 = 67.5^\circ$ and then decreases to $\Phi_1 = 90^\circ$. The pressure coefficient C_{pe} again increases from $\Phi_1 = 90^\circ$ to $\Phi_1 = 135^\circ$ and then again started decreasing. On the second blade, pressure distribution over the concave surfaces shows the same characteristics as for $\alpha = 20^\circ$. On the third blade pressure decreases from $\Phi_3 = 0^\circ$ to $\Phi_3 = 45^\circ$. Then it increases from $\Phi_3 = 45^\circ$ to $\Phi_3 = 90^\circ$. From $\Phi_3 = 90^\circ$ to $\Phi_3 = 135^\circ$, pressure decreases and from Φ_3 = 135° pressure again started increasing. On the concave surface of the fourth blade pressure remains constant. Therefore on the first and four blades, pressure coefficient C_{pe} is positive.

At rotor angle α = 50° (Figure 5.1(f)) pressure on the convex surface of the first blade increases from Φ_1 = 0° to Φ_1 = 135° and pressure decreases smoothly from Φ_1 = 135° to Φ_1 = 180°. On the second blade pressure increases slightly from Φ_2 = 0° to Φ_2 = 45° and then slightly decreases to Φ_2 = 67.5°. From Φ_2 = 67.5° to Φ = 112.5° pressure again increases and from Φ_2 = 112.5° pressure decreases to negative value. On the third blade pressure increases to positive value from negative from Φ_3 = 0° to Φ_3 = 45° and then slightly decreases from Φ_3 = 45° to Φ_3 = 90°. From Φ_3 = 90°, pressure again started increasing and becomes positive. On the fourth blade pressure drastically increases up to Φ_4 = 22.5° and decreases from Φ_4 = 22.5° to Φ_4 = 67.5°. Then pressure slightly rises from Φ_4 = 67.5° to Φ_4 = 90°. Between pressure tapping angle Φ_4 = 90° to Φ_4 = 135° pressure slightly decreases and from Φ_4 = 135° again started increasing.

On the concave surface of the first blade pressure remains constant from Φ_1 = 0° to Φ_1 = 112.5° and then increases from Φ_1 = 112.5° to Φ_1 = 135°. From Φ_1 = 135°, C_{pe} decreases up to Φ_1 = 157° and then remains again constant. On the second blade pressure remains approximately constant from Φ_2 = 0° to Φ_2 = 90°. Then it slightly increases to positive value from Φ_2 = 90° to Φ_2 = 112.5° and again decreases to negative value. Considering the third blade pressure decreases linearly from Φ_3 = 0° to Φ_3 = 135° and then it started increasing. On the fourth blade pressure drastically increases from Φ_4 = 0° to Φ_4 = 22.5° and remains constant between Φ_4 = 22.5° to Φ_4 = 112.5° and then it slightly decreases.

At rotor angle α = 60° (Figure 5.1(g)) pressure on the convex surface of the first blade increases from Φ_1 = 0° to Φ_1 = 157° and pressure decreases smoothly from Φ_1 = 157° to Φ_1 = 180°. On the second blade pressure decreases from Φ_2 = 0° to Φ_2 = 45° and becomes negative and then slightly increases up to Φ_2 = 90°. At Φ_2 = 90°, pressure started decreasing. However, on the third blade pressure increases from pressure tapping angle Φ_3 = 0° to Φ_3 = 22.5° and then remains constant at atmospheric value from Φ_3 = 22.5° to Φ_3 = 112.5°. After that pressure slightly increases from Φ_3 = 112.5° to Φ_3 = 180°. In the case of the fourth blade pressure drastically increases from Φ_4 = 0° to Φ_4 = 22.5° and then decreases up to Φ_4 = 67.5°. Then again pressure increases from Φ_4 = 67.5° to Φ_4 = 112.5°. From Φ_4 = 112.5° it slightly decreases and from Φ_4 = 135° again started increasing.

On the concave surface of the first blade pressure remains almost constant from Φ_1 = 0° to Φ_1 = 112.5° and then increases up to Φ_1 = 135°. The pressure coefficient C_{pe} decreases from Φ_1 = 135° to Φ_1 = 157° and then again remains constant. On the second blade pressure increases from Φ_2 = 0° to Φ_2 = 22.5° and then decreases to Φ_2 = 45°. From Φ_2 = 45° pressure increases up to Φ_2 = 135° and after that it slightly decreases to negative value. Whereas, on the third blade pressure decreases linearly from Φ_3 = 0° to Φ_3 = 135° and then from Φ_3 = 135° it increases. For the fourth blade pressure increases from Φ_4 = 0° to Φ_4 = 22.5° and then remains constant between Φ_4 = 22.5° to Φ_4 = 112.5°. However at Φ_4 = 112.5° it started decreasing.

At α = 70° (Figure 5.1(h)) pressure on the convex surface of the first blade increases from Φ_1 = 0° to Φ_1 = 135° and after that pressure decreases smoothly from Φ_1 = 135° to Φ_1 = 180°. Considering the second blade pressure remains constant at atmospheric value from Φ_2 = 0° to Φ_2 = 180°. On the third blade pressure remains constant in positive value from Φ_3 = 0° to Φ_3 = 180°. For the fourth blade pressure drastically increases from Φ_4 = 0° to Φ_4 = 22.5° and after that it decreases till Φ_4 = 67.5°. In the range of Φ_4 = 67.5° to Φ_4 = 90° pressure again increases. From the pressure tapping angle Φ_4 = 90° to Φ_4 = 157°, pressure decreases and after the value of Φ_4 = 157° pressure again started increasing.

Considering the concave surface of the first blade pressure remains almost constant from Φ_1 = 0° to Φ_1 = 67.5° and then slightly increases up to Φ_1 = 90°. From Φ_1 = 90° pressure coefficient C_{pe} decreases up to Φ_1 = 112.5° and then again increases up to Φ_1 = 135° to positive value. After the angle Φ_1 = 135° pressure again decreases. For the second blade pressure increases at the beginning and remains constant from Φ_2 = 22.5° to Φ_2 = 112.5° and then again it increases. In the case of the third blade pressure increases from $\Phi_3 = 0°$ to $\Phi_3 = 22.5°$and then it remains constant till $\Phi_3 = 90°$. After that pressure decreases slightly from $\Phi_3 = 90°$ to $\Phi_3 = 135°$. From the pressure tapping angle $\Phi_3 = 135°$ it slightly increases. But for the fourth blade pressure fluctuates slightly.

At rotor angle $\alpha = 80°$ (Figure 5.1(i)) pressure on the convex surface of the first blade decreases from $\Phi_1 = 0°$ to $\Phi_1 = 45°$ and then pressure increases smoothly from $\Phi_1 = 45°$ to $\Phi_1 = 157°$. Continuing from $\Phi_1 = 157°$ it again decreases. On the second blade pressure remains constant at atmospheric value from $\Phi_2 = 0°$ to $\Phi_2 = 180°$. On the third blade pressure remains constant in positive value from $\Phi_3 = 0°$ to $\Phi_3 = 180°$. Whereas for the fourth blade pressure increases from $\Phi_4 = 0°$ to $\Phi_4 = 22.5°$ and then decreases from $\Phi_4 = 22.5°$ to $\Phi_4 = 180°$.

For the concave surface of the first blade pressure decreases from $\Phi_1 = 0°$ to $\Phi_1 = 45°$ and then remains constant up to $\Phi_1 = 112.5°$. Pressure coefficient C_{pe} increases slightly from $\Phi_1 = 112.5°$ to $\Phi_1 = 135°$ and then again decreases from $\Phi_1 = 135°$ to negative value. On the second blade pressure remains constant from $\Phi_2 = 0°$ to $\Phi_2 = 112.5°$ and then increases from $\Phi_2 = 112.5°$ to $\Phi_2 = 135°$. Pressure decreases from $\Phi_2 = 135°$ to $\Phi_2 = 157°$ and then remains constant. In the case of the third blade pressure increases from $\Phi_3 = 0°$ to $\Phi_3 = 22.5°$ at atmospheric level and from $\Phi_3 = 22.5°$ it remains constant till $\Phi_3 = 180°$. Considering the fourth blade pressure fluctuates slightly between $\Phi_4 = 0°$ to $\Phi_4 = 180°$. C_{pe} is positive on the fourth blade.

The pressure distribution over the surfaces for angle of rotation from $\alpha = 90°$ to 170°, from $\alpha = 180°$ to 260° and from $\alpha = 270°$ to 350°, shows the same characteristics as for $\alpha = 0°$ to 80°.

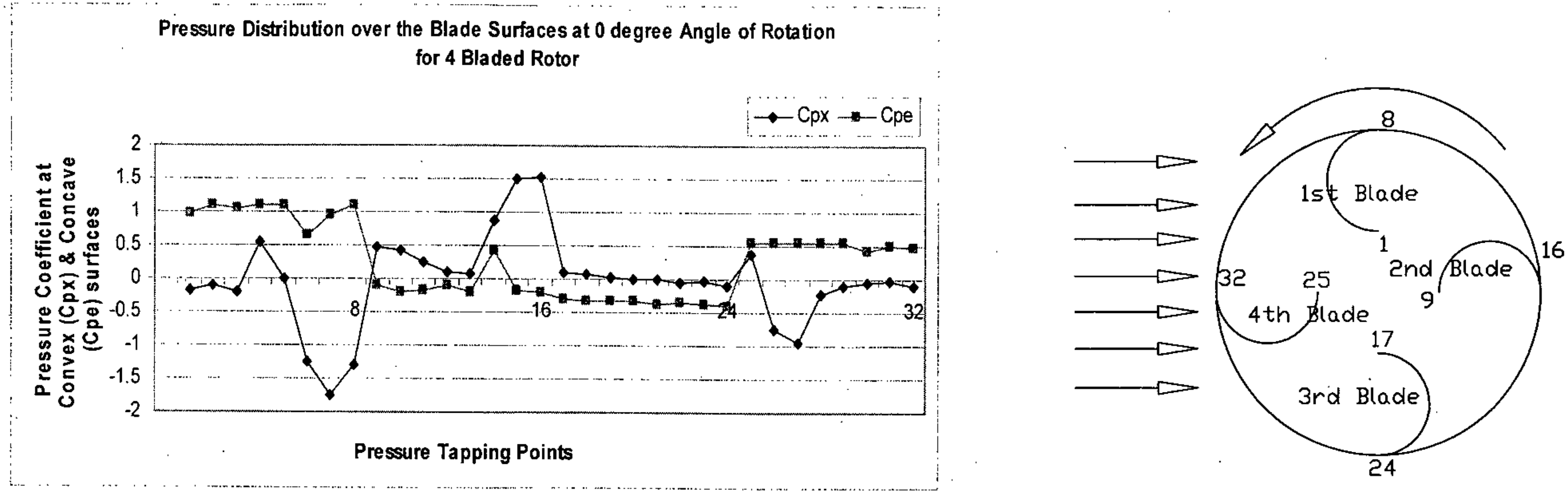

Figure 5.1 (a): Pressure distribution over the blade surfaces at 0° angle of rotation

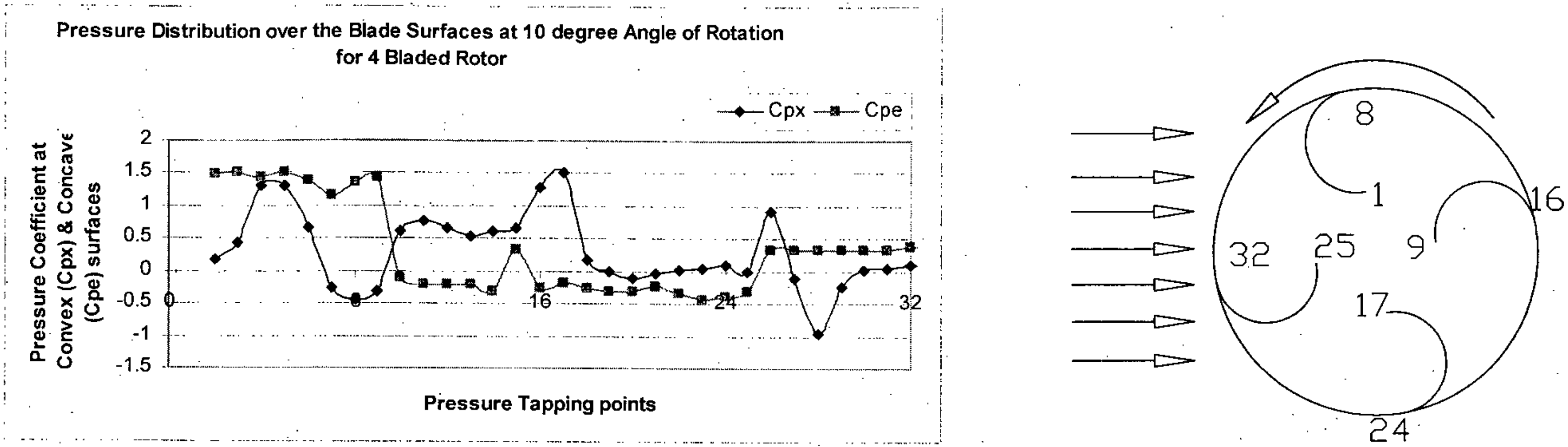

Figure 5.1 (b): Pressure distribution over the blade surfaces at 10° angle of rotation

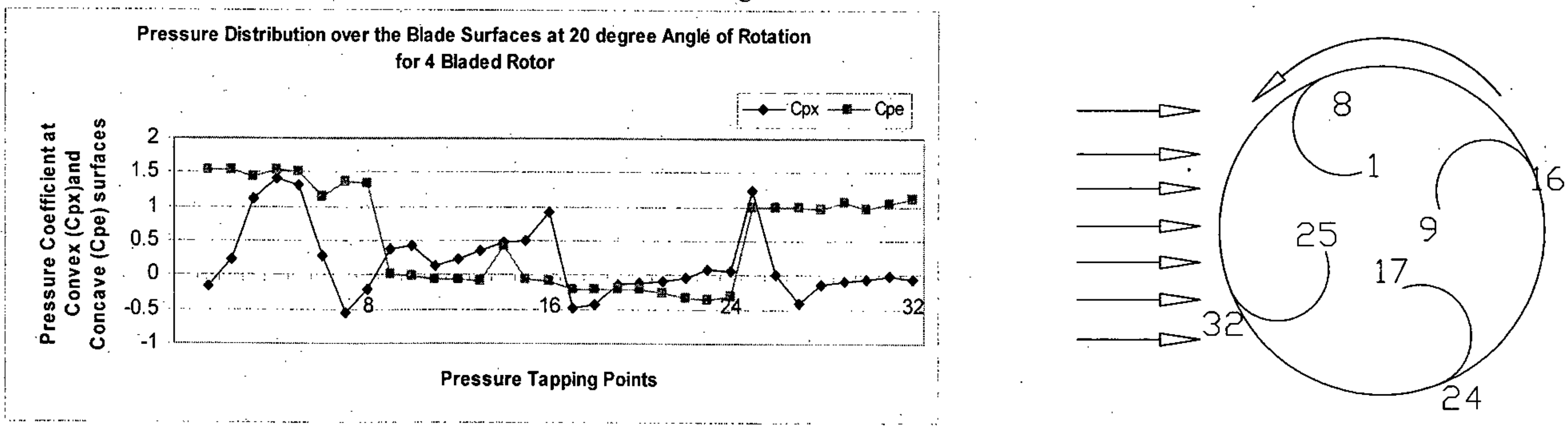

Figure 5.1 (c): Pressure distribution over the blade surfaces at 20° angle of rotation

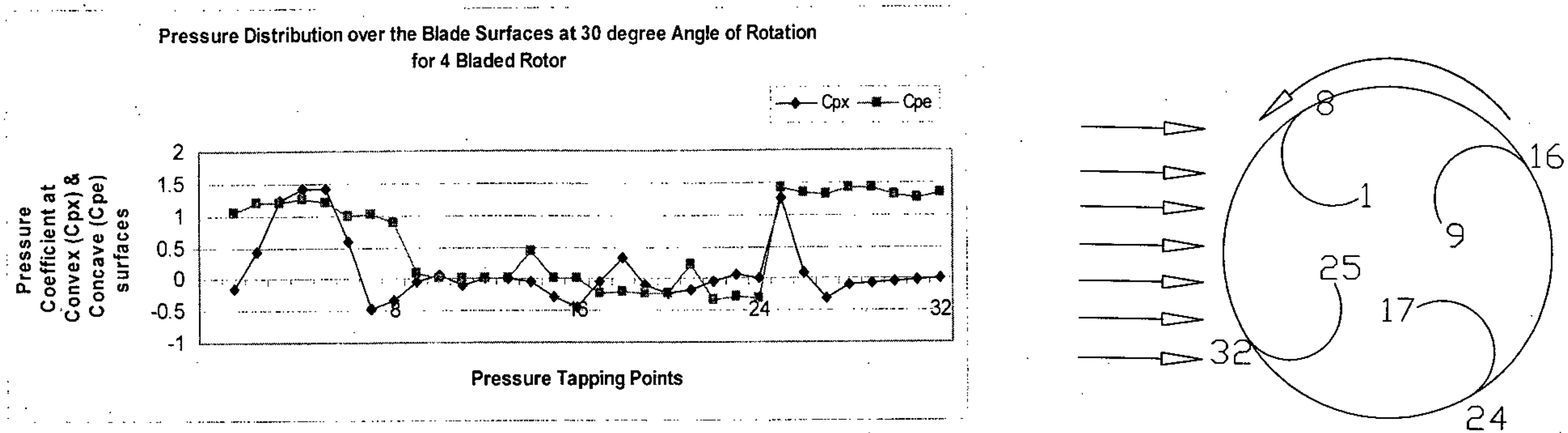

Figure 5.1 (d): Pressure distribution over the blade surfaces at 30° angle of rotation

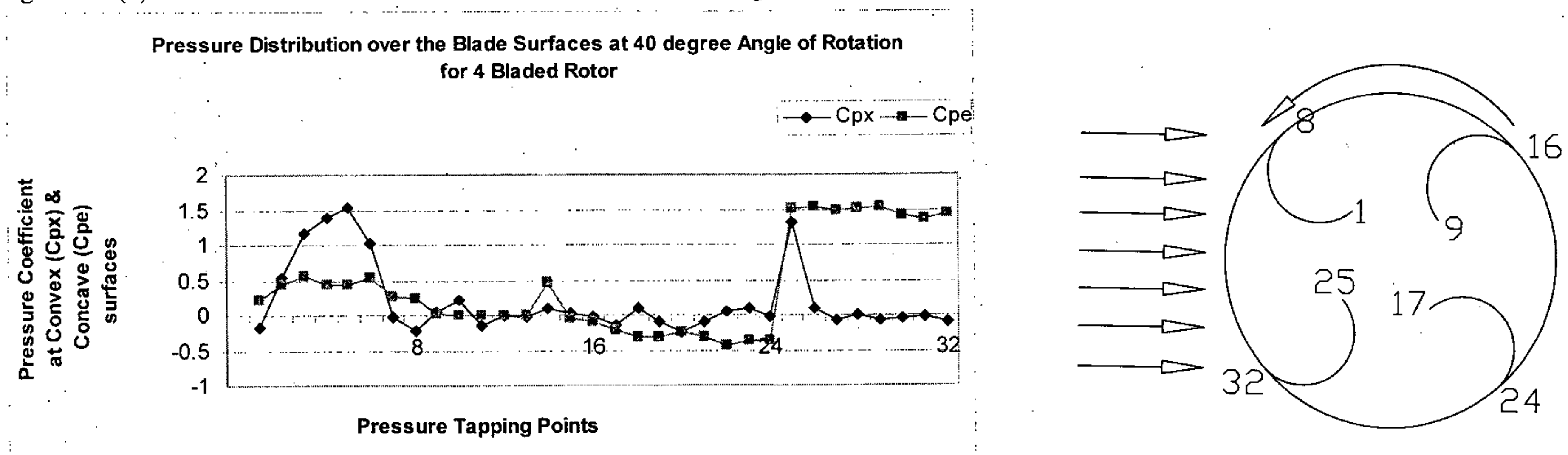

Figure 5.1 (e): Pressure distribution over the blade surfaces at 40° angle of rotation

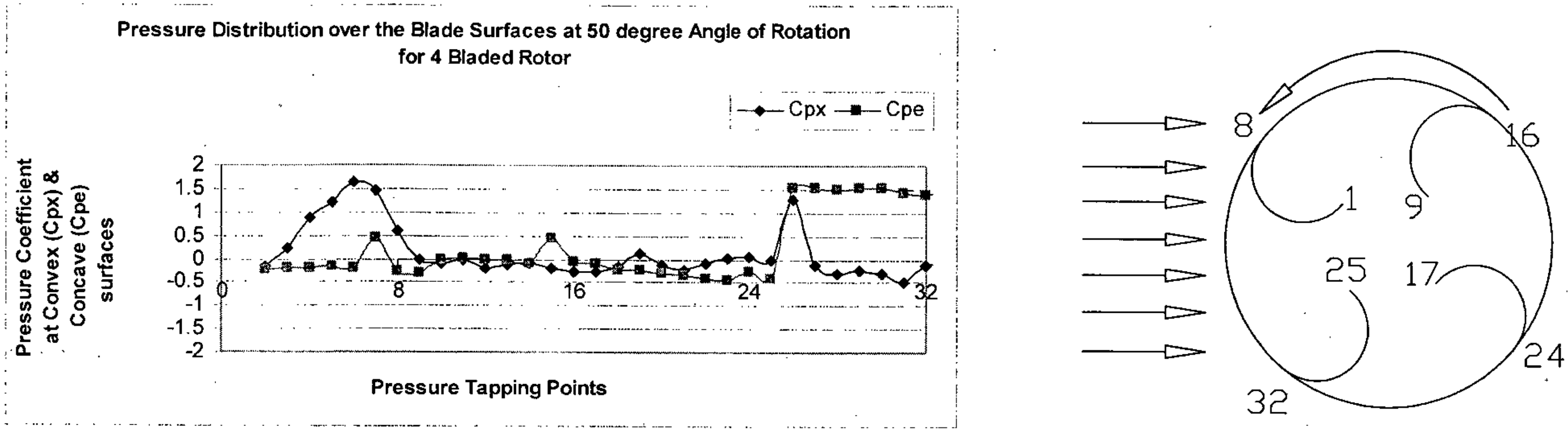

Figure 5.1 (f): Pressure distribution over the blade surfaces at 50° angle of rotation

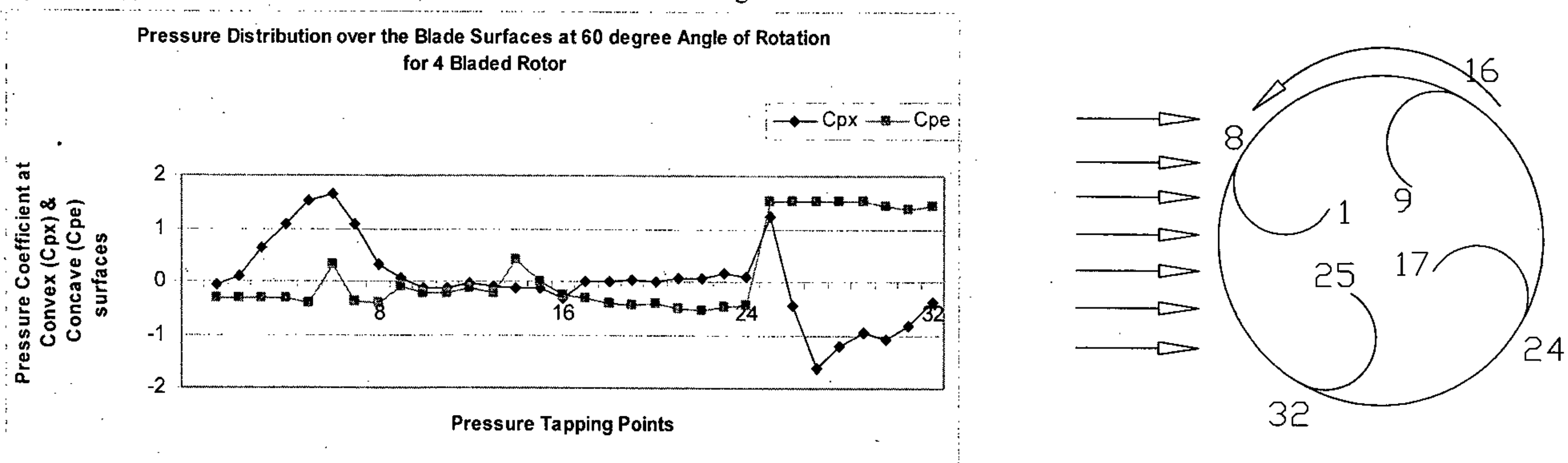

Figure 5.1 (g): Pressure distribution over the blade surfaces at 60° angle of rotation

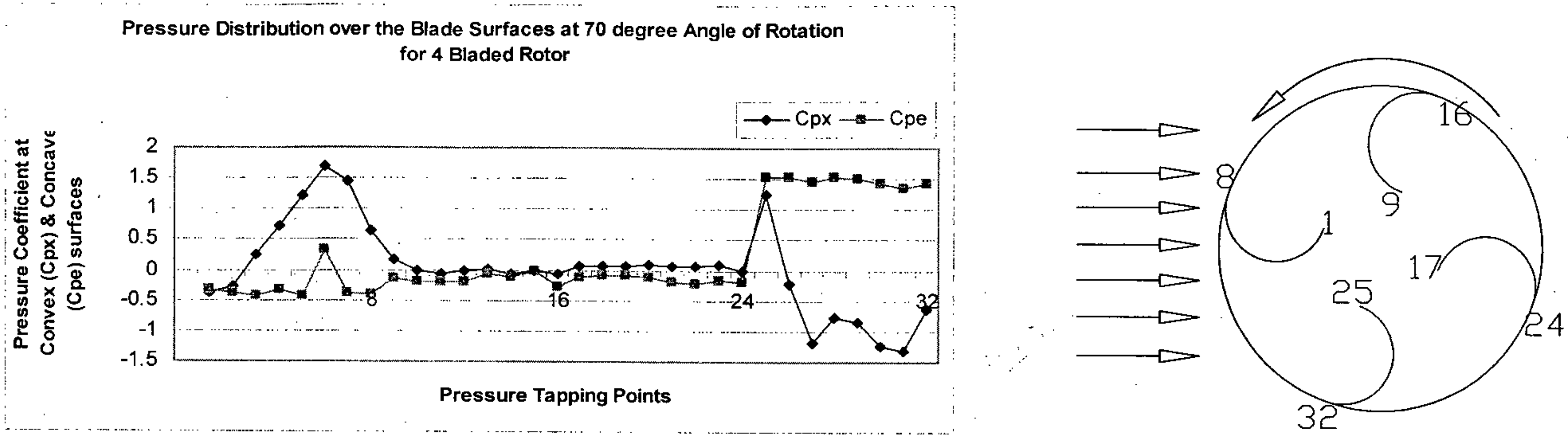

Figure 5.1 (h): Pressure distribution over the blade surfaces at 70° angle of rotation

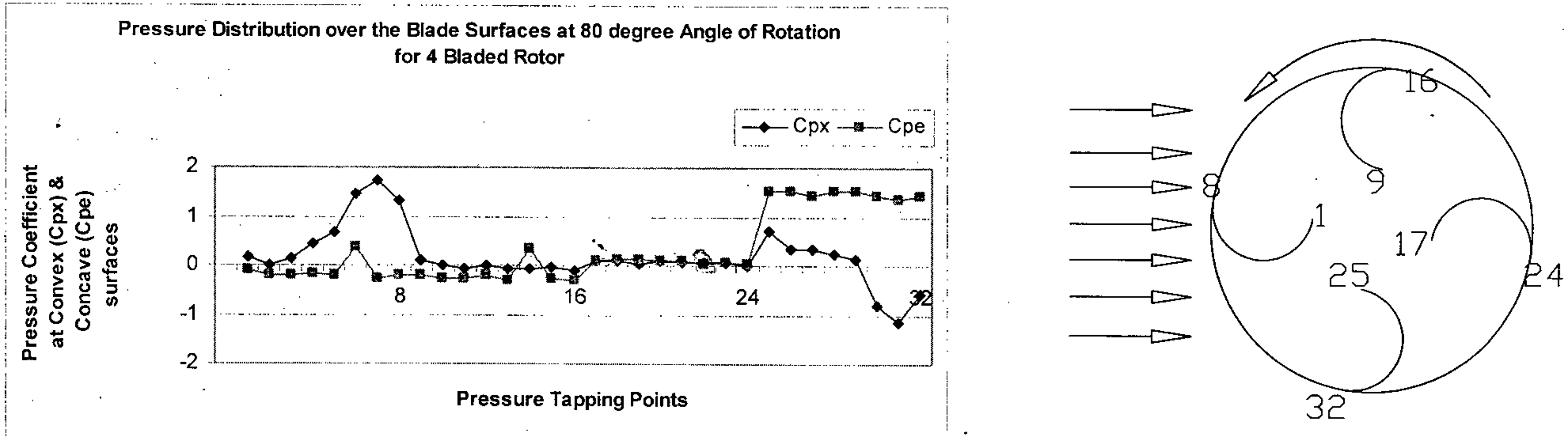

Figure 5.1 (i): Pressure distribution over the blade surfaces at 80° angle of rotation

(b) Pressure Distribution for Five bladed Vertical Axis Vane Type Rotor:

The pressure distributions over the surfaces of the blades were measured at every 10° interval of rotor angle between $0° \leq \alpha \leq 60°$. The results are presented in the Figures 5.2(a) to 5.2(g).

For rotor angle $\alpha = 0°$ (Figure 5.2(a)) as the flow accelerates over the leading edge of the convex surface of the first blade, the pressure decreases up to $\Phi_1 = 67.5°$ and becomes negative value. From pressure tapping angle $\Phi_1 = 67.5°$ to $\Phi_1 = 112.5°$, pressure smoothly increases and corresponding to $\Phi_1 = 112.5°$ to $\Phi_1 = 180°$ it decreases. In the case of the second blade pressure increases to positive value from $\Phi_2 = 0°$ to $\Phi_2 = 22.5°$ and then decrease from $\Phi_3 = 22.5$ to $\Phi_3 = 67.5°$ to negative value. From pressure tapping angle $\Phi_2 = 67.5°$ to $\Phi_2 = 112.5°$, pressure again increases and after $\Phi_2 = 112.5°$ it remains constant. For the third blade pressure decreases in negative value from the pressure tapping angle $\Phi_3 = 22.5°$ to $\Phi_3 = 90°$ and after that it slightly increases. Whereas, on the fourth blade pressure increases to positive value from $\Phi_4 = 0°$ to $\Phi_4 = 67.5°$ and then it decreases to negative value up to $\Phi_4 = 90°$. From $\Phi_4 = 90°$ it reaches to atmospheric value and at $\Phi_4 = 135°$ it started decreasing to negative value. On the fifth blade pressure increases from $\Phi_5 = 0°$ to $\Phi_5 = 157°$ and becomes positive value. Again, from pressure tapping angle $\Phi_5 = 157°$ it started decreasing.

On the concave surface of the first blade pressure, fluctuates slightly in positive value between $\Phi_1 = 0°$ to $\Phi_1 = 90°$. From the pressure tapping angle $\Phi_1 = 90°$ to $\Phi_1 = 180°$, pressure slightly increases. On the second blade pressure fluctuates slightly in negative value from $\Phi_2 = 0°$ to $\Phi_2 = 180°$. Whereas, on the third blade pressure increases linearly in the negative region from $\Phi_3 = 0°$ to $\Phi_3 = 90°$ and then decreases from $\Phi_3 = 90°$ to $\Phi_3 = 180°$. For the fourth blade pressure remains constant value from $\Phi_4 = 0°$ to $\Phi_4 = 180°$. Considering the fifth blade pressure increases from $\Phi_5 = 0°$ to $\Phi_5 = 90°$. From the pressure tapping angle $\Phi_5 = 90°$, it slightly decreases up to $\Phi_5 = 112.5°$ and then remains constant.

At rotor angle $\alpha = 10^\circ$ (Figure 5.2(b)) pressure on the convex surface of the first blade decreases up to $\Phi_1 = 67.5^\circ$ and becomes negative value. From then the pressure smoothly increases between $\Phi_1 = 67.5^\circ$ to $\Phi_1 = 180^\circ$. For the second blade pressure decreases from $\Phi_2 = 22.5$ to $\Phi_2 = 67.5^\circ$ to negative value. Between pressure tapping angle $\Phi_2 = 67.5^\circ$ to $\Phi_2 = 180^\circ$, pressure again increases. On the third blade pressure decreases in negative values from $\Phi_3 = 0^\circ$ to $\Phi_3 = 90^\circ$. Then it slightly increases from $\Phi_3 = 90^\circ$ to $\Phi_3 = 180^\circ$. In case of the fourth blade pressure increases to positive value from $\Phi_4 = 0^\circ$ to $\Phi_4 = 67.5^\circ$ and then it decreases to negative value up to $\Phi_4 = 90^\circ$. After pressure tapping angle $\Phi_4 = 90^\circ$ it increases to positive value. On the fifth blade pressure increases from $\Phi_5 = 0^\circ$ to $\Phi_5 = 135^\circ$ and becomes positive value. It is found that from $\Phi_5 = 135^\circ$ it started decreasing.

On the concave surface of the first blade pressure fluctuates slightly in positive value between $\Phi_1 = 0^\circ$ to $\Phi_1 = 90^\circ$. From $\Phi_1 = 90^\circ$ to $\Phi_1 = 180^\circ$, pressure slightly increases. Whereas, on the second blade pressure fluctuates slightly in negative values from $\Phi_2 = 0^\circ$ to $\Phi_2 = 180^\circ$. But on the third blade pressure remains constant in the negative region from $\Phi_3 = 0^\circ$ to $\Phi_3 = 180^\circ$. On the fourth blade pressure remains constant value from $\Phi_4 = 0^\circ$ to $\Phi_4 = 180^\circ$. Whereas, on the fifth blade pressure increases slightly.

At rotor angle $\alpha = 20^\circ$ (Figure 5.2(c)) pressure on the convex surface of the first blade decreases up to $\Phi_1 = 67.5^\circ$ and becomes negative value. From $\Phi_1 = 67.5^\circ$ to $\Phi_1 = 180^\circ$, pressure increases smoothly. In case of the second blade pressure increases to positive value from $\Phi_2 = 0^\circ$ to $\Phi_2 = 22.5^\circ$ and then decrease from $\Phi_2 = 22.5$ to $\Phi_2 = 67.5^\circ$ to negative value. Pressure again increases from $\Phi_2 = 67.5^\circ$ to $\Phi_2 = 180^\circ$. On the third blade pressure remains constant in negative values from $\Phi_3 = 0^\circ$ to $\Phi_3 = 180^\circ$. For the fourth blade pressure increases to positive value from $\Phi_4 = 0^\circ$ to $\Phi_4 = 180^\circ$. On the fifth blade pressure decreases from $\Phi_5 = 0^\circ$ to $\Phi_5 = 22.5^\circ$ and from $\Phi_5 = 22.5^\circ$ it increases up to $\Phi_5 = 135^\circ$. It is evident that pressure decreases from $\Phi_5 = 135^\circ$ to $\Phi_5 = 180^\circ$ and ultimately becomes negative, which can be seen from the same figure.

On the concave surface of the first blade pressure fluctuates slightly in positive value between $\Phi_1 = 0^\circ$ to $\Phi_1 = 90^\circ$. When the pressure tapping angle is between From $\Phi_1 =$

90° to Φ = 180°, pressure slightly increases. But on the second blade pressure fluctuates slightly in negative value from Φ_2 = 0° to Φ_2 = 180°. On the third and fourth blade, pressure distribution over the concave surfaces shows the same characteristics as for α = 10°. For the fifth blade pressure remains almost constant in the positive region from Φ_5 = 0° to Φ_5 = 180°.

At rotor angle α = 30° (Figure 5.2(d)) pressure on the convex surface of the first blade decreases up to Φ_1 = 67.5° and becomes negative value. Pressure smoothly increases from Φ_1 = 67.5° to Φ_1 = 180°. However, on the second blade pressure increases to positive value from Φ_2 = 0° to Φ_2 = 22.5° and then decrease from Φ_2 = 22.5 to Φ_2 = 67.5° to negative value. From Φ_2 = 67.5° to Φ_2 = 157°, pressure again increases. And from Φ_2 = 157° to Φ_2 = 180°, pressure decreases. For the third blade pressure remains almost constant in negative values from Φ_3 = 0° to Φ_3 = 180°. On the fourth blade pressure increases to positive value from Φ_4 = 0° to Φ_4 = 180°. For the fifth blade pressure increases from Φ_5 = 0° to Φ_5 = 22.5° and from Φ_5 = 22.5° it decreases up to Φ_5 = 67.5°. From Φ_5 = 67.5° to Φ_5 = 135°, pressure again increases. From Φ_5 = 135° it decreases and becomes negative.

Considering the concave surface of the first blade it is found that pressure fluctuates slightly in positive value between Φ_1 = 0° to Φ_1 = 90°. From Φ_1 = 90° to Φ_1 = 180°, pressure increases. The pressure fluctuates on the second blade slightly in negative value from Φ_2 = 0° to Φ_2 = 180°. Whereas, on the third and fourth blade, pressure distribution over the concave surfaces shows the same characteristics as for α = 10° with slightly different in the separation point. The fifth blade experiences pressure fluctuating in the positive region from Φ_5 = 0° to Φ_5 = 180°.

When the rotor angle α = 40° (Figure 5.2(e)) pressure on the convex surface of the first blade decreases from Φ_1 = 0° to Φ_1 = 67.5° and becomes negative value. It is also found from the same figure that the pressure tapping angle Φ_1 = 67.5° to Φ_1 = 180°, pressure increases smoothly. However, on the second blade pressure increases to positive value from Φ_2 = 0° to Φ_2 = 22.5° and then decreases from Φ_2 = 22.5 to Φ_2 = 67.5° to negative value. In the range of Φ_2 = 67.5° to Φ_2 = 180°, pressure again increases. For the third blade pressure fluctuates slightly in negative values from Φ_3 = 0° to Φ_3 = 180°. The pressure increases to positive value from Φ_4 = 0° to Φ_4 = 67.5° on the fourth blade. From Φ_4 = 67.5° to Φ_4 = 112.5°, pressure decreases and then again increases from Φ_4 = 112.5 to Φ_4 = 180° to positive value. For the fifth blade pressure decreases from Φ_5 = 0° to Φ_5 = 112.5° and again it increases from Φ_5 = 112.5°.

The pressure fluctuates slightly in positive value on the concave surface of the first blade between Φ_1 = 0° to Φ_1 = 180°. However, on the second blade pressure fluctuates slightly in negative value from Φ_2 = 0° to Φ_2 = 180°. In the case of the third and fourth blade, pressure distribution over the concave surfaces shows the same characteristics as for α = 30°. On the fifth blade pressure increases in the positive region from Φ_5 = 0° to Φ_5 = 112.5° and decreases from Φ_5 = 112.5° to Φ_5 = 135° and from then it remains constant.

At rotor angle α = 50° (Figure 5.2(f)) pressure on the convex surface of the first blade decreases up to Φ_1 = 67.5° and becomes negative value. From Φ_1 = 67.5° to Φ_1 = 180°, pressure increases smoothly. On the second blade pressure fluctuates little from Φ_2 = 0° to Φ_2 = 45° and then decreases from Φ_2 = 45° to Φ_2 = 90° in negative value. Pressure again increases from Φ_2 = 90° to Φ_2 = 180°. For the third blade pressure remains almost constant in negative values from Φ_3 = 0° to Φ_3 = 180°. On the fourth blade pressure increases from negative to positive value from Φ_4 = 0° to Φ_4 = 180°. Whereas, on the fifth blade pressure decreases from Φ_5 = 0° to Φ_5 = 90° and from Φ_5 = 90° it again increases up to Φ_5 = 135° and ultimately pressure decreases again.

The pressure is almost constant in positive value between Φ_1 = 0° to Φ_1 = 180° on the concave surface of the first blade. For the second blade pressure fluctuates slightly in negative values from Φ_2 = 0° to Φ_2 = 180°. On the third blade, pressure distribution over the concave surfaces shows the same characteristics as for α = 40°. In case of the fourth blade pressure fluctuates slightly in negative value from Φ_4 = 0° to Φ_4 = 180°. But on the fifth blade pressure fluctuates in the positive region from Φ_5 = 0° to Φ_5 = 67.5° and goes on increasing from Φ_5 = 67.5° to Φ_5 = 180°.

At rotor angle $\alpha = 60^\circ$ (Figure 5.2(g)) the pressure on the convex surface of the first blade decreases up to $\Phi_1 = 67.5^\circ$. The flow separation occurs at $\Phi_1 = 67.5^\circ$ by an adverse pressure gradient on the first blade of the convex surface and ultimately becomes negative. From the pressure tapping angle $\Phi_1 = 67.5^\circ$ to $\Phi_1 = 180^\circ$, pressure increases smoothly. On the second blade pressure increases to positive value from $\Phi_2 = 0^\circ$ to $\Phi_2 = 22.5^\circ$ and then decreases from $\Phi_2 = 22.5^\circ$ to $\Phi_2 = 67.5^\circ$ to negative value. Pressure again increases from $\Phi_2 = 67.5^\circ$ to $\Phi_2 = 180^\circ$. On the third blade pressure fluctuates slightly in negative values from $\Phi_3 = 0^\circ$ to $\Phi_3 = 180^\circ$. When the fourth blade is considered it is evident that the pressure increases from negative to positive value from $\Phi_4 = 0^\circ$ to $\Phi_4 = 180^\circ$. However on the fifth blade pressure decreases from $\Phi_5 = 0^\circ$ to $\Phi_5 = 67.5^\circ$ and it again increases from $\Phi_5 = 67.5$ to $\Phi_3 = 112.5^\circ$ and ultimately pressure decreases again.

The pressure remains at atmospheric level between $\Phi_1 = 0^\circ$ to $\Phi_1 = 180^\circ$ on the concave surface of the first blade. On the second blade pressure fluctuates slightly in negative value from $\Phi_2 = 0^\circ$ to $\Phi_2 = 180^\circ$. In case of the third blade pressure remains constant in the negative region from $\Phi_3 = 0^\circ$ to $\Phi_3 = 180^\circ$. Whereas, on the fourth blade pressure fluctuates slightly in negative value from $\Phi_4 = 0^\circ$ to $\Phi_4 = 180^\circ$. On the fifth blade pressure fluctuates slightly in the positive region from $\Phi_5 = 0^\circ$ to $\Phi_5 = 67.5^\circ$ and increases from $\Phi_5 = 67.5^\circ$ to $\Phi_5 = 180^\circ$.

The pressure distribution over the surfaces for angle of rotation from $\alpha = 72^\circ$ to 144°, from $\alpha = 144^\circ$ to 216°, from $\alpha = 216^\circ$ to 288° and from $\alpha = 288^\circ$ to 350°, shows the same characteristics as for $\alpha = 0^\circ$ to 60°.

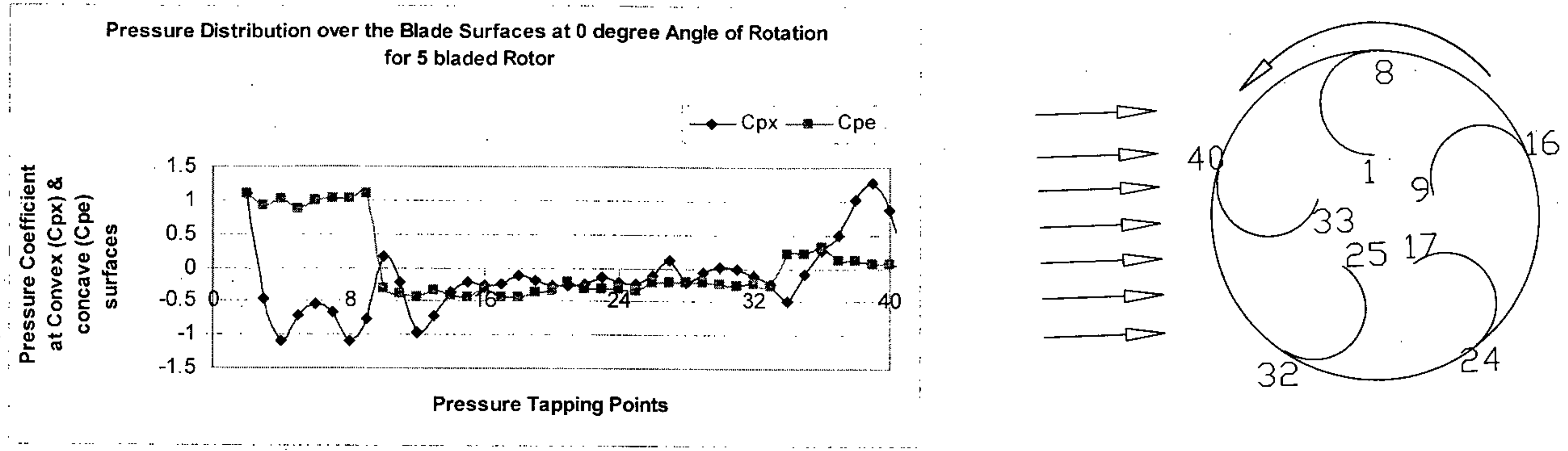

Figure 5.2 (a): Pressure distribution over the blade surfaces at 0° angle of rotation

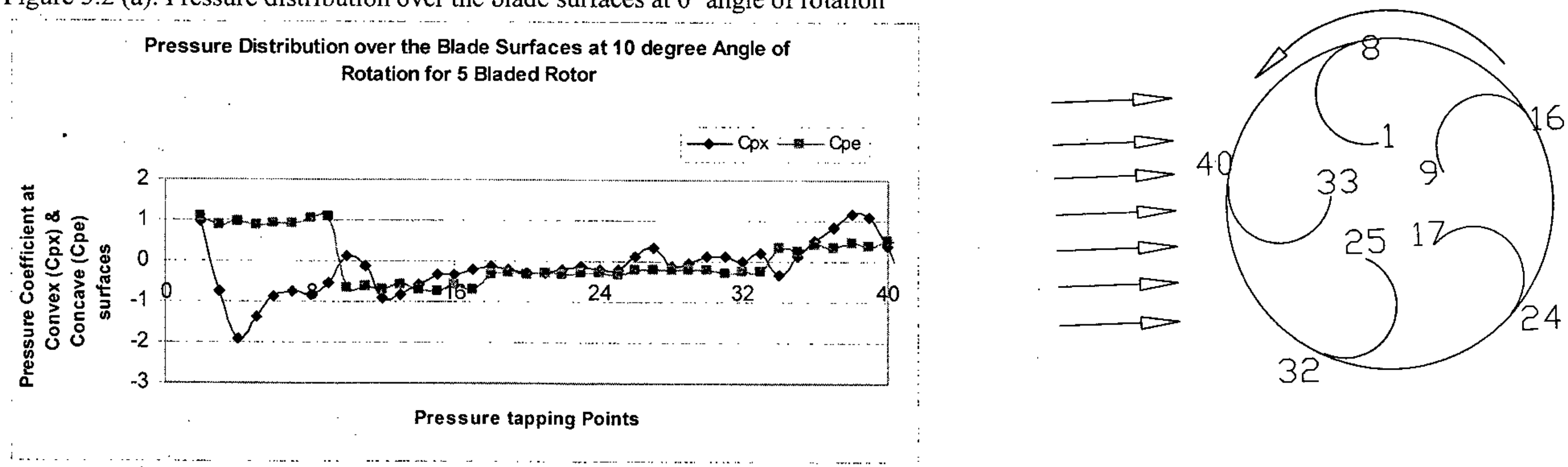

Figure 5.2 (b): Pressure distribution over the blade surfaces at 10° angle of rotation

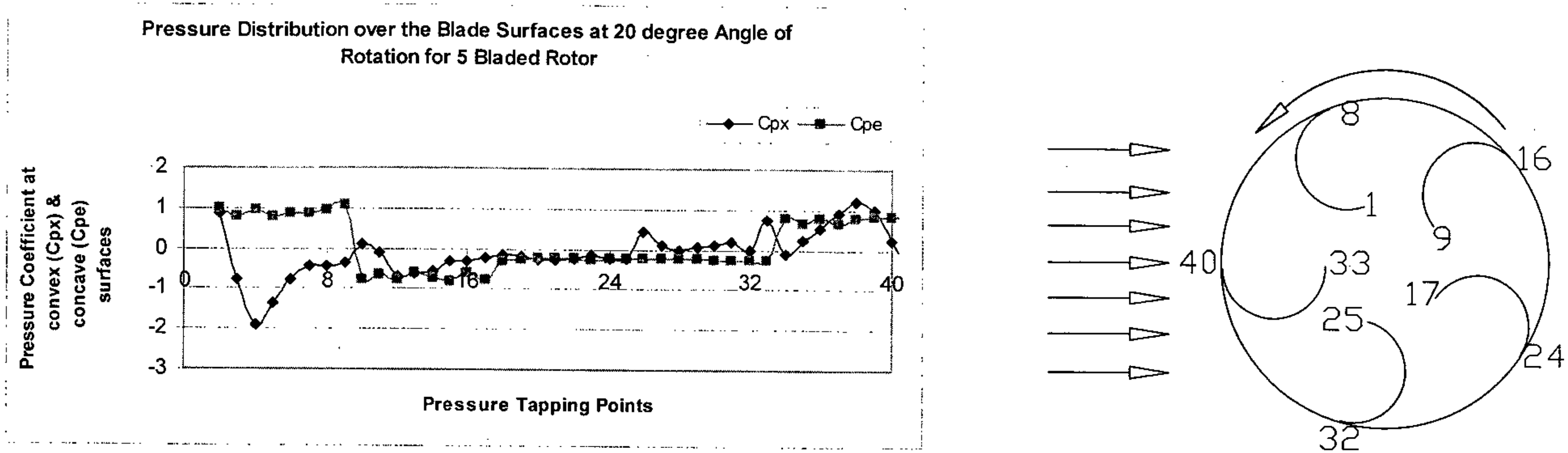

Figure 5.2 (c): Pressure distribution over the blade surfaces at 20° angle of rotation

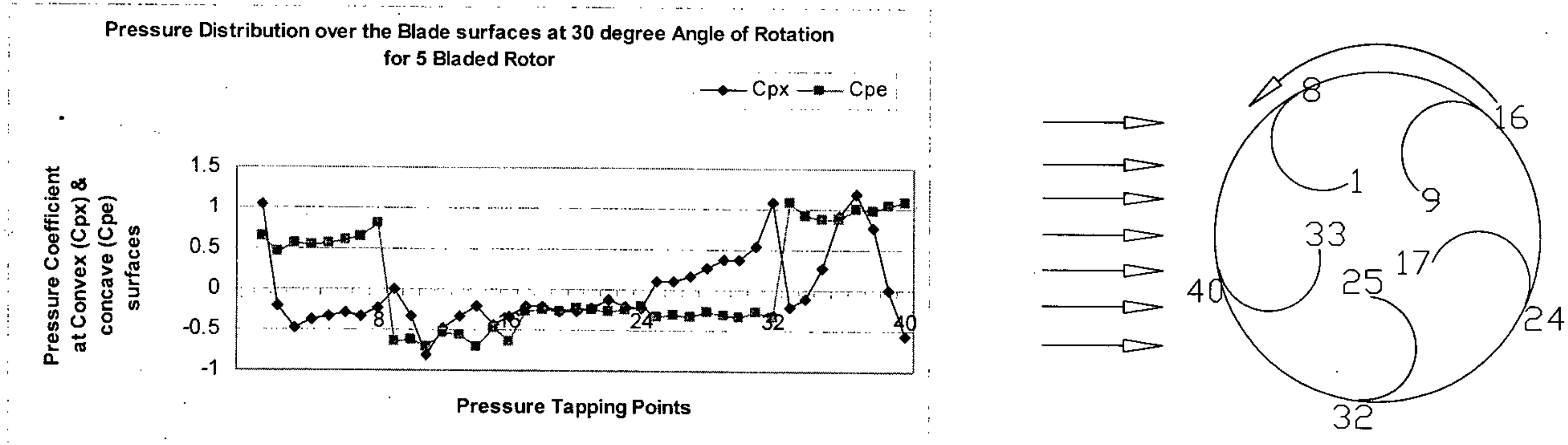

Figure 5.2 (d): Pressure distribution over the blade surfaces at 30° angle of rotation

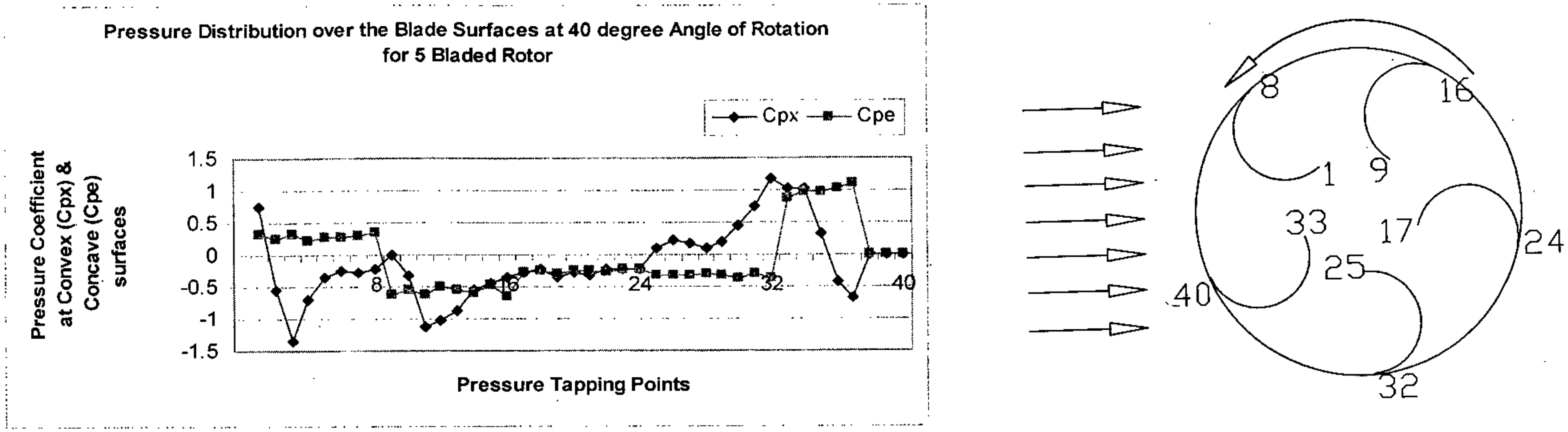

Figure 5.2 (e): Pressure distribution over the blade surfaces at 40° angle of rotation

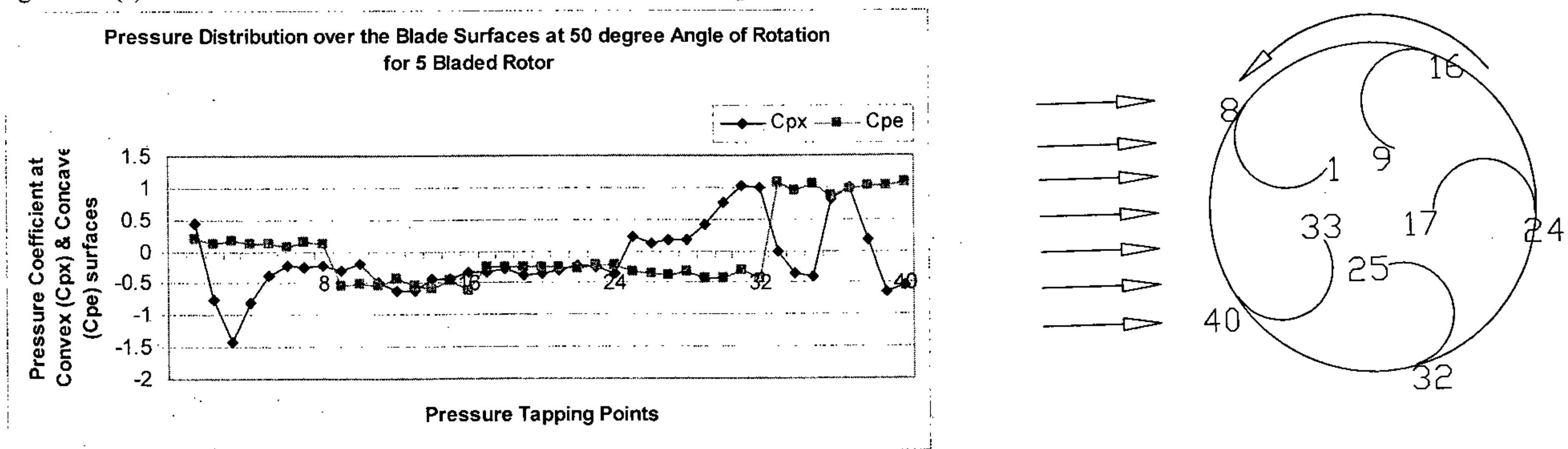

Figure 5.2 (f): Pressure distribution over the blade surfaces at 50° angle of rotation

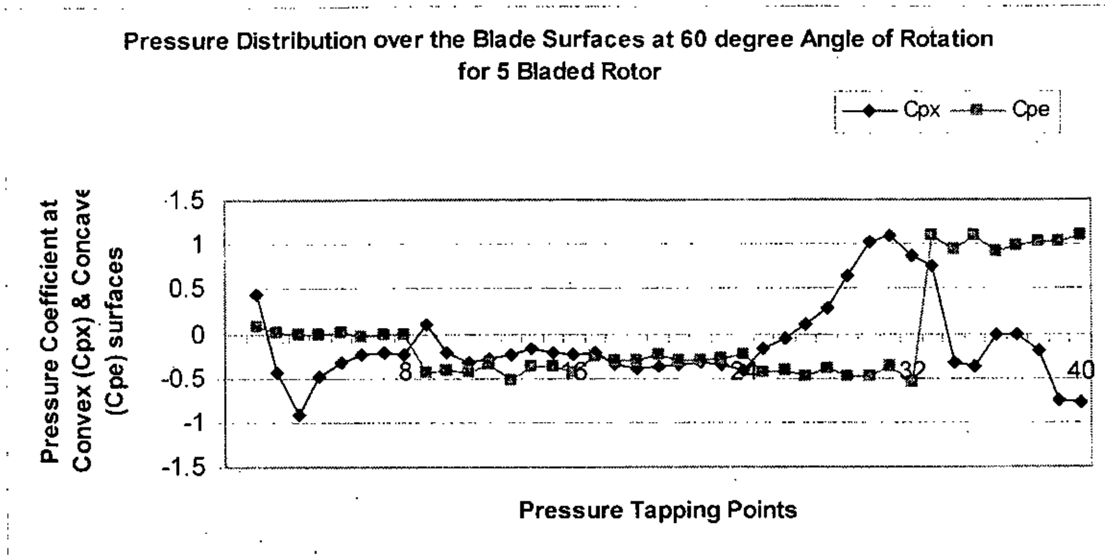

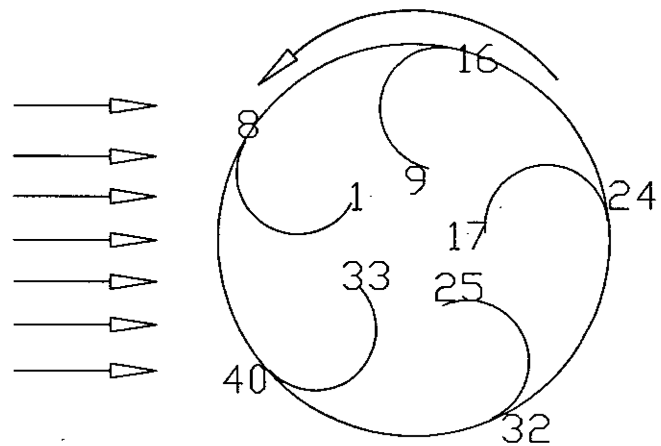

Figure 5.2 (g): Pressure distribution over the blade surfaces at 60° angle of rotation

(c) Pressure Distribution for Six bladed Vertical Axis Vane Type Rotor:

The pressure distributions over the surfaces of the blades were measured at every 10° interval of rotor angle between $0° \leq \alpha \leq 50°$. The results are presented in the Figures 5.3(a) to 5.3(f).

At rotor angle $\alpha = 0°$ (Figure 5.3(a)) as the flow accelerates over the leading edge of the convex surface of the first blade, the pressure decreases up to $\Phi_1 = 67.5°$. The flow separation occurs at $\Phi_1 = 67.5°$ by an adverse pressure gradient on the first blade of the convex surface and becomes negative value. After that pressure smoothly increases from pressure tapping angle $\Phi_1 = 67.5°$ to $\Phi_1 = 180°$. The pressure increases to positive value from $\Phi_2 = 0°$ to $\Phi_2 = 22.5°$ for the second blade and then decreases from $\Phi_2 = 22.5$ to $\Phi_2 = 67.5°$ to negative value. From $\Phi_2 = 67.5°$ to $\Phi_2 = 180°$, pressure again increases. On the third blade pressure decreases in negative values between $\Phi_3 = 22.5°$ to $\Phi_3 = 45°$ and then pressure remains constant. Whereas, on the fourth blade pressure decreases from $\Phi_4 = 22.5°$ to $\Phi_4 = 45°$ and after that it remains almost constant. However, on the fifth blade pressure increases from $\Phi_5 = 0°$ to $\Phi_5 = 45°$ and then decreases from $\Phi_5 = 40°$ to $\Phi_5 = 90°$ and then again it increases from $\Phi_5 = 90°$. On the sixth blade pressure increases from $\Phi_6 = 0°$ to $\Phi_6 = 22.5°$ and decreases from $\Phi_6 = 22.5°$ to $\Phi_6 = 45°$ and after $\Phi_6 = 45°$ it started increasing to positive value.

Considering the concave surface of the first blade pressure remains approximately constant. On the second blade pressure fluctuates slightly in positive values from $\Phi_2 = 0°$ to $\Phi_2 = 67.5°$. From the pressure tapping angle $\Phi_2 = 67.5°$ to $\Phi_2 = 180°$, pressure slightly increases. In the case of the third blade pressure remains constant from $\Phi_3 = 0°$ to $\Phi_3 = 90°$ and then decreases up to $\Phi_3 = 135°$. From $\Phi_3 = 135°$ to $\Phi_3 = 180°$, it slightly increases. However, on the fourth, fifth and sixth blade pressure remains almost constant value from $\Phi = 0°$ to $\Phi = 180°$.

At rotor angle $\alpha = 10°$ (Figure 5.3(b)) pressure on the convex surface of the first blade decreases up to $\Phi_1 = 67.5°$. The flow separation occurs at $\Phi_1 = 67.5°$ by an adverse pressure gradient on the first blade of the convex surface and becomes negative. The pressure increases after $\Phi_1 = 67.5^\circ$ to $\Phi_1 = 180^\circ$. On the second blade pressure increases to positive value from $\Phi_2 = 0^\circ$ to $\Phi_2 = 22.5^\circ$ and then decrease from $\Phi_2 = 22.5$ to $\Phi_2 = 67.5^\circ$ to negative value. From the pressure tapping angle $\Phi_2 = 67.5^\circ$ to $\Phi_2 = 90^\circ$, pressure again increases. Again pressure decreases from $\Phi_2 = 90$ to $\Phi_2 = 112.5^\circ$ and then increases from $\Phi_2 = 112.5^\circ$ to $\Phi_2 = 180^\circ$. Whereas, on the third blade pressure increases from $\Phi_3 = 0^\circ$ to $\Phi_3 = 22.5^\circ$ and then pressure decreases to negative value from $\Phi_3 = 22.5^\circ$ to $\Phi_3 = 67.5^\circ$. Again pressure increases from $\Phi_3 = 67.5^\circ$ to $\Phi_3 = 135^\circ$ and after $\Phi_3 = 135^\circ$ to the pressure tapping angle $\Phi_3 = 180^\circ$ pressure remains constant. On the fourth blade pressure remains almost constant. In the case of the fifth blade pressure increases from $\Phi_5 = 0^\circ$ to $\Phi_5 = 180^\circ$ smoothly. The pressure increases from $\Phi_6 = 0^\circ$ to $\Phi_6 = 112.5^\circ$ on the sixth blade and then decreases from $\Phi_6 = 112.5^\circ$ to $\Phi_6 = 180^\circ$ and reaches to negative value.

The pressure remains approximately constant on the concave surface of the first blade. On the second blade pressure fluctuates slightly in positive values from $\Phi_2 = 0^\circ$ to $\Phi_2 = 67.5^\circ$. Again from pressure tapping angle $\Phi_2 = 67.5^\circ$ to $\Phi_2 = 180^\circ$, the pressure remains constant. On the third blade, the pressure coefficient C_{px} fluctuates slightly. It is found that on the fourth, fifth and sixth blade, pressure distribution over the concave surfaces shows the same characteristics as for $\alpha = 0^\circ$.

From the Figure 5.3(c) at rotor angle $\alpha = 20^\circ$, it is found that the pressure on the convex surface of the first blade decreases from $\Phi_1 = 0^\circ$ to $\Phi_1 = 67.5^\circ$. The flow separation occurs at $\Phi_1 = 67.5^\circ$ by an adverse pressure gradient on the first blade of the convex surface and becomes negative value. Then pressure increases from $\Phi_1 = 67.5^\circ$ to $\Phi_1 = 180^\circ$. For the second blade pressure increases to positive value from $\Phi_2 = 0^\circ$ to $\Phi_2 = 22.5^\circ$ and then decreases from $\Phi_2 = 22.5$ to $\Phi_2 = 67.5^\circ$ to negative value and pressure again increases from $\Phi_2 = 67.5^\circ$ to $\Phi_2 = 180^\circ$. Whereas, on the third blade pressure decreases from $\Phi_3 = 0^\circ$ to $\Phi_3 = 67.5^\circ$ and then again pressure increases from $\Phi_3 = 67.5^\circ$ to $\Phi_3 = 180^\circ$. However, on the fourth blade pressure remains almost constant. But on the fifth blade pressure increases from $\Phi_5 = 0^\circ$ to $\Phi_5 = 67.5^\circ$ smoothly. Then from pressure tapping angle $\Phi_5 = 67.5^\circ$ to $\Phi_5 = 90^\circ$ pressure decreases and again increases from $\Phi_5 = 90^\circ$ to $\Phi_5 = 180^\circ$. For the sixth blade pressure increases from $\Phi_6 = 0^\circ$ to $\Phi_6 = 112.5^\circ$ and decreases in the range of pressure tapping angle $\Phi_6 = 112.5^\circ$ to $\Phi_6 = 180^\circ$ and reaches to the negative value.

It is found that on the concave surface of the first blade pressure fluctuates slightly. However, on the second blade pressure remains almost constant at atmospheric level. For the third blade, the pressure coefficient C_{px} decreases from $\Phi_3 = 0^\circ$ to $\Phi_3 = 67.5^\circ$ and then increases in the range of $\Phi_3 = 67.5^\circ$ to $\Phi_3 = 135^\circ$ and then remains almost constant. Whereas, on the fourth, fifth and sixth blade, pressure distribution over the concave surfaces shows the same characteristics at rotor angle of $\alpha = 10^\circ$.

When the rotor angle $\alpha = 30^\circ$ (Figure 5.3(d)) the pressure on the convex surface of the first blade decreases from $\Phi_1 = 0^\circ$ to $\Phi_1 = 67.5^\circ$. The flow separation occurs at $\Phi_1 = 67.5^\circ$ by an adverse pressure gradient on the first blade of the convex surface and becomes negative value. Pressure increases from $\Phi_1 = 67.5^\circ$ to $\Phi_1 = 180^\circ$. On the second blade, pressure distribution over the convex surfaces shows the same characteristics as for $\alpha = 20^\circ$. It is found that pressure decreases from $\Phi_3 = 0^\circ$ to $\Phi_3 = 67.5^\circ$ on the third blade. Then pressure increases in negative value from $\Phi_3 = 67.5^\circ$ to $\Phi_3 = 135^\circ$ and then remains constant. On the fourth blade pressure decreases from $\Phi_4 = 0^\circ$ to $\Phi_4 = 67.5^\circ$ and increases from $\Phi_4 = 67.5^\circ$ to $\Phi_4 = 135^\circ$ and then remains almost constant. Whereas, on the fifth blade pressure increases from $\Phi_5 = 0^\circ$ to $\Phi_5 = 67.5^\circ$ smoothly. It decreases from $\Phi_5 = 67.5^\circ$ to $\Phi_5 = 90^\circ$ and again increases from $\Phi_5 = 90^\circ$ to $\Phi_5 = 180^\circ$. On the sixth blade, pressure distribution over the convex surfaces shows the same characteristics as for $\alpha = 20^\circ$ with slightly different in the separation point.

In case of the concave surface of the first blade pressure fluctuates slightly. On the second blade pressure remains constant at atmospheric level. On the third blade, the C_{px} decreases from $\Phi_3 = 0^\circ$ to $\Phi_3 = 67.5^\circ$. It increases from $\Phi_3 = 67.5^\circ$ to $\Phi_3 = 135^\circ$ and then remains constant. The pressure distribution on the fourth and fifth blade over the concave surfaces shows the same characteristics as for $\alpha = 20^\circ$. However, on the sixth blade pressure slightly decreases in negative value from $\Phi = 0^\circ$ to $\Phi = 180^\circ$.

Considering the rotor angle α = 40° (Figure 5.3(e)), the pressure on the convex surface of the first blade decreases up to Φ_1 = 67.5° and then increases from Φ_1 = 67.5° to Φ_1 = 180°. On the second blade pressure decreases from Φ_2 = 0° to Φ_2 = 67.5° and then increases from Φ_2 = 67.5° to Φ_2 = 180°. On the third blade pressure decreases from Φ_3 = 0° to Φ_3 = 90° and increases from Φ_3 = 90° to Φ_3 = 180°. But on the fourth blade pressure fluctuates slightly between Φ_4 = 0° to Φ_4 = 180°. Whereas, on the fifth blade pressure increases from Φ_5 = 0° to Φ_5 = 135° smoothly and decreases from Φ_5 = 135° to Φ_5 = 180°. For the sixth blade pressure at first increases from Φ_6 = 0° to Φ_6 = 22.5° and then decreases from Φ_6 = 22.5° to Φ_6 = 67.5°. Again, pressure increases from Φ_6 = 67.5° to Φ_6 = 135° pressure tapping angle and again started decreasing from Φ_6 = 135°.

For the concave surface of the first blade pressure fluctuates slightly. But on the second blade pressure remains constant at atmospheric level. However, on the third blade, pressure distribution over the concave surface shows the same characteristics as for rotor α = 30°. On the fourth blade, pressure distribution over the concave surface shows the same characteristics as for α = 20°. On the fifth blade pressure coefficient C_{pe} remains almost constant from Φ = 0° to Φ = 180°. However, on the sixth blade pressure coefficient C_{pe} remains constant from Φ = 0° to Φ = 180°.

When the rotor angle α = 50° (Figure 5.3(e)) pressure on the convex surface of the first blade decreases from Φ_1 = 0° to Φ_1 = 67.5°. The flow separation occurs at Φ_1 = 67.5° by an adverse pressure gradient on the first blade of the convex surface and then increases from Φ_1 = 67.5° to Φ_1 = 180°. On the second blade pressure decreases from Φ_2 = 0° to Φ_2 = 67.5° and increase from Φ_2 = 67.5° to Φ_2 = 135° and then it again decreases. But on the third blade, pressure distribution over the convex surface shows the same characteristics as for α = 40°. On the fourth blade pressure fluctuates between Φ_4 = 0° to Φ_4 = 180°. Whereas, on the fifth blade pressure increases from Φ_5 = 0° to Φ_5 = 135° smoothly and decreases from Φ_5 = 135° to Φ_5 = 180°. On the sixth blade pressure decreases from Φ_6 = 0° to Φ_6 = 67.5° and then it increases from Φ_6 = 67.5° to Φ_6 = 135° and again decreases from Φ_6 = 135°.

The pressure fluctuates slightly on the concave surface of the first blade. But on the second, and third blade pressure coefficient C_{pe} remains constant from $\Phi = 0°$ to $\Phi = 180°$. On the fourth and fifth blade, same nature of pressure distribution prevail on the concave surfaces as for $\alpha = 20°$. In case of the sixth blade pressure coefficient C_{pe} increases slightly with compare to $\alpha = 50°$.

The pressure distribution over the surfaces for angle of rotation from $\alpha = 60°$ to 110°, from $\alpha = 120°$ to 170°, from $\alpha = 180°$ to 230°, from $\alpha = 240°$ to 290°, and from $\alpha = 300°$ to 350°, shows the same characteristics as for $\alpha = 0°$ to 50°.

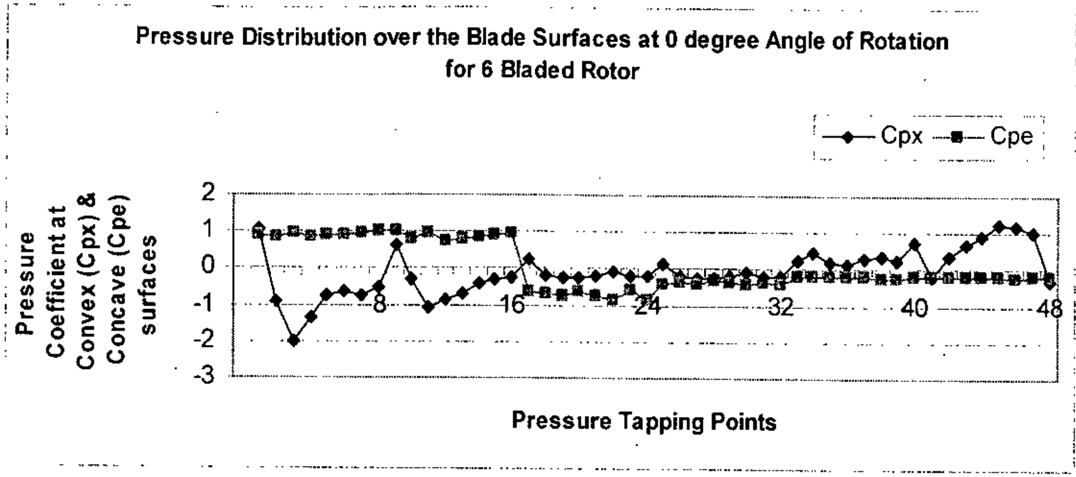

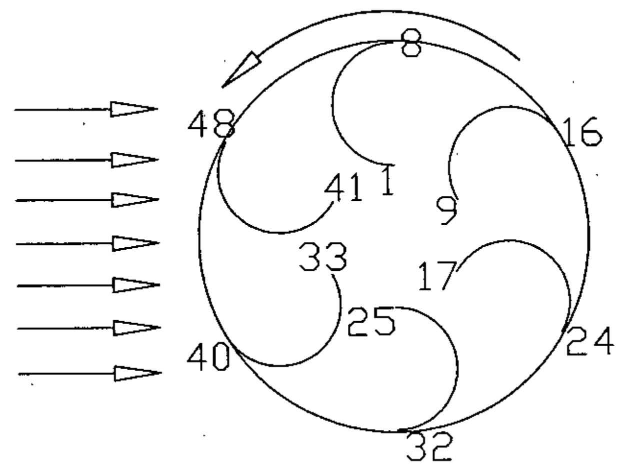

Figure 5.3 (a): Pressure distribution over the blade surfaces at 0° angle of rotation

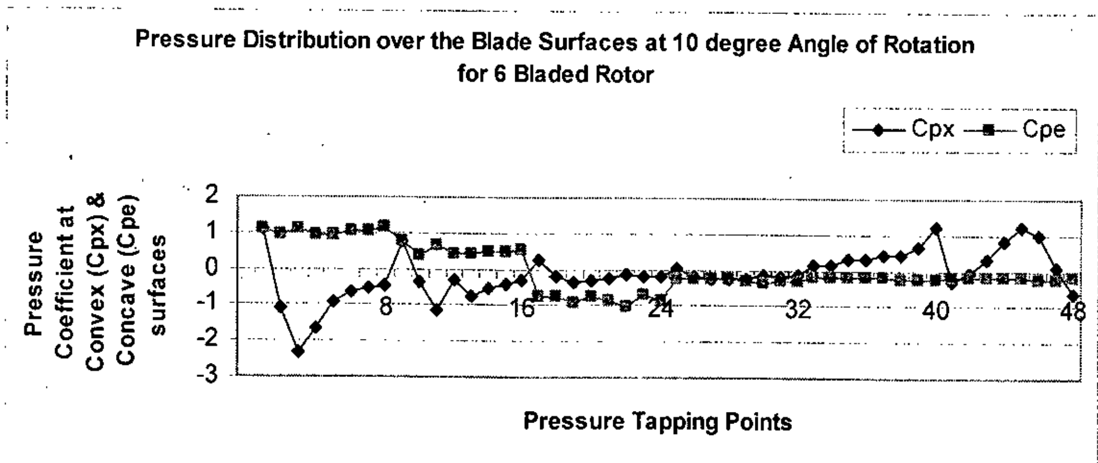

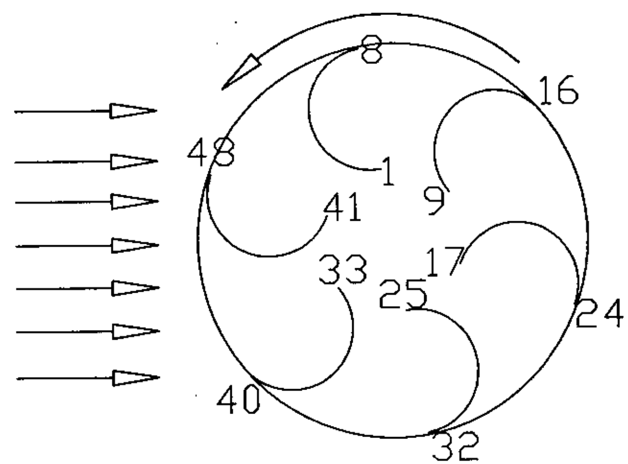

Figure 5.3 (b): Pressure distribution over the blade surfaces at 10° angle of rotation

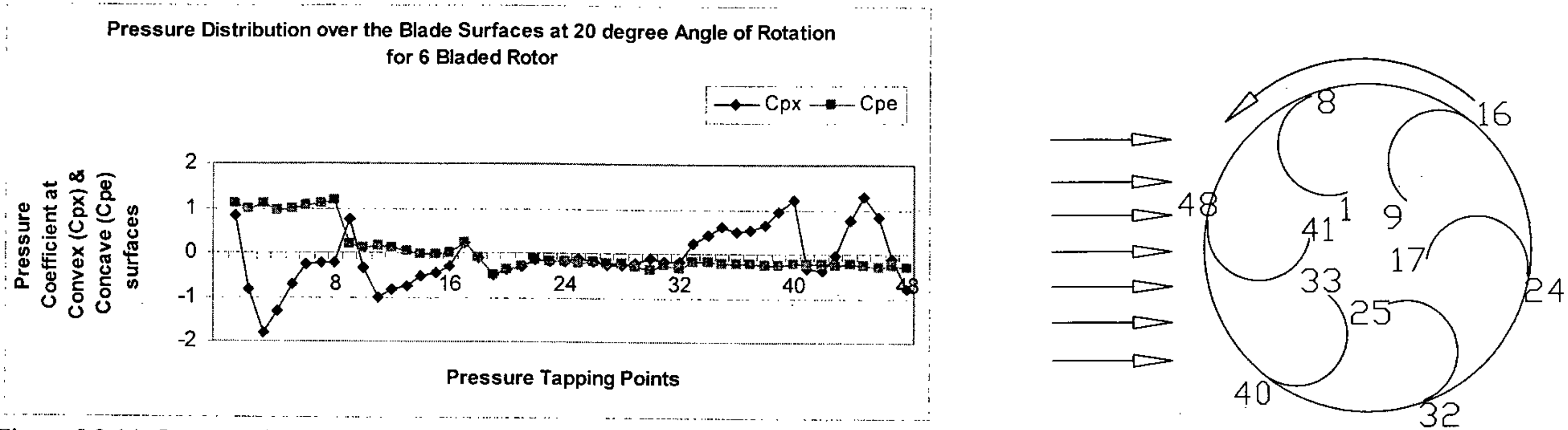

Figure 5.3 (c): Pressure distribution over the blade surfaces at 20° angle of rotation

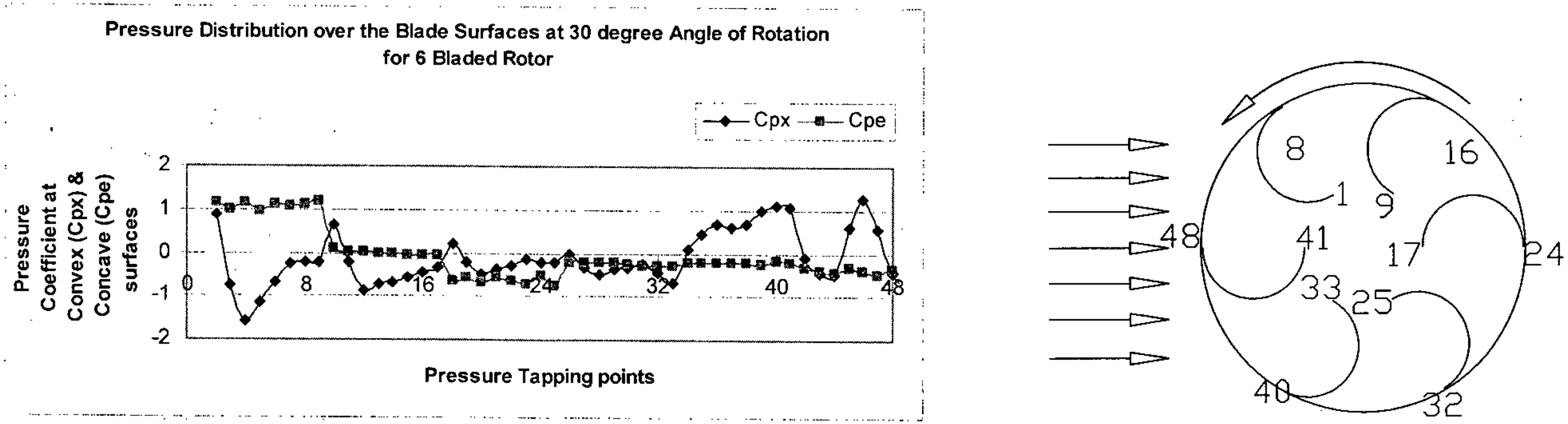

Figure 5.3 (d): Pressure distribution over the blade surfaces at 30° angle of rotation

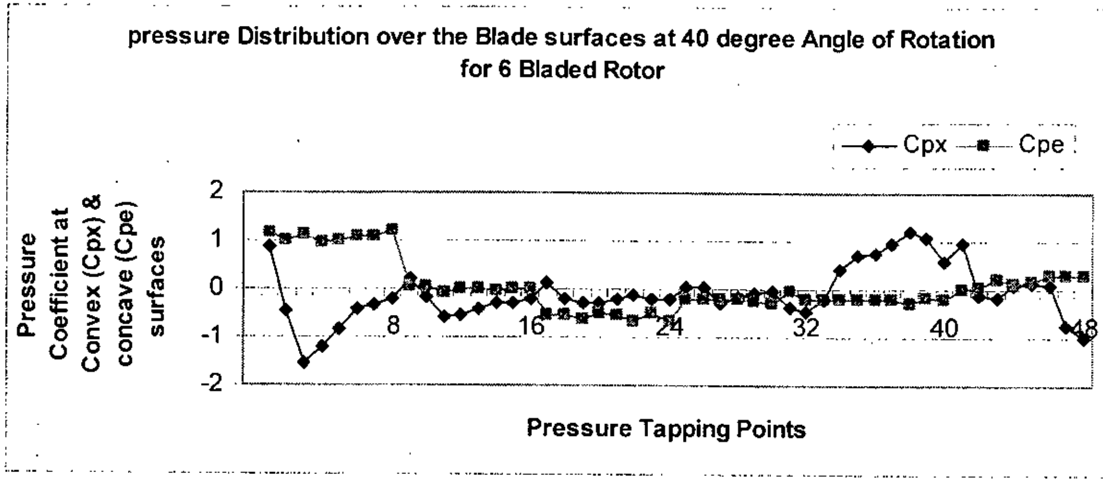

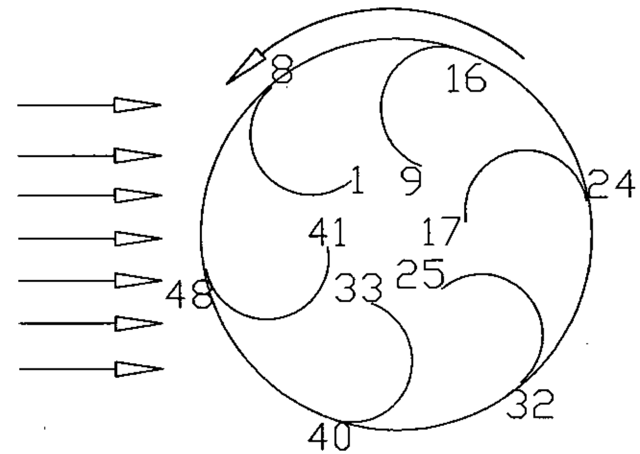

Figure 5.3 (e): Pressure distribution over the blade surfaces at 40° angle of rotation

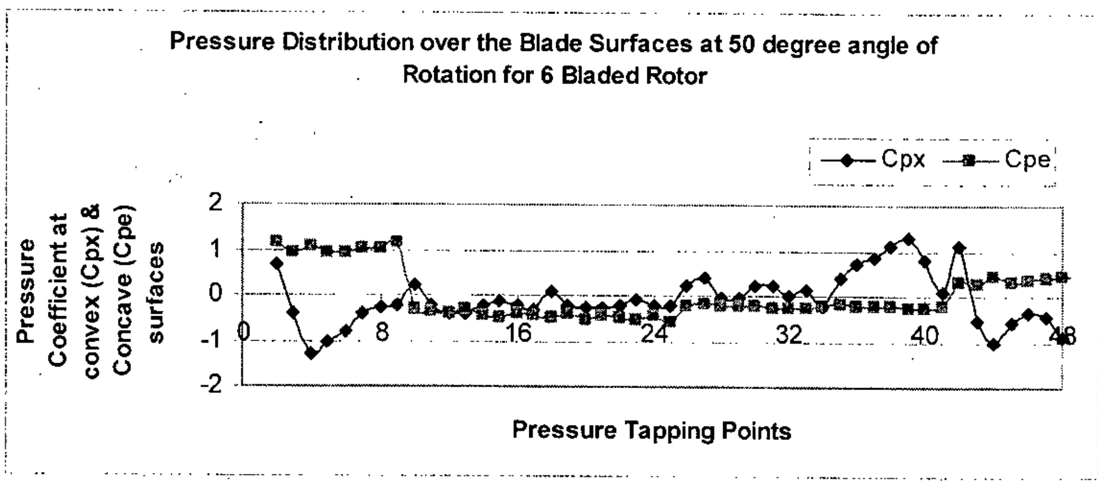

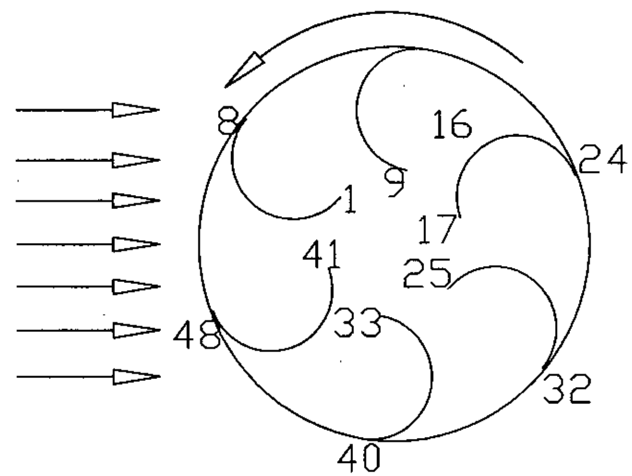

Figure 5.3 (f): Pressure distribution over the blade surfaces at 50° angle of rotation

5.2.2 Normal Drag Coefficient

(a) Normal Drag Coefficient for Four Bladed Vane Rotor:

Normal drag coefficient, C_n of an individual blade effect of four bladed vane rotor is shown in Figure 5.4(a) for different rotor angles. For the flow over the four-bladed system, considering a single blade the normal drag coefficient $C_n(\alpha)$ increases with the increase of the rotor angle from $\alpha=0^\circ$ to 10°. The coefficient decreases from $\alpha=10^\circ$ to 20°, and then increases up to $\alpha=60^\circ$. After that it decreases up to 90°. The value of C_n increases from $\alpha=90^\circ$ to $\alpha=100^\circ$ and decreases up to $\alpha=120^\circ$. It slightly rises to $\alpha=130^\circ$ and falls to $\alpha=140^\circ$. The value of C_n increases from $\alpha=140^\circ$ to $\alpha=160^\circ$ and slightly drops to $\alpha=170^\circ$. Again it increases from $\alpha=170^\circ$ to $\alpha=180^\circ$ and then decreases up to $\alpha=200^\circ$. After that the coefficient increases from $\alpha=200^\circ$ to $\alpha=240^\circ$ and decreases up to $\alpha=270^\circ$. Then it slightly increases up to $\alpha=280^\circ$. Between $\alpha=280^\circ$ to $\alpha=330^\circ$, the value of C_n sharply falls and becomes negative. After that C_n increases up to $\alpha=360^\circ$. The positive torque is available between $\alpha=40^\circ$ to $\alpha=110^\circ$ and from $\alpha=150^\circ$ to $\alpha=260^\circ$. Negative torque is available between $\alpha=0^\circ$ to $\alpha=30^\circ$, at $\alpha=120^\circ$, at $\alpha=140^\circ$ and from $\alpha=270^\circ$ to $\alpha=360^\circ$. Therefore, the drag coefficient $C_n(\alpha)$ for the first blade which contributes more for the torque production, is positive for a rotor angle of $\alpha=40^\circ$ to 90° and is negative in the range between $\alpha=0^\circ$ to 40°. The drag coefficient $C_n(\alpha)$, for the second blade, is small compared to that of the first blade. The drag coefficient $C_n(\alpha)$, is positive for the third blade, which produces positive torque. For the fourth blade, it produces positive torque as well as negative torque.

Normal drag coefficient, C_n with four blades combined effect is presented in Figure 5.4(b) for different rotor angles. Drag coefficient, C_n increases with the increase of the rotor angle from $\alpha=0^\circ$ to $\alpha=10^\circ$, and then decreases up to $\alpha=50^\circ$. The drag coefficient again increases from $\alpha=50^\circ$ to $\alpha=60^\circ$ and then decreases from $\alpha=60^\circ$ to $\alpha=70^\circ$. It again increases slightly to $\alpha=80^\circ$ and falls sharply to $\alpha=90^\circ$. So the drag coefficient, C_n for the four blades is negative for a rotor angle of 0° to 90°. The system repeats from $\alpha=90^\circ$ to $\alpha=170^\circ$, $\alpha=180^\circ$ to $\alpha=260^\circ$ and $\alpha=270^\circ$ to $\alpha=350^\circ$. In the four bladed system, the C_n rises and falls sharply.

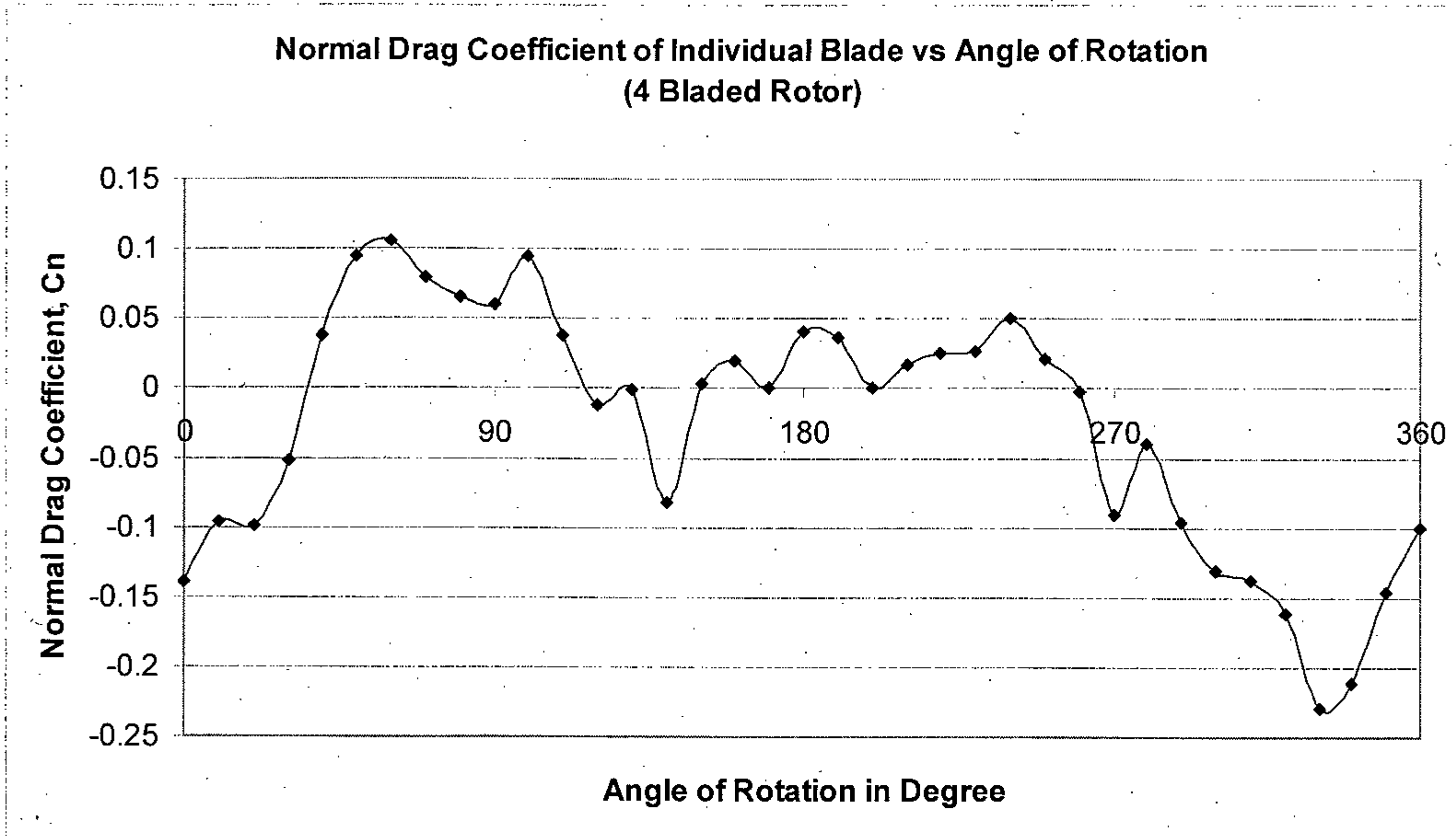

Figure 5.4(a): Normal drag coefficient of individual blade effect (for 4 bladed rotor)

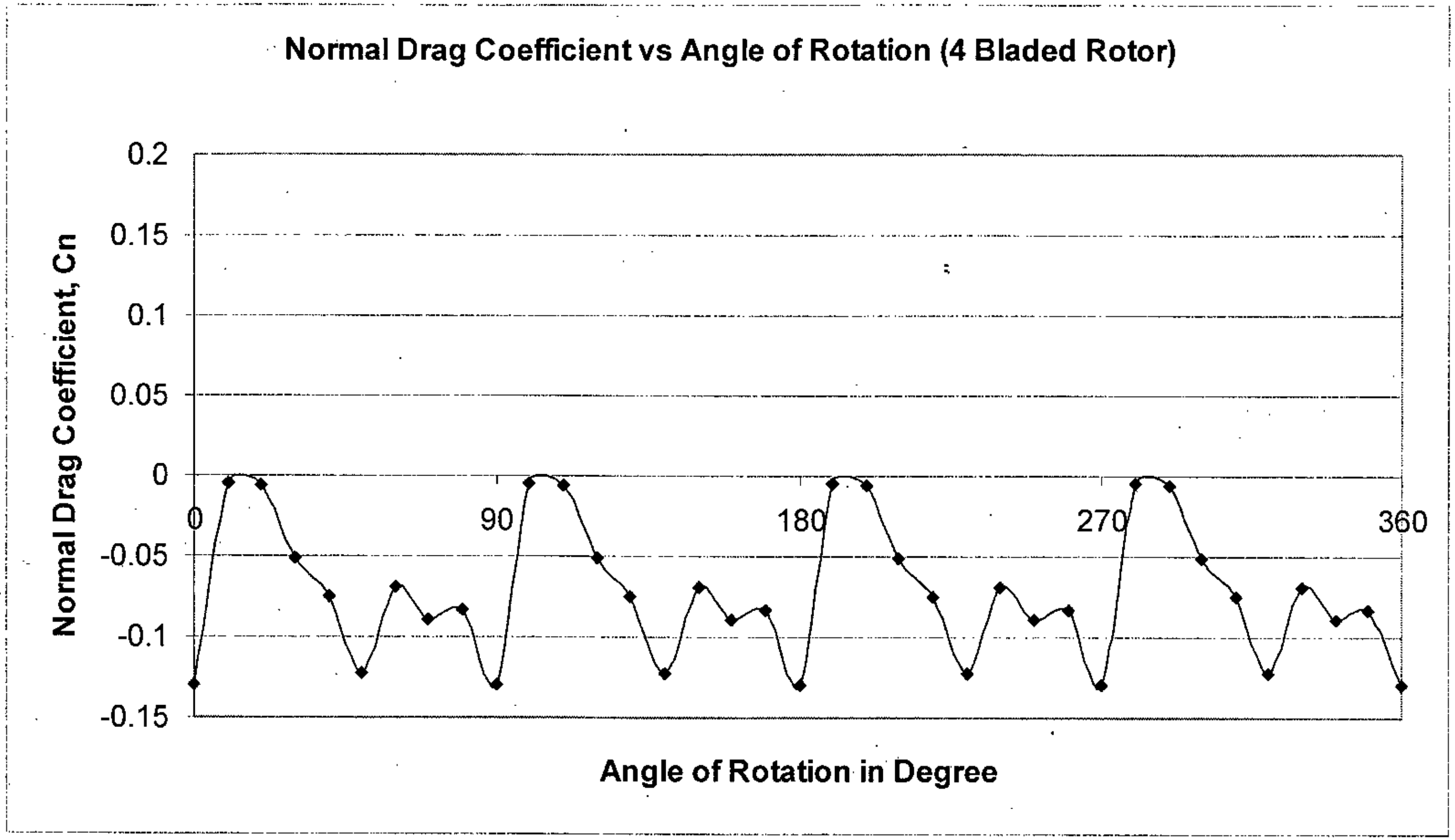

Figure 5.4(b): Normal drag coefficient with the combined blade effect (for 4 bladed rotor)

(b) Normal Drag Coefficient for Five Bladed Vane Rotor:

Normal drag coefficient, C_n of an individual blade effect of five bladed vane rotor is shown in Figure 5.5(a) for different rotor angles. For the flow over the five-bladed system, considering a single blade the normal drag coefficient $C_n(\alpha)$ decreases with the increase of the rotor angle from $\alpha=0^\circ$ to 10°, and then increases up to 30°. Between $\alpha=30^\circ$ to $\alpha=50^\circ$, drag coefficient $C_n(\alpha)$ remains constant and after that it increases up to $\alpha=90^\circ$. The value of C_n decreases from $\alpha=90^\circ$ to $\alpha=110^\circ$ and increases up to $\alpha=130^\circ$. It slightly decreases from $\alpha=130^\circ$ to $\alpha=180^\circ$ and increases from $\alpha=190^\circ$ to $\alpha=270^\circ$. At $\alpha=280^\circ$ it falls sharply up to $\alpha=360^\circ$. Therefore, positive torque is available from $\alpha=70^\circ$ to $\alpha=180^\circ$ and from $\alpha=210^\circ$ to $\alpha=300^\circ$. Negative torque is available in the range of $\alpha=0^\circ$ to $\alpha=60^\circ$, from $\alpha=190^\circ$ to $\alpha=200^\circ$ and from $\alpha=310^\circ$ to $\alpha=360^\circ$. Therefore, the drag coefficient $C_n(\alpha)$ for the first blade, which contributes for the torque production, is negative for a rotor angle of 0° to 60° and reaches its maximum value at $\alpha=60^\circ$.The drag coefficient $C_n(\alpha)$, for the second blade, is positive, which is in favour of positive torque production. In case of the third blade, it is in favour of positive torque production and also negative torque production. The drag coefficient $C_n(\alpha)$, for the fourth blade is positive, which is in favour of positive torque production. For the fifth blade, it is in favour of positive torque production as well as negative.

Normal drag coefficient, C_n with five blades combined effect is shown in Figure 5.5(b) for different rotor angles. Drag coefficient, C_n decreases with the increase of the rotor angle from $\alpha=0^\circ$ to $\alpha=10^\circ$, and increases up to $\alpha=30^\circ$. Then it decreases from $\alpha=30^\circ$ to $\alpha=60^\circ$. The system repeats from $\alpha=72^\circ$ to $\alpha=144^\circ$, $\alpha=144^\circ$ to $\alpha=216^\circ$, $\alpha=216^\circ$ to $\alpha=288^\circ$, and $\alpha=288^\circ$ to $\alpha=350^\circ$.In the five bladed system, the C_n rises and falls sharply.

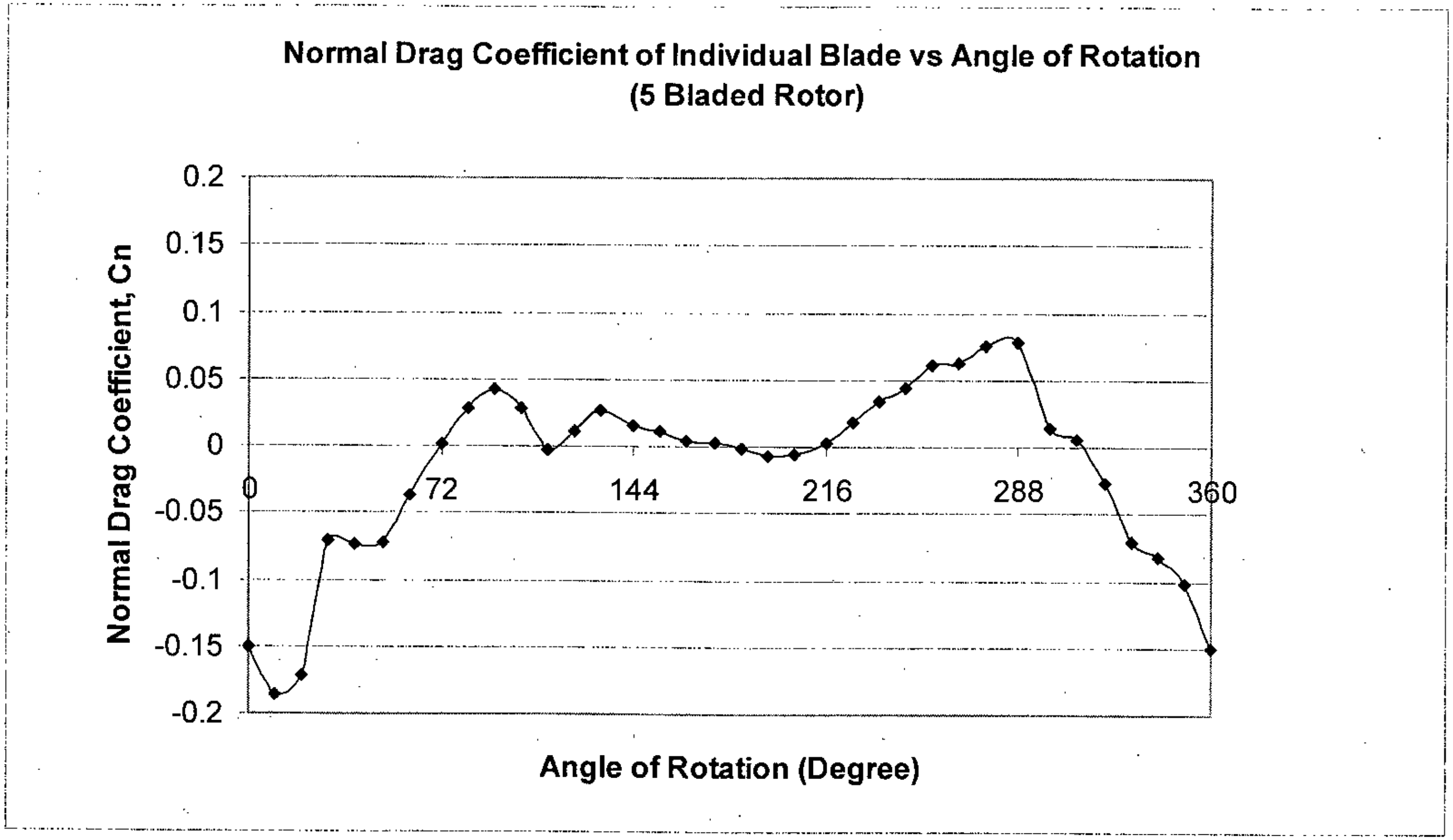

Figure 5.5(a): Normal drag coefficient of individual blade effect (for 5 bladed rotor)

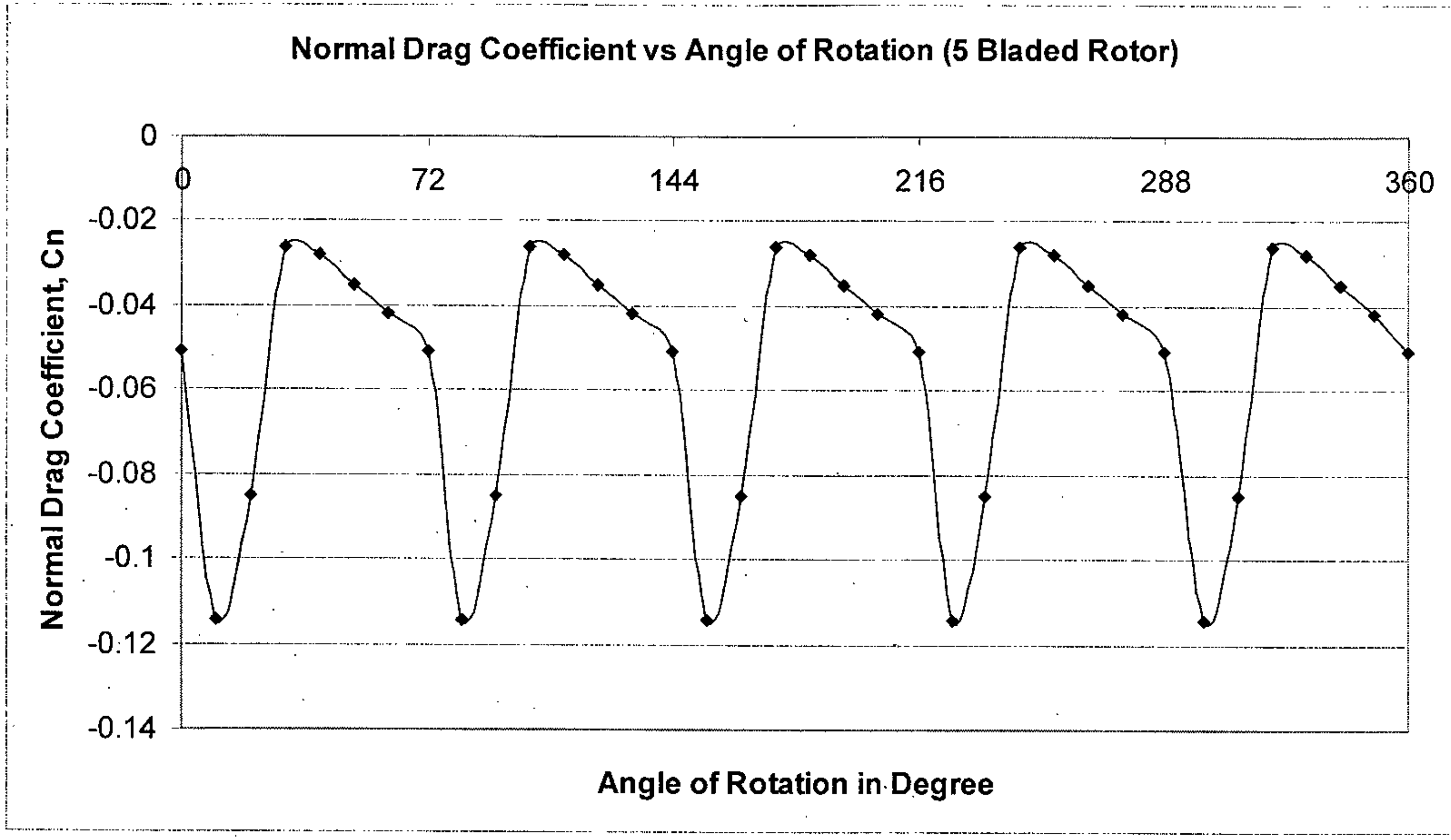

Figure 5.5(b): Normal drag coefficient with the combined blade effect (for 5 bladed rotor)

(c) Normal Drag Coefficient for Six Bladed Vane Rotor:

Normal drag coefficient, C_n of an individual blade effect of six bladed vane rotor is shown in Figure 5.6(a) for different rotor angles. For the flow over the six-bladed system, considering a single blade the normal drag coefficient $C_n(\alpha)$ decreases with the increase of the rotor angle from $\alpha=0°$ to 10°, and then increases up to 130°. From $\alpha=130°$ to $\alpha=210°$, drag coefficient $C_n(\alpha)$ decreases linearly. Between $\alpha=0°$ to $\alpha=180°$, drag coefficient $C_n(\alpha)$, is positive for a rotor angle of 110° to 180° and reaches its maximum value at $\alpha=130°$. The value of C_n increases from $\alpha=210°$ to $\alpha=300°$ and then decreases from $\alpha=300°$ to $\alpha=320$. After that it slightly rises up to $\alpha=330°$. From $\alpha=330°$, the value of C_n sharply falls till $\alpha=360°$. Therefore, positive torque is available between $\alpha=110°$ to $\alpha=200°$ and $\alpha=220°$ to $\alpha=340°$. Negative torque is available between $\alpha=0°$ to $\alpha=100°$, $\alpha=210°$ and $\alpha=350°$ to $\alpha=360°$. Therefore, The drag coefficient $C_n(\alpha)$ for the first blade contributes for the torque production, is negative for a rotor angle of 0° to 50° and reaches its maximum value at $\alpha=50°$. Drag coefficient $C_n(\alpha)$ for the second blade is favourable for production of positive as well as negative torque. In the case of the third blade it is positive, which is in favour of positive torque production. The drag coefficient for the fourth blade, produces positive torque as well as negative torque. The drag coefficient $C_n(\alpha)$, for the fifth blade is positive, which is in favour of positive torque production. The drag coefficient $C_n(\alpha)$, for the sixth blade, is in favour of positive torque production as well as negative.

Normal drag coefficient, C_n with six blades combined effect is shown in Figure 5.6(b) for different rotor angles. Drag coefficient, C_n increases with the increase of the rotor angle from $\alpha=0°$ to $\alpha=20°$, and then decreases up to $\alpha=60°$. The system repeats from $\alpha=60°$ to $\alpha=110°$, $\alpha=120°$ to $\alpha=170°$, $\alpha=180°$ to $\alpha=230°$, $\alpha=240°$ to $\alpha=290°$, and $\alpha=300°$ to $\alpha=350°$. In the six bladed system, the C_n rises and falls sharply.

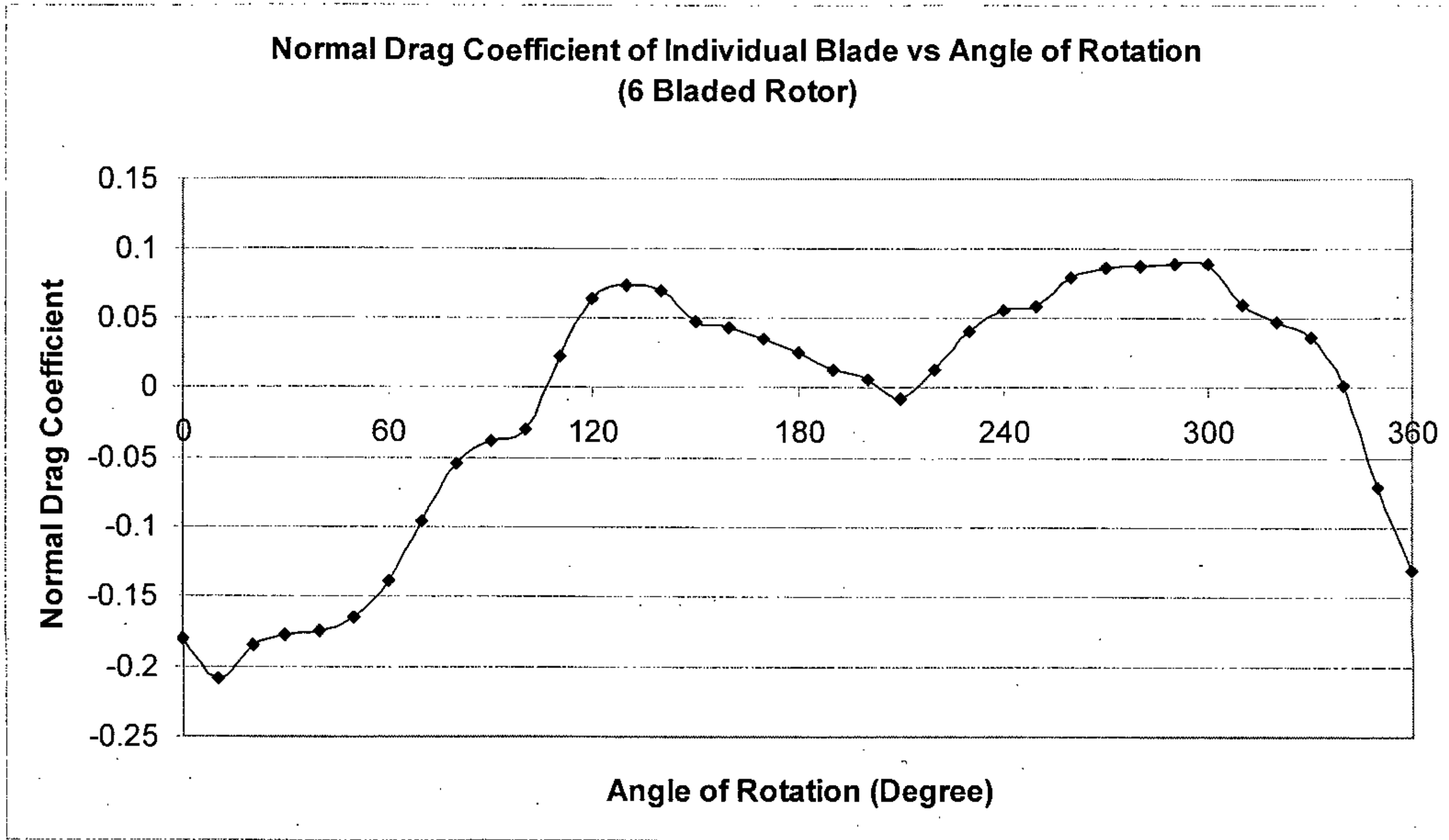

Figure 5.6(a): Normal drag coefficient of individual blade effect (for 6 bladed rotor)

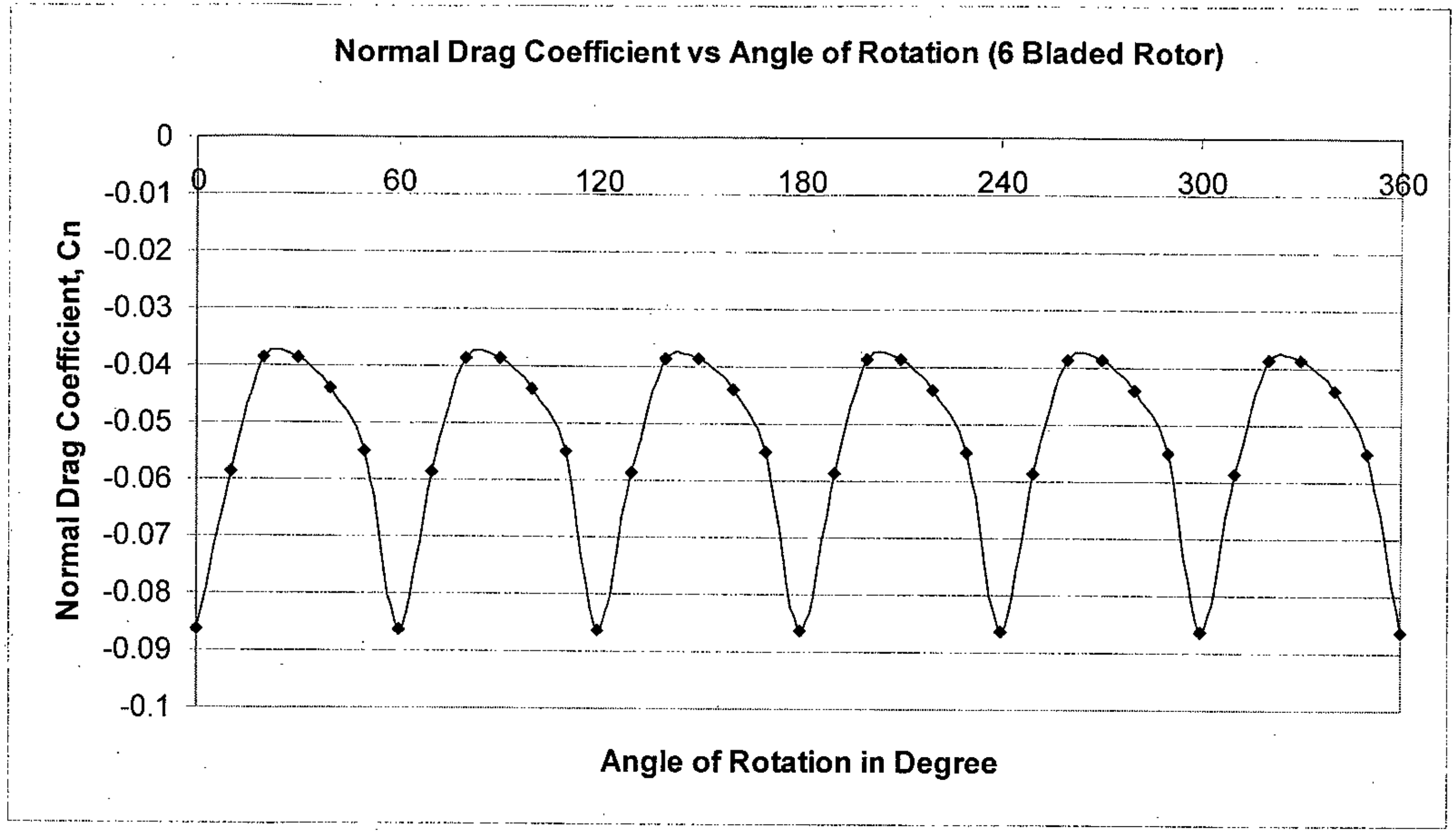

Figure 5.6(b): Normal drag coefficient with the combined blade effect (for 6 bladed rotor)

5.2.3 Tangential Drag Coefficient

(a) Tangential Drag Coefficient for Four Bladed Vane Rotor:

Tangential drag coefficient, C_t of an individual blade effect of four bladed Vane rotor is shown in Figure 5.7(a) for different rotor angles. Considering the flow over the four-bladed system, on the first blade, the tangential drag coefficient, C_t increases with the increase of the rotor angle from $\alpha=0^\circ$ to 60°, and decreases up to 120°. It rises from $\alpha=120^\circ$ to $\alpha=130^\circ$ and falls up to $\alpha=150^\circ$. Again it rises from $\alpha=150^\circ$ to $\alpha=160^\circ$. The tangential coefficient falls from $\alpha=160^\circ$ to $\alpha=170^\circ$ and increases till $\alpha=190^\circ$. From $\alpha=190^\circ$ it decreases up to $\alpha=210^\circ$. Again it rises from $\alpha=210^\circ$ to $\alpha=240^\circ$ and decreases up to $\alpha=270^\circ$. Then the coefficient slightly rises from $\alpha=270^\circ$ to $\alpha=280^\circ$, and then decreases up to $\alpha=340^\circ$. Finally, the tangential drag coefficient sharply increases from $\alpha=340^\circ$ to $\alpha = 360^\circ$. Therefore positive thrust is available between 40° to 110° and 160° to 260° angle of rotation. Negative thrust is available from 120° to 150° and 270° to 360° angle of rotation. In other words, The drag coefficient $C_t(\alpha)$ for the first blade which contributes for thrust production on the support of the rotor, is positive for the rotor angle 35° to 90° and negative thrust for 0° to 35° angle of rotation. The drag coefficient, for the second blade, is small compared to that of the first blade. It produces positive thrust as well as negative thrust. The drag coefficient, $C_t(\alpha)$ for the third blade is positive, is in favour of positive thrust production. The drag coefficient $C_t(\alpha)$, for the fourth blade, produces negative thrust.

Tangential drag coefficient, C_t with four blades combined effect is shown in Figure 5.7(b) for different rotor angles. Drag coefficient, C_t increases sharply with the increase of the rotor angle from $\alpha=0^\circ$ to $\alpha=10^\circ$, and then sharp decrease occurs up to 30°. It increases smoothly from $\alpha=30^\circ$ to $\alpha=60^\circ$ and decreases up to $\alpha=80^\circ$. So, the drag coefficient C_t for four blades, which contributes more for the thrust production, is always negative between 0° to 80° angle of rotation. The system repeats from $\alpha=90^\circ$ to $\alpha=170^\circ$, $\alpha=180^\circ$ to $\alpha=260^\circ$ and $\alpha=270^\circ$ to $\alpha=350^\circ$.

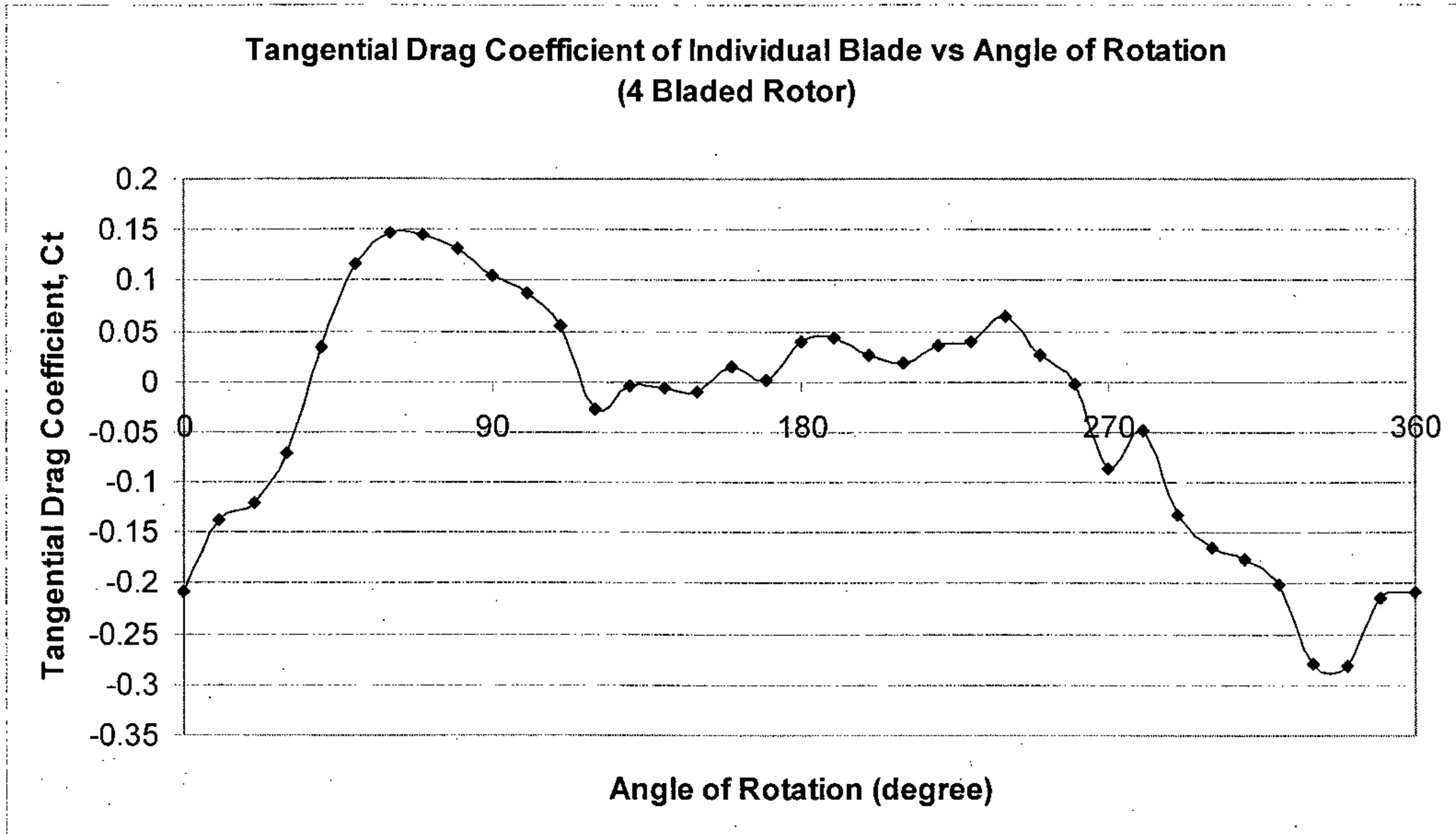

Figure 5.7(a): Tangential drag coefficient of individual blade effect (for 4 bladed rotor)

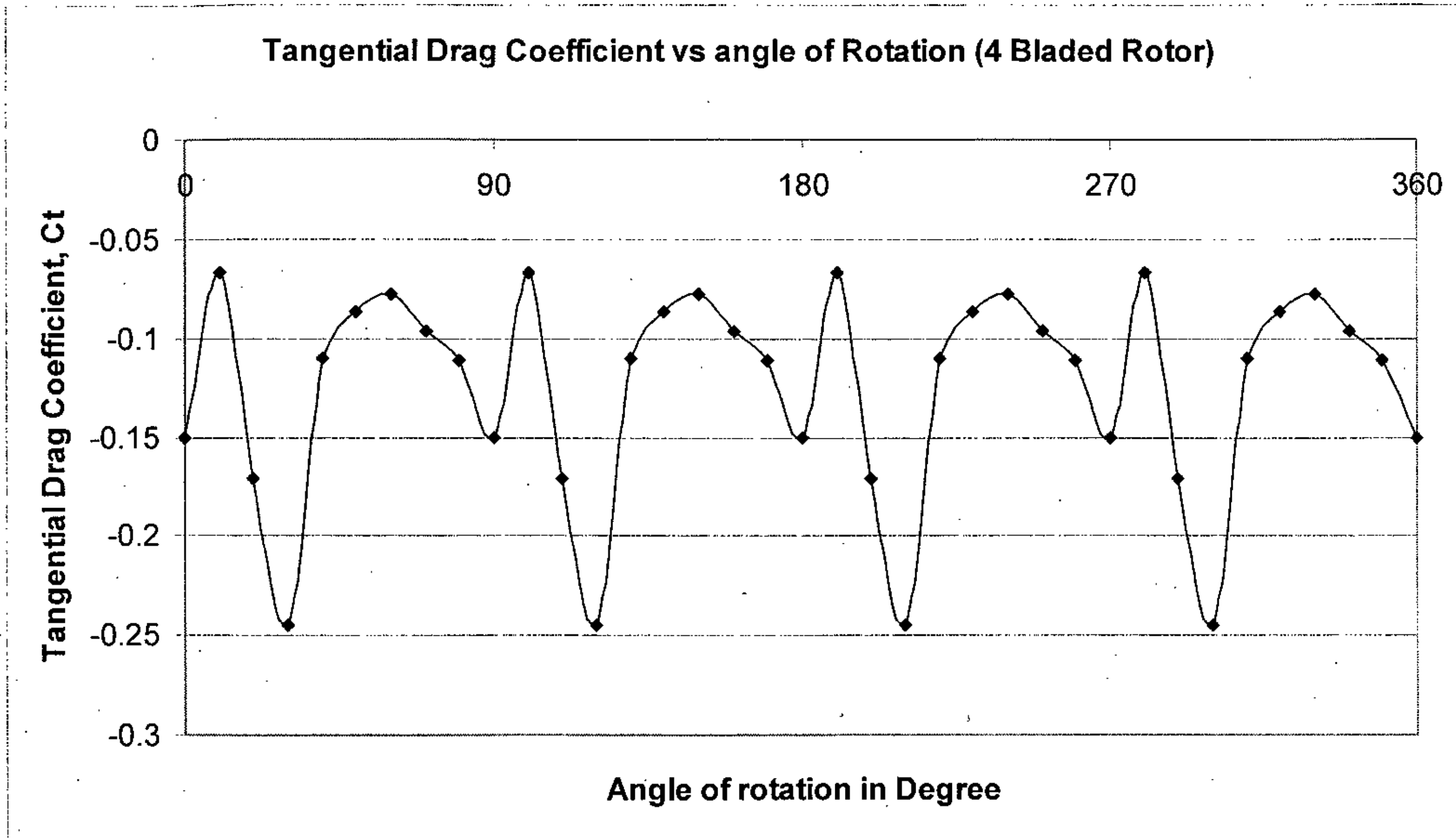

Figure 5.7(b): Tangential drag coefficient with the combined blade effect (for 4 bladed rotor)

(b) Tangential Drag Coefficient for Five Bladed Vertical Axis Vane Type Rotor:

Tangential drag coefficient, C_t of an individual blade effect of five bladed Vane rotor is shown in Figure 5.8(a) for different rotor angles. For the five-bladed system, on the first blade, the tangential drag coefficient, C_t decreases with the increase of the rotor angle from $\alpha=0^\circ$ to 10°, and then increases up to 90°. From $\alpha=90^\circ$ drag coefficient C_t falls smoothly till $\alpha=110$. It rises from $\alpha=110^\circ$ to $\alpha=130^\circ$ and decreases from $\alpha=130^\circ$ to $\alpha=210^\circ$. From $\alpha=210^\circ$ it increases up to $\alpha=280^\circ$. From then onwards the drag coefficient, C_t decreases sharply till $\alpha=360^\circ$. Therefore, positive thrust is available between 70° to 180° and 220° to 300° angle of rotation. Negative thrust is available from 0° to 60° and 220° to 300° angle of rotation. Therefore, the drag coefficient $C_t(\alpha)$ for the first blade which contributes for thrust production on the support of the rotor, is negative. The drag coefficient $C_t(\alpha)$, for the second blade, is mostly positive. Drag coefficient $C_t(\alpha)$, for the third blade, is in favour of positive thrust production as well as negative thrust production. The drag coefficient $C_t(\alpha)$, for the fourth blade, produces positive thrust. Drag coefficient $C_t(\alpha)$, for the fifth blade, is in favour of positive thrust production and also negative thrust.

Tangential drag coefficient, C_t with five blades combined effect is shown in Figure 5.8(b) for different rotor angles. Drag coefficient, C_t decreases with the increase of the rotor angle from $\alpha=0^\circ$ to $\alpha=10^\circ$, and then increases up to $\alpha=30^\circ$. Then it again decreases to $\alpha=40^\circ$. The coefficient increases from $\alpha=40^\circ$ to $\alpha=60^\circ$ and decreases from $\alpha=60^\circ$ to $\alpha=72^\circ$. The system repeats from $\alpha=72^\circ$ to $\alpha=144^\circ$, $\alpha=144^\circ$ to $\alpha=216^\circ$, $\alpha=216^\circ$ to $\alpha=288^\circ$, and $\alpha=288^\circ$ to $\alpha=350^\circ$.

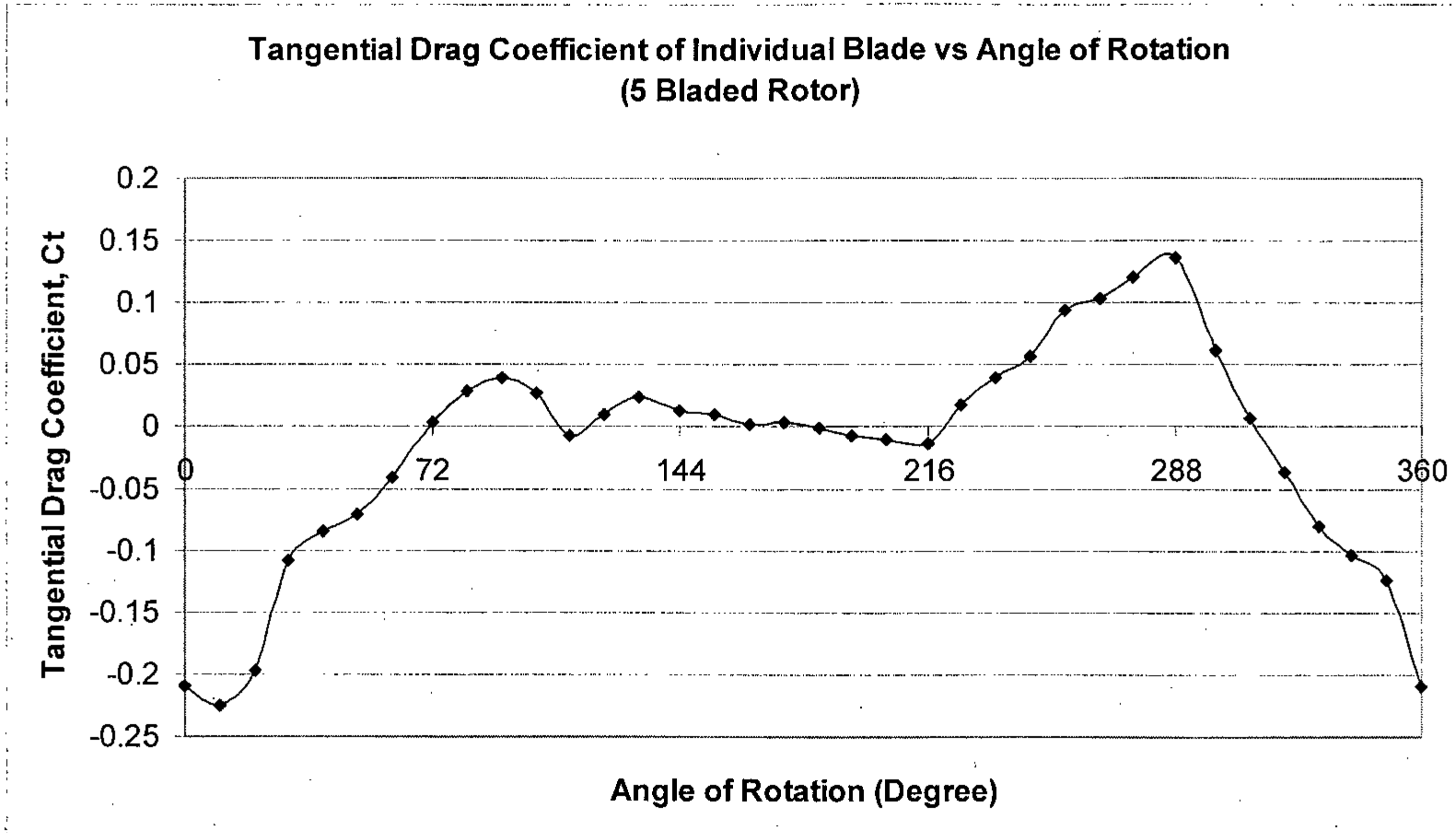

Figure 5.8(a): Tangential drag coefficient of individual blade effect (for 5 bladed rotor)

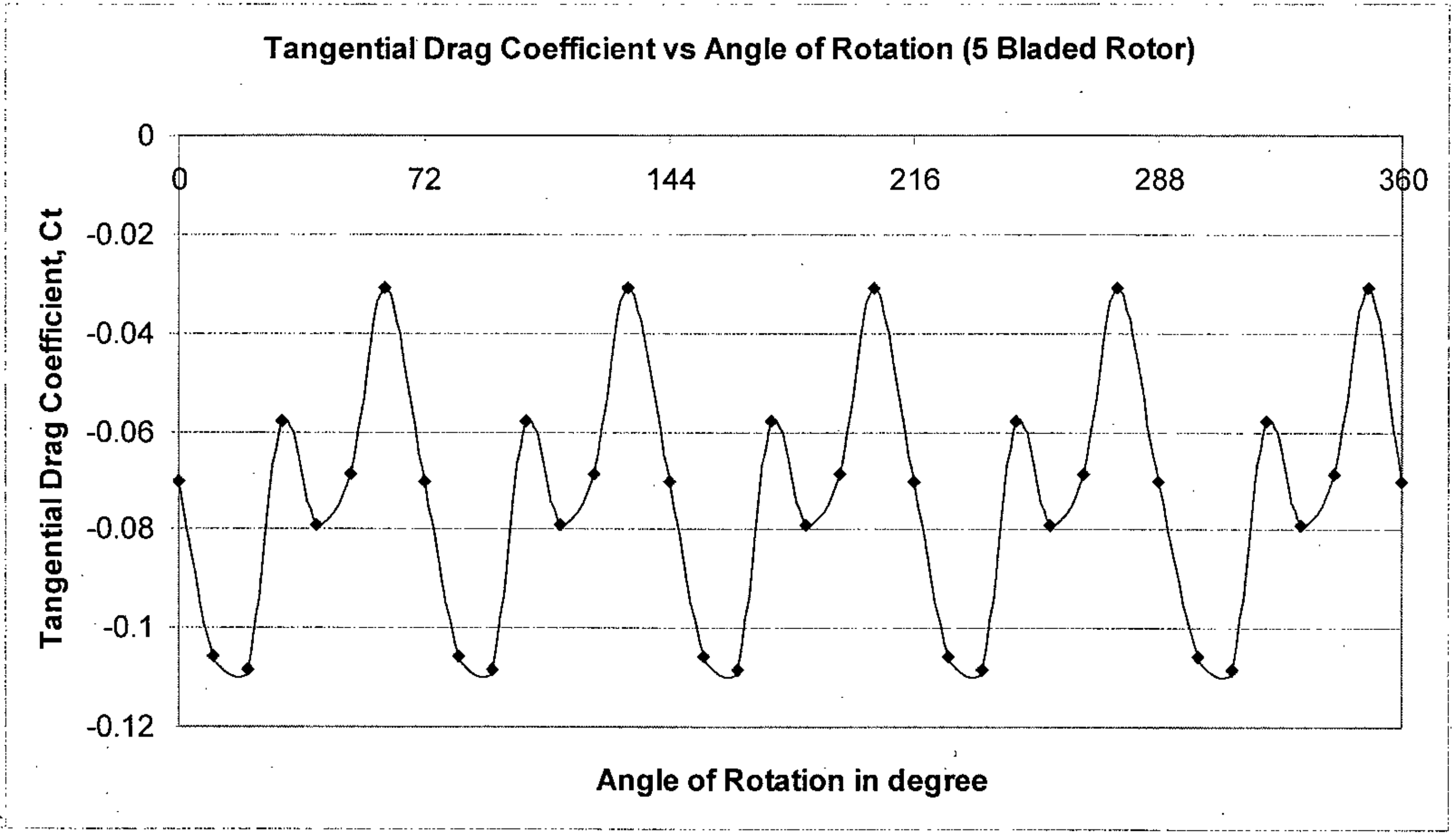

Figure 5.8(b): Tangential drag coefficient with the combined blade effect (for 5 bladed rotor)

(c) Tangential Drag Coefficient for Six Bladed Vertical Axis Vane Type Rotor:

Tangential drag coefficient, C_t of an individual blade effect of six bladed Vane rotor is shown in Figure 5.9(a) for different rotor angles. For the six-bladed system, on the first blade, the tangential drag coefficient, C_t decreases with the increase of the rotor angle from α=0° to 10°, and then increases up to 30°. The tangential drag coefficient, C_t falls slightly from α=30° to α=40°, and increases up to 130°. The drag coefficient decreases from α=130° to α=210° and increases from α=210° to α=280°. From α=280° it decreases till α=320° and remains constant to α=330°. The drag coefficient C_t decreases sharply from α=330° to α=350° and then remains constant to α=360°. Positive thrust is available between 110° to 200° and 220° to 330° angle of rotation. Negative thrust is available from 0° to 100°, at 210° and 340° to 360° angle of rotation. Therefore, the drag coefficient $C_t(\alpha)$ for the first blade which contributes for thrust production on the support of the rotor, is negative for the rotor angle 0° to 50°. The drag coefficient $C_t(\alpha)$, for the second blade, produces positive as well as negative thrust. The drag coefficient $C_t(\alpha)$ for the third blade, is in favour of positive thrust production. The drag coefficient $C_t(\alpha)$, for the fourth blade, produces positive thrust as well as negative. Drag coefficient $C_t(\alpha)$ for the fifth blade is positive, i.e. it is in favour of positive thrust production. The drag coefficient $C_t(\alpha)$, for the sixth blade, is in favour of positive thrust as well as negative thrust production.

Tangential drag coefficient, C_t with six blades combined effect is shown in Figure 5.9(b) for different rotor angles. Drag coefficient, C_t increases with the increase of the rotor angle from α=0° to α=20°, and decreases up to α=60°. The system repeats from α=60° to α=110°, α=120° to α=170°, α=180° to α=230°, α=240° to α=290° and α=300° to α=350°.

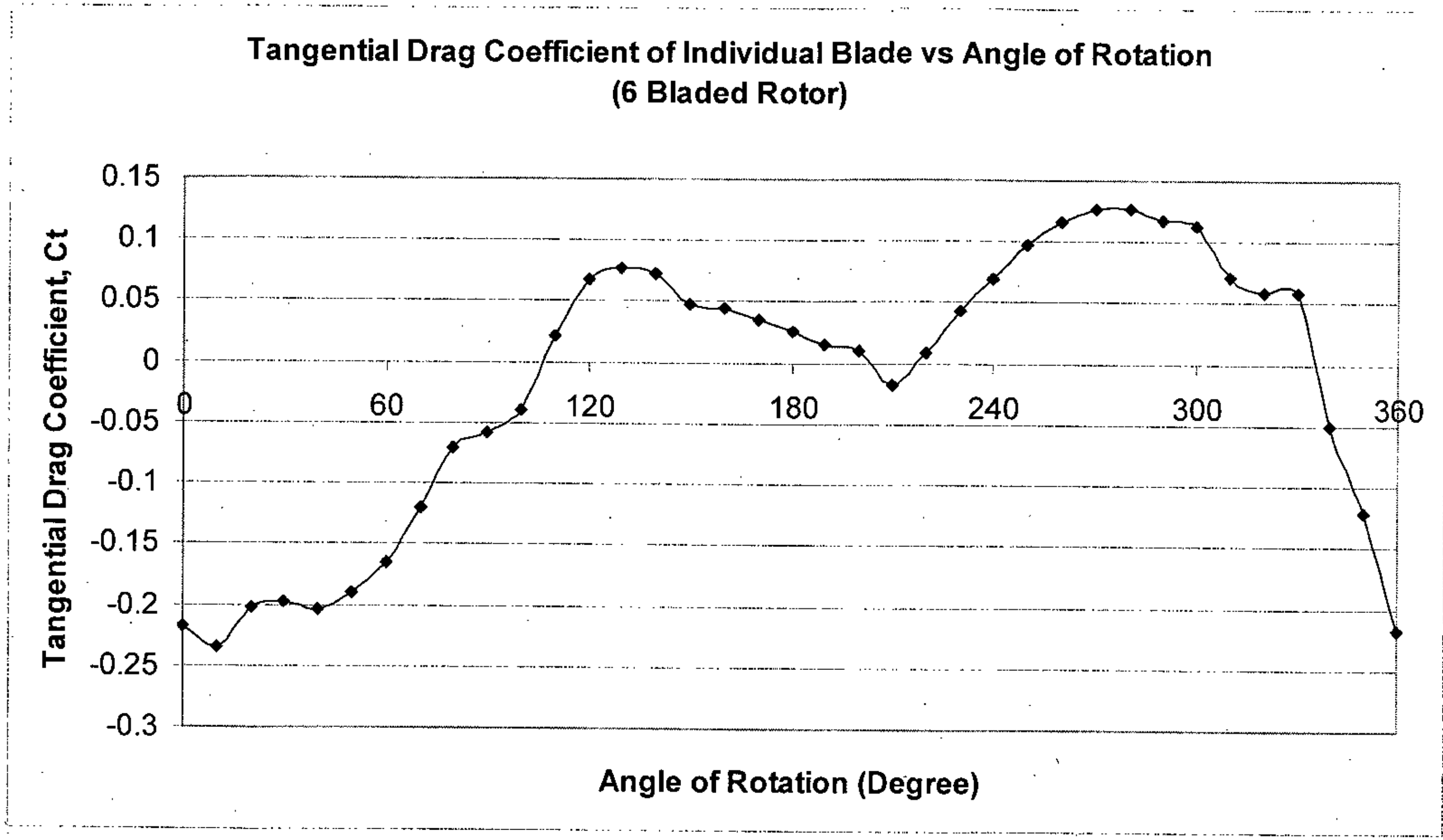

Figure 5.9(a): Tangential drag coefficient of individual blade effect (for 6 bladed rotor)

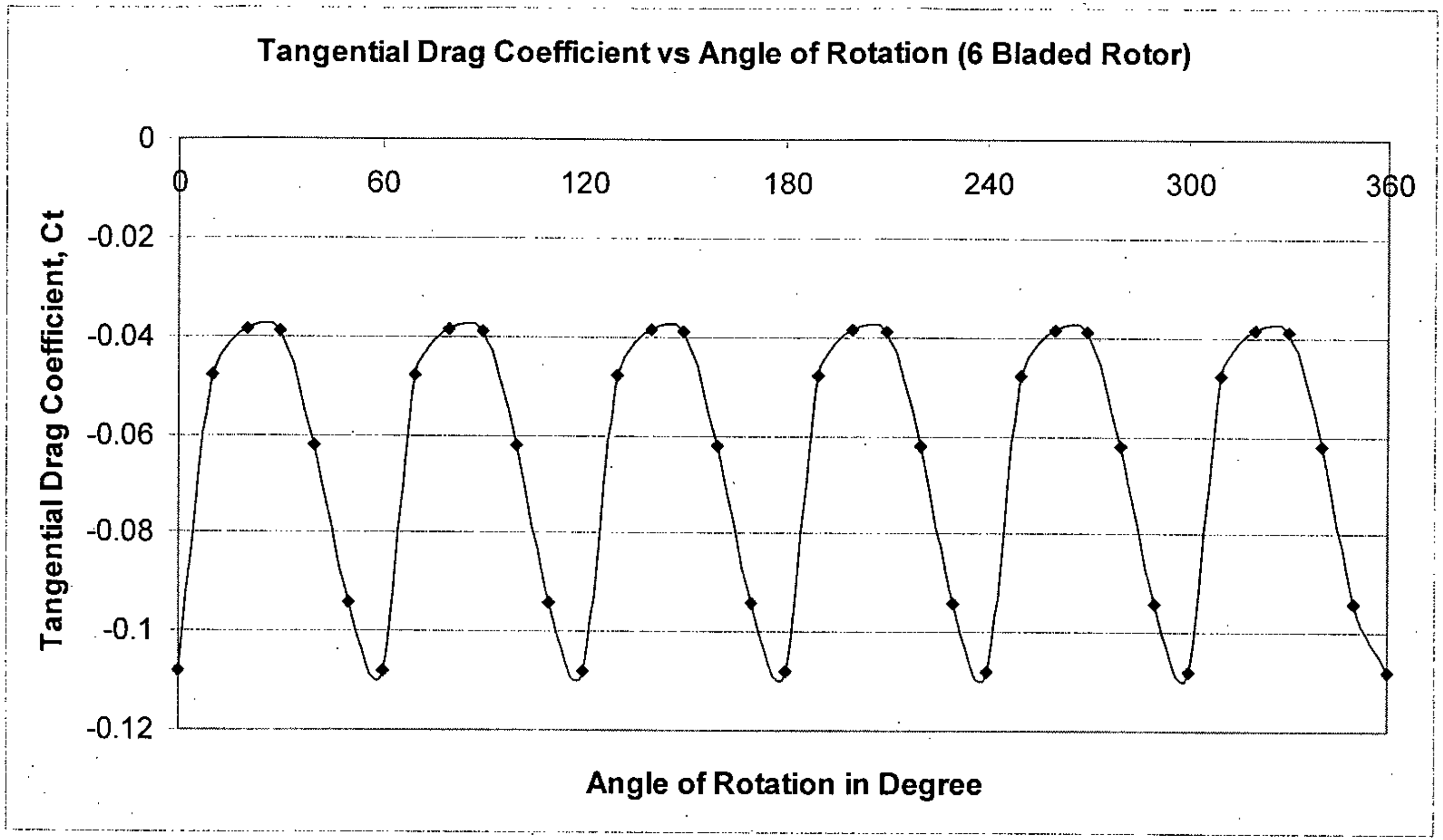

Figure 5.9(b): Tangential drag coefficient with the combined blade effect (for 6 bladed rotor)

5.2.4 Torque Coefficient

(a) Torque Coefficient for Four Bladed Vertical Axis Vane Type Rotor:

Torque coefficient, C_q with individual blade effect of four bladed vane rotor is shown in Figure 5.10(a) for different rotor angles. Considering the flow over the four-bladed system, on the first blade, the torque coefficient decreases with the increases of the rotor angle from α=0° to 10°, and increases slightly to 20° and then decreases up to 60°. The coefficient rises from α=60° to α=90° and decreases from α=90° to α=100°. From α=100° it increases till α=120°. The torque coefficient falls to α=130° and again rises to α=140°. It decreases in the range of α=140° to α=160°. Then the C_q increases to α=170° and again decreases to α=180°. It again increases from α=180° to α=200°. Between α=200° to α=240°, the C_q falls sharply and becomes negative. It increases sharply from α=240° to α=270°, and then falls to α=280°. The drag coefficient C_q increases from α=280° to α=330°, and then C_q decreases till α=360°. Therefore, the positive torque is available for a rotor angle of 0° to 30°, 120° to 150°, at 170°, at 200° and 260° to 360°. Negative torque is available for a rotor angle of 40° to 110°, 180° to 190° and 210° to 250°. It is observed that the fourth blade torque coefficient is highest among the four blades. For the four-bladed system, the nature of this curve is opposite to that of the normal drag coefficient, C_n with individual blade effect, which contributes more for producing torque. The difference is that the value of torque coefficient is smaller than that of normal drag coefficient with individual blade effect.

Total static torque coefficient, C_Q with four blades vane rotor is shown in Figure 5.10 (b) at different rotor angles. For the four-bladed system, the nature of the curve is opposite to that of the normal drag coefficient with four blades combined effect. The difference is that the value of torque coefficient is smaller than that of normal drag coefficient with combined blade effect. And total static torque coefficient is positive where normal drag coefficient for combined blade effect is negative value. Here the total static torque decreases from α=0° to α=10°, and then increases up to α=50°. It decreases to α=60° and slightly rises to α=70°. It again falls from α=70° to α=80°, and then increases up to 90°. The curve repeats from 90° to 170°, from 180° to 260° and from 270° to 350°.

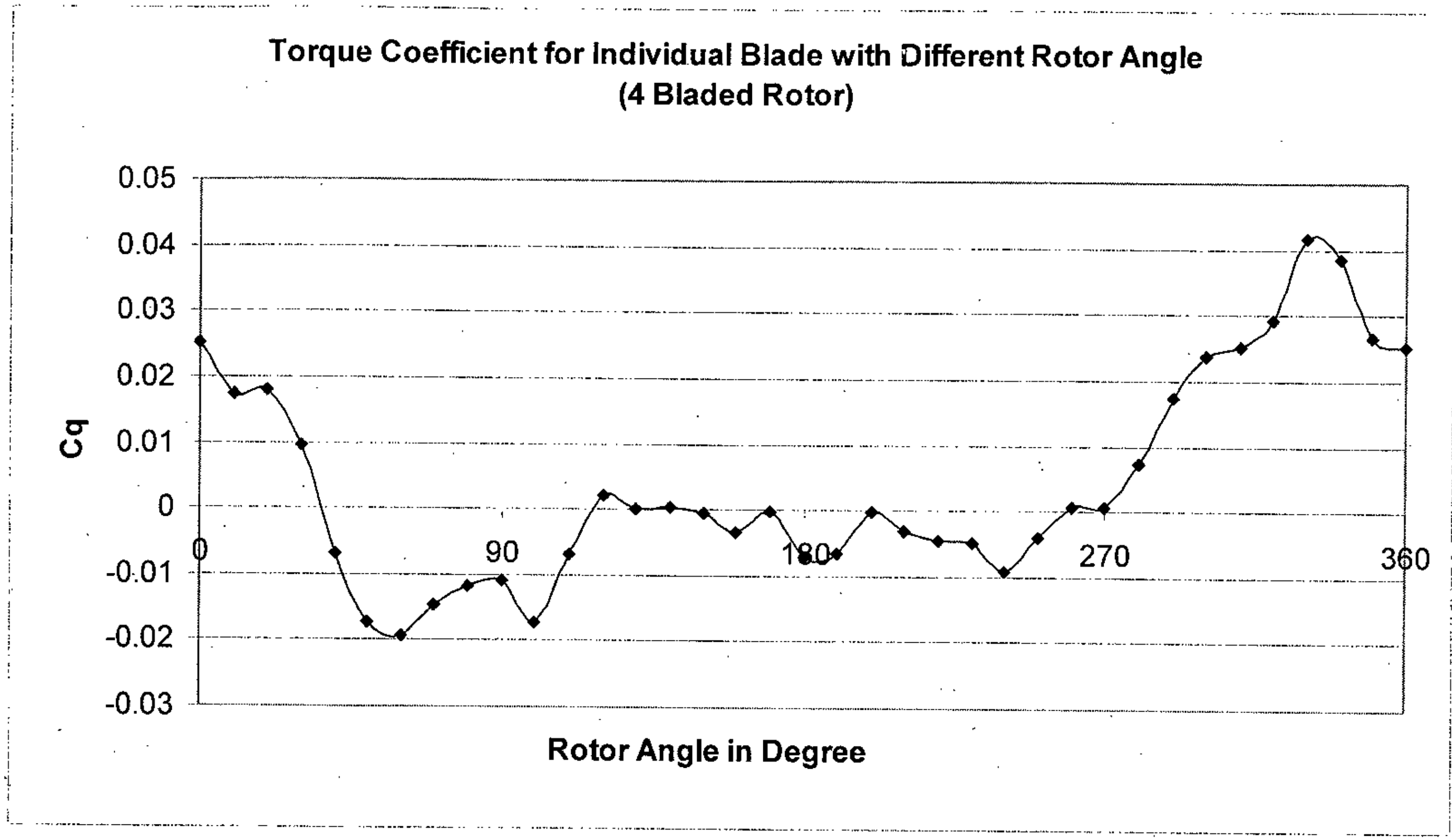

Figure 5.10(a): Torque coefficient with individual blade effect (for 4 bladed rotor)

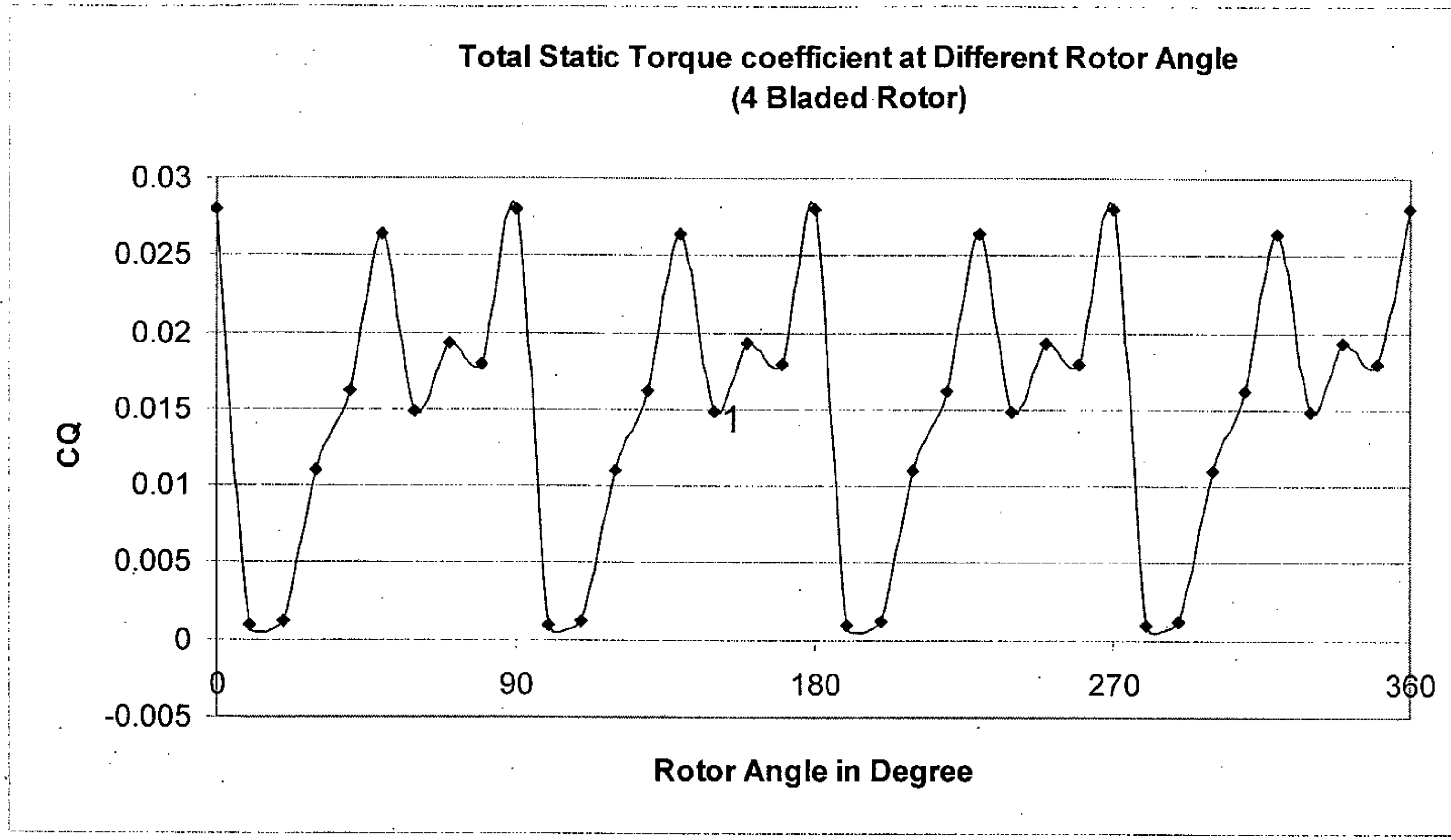

Figure 5.10(b): Total static torque coefficient at different rotor angle (for 4 bladed rotor)

(b) Torque Coefficient for Five Bladed Vertical Axis Vane Type Rotor:

Torque coefficient, C_q with individual blade effect of five bladed vane rotor is shown in Figure 5.11(a) for different rotor angles. Considering the flow over the five-bladed system, on the first blade, the torque coefficient increases with the increase of the rotor angle from $\alpha=0^\circ$ to 10°, and then decreases slightly to 30° and remains constant till 50°. The coefficient, C_q decreases with the increase of rotor angle α, up to 90°. Between $\alpha=0^\circ$ to $\alpha=90^\circ$, the torque coefficient is positive for a rotor angle of 0° to 70° and reaches its maximum value at $\alpha=10^\circ$. The coefficient rises from $\alpha=90^\circ$ to $\alpha=110^\circ$. After that it decreases from $\alpha=110^\circ$ to $\alpha=130^\circ$, and increases up to $\alpha=190^\circ$ smoothly. Then C_q falls from $\alpha=190^\circ$ to $\alpha=280^\circ$ smoothly. From then onwards, it increases till $\alpha=360^\circ$. Therefore, the positive torque is available for a rotor angle of 0° to 70°, at 110°, 170° to 200° and 300° to 360°. Negative torque is available for a rotor angle of 80° to 100°, 120° to 160° and 210° to 290°. It is observed that for the second blade torque coefficient is comparatively smaller than that of the first blade. For the third blade, torque coefficient increases from negative to positive value. In the case of fourth blade, torque is negative. For the fifth blade, the coefficient produces positive as well as negative torque. The first blade torque is highest among the five blades. For the five-bladed system, the nature of this curve is opposite to that of the normal drag coefficient, C_n with individual blade effect. The difference is that the value of torque coefficient is smaller than normal drag coefficient with individual blade effect.

Total static torque coefficient, C_q with five blades vane rotor is shown in Figure 5.11 (b) at different rotor angles. For the five-bladed system, the nature of the curve is opposite to the normal drag coefficient, C_n with five blades combined effect. The difference is that the value of torque coefficient is smaller than that of the normal drag coefficient with combined blade effect. And total static torque coefficient is positive where normal drag coefficient for combined blade effect is negative value. Here the total static torque increases with the increase of the rotor angle up to $\alpha=10^\circ$ and reaches its maximum value and then decreases up to $\alpha=30^\circ$. From this point the coefficient C_q increases up to 72°. The curve repeats from 72° to 144°, from 144° to 216°, from 216° to 288° and from 288° to 350°.

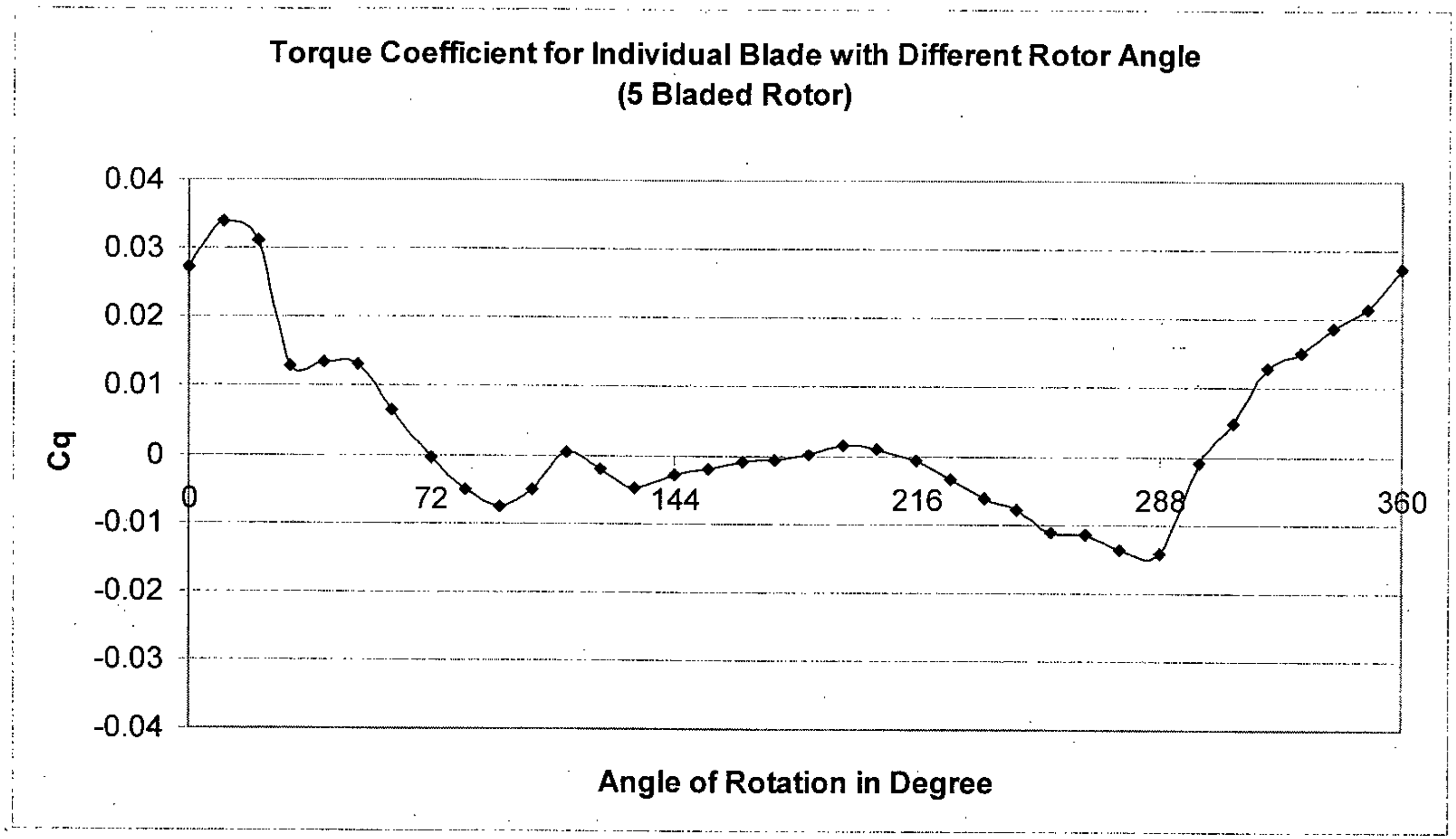

Figure 5.11(a): Torque coefficient with individual blade effect (for 5 bladed rotor)

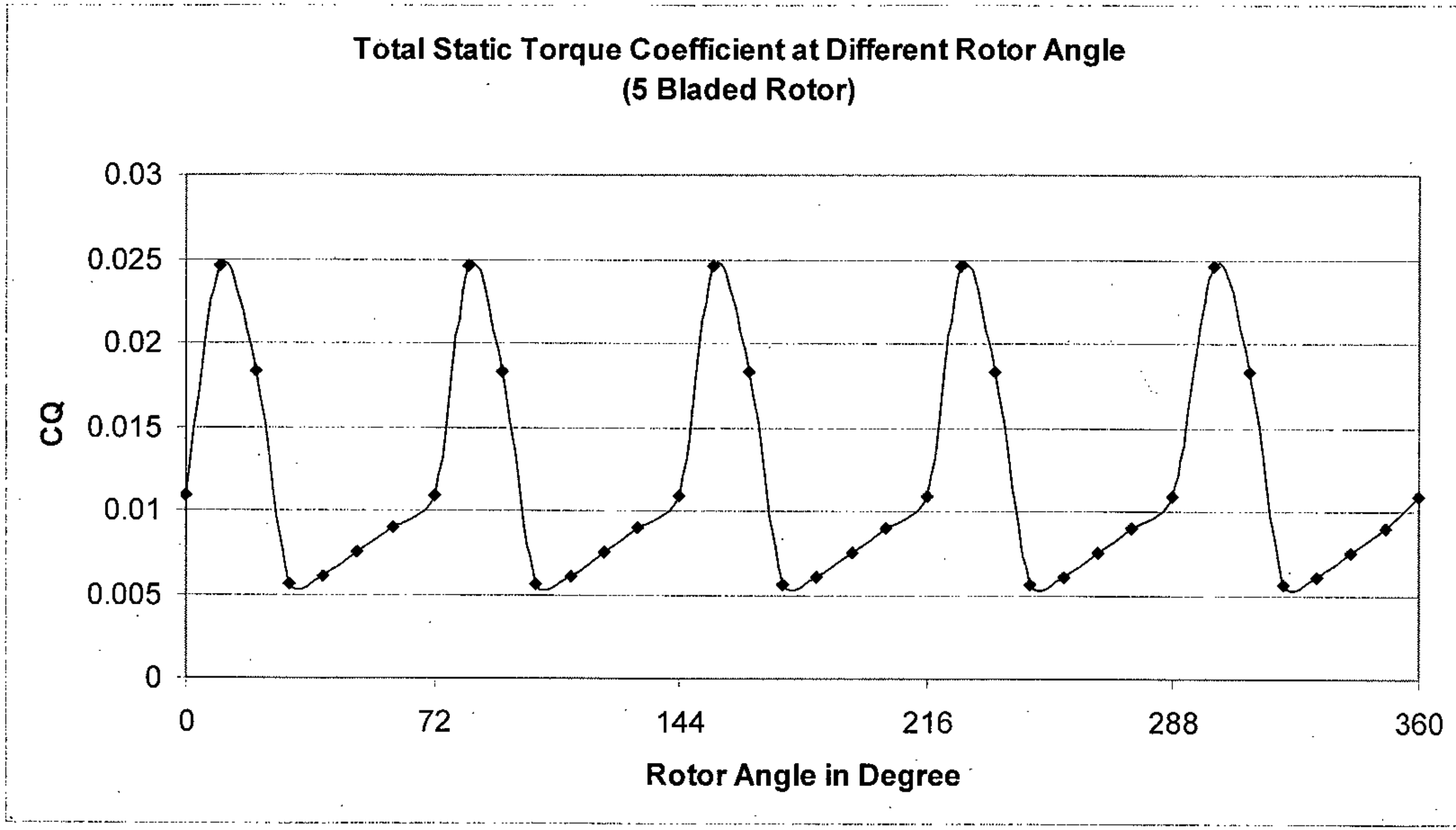

Figure 5.11(b): Total static torque coefficient at different rotor angle (for 5 bladed rotor)

(c) Torque Coefficient for Six Bladed Vertical Axis Vane Type Rotor:

Torque coefficient, C_q with individual blade effect of six bladed vane rotor is shown in Figure 5.12(a) for different rotor angles. Considering the flow over the six-bladed system, on the first blade, the torque coefficient, C_q increases with the increase of the rotor angle from $\alpha=0^\circ$ to 10°, and then decreases up to 130°. From this point the drag coefficient increases up to 210°. Between $\alpha=0^\circ$ to $\alpha=100^\circ$, the torque coefficient C_q is positive for a rotor angle of 0° to 100° and reaches its maximum value at $\alpha=10^\circ$. The coefficient decreases from $\alpha=210^\circ$ to $\alpha=300^\circ$. From then onwards, the C_q increases from $\alpha=300^\circ$ to $\alpha=320^\circ$ and slightly falls at $\alpha=330^\circ$. It increases from $\alpha=330^\circ$ to $\alpha=360^\circ$. Therefore, the positive torque is available for a rotor angle of 0° to 100°, at 210° and from 340° to 360°. Negative torque is available for a rotor angle of 110° to 200° and from 220° to 330°. It is observed that the first blade produces highest torque among the six blades. For the six-bladed system, the nature of this curve is opposite to that of the normal drag coefficient, C_n with individual blade effect, which is responsible for producing torque. The difference is that the value of torque coefficient is smaller than normal drag coefficient with individual blade effect.

Total static torque coefficient, C_q with six blades Vane rotor is shown in Figure 5.12 (b) at different rotor angles. For the six-bladed system, the nature of the curve repeats after 50° angle of rotation like that of the normal drag coefficient due to combined effect. The value of torque coefficient is smaller than that of normal drag coefficient with combined blade effect. And total static torque coefficient is positive where normal drag coefficient for combined blade effect is negative value. Here the total static torque decreases with the increase of the rotor angle up to $\alpha=20^\circ$. From this point the coefficient C_q increases till $\alpha=60^\circ$. Then the curve repeats. The curve repeats from 60° to 110°, from 120° to 170°, from 180° to 230°, 240° to 290° and from 300° to 350°.

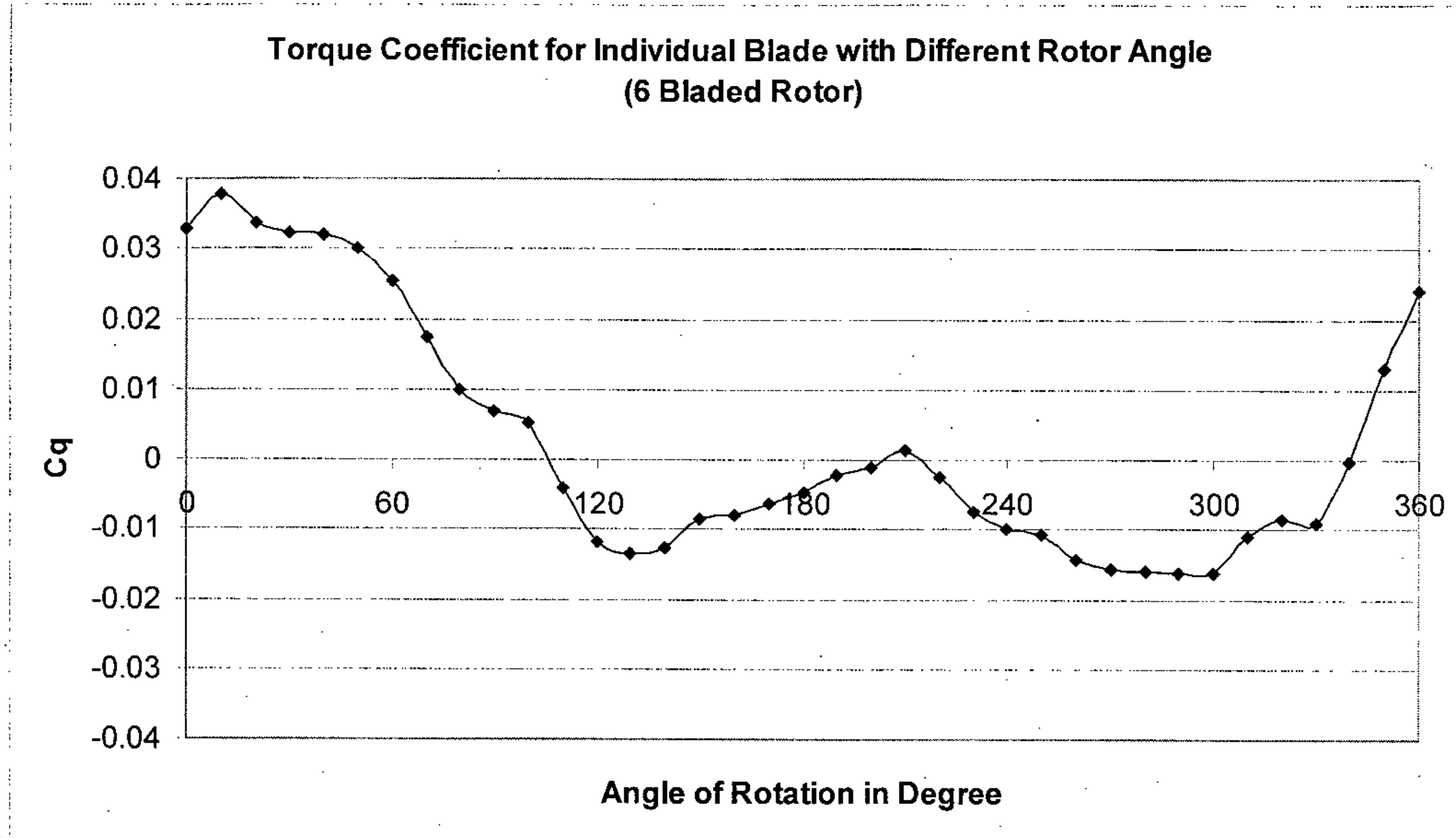

Figure 5.12(a): Torque coefficient with individual blade effect (for 6 bladed rotor)

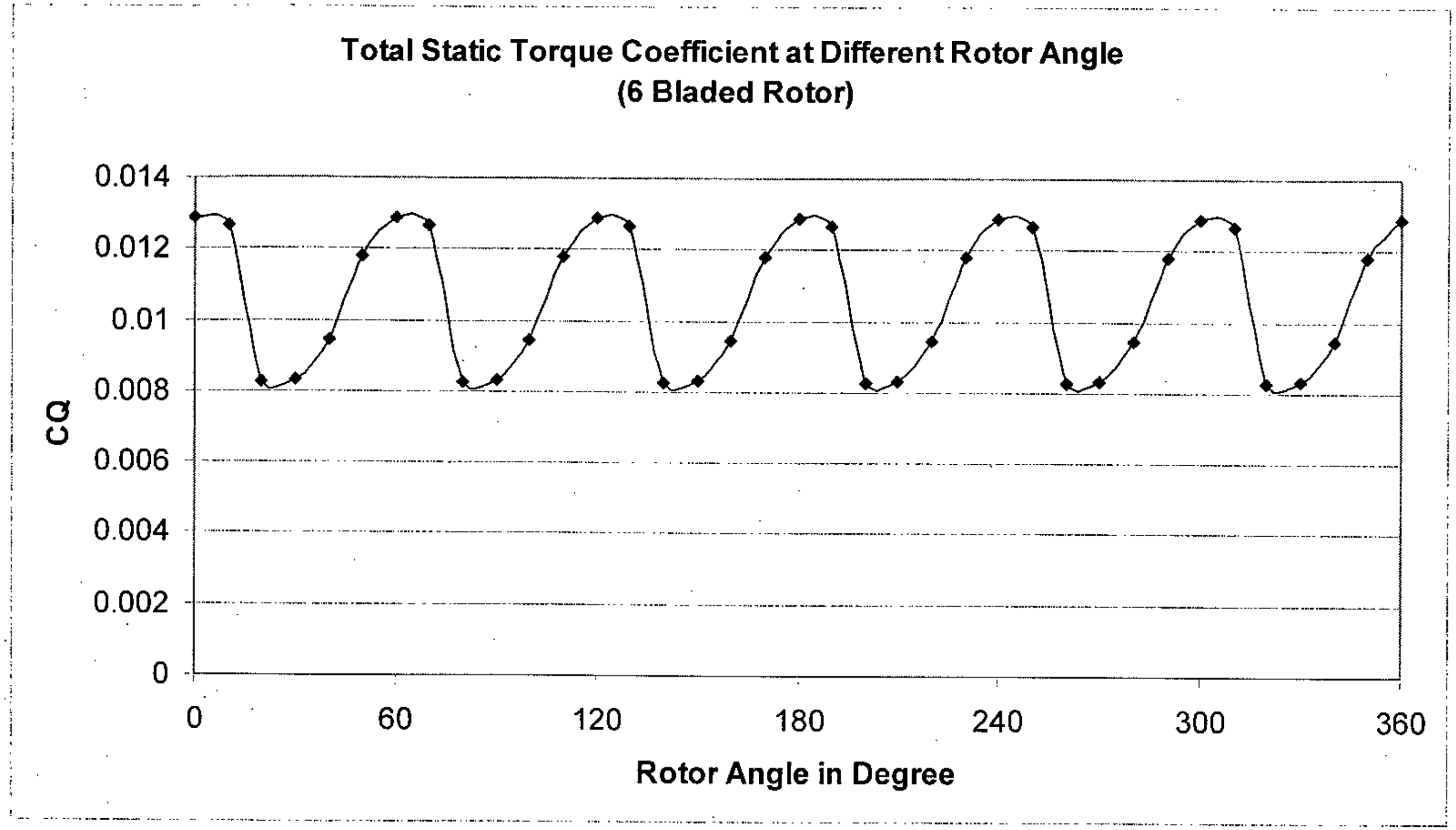

Figure 5.12(b): Total static torque coefficient at different rotor angle (for 6 bladed rotor)

5.3 Dynamic Aerodynamic Characteristics

5.3.1 Power Coefficient

The power coefficients for different speed ratios of 4 bladed, 5 bladed and 6 bladed vane rotors are shown in Figure 5.13, Figure 5.14 and Figure 5.15 respectively. Comparison of power coefficient for different speed ratio of 4, 5 and 6 bladed vane rotor is shown in Figure 5.16.

The power coefficients for different speed ratios are shown in Figure 5.17 along with measured data of Ogawa & Yashida [18], Islam et al [12], Rahman [2] and Bhuiyan [33]. Ogawa & Yashida [18] and Islam et al [12] both researchers worked with two bladed Savonius rotor. Rahman [2] studied three bladed Savonius rotor and Bhuiyan [33] experimented and analyzed aerodynamic characteristics of four bladed Savonius rotor. The power coefficient obtained in the present experiment matches qualitatively with the measured data, but shows a greater deviation.

The nature of curves for all the cases is similar. The present method assumes a potential vortex, however, in reality the flow field around a rotating rotor is also dependent and governed by shear layers, flow separation, high turbulence level, etc. Furthermore, the effect of wake formation has not been considered in the present study.

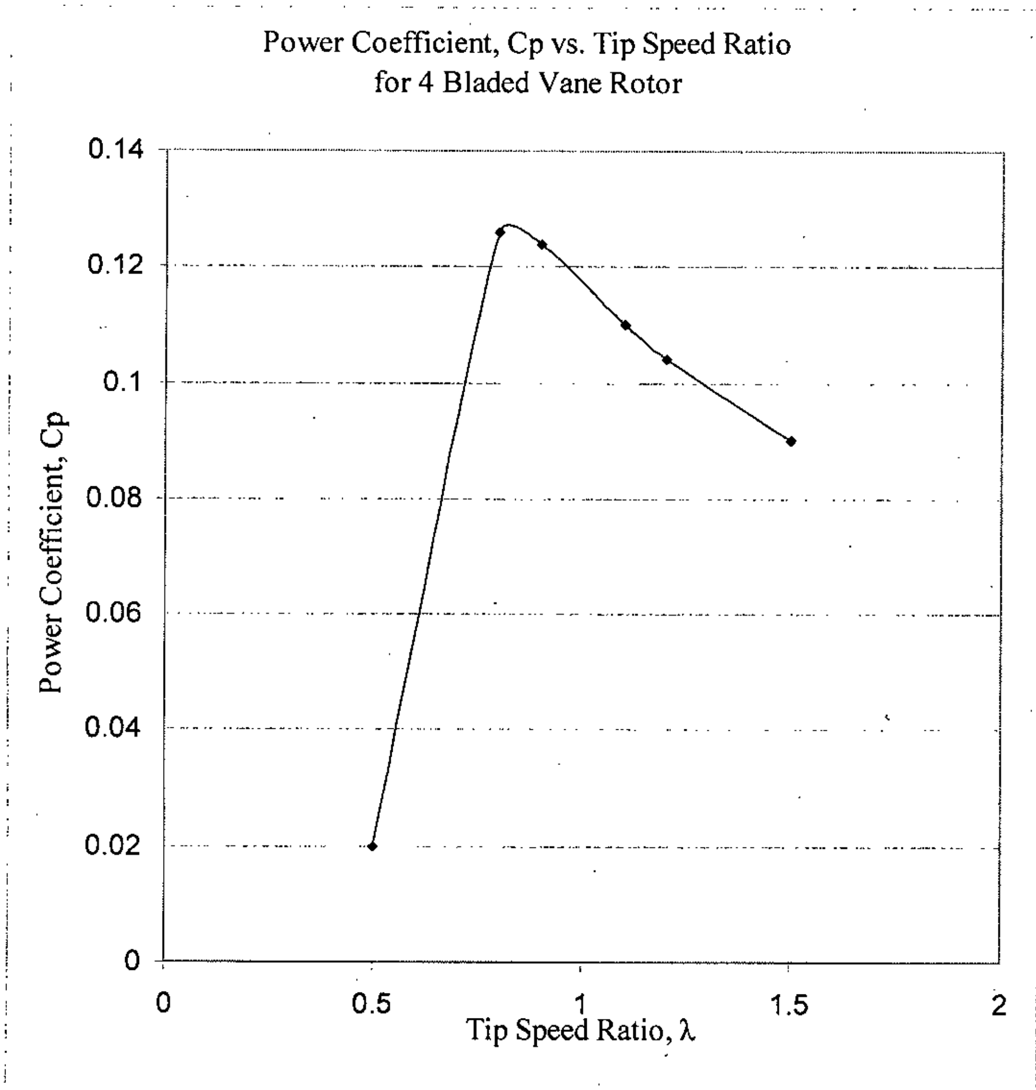

Figure 5.13: Power Coefficient vs. Tip speed ratio curve for 4 bladed Vane rotor.

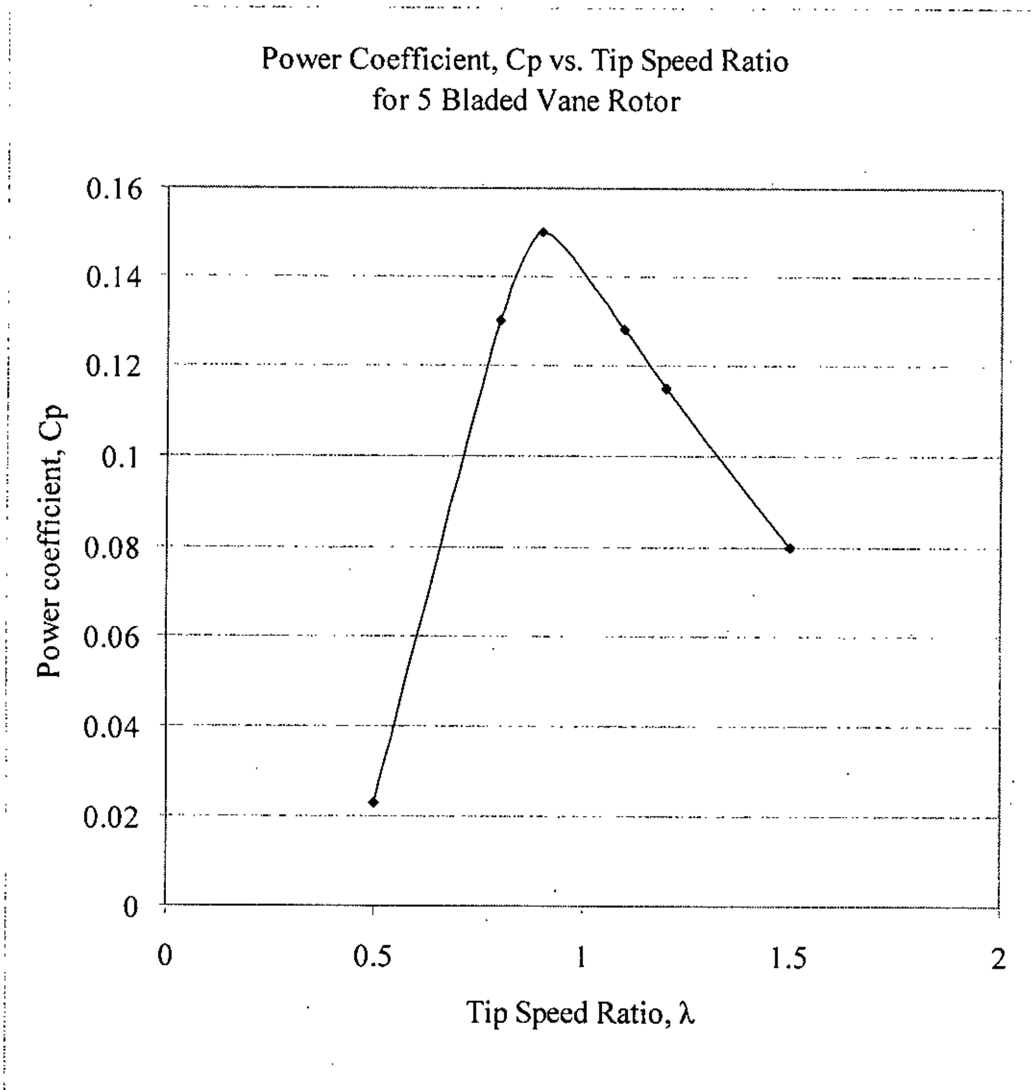

Figure 5.14: Power Coefficient vs. Tip speed ratio curve for 5 bladed Vane rotor.

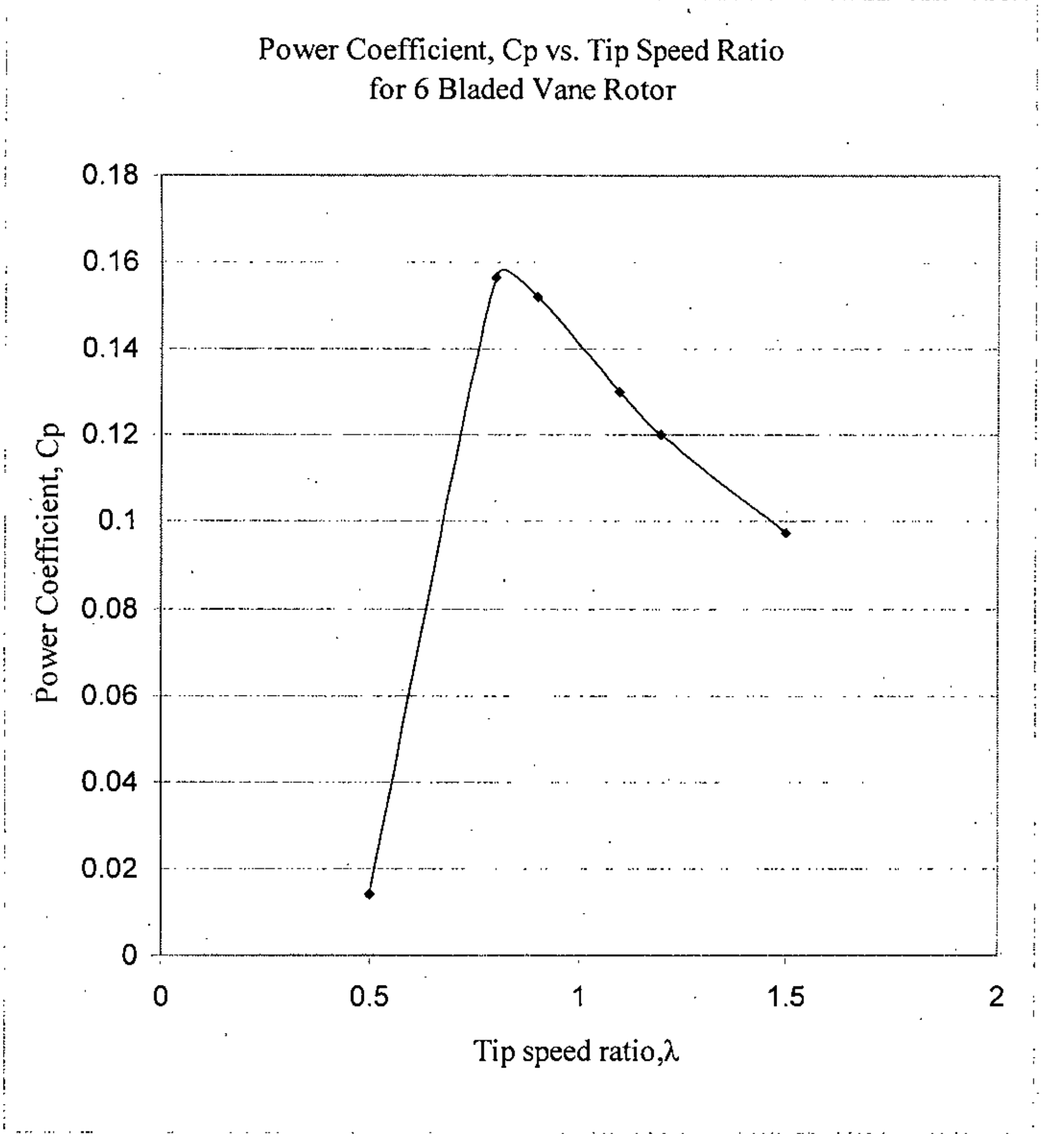

Figure 5.15: Power Coefficient vs. Tip Speed Ratio curve for 6 bladed Vane Rotor.

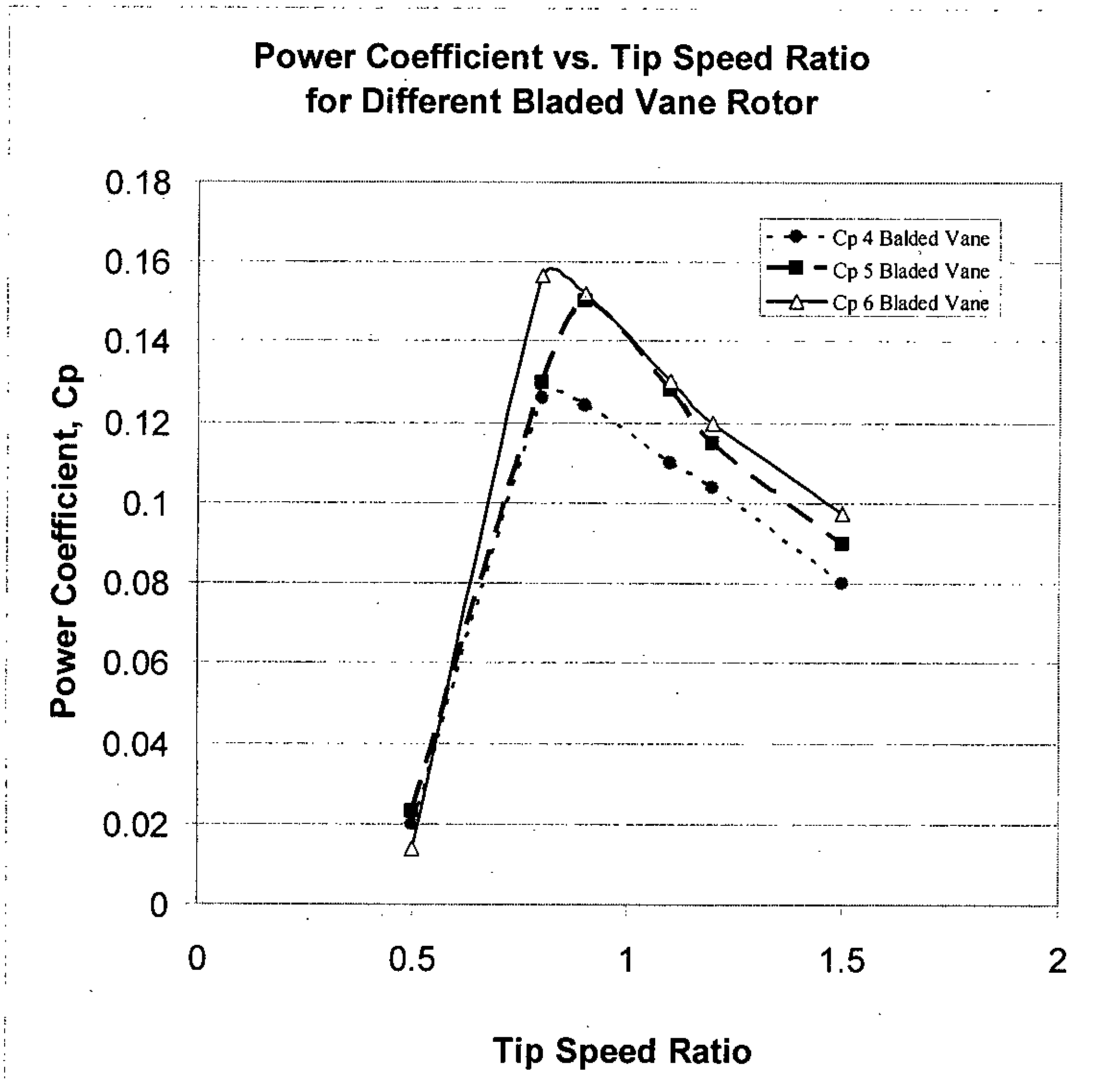

Figure 5.16: Comparison of power coefficient vs. tip speed ratio curve for 4 bladed, 5 bladed and 6 bladed vane rotor.

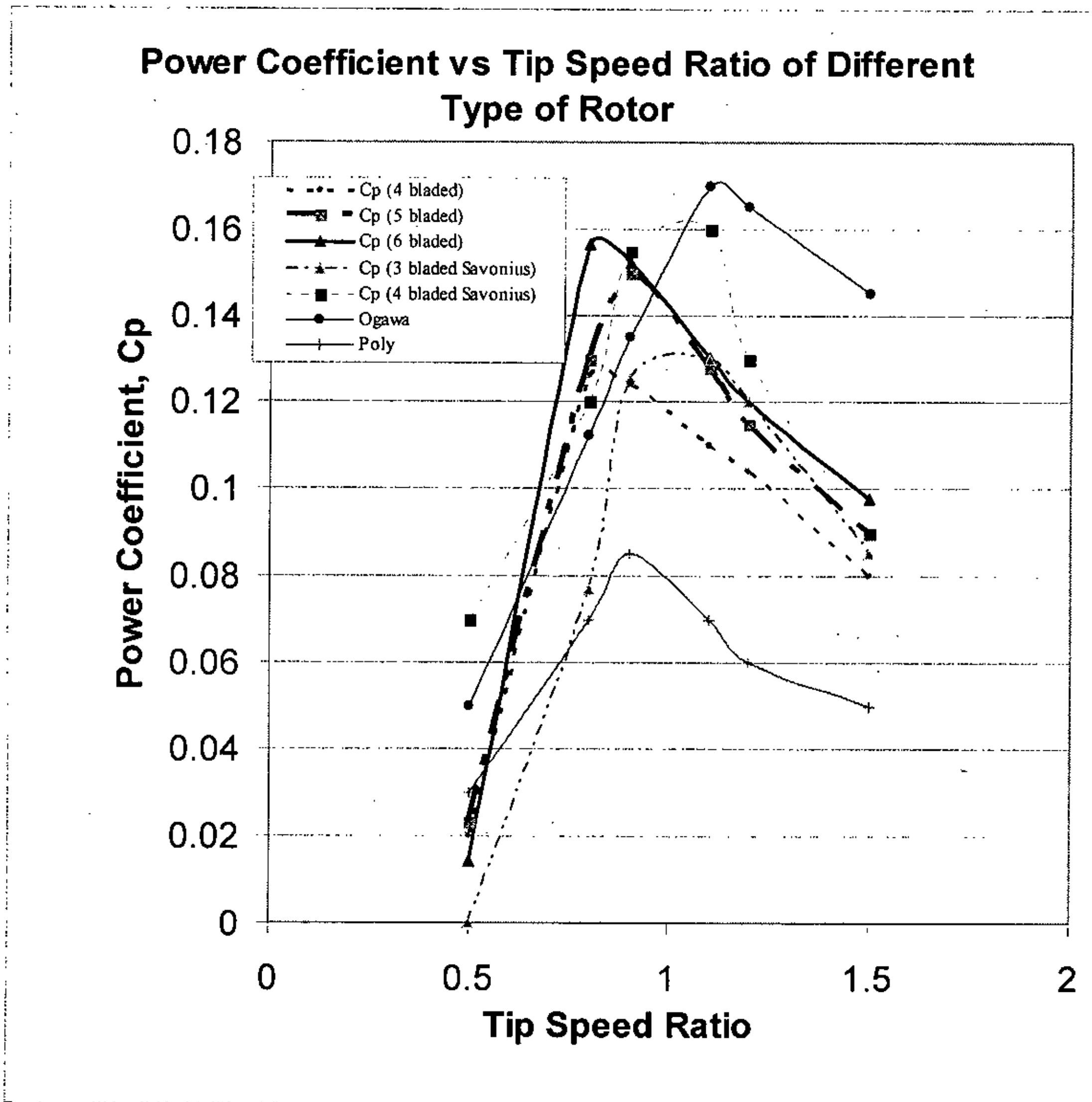

Figure 5.17: Comparison of power coefficient vs. tip speed ratio for different type of rotor.

CHAPTER 6

CONCLUSIONS AND RECOMMENDATIONS

Chapter-6

CONCLUSIONS AND RECOMMENDATIONS

6.1 Conclusions

The present work concerns study of the pressure distribution over the individual blades of the four-bladed, five-bladed and six-bladed vane rotor on both the convex and the concave surfaces at different angles of rotation. A computer programming was performed using C++ language to calculate forces experienced by the rotor blades and also the drag coefficients and torque coefficients by using raw data from the experiment. In the dynamic part of this research work, the power coefficient (C_p) was calculated using the value of the component of relative velocity V_w, along the free stream velocity U_o, and the static normal drag coefficient C_n for different tip speed ratio, λ. From the study, analysis and result of this research work, the following conclusions can be made:

1. It is concluded from the present work that flow separation takes place over the convex and concave surfaces of the blade and location of such separation point depends on the rotor angle.

2. The nature of the torque coefficient is opposite to that of the normal drag coefficient on the individual blade of the four, five and six bladed vane type rotor. This contributes significantly for producing torque. The value of torque coefficient is smaller than that of normal drag coefficient experienced with individual blade.

3. Total static torque coefficients for four, five and six bladed vane rotor at different rotor angle were analyzed in the present research work. For four and five bladed rotor, it is observed that the nature of the curve is opposite to that of the normal drag coefficient due to combined effect. And the value of torque

coefficients is smaller than that of normal drag coefficient because of combined effect.

4. In the case of six bladed rotor, it is found that the curve repeats after 50° angle of rotation like that of the normal drag coefficient due to combined effect. And the value of torque coefficient is smaller than that of normal drag coefficient as a result of the combined effect.

5. For four, five and six bladed vane type rotor, the net torque is always positive.

6. It is concluded from the present study that six bladed vane type rotor provides more power among the four, five and six bladed vane rotor and five bladed rotor provides more power than four bladed rotor. In other words, more blades meant more power. However, there is an optimum limit depending on the diameter of the rotor, and size and shape of the blades, etc.

7. For study of dynamic characteristics, the measured power coefficients (C_p) for different tip speed ratio (λ) of the present research work matches with the nature of the theoretical C_p vs. λ curve. Comparing with the existing measured data, the present study agrees well with the curves of other research works. It is observed that the increase in the number of blades makes the nature of the C_p vs. λ curve steeper. Thus it can be concluded that by increasing the number of blades, the power output can also be increased.

6.2 Recommendations

1. The same experiment may be done with rotors having different shapes of the blades.

2. The effect of Reynolds number on the flow characteristics over four bladed, five bladed and six bladed vane and Savonius rotor may be investigated.

3. The same experiment can be done with flow visualization technique utilizing smoke tunnel or similar type of devices to get a better understanding about the pressure distribution, drag coefficient and torque coefficient and other parameter.

4. Further detailed research could also be conducted in this field by varying the numbers of blades.

REFERENCES

REFERENCES

[1] Islam, A.K.M.S, Islam, M.Q., Razzaque, M.M. and Ashraf, R. (1995), "Static Torque and Drag Characteristics of an S-shaped Savonius Rotor and Prediction of Dynamic Characteristics", Wind Engineering, Vol. 19, No. 6, U.K.

[2] Rahman, M. (2000), "Aerodynamic Characteristics of a Three Bladed Savonius Rotor", M.Sc. Engg. Thesis, Dept of Mech. Engg., BUET.

[3] Fujisawa, N. (1996), "Velocity Measurements and Numerical Calculations of Flow fields in and Around Savonius Rotors", Journal of Wind Engineering and Industrial Aerodynamics, Vol. 59, U.K.

[4] Gavalda, J.,Massons J.and Diaz, F. (1991) "Drag and Lift Coefficients of the Savonius Wind Machine", Wind Engineering, Vol. 15, No. 5, U.K.

[5] Huda, M.D., Selim, M.A., Islam, A.K., M., S. and Islam, M.Q. (1992), "The Performance of an S-shaped Savonius Rotor with a Deflecting Plate", RERIC Int. Energy Journal, Vol. 14, No. 1, Bangkok, Thailand.

[6] Aldos, T.K. (1984), "Savonius Rotor Using Swinging Blades as an Augmentation System", Wind Engineering, Vol. 18, No. 4, U.K.

[7] Aldos, T.K. and Obeidat, K.M. (1987), "Performance Analysis of Two Savonius Rotors Running Side by Side Using The Discrete Vortex Method", Wind Engineering, Vol. 11, No.5, U.K.

[8] Modi, V. J. and Fernando, M.S.U.K. (1981), "On The Performance of the Savonius Wind Turbine", Journal of Solar Energy Engineering, Vol. 111/71, U.K.

[9] Park, J. (1975), "Simplified Wind Power System for Experimentry", Helion Inc., California, USA.

[10] Ogowa, T., Tahara, K. and Suzuki, N. (1986), "Wind Tunnel Performance Data of the Savonius Rotor with Circular Guide Vanes", Bulletin of JSME, Vol. 29, No.253, Tokyo, Japan.

[11] Lysen, E.H., Bos, H.G. and Cordes, E.H. (1978), "Savonius Rotors for Water Pumping", SWD Publication, Amersfoort, The Netherlands.

[12] Islam, A.K.M.S, Islam, M.Q., Mandal, A.C. and Razzaque, M.M. (1993), "Aerodynamic Characteristics of a Stationary Savonius rotor", RERIC Int. Energy Journal, Vol. 15, No. 2. pp. 125-135.

[13] Bowdin, G.J. and McAleese, S.A. (1984), "The Properties of Isolated and Coupled Savonius Rotors", Wind Engineering, Vol. 8, No. 4, pp. 271-288.

[14] Templin, R. J. (1974), "Aerodynamic Performance Theory for the NRC Vertical Vertical-Axis Wind Turbine", National Research Council of Canada, Report LTR-LA-160.

[15] Noll, R.B. and Ham, N.D. (1980), "Analytical Evaluation of the Aerodynamics Performance of a High-Reliability Vertical- Axis Wind Turbine", Proceedings of AWEA National Conference.

[16] Wilson, R.E. and Lissaman, P.B.S. (1974), "Applied Aerodynamics of Wind Power Machines", Oregon State University, USA.

[17] Strickland, J.H. (1975), "The Darrieus Turbine: A Performance Prediction Model Using Multiple Streamtubes, Sanida Laboratories Report", SAND75-0431.

[18] Ogawa, T. and Yoshida, H. (1986), "The Effects of a Deflecting Plate and Rotor and Plates", Bull. JSME, vol. 29, pp. 2115-2121.

[19] Paraschivoiu, I. and Delclaux, F. (1983), "Double Multiple Streamtube Model with Recent Improvements", Journal of Energy, Vol. 7, No. 3, pp. 250-255.

[20] Paraschiviu, I., Fraunie, P. and Beguier, C. (1985), "Streamtube Expansion Effects on thr Darrieus Wind Turbine", Journal of Propulsion, Vol. 1, No. 2, pp. 150-155.

[21] Fanucci, J.B. and Watters, R.E. (1976), "Innovative Wind Machines: The Theoretical Performance of a Vertical-Axis Wind Turbine", Proceedings of the Vertical-Axis Wind Turbine Technology Workshop, Sandia Laboratories, SAND 76-5586, pp. 111-61-95.

[22] Holme, O. (1976), "A Contribution to the Aerodynamic Theory of the Vertical Axis Wind Turbine", Proceedings of the International Symposium on Wind Energy Systems, Cambridge, pp. c4-55-72.

[23] Wilson, R.E. (1978), "Vortex Sheet Analysis of the Giromill", ASME Journal of Fluid Engineering, Vol. 100, No. 3, pp. 340-342.

[24] Sawada, T., Nakamura, M. and Kamada, S. (1986), "Blade Force Measurement and Flow Visualization of Savonius Rotors", Bulletin of JSME. Vol. 29, No.253. Tokyo, Japan.

[25] Aldos, T.K. and Obeidat, K.M. (1987), "Performance Analysis of Two Savonius Rotors Running Side by Side Using The Discrete Vortex method", Wind Engineering, Vol. 11, No. 5.

[26] Jones, C. N., Littler, R.D. and Manser, B.L. (1979), "The Savonius Rotor Performance and Flow", 1st BWEA Workshop.

[27] Sivasegaram, S. and Sivapalan, S. (1983), "Augmentation of Power in Slow Running Vertical-Axis Wind Rotors Using Multiple Vanes", Wind Engineering, Vol. 7, No. 1.

[28] Newman, B.G. (1974), "Measurements on a Savonius Rotor with a Variable Gap", Proc. Symposium on Wind Energy: Achievements and Potential, Sherbrooke, Canada.

[29] Lysen, E. H. (1983), "Introduction to Wind Energy", Steering Committee of Wind Energy for Developing Countries, P.O. Box 85, Amersfoort, The Netherlands.

[30] Wilson, R.E. and Walker, S.N. (1981), "Performance Analysis Program for propeller Type Wind Turbines", Oregon State University, March, USA.

[31] Sivasegaram, S. (1977), "Design Parameters Affecting the performance of Resistance Type Rotors", Wind Engineering, Vol. 1, pp. 207-217.

[32] Beurskens, H.J.M. (1980), "Low Speed Water Pumping Wind Mills: Rotor Tests and Overall Performance", Proc. Of 3rd Int. Symp. on Wind Energy Systems, Copenhagen, Denmark.

[33] Bhuiyan, H. K. (2003), "Aerodynamic Characteristics of a Four Bladed Savonius Rotor", M.Sc. Engg. Thesis, Dept of Mech. Engg., BUET.

APPENDIX-A

PROGRAMMING CODE

```
/* PROGRAM FOR CALCULATING NORMAL & TANGENTIAL FORCE
   AND TORQUE USING EXPERIMENTAL RAW DATA  */

#include<iostream.h>
#include<math.h>
#include<conio.h>

void main()
{
 clrscr();
 int i, j;
 float DP[100][100],FN[100][100],ANG[100][100],FT[100][100],TQ[100][100];
 float dell,gama,d,pie,a,s;
 float FNF[100],FTF[100],TQF[100];

 gama=9.81;
 d= 0.065;
 a= 0.075;
 s= a/d;
 pie= 22/7;
 dell= d*10*pie/360;

 cout<<"enter the values of DP"<<endl;
 for(i=1;i<37;i++)
        for(j=1;j<9;j++)
        {
               cin>>DP[i][j];
        }

  for (i=1;i<37;i++)
        {
        FNF[i]=0.0;
```

```
TQF[i]=0.0;
FTF[i]=0.0;
        for (j=1;j<9;j++)
        {
        ANG[i][j]= (180/8)*(j-1);
        FN[i][j]= dell*gama*0.342*cos(ANG[i][j])*DP[i][j];
        FNF[i]=FNF[i]+FN[i][j];
        TQ[i][j]=FN[i][j]*(d/2)*(1-s);
        TQF[i]=TQF[i]+TQ[i][j];
        FT[i][j]= dell*gama*0.342*sin(ANG[i][j])*DP[i][j];
        FTF[i]=FTF[i]+FT[i][j];
        }
cout<<"FNF="<<FNF[i]<<'\t'<<"TQF ="<<TQF[i]<<'\t'<<"FTF
="<<FTF[i]<<endl;
FNF[i]=0.0;
TQF[i]=0.0;
FTF[i]=0.0;
}

  for (i=1;i<37;i++)
        {
        for (j=1;j<9;j++)
        {
        cout<<"DP ="<< DP[i][j]<<'\t'<<"FN ="<<FN[i][j]<<'\t'<<"TQ ="<<TQ[i][j]
        <<'\t'<<"FT ="<<FT[i][j]<<endl;
        }
        }
getch();
}
```

/* PROGRAM FOR INTEGRATION */

```
#include<iostream.h>
#include<math.h>
#include<conio.h>

void main()
{
 clrscr();
 int i, j;
 float DP[100][100],FN[100][100],ANG[100][100],FT[100][100],TQ[100][100];
 float dell,gama,d,pie,a,s,RO,U;
 float FNF[100],FTF[100],TQF[100],CN[100],CQ[100],CT[100];

 gama=9.81;
 d= 0.065;
 a= 0.075;
 s= a/d;
 pie= 22/7;
 dell= d*10*pie/360;
 RO=1.2;
 U=13;

 cout<<"enter the values of DP"<<endl;
 for(i=1;i<37;i++)
        for(j=1;j<9;j++)
                {
                cin>>DP[i][j];
                }

 for (i=1;i<37;i++)
        {
```

```
FNF[i]=0.0;
TQF[i]=0.0;
FTF[i]=0.0;
    for (j=1;j<9;j++)
    {
    ANG[i][j]= (180/8)*(j-1);
    FN[i][j]= dell*gama*0.342*cos(ANG[i][j])*DP[i][j];
    FNF[i]=FNF[i]+FN[i][j];
    TQ[i][j]=FN[i][j]*(d/2)*(1-s);
    TQF[i]=TQF[i]+TQ[i][j];
    FT[i][j]= dell*gama*0.342*sin(ANG[i][j])*DP[i][j];
    FTF[i]=FTF[i]+FT[i][j];
    }
CN[i]=FNF[i]/(0.5*RO*U*U*d);
CQ[i]=CN[i]*((1-s)/(2-s));
CT[i]=FTF[i]/(0.5*RO*U*U*d);
cout<<"CN ="<<CN[i]<<'\t'<<"CQ ="<<CQ[i]<<'\t'<<"CT= "<<CT[i]<<endl;
FNF[i]=0.0;
TQF[i]=0.0;
FTF[i]=0.0;
}

getch();
}
```

/* PROGRAM FOR COMBING THE EFFECT OF FOUR BLADES */

```
#include<iostream.h>
#include<math.h>
#include<conio.h>

void main()
{
        clrscr();
        int i, j;
        //float DP[100][100];
        float FN[100][100],ANG[100][100],FT[100][100],TQ[100][100];
        float dell,gama,d,pie,a,s,RO,U;
        float FNF[100],FTF[100],TQF[100],CN[100],CQ[100],CT[100];
        gama=9.81;
        d= 0.065;
        a= 0.075;
        s= a/d;
        pie= 22/7;
        dell= d*10*pie/360;
        RO=1.2;
        U=13;

        cout<<"Enter the values of DP"<<endl;
          for(i=1;i<37;i++)
                for(j=1;j<9;j++)
                        {
                        cin>>DP[i][j];
                        }
        for (i=1;i<37;i++)
                {FNF[i]=0.0;
                TQF[i]=0.0;
```

```
FTF[i]=0.0;
for (j=1;j<9;j++)
{
        ANG[i][j]= (180/8)*(j-1);
        FN[i][j]= dell*gama*0.342*cos(ANG[i][j])*DP[i][j];
        FNF[i]=FNF[i]+FN[i][j];
        TQ[i][j]=FN[i][j]*(d/2)*(1-s);
        TQF[i]=TQF[i]+TQ[i][j];
        FT[i][j]= dell*gama*0.342*sin(ANG[i][j])*DP[i][j];
        FTF[i]=FTF[i]+FT[i][j];
        }
CN[i]=FNF[i]/(0.5*RO*U*U*d);
CQ[i]=CN[i]*((1-s)/(2-s));
CT[i]=FTF[i]/(0.5*RO*U*U*d);
FNF[i]=0.0;
TQF[i]=0.0;
FTF[i]=0.0;
}

for(j=1;j<5;j++)
    for(i=1;i<10;i++)
    {
    CFNF[i]=FNF[i]+FNF[i+9]+FNF[i+18]+FNF[i+27];
    CFTF[i]=FTF[i]+FTF[i+9]+FTF[i+18]+FTF[i+27];
    CTQF[i]=TQF[i]+TQF[i+9]+TQF[i+18]+TQF[i+27];
    CCN[i]=CN[i]+CN[i+9]+CN[i+18]+CN[i+27];
    CCT[i]=CT[i]+CT[i+9]+CT[i+18]+CT[i+27];
    CCQ[i]=(CN[i]+CN[i+9]+CN[i+18]+CN[i+27])*((1-s)/((2-s)*(2-s)));
    cout<<"CCN ="<<CCN[i]<<'\t'<<"CCQ ="<<CCQ[i]<<'\t'<<"CCT=
    "<<CCT[i]<<endl;
    }
getch(); }
```

APPENDIX-B

EXPERIMENTAL DATA

4 Bladed Vertical Axis Vane Type Rotor

α = 0°

Tapping Point	Initial Reading (in of H2O)	α = 0° (in of H2O) (Convex surface)		Initial Reading (in of H2O)	α = 0° (in of H2O) (Concave surface)		Pressure Dff. DP (in of H2O)
1	2.15	2.3	-0.15	2.3	1.4	0.9	-1.05
2	2.3	2.4	-0.1	2.31	1.3	1.01	-1.11
3	2.22	2.4	-0.18	2.31	1.35	0.96	-1.14
4	2.1	1.6	0.5	2.4	1.4	1	-0.5
5	2.21	2.2	0.01	2.51	1.5	1.01	-1
6	2.35	3.5	-1.15	2.6	2	0.6	-1.75
7	2.48	4.1	-1.62	2.25	1.38	0.87	-2.49
8	2.3	3.5	-1.2	2.42	1.4	1.02	-2.22

4 Bladed Vertical Axis Vane Type Rotor

α = 10°

Tapping Point	Initial Reading (in of H2O)	α = 10° (in of H2O) (Convex surface)		Initial Reading (in of H2O)	α = 10° (in of H2O) (Concave surface)		Pressure Dff. DP (in of H2O)
1	2.15	2	0.15	2.3	0.93	1.37	-1.22
2	2.3	1.9	0.4	2.31	0.93	1.38	-0.98
3	2.22	1.02	1.2	2.31	1	1.31	-0.11
4	2.1	0.9	1.2	2.4	1.01	1.39	-0.19
5	2.21	1.6	0.61	2.51	1.25	1.26	-0.65
6	2.35	2.6	-0.25	2.6	1.55	1.05	-1.3
7	2.48	2.88	-0.4	2.25	1	1.25	-1.65
8	2.3	2.6	-0.3	2.42	1.1	1.32	-1.62

4 Bladed Vertical Axis Vane Type Rotor

α = 20°

Tapping Point	Initial Reading (in of H2O)	α = 20° (in of H2O) (Convex surface)		Initial Reading (in of H2O)	α = 20° (in of H2O) (Concave surface)		Pressure Dff. DP (in of H2O)
1	2.15	2.3	-0.15	2.3	0.9	1.4	-1.55
2	2.3	2.1	0.2	2.31	0.9	1.41	-1.21
3	2.22	1.2	1.02	2.31	1	1.31	-0.29
4	2.1	0.8	1.3	2.4	1	1.4	-0.1
5	2.21	1.01	1.2	2.51	1.12	1.39	-0.19
6	2.35	2.1	0.25	2.6	1.55	1.05	-0.8
7	2.48	3	-0.52	2.25	1	1.25	-1.77
8	2.3	2.5	-0.2	2.42	1.2	1.22	-1.42

4 Bladed Vertical Axis Vane Type Rotor
α = 30°

Tapping Point	Initial Reading (in of H2O)	α = 30° (in of H2O) (Convex surface)		Initial Reading (in of H2O)	α = 30° (in of H2O) (Concave surface)		Pressure Dff. DP (in of H2O)
1	2.15	2.3	-0.15	2.3	1.35	0.95	-1.1
2	2.3	1.9	0.4	2.31	1.2	1.11	-0.71
3	2.22	1.1	1.12	2.31	1.2	1.11	0.01
4	2.1	0.8	1.3	2.4	1.25	1.15	0.15
5	2.21	0.9	1.31	2.51	1.4	1.11	0.2
6	2.35	1.8	0.55	2.6	1.7	0.9	-0.35
7	2.48	2.9	-0.42	2.25	1.32	0.93	-1.35
8	2.3	2.6	-0.3	2.42	1.6	0.82	-1.12

4 Bladed Vertical Axis Vane Type Rotor
α = 40°

Tapping Point	Initial Reading (in of H2O)	α = 40° (in of H2O) (Convex surface)		Initial Reading (in of H2O)	α = 40° (in of H2O) (Concave surface)		Pressure Dff. DP (in of H2O)
1	2.15	2.3	-0.15	2.3	2.1	0.2	-0.35
2	2.3	1.8	0.5	2.31	1.9	0.41	0.09
3	2.22	1.15	1.07	2.31	1.8	0.51	0.56
4	2.1	0.82	1.28	2.4	2	0.4	0.88
5	2.21	0.8	1.41	2.51	2.1	0.41	1
6	2.35	1.4	0.95	2.6	2.1	0.5	0.45
7	2.48	2.5	-0.02	2.25	2	0.25	-0.27
8	2.3	2.5	-0.2	2.42	2.2	0.22	-0.42

4 Bladed Vertical Axis Vane Type Rotor
α = 50°

Tapping Point	Initial Reading (in of H2O)	α = 50° (in of H2O) (Convex surface)		Initial Reading (in of H2O)	α = 50° (in of H2O) (Concave surface)		Pressure Dff. DP (in of H2O)
1	2.15	2.3	-0.15	2.3	2.5	-0.2	0.05
2	2.3	2.1	0.2	2.31	2.5	-0.19	0.39
3	2.22	1.4	0.82	2.31	2.48	-0.17	0.99
4	2.1	1	1.1	2.4	2.55	-0.15	1.25
5	2.21	0.7	1.51	2.51	2.7	-0.19	1.7
6	2.35	1	1.35	2.6	2.2	0.4	0.95
7	2.48	1.95	0.53	2.25	2.5	-0.25	0.78
8	2.3	2.3	0	2.42	2.7	-0.28	0.28

4 Bladed Vertical Axis Vane Type Rotor

α = 60°

Tapping Point	Initial Reading (in of H2O)	α = 60° (in of H2O) (Convex surface)		Initial Reading (in of H2O)	α = 60° (in of H2O) (Concave surface)		Pressure Dff. DP (in of H2O)
1	2.15	2.2	-0.05	2.3	2.6	-0.3	0.25
2	2.3	2.22	0.08	2.31	2.6	-0.29	0.37
3	2.22	1.65	0.57	2.31	2.6	-0.29	0.86
4	2.1	1.12	0.98	2.4	2.68	-0.28	1.26
5	2.21	0.82	1.39	2.51	2.9	-0.39	1.78
6	2.35	0.82	1.53	2.6	2.3	0.3	1.23
7	2.48	1.5	0.98	2.25	2.6	-0.35	1.33
8	2.3	2	0.3	2.42	2.8	-0.38	0.68

4 Bladed Vertical Axis Vane Type Rotor

α = 70°

Tapping Point	Initial Reading (in of H2O)	α = 70° (in of H2O) (Convex surface)		Initial Reading (in of H2O)	α = 70° (in of H2O) (Concave surface)		Pressure Dff. DP (in of H2O)
1	2.15	2.5	-0.35	2.3	2.6	-0.3	-0.05
2	2.3	2.55	-0.25	2.31	2.65	-0.34	0.09
3	2.22	2	0.22	2.31	2.7	-0.39	0.61
4	2.1	1.45	0.65	2.4	2.7	-0.3	0.95
5	2.21	1.1	1.11	2.51	2.9	-0.39	1.5
6	2.35	0.8	1.55	2.6	2.3	0.3	1.25
7	2.48	1.15	1.33	2.25	2.6	-0.35	1.68
8	2.3	1.7	0.6	2.42	2.8	-0.38	0.98

4 Bladed Vertical Axis Vane Type Rotor

α = 80°

Tapping Point	Initial Reading (in of H2O)	α = 80° (in of H2O) (Convex surface)		Initial Reading (in of H2O)	α = 80° (in of H2O) (Concave surface)		Pressure Dff. DP (in of H2O)
1	2.15	2	0.15	2.3	2.4	-0.1	0.25
2	2.3	2.3	0	2.31	2.5	-0.19	0.19
3	2.22	2.1	0.12	2.31	2.5	-0.19	0.31
4	2.1	1.7	0.4	2.4	2.56	-0.16	0.56
5	2.21	1.6	0.61	2.51	2.7	-0.19	0.8
6	2.35	1	1.35	2.6	2.25	0.35	1
7	2.48	0.9	1.58	2.25	2.5	-0.25	1.83
8	2.3	1.1	1.2	2.42	2.6	-0.18	1.38

4 Bladed Vertical Axis Vane Type Rotor
α = 90°

Tapping Point	Initial Reading (in of H2O)	α = 90° (in of H2O) (Convex surface)		Initial Reading (in of H2O)	α = 90° (in of H2O) (Concave surface)		Pressure Dff. DP (in of H2O)
1	2.15	1.72	0.43	2.3	2.4	-0.1	0.53
2	2.3	1.9	0.4	2.31	2.5	-0.19	0.59
3	2.22	2	0.22	2.31	2.48	-0.17	0.39
4	2.1	2	0.1	2.4	2.5	-0.1	0.2
5	2.21	2.15	0.06	2.51	2.7	-0.19	0.25
6	2.35	1.55	0.8	2.6	2.2	0.4	0.4
7	2.48	1.1	1.38	2.25	2.4	-0.15	1.53
8	2.3	0.9	1.4	2.42	2.6	-0.18	1.58

4 Bladed Vertical Axis Vane Type Rotor
α = 100°

Tapping Point	Initial Reading (in of H2O)	α = 100° (in of H2O) (Convex surface)		Initial Reading (in of H2O)	α = 100° (in of H2O) (Concave surface)		Pressure Dff. DP (in of H2O)
1	2.15	1.6	0.55	2.3	2.4	-0.1	0.65
2	2.3	1.6	0.7	2.31	2.5	-0.19	0.89
3	2.22	1.6	0.62	2.31	2.5	-0.19	0.81
4	2.1	1.6	0.5	2.4	2.6	-0.2	0.7
5	2.21	1.65	0.56	2.51	2.8	-0.29	0.85
6	2.35	1.75	0.6	2.6	2.3	0.3	0.3
7	2.48	1.3	1.18	2.25	2.5	-0.25	1.43
8	2.3	0.92	1.38	2.42	2.6	-0.18	1.56

Figure 4.1 : Schematic diagram of wind tunnel

4 Bladed Vertical Axis Vane Type Rotor
α = 110°

Tapping Point	Initial Reading (in of H2O)	α = 110° (in of H2O) (Convex surface)		Initial Reading (in of H2O)	α = 110° (in of H2O) (Concave surface)		Pressure Dff. DP (in of H2O)
1	2.15	1.8	0.35	2.3	2.3	0	0.35
2	2.3	1.9	0.4	2.31	2.32	-0.01	0.41
3	2.22	2.1	0.12	2.31	2.36	-0.05	0.17
4	2.1	1.9	0.2	2.4	2.45	-0.05	0.25
5	2.21	1.88	0.33	2.51	2.6	-0.09	0.42
6	2.35	1.92	0.43	2.6	2.2	0.4	0.03
7	2.48	2.02	0.46	2.25	2.3	-0.05	0.51
8	2.3	1.45	0.85	2.42	2.5	-0.08	0.93

4 Bladed Vertical Axis Vane Type Rotor
α = 120°

Tapping Point	Initial Reading (in of H2O)	α = 120° (in of H2O) (Convex surface)		Initial Reading (in of H2O)	α = 120° (in of H2O) (Concave surface)		Pressure Dff. DP (in of H2O)
1	2.15	2.2	-0.05	2.3	2.22	0.08	-0.13
2	2.3	2.25	0.05	2.31	2.3	0.01	0.04
3	2.22	2.3	-0.08	2.31	2.3	0.01	-0.09
4	2.1	2.1	0	2.4	2.4	0	0
5	2.21	2.2	0.01	2.51	2.5	0.01	0
6	2.35	2.4	-0.05	2.6	2.2	0.4	-0.45
7	2.48	2.75	-0.27	2.25	2.25	0	-0.27
8	2.3	2.7	-0.4	2.42	2.42	0	-0.4

4 Bladed Vertical Axis Vane Type Rotor
α = 130°

Tapping Point	Initial Reading (in of H2O)	α = 130° (in of H2O) (Convex surface)		Initial Reading (in of H2O)	α = 130° (in of H2O) (Concave surface)		Pressure Dff. DP (in of H2O)
1	2.15	2.1	0.05	2.3	2.28	0.02	0.03
2	2.3	2.1	0.2	2.31	2.3	0.01	0.19
3	2.22	2.35	-0.13	2.31	2.3	0.01	-0.14
4	2.1	2.1	0	2.4	2.4	0	0
5	2.21	2.24	-0.03	2.51	2.52	-0.01	-0.02
6	2.35	2.25	0.1	2.6	2.18	0.42	-0.32
7	2.48	2.45	0.03	2.25	2.3	-0.05	0.08
8	2.3	2.32	-0.02	2.42	2.5	-0.08	0.06

4 Bladed Vertical Axis Vane Type Rotor
α = 140°

Tapping Point	Initial Reading (in of H2O)	α = 140° (in of H2O) (Convex surface)		Initial Reading (in of H2O)	α = 140° (in of H2O) (Concave surface)		Pressure Dff. DP (in of H2O)
1	2.15	2.22	-0.07	2.3	2.3	0	-0.07
2	2.3	2.3	0	2.31	2.3	0.01	-0.01
3	2.22	2.4	-0.18	2.31	2.32	-0.01	-0.17
4	2.1	2.2	-0.1	2.4	2.4	0	-0.1
5	2.21	2.3	-0.09	2.51	2.6	-0.09	4.44089E-16
6	2.35	2.52	-0.17	2.6	2.2	0.4	-0.57
7	2.48	3.2	-0.72	2.25	2.3	-0.05	-0.67
8	2.3	31	-28.7	2.42	2.5	-0.08	-28.62

4 Bladed Vertical Axis Vane Type Rotor
α = 150°

Tapping Point	Initial Reading (in of H2O)	α = 150° (in of H2O) (Convex surface)		Initial Reading (in of H2O)	α = 150° (in of H2O) (Concave surface)		Pressure Dff. DP (in of H2O)
1	2.15	2.1	0.05	2.3	2.4	-0.1	0.15
2	2.3	2.42	-0.12	2.31	2.5	-0.19	0.07
3	2.22	2.35	-0.13	2.31	2.5	-0.19	0.06
4	2.1	2.12	-0.02	2.4	2.52	-0.12	0.1
5	2.21	2.3	-0.09	2.51	2.7	-0.19	0.1
6	2.35	2.48	-0.13	2.6	2.22	0.38	-0.51
7	2.48	2.6	-0.12	2.25	2.25	0	-0.12
8	2.3	2.6	-0.3	2.42	2.66	-0.24	-0.06

4 Bladed Vertical Axis Vane Type Rotor
α = 160°

Tapping Point	Initial Reading (in of H2O)	α = 160° (in of H2O) (Convex surface)		Initial Reading (in of H2O)	α = 160° (in of H2O) (Concave surface)		Pressure Dff. DP (in of H2O)
1	2.15	2	0.15	2.3	2.44	-0.14	0.29
2	2.3	2.3	0	2.31	2.5	-0.19	0.19
3	2.22	2.28	-0.06	2.31	2.5	-0.19	0.13
4	2.1	2.1	0	2.4	2.58	-0.18	0.18
5	2.21	2.2	0.01	2.51	2.58	-0.07	0.08
6	2.35	2.4	-0.05	2.6	2.7	-0.1	0.05
7	2.48	2.5	-0.02	2.25	2.25	0	-0.02
8	2.3	2.36	-0.06	2.42	2.66	-0.24	0.18

4 Bladed Vertical Axis Vane Type Rotor
α = 170°

Tapping Point	Initial Reading (in of H2O)	α = 170° (in of H2O) (Convex surface)		Initial Reading (in of H2O)	α = 170° (in of H2O) (Concave surface)		Pressure Dff. DP (in of H2O)
1	2.15	2.05	0.1	2.3	2.5	-0.2	0.3
2	2.3	2.3	0	2.31	2.55	-0.24	0.24
3	2.22	2.28	-0.06	2.31	2.56	-0.25	0.19
4	2.1	2.1	0	2.4	2.6	-0.2	0.2
5	2.21	2.28	-0.07	2.51	2.8	-0.29	0.22
6	2.35	2.4	-0.05	2.6	2.3	0.3	-0.35
7	2.48	2.5	-0.02	2.25	2.5	-0.25	0.23
8	2.3	2.4	-0.1	2.42	2.7	-0.28	0.18

4 Bladed Vertical Axis Vane Type Rotor
α = 180°

Tapping Point.	Initial Reading (in of H2O)	α = 180° (in of H2O) (Convex surface)		Initial Reading (in of H2O)	α = 180° (in of H2O) (Concave surface)		Pressure Dff. DP (in of H2O)
1	2.15	2.05	0.1	2.3	2.58	-0.28	0.38
2	2.3	2.24	0.06	2.31	2.6	-0.29	0.35
3	2.22	2.2	0.02	2.31	2.62	-0.31	0.33
4	2.1	2.1	0	2.4	2.7	-0.3	0.3
5	2.21	2.22	-0.01	2.51	2.85	-0.34	0.33
6	2.35	2.4	-0.05	2.6	2.92	-0.32	0.27
7	2.48	2.5	-0.02	2.25	2.6	-0.35	0.33
8	2.3	2.4	-0.1	2.42	2.78	-0.36	0.26

4 Bladed Vertical Axis Vane Type Rotor
α = 190°

Tapping Point	Initial Reading (in of H2O)	α = 190° (in of H2O) (Convex surface)		Initial Reading (in of H2O)	α = 190° (in of H2O) (Concave surface)		Pressure Dff. DP (in of H2O)
1	2.15	2	0.15	2.3	2.55	-0.25	0.4
2	2.3	2.3	0	2.31	2.6	-0.29	0.29
3	2.22	2.32	-0.1	2.31	2.6	-0.29	0.19
4	2.1	2.12	-0.02	2.4	2.62	-0.22	0.2
5	2.21	2.2	0.01	2.51	2.82	-0.31	0.32
6	2.35	2.3	0.05	2.6	3	-0.4	0.45
7	2.48	2.4	0.08	2.25	2.6	-0.35	0.43
8	2.3	2.3	0	2.42	2.72	-0.3	0.3

4 Bladed Vertical Axis Vane Type Rotor
α = 200°

Tapping Point	Initial Reading (in of H2O)	α = 200° (in of H2O) (Convex surface)		Initial Reading (in of H2O)	α = 200° (in of H2O) (Concave surface)		Pressure Dff. DP (in of H2O)
1	2.15	2.6	-0.45	2.3	2.5	-0.2	-0.25
2	2.3	2.7	-0.4	2.31	2.5	-0.19	-0.21
3	2.22	2.35	-0.13	2.31	2.5	-0.19	0.06
4	2.1	2.2	-0.1	2.4	2.6	-0.2	0.1
5	2.21	2.3	-0.09	2.51	2.74	-0.23	0.14
6	2.35	2.38	-0.03	2.6	2.9	-0.3	0.27
7	2.48	2.4	0.08	2.25	2.58	-0.33	0.41
8	2.3	2.25	0.05	2.42	2.7	-0.28	0.33

4 Bladed Vertical Axis Vane Type Rotor
α = 210°

Tapping Point	Initial Reading (in of H2O)	α = 210° (in of H2O) (Convex surface)		Initial Reading (in of H2O)	α = 210° (in of H2O) (Concave surface)		Pressure Dff. DP (in of H2O)
1	2.15	2.2	-0.05	2.3	2.5	-0.2	0.15
2	2.3	2.01	0.29	2.31	2.5	-0.19	0.48
3	2.22	2.3	-0.08	2.31	2.51	-0.2	0.12
4	2.1	2.3	-0.2	2.4	2.6	-0.2	4.44089E-16
5	2.21	2.38	-0.17	2.51	2.3	0.21	-0.38
6	2.35	2.4	-0.05	2.6	2.9	-0.3	0.25
7	2.48	2.42	0.06	2.25	2.5	-0.25	0.31
8	2.3	2.3	0	2.42	2.7	-0.28	0.28

4 Bladed Vertical Axis Vane Type Rotor
α = 220°

Tapping Point	Initial Reading (in of H2O)	α = 220° (in of H2O) (Convex surface)		Initial Reading (in of H2O)	α = 220° (in of H2O) (Concave surface)		Pressure Dff. DP (in of H2O)
1	2.15	2.28	-0.13	2.3	2.5	-0.2	0.07
2	2.3	2.22	0.08	2.31	2.6	-0.29	0.37
3	2.22	2.32	-0.1	2.31	2.6	-0.29	0.19
4	2.1	2.32	-0.22	2.4	2.62	-0.22	4.44089E-16
5	2.21	2.3	-0.09	2.51	2.8	-0.29	0.2
6	2.35	2.31	0.04	2.6	3	-0.4	0.44
7	2.48	2.4	0.08	2.25	2.58	-0.33	0.41
8	2.3	2.32	-0.02	2.42	2.75	-0.33	0.31

4 Bladed Vertical Axis Vane Type Rotor
α = 230°

Tapping Point	Initial Reading (in of H2O)	α = 230° (in of H2O) (Convex surface)		Initial Reading (in of H2O)	α = 230° (in of H2O) (Concave surface)		Pressure Dff. DP (in of H2O)
1	2.15	2.3	-0.15	2.3	2.5	-0.2	0.05
2	2.3	2.2	0.1	2.31	2.52	-0.21	0.31
3	2.22	2.32	-0.1	2.31	2.6	-0.29	0.19
4	2.1	2.3	-0.2	2.4	2.7	-0.3	0.1
5	2.21	2.3	-0.09	2.51	2.9	-0.39	0.3
6	2.35	2.32	0.03	2.6	3.01	-0.41	0.44
7	2.48	2.42	0.06	2.25	2.51	-0.26	0.32
8	2.3	2.3	0	2.42	2.8	-0.38	0.38

4 Bladed Vertical Axis Vane Type Rotor
α = 240°

Tapping Point	Initial Reading (in of H2O)	α = 240° (in of H2O) (Convex surface)		Initial Reading (in of H2O)	α = 240° (in of H2O) (Concave surface)		Pressure Dff. DP (in of H2O)
1	2.15	2.16	-0.01	2.3	2.6	-0.3	0.29
2	2.3	2.3	0	2.31	2.7	-0.39	0.39
3	2.22	2.2	0.02	2.31	2.72	-0.41	0.43
4	2.1	2.1	0	2.4	2.78	-0.38	0.38
5	2.21	2.15	0.06	2.51	2.98	-0.47	0.53
6	2.35	2.3	0.05	2.6	3.1	-0.5	0.55
7	2.48	2.32	0.16	2.25	2.7	-0.45	0.61
8	2.3	2.22	0.08	2.42	2.82	-0.4	0.48

4 Bladed Vertical Axis Vane Type Rotor
α = 250°

Tapping Point	Initial Reading (in of H2O)	α = 250° (in of H2O) (Convex surface)		Initial Reading (in of H2O)	α = 250° (in of H2O) (Concave surface)		Pressure Dff. DP (in of H2O)
1	2.15	2.1	0.05	2.3	2.4	-0.1	0.15
2	2.3	2.25	0.05	2.31	2.4	-0.09	0.14
3	2.22	2.15	0.07	2.31	2.4	-0.09	0.16
4	2.1	2.02	0.08	2.4	2.5	-0.1	0.18
5	2.21	2.15	0.06	2.51	2.68	-0.17	0.23
6	2.35	2.28	0.07	2.6	2.8	-0.2	0.27
7	2.48	2.4	0.08	2.25	2.4	-0.15	0.23
8	2.3	2.3	0	2.42	2.6	-0.18	0.18

4 Bladed Vertical Axis Vane Type Rotor
α = 260°

Tapping Point	Initial Reading (in of H2O)	α = 260° (in of H2O) (Convex surface)		Initial Reading (in of H2O)	α = 260° (in of H2O) (Concave surface)		Pressure Dff. DP (in of H2O)
1	2.15	2.05	0.1	2.3	2.2	0.1	4.44089E-16
2	2.3	2.2	0.1	2.31	2.2	0.11	-0.01
3	2.22	2.2	0.02	2.31	2.2	0.11	-0.09
4	2.1	2	0.1	2.4	2.3	0.1	0
5	2.21	2.15	0.06	2.51	2.42	0.09	-0.03
6	2.35	2.3	0.05	2.6	2.58	0.02	0.03
7	2.48	2.42	0.06	2.25	2.2	0.05	0.01
8	2.3	2.3	0	2.42	2.4	0.02	-0.02

4 Bladed Vertical Axis Vane Type Rotor

$\alpha = 270°$

Tapping Point	Initial Reading (in of H2O)	α = 270° (in of H2O) (Convex surface)		Initial Reading (in of H2O)	α = 270° (in of H2O) (Concave surface)		Pressure Dff. DP (in of H2O)
1	2.15	1.8	0.35	2.3	1.8	0.5	-0.15
2	2.3	3	-0.7	2.31	1.8	0.51	-1.21
3	2.22	3.1	-0.88	2.31	1.8	0.51	-1.39
4	2.1	2.3	-0.2	2.4	1.9	0.5	-0.7
5	2.21	2.3	-0.09	2.51	2	0.51	-0.6
6	2.35	2.4	-0.05	2.6	2.2	0.4	-0.45
7	2.48	2.5	-0.02	2.25	1.8	0.45	-0.47
8	2.3	2.4	-0.1	2.42	1.98	0.44	-0.54

4 Bladed Vertical Axis Vane Type Rotor

$\alpha = 280°$

Tapping Point	Initial Reading (in of H2O)	α = 280° (in of H2O) (Convex surface)		Initial Reading (in of H2O)	α = 280° (in of H2O) (Concave surface)		Pressure Dff. DP (in of H2O)
1	2.15	1.3	0.85	2.3	2	0.3	0.55
2	2.3	2.4	-0.1	2.31	2	0.31	-0.41
3	2.22	3.1	-0.88	2.31	2	0.31	-1.19
4	2.1	2.32	-0.22	2.4	2.1	0.3	-0.52
5	2.21	2.2	0.01	2.51	2.2	0.31	-0.3
6	2.35	2.3	0.05	2.6	2.3	0.3	-0.25
7	2.48	2.4	0.08	2.25	1.9	0.35	-0.27
8	2.3	2.22	0.08	2.42	2.1	0.32	-0.24

4 Bladed Vertical Axis Vane Type Rotor

$\alpha = 290°$

Tapping Point	Initial Reading (in of H2O)	α = 290° (in of H2O) (Convex surface)		Initial Reading (in of H2O)	α = 290° (in of H2O) (Concave surface)		Pressure Dff. DP (in of H2O)
1	2.15	1.01	1.14	2.3	1.38	0.92	0.22
2	2.3	2.3	0	2.31	1.4	0.91	-0.91
3	2.22	2.6	-0.38	2.31	1.4	0.91	-1.29
4	2.1	2.22	-0.12	2.4	1.5	0.9	-1.02
5	2.21	2.3	-0.09	2.51	1.52	0.99	-1.08
6	2.35	2.4	-0.05	2.6	1.7	0.9	-0.95
7	2.48	2.5	-0.02	2.25	1.3	0.95	-0.97
8	2.3	2.35	-0.05	2.42	1.4	1.02	-1.07

4 Bladed Vertical Axis Vane Type Rotor
α = 300°

Tapping Point	Initial Reading (in of H2O)	α = 300° (in of H2O) (Convex surface)		Initial Reading (in of H2O)	α = 300° (in of H2O) (Concave surface)		Pressure Dff. DP (in of H2O)
1	2.15	1	1.15	2.3	1	1.3	-0.15
2	2.3	2.22	0.08	2.31	1.08	1.23	-1.15
3	2.22	2.5	-0.28	2.31	1.1	1.21	-1.49
4	2.1	2.2	-0.1	2.4	1.1	1.3	-1.4
5	2.21	2.28	-0.07	2.51	1.22	1.29	-1.36
6	2.35	2.4	-0.05	2.6	1.4	1.2	-1.25
7	2.48	2.5	-0.02	2.25	1.1	1.15	-1.17
8	2.3	2.3	0	2.42	1.2	1.22	-1.22

4 Bladed Vertical Axis Vane Type Rotor
α = 310°

Tapping Point	Initial Reading (in of H2O)	α = 310° (in of H2O) (Convex surface)		Initial Reading (in of H2O)	α = 310° (in of H2O) (Concave surface)		Pressure Dff. DP (in of H2O)
1	2.15	0.95	1.2	2.3	0.9	1.4	-0.2
2	2.3	2.2	0.1	2.31	0.9	1.41	-1.31
3	2.22	2.28	-0.06	2.31	0.95	1.36	-1.42
4	2.1	2.1	0	2.4	1	1.4	-1.4
5	2.21	2.28	-0.07	2.51	1.1	1.41	-1.48
6	2.35	2.4	-0.05	2.6	1.3	1.3	-1.35
7	2.48	2.5	-0.02	2.25	1	1.25	-1.27
8	2.3	2.38	-0.08	2.42	1.1	1.32	-1.4

4 Bladed Vertical Axis Vane Type Rotor
α = 320°

Tapping Point	Initial Reading (in of H2O)	α = 320° (in of H2O) (Convex surface)		Initial Reading (in of H2O)	α = 320° (in of H2O) (Concave surface)		Pressure Dff. DP (in of H2O)
1	2.15	0.99	1.16	2.3	0.89	1.41	-0.25
2	2.3	2.4	-0.1	2.31	0.89	1.42	-1.52
3	2.22	2.5	-0.28	2.31	0.94	1.37	-1.65
4	2.1	2.3	-0.2	2.4	0.99	1.41	-1.61
5	2.21	2.5	-0.29	2.51	1.1	1.41	-1.7
6	2.35	2.8	-0.45	2.6	1.28	1.32	-1.77
7	2.48	2.58	-0.1	2.25	0.99	1.26	-1.36
8	2.3	2.39	-0.09	2.42	1.09	1.33	-1.42

4 Bladed Vertical Axis Vane Type Rotor

α = 330°

Tapping Point	Initial Reading (in of H2O)	α = 330° (in of H2O) (Convex surface)		Initial Reading (in of H2O)	α = 330° (in of H2O) (Concave surface)		Pressure Dff. DP (in of H2O)
1	2.15	1	1.15	2.3	0.9	1.4	-0.25
2	2.3	2.7	-0.4	2.31	0.9	1.41	-1.81
3	2.22	3.7	-1.48	2.31	0.92	1.39	-2.87
4	2.1	3.2	-1.1	2.4	1	1.4	-2.5
5	2.21	3.1	-0.89	2.51	1.1	1.41	-2.3
6	2.35	3.35	-1	2.6	1.3	1.3	-2.3
7	2.48	3.25	-0.77	2.25	1	1.25	-2.02
8	2.3	2.66	-0.36	2.42	1.1	1.32	-1.68

4 Bladed Vertical Axis Vane Type Rotor

α = 340°

Tapping Point	Initial Reading (in of H2O)	α = 340° (in of H2O) (Convex surface)		Initial Reading (in of H2O)	α = 340° (in of H2O) (Concave surface)		Pressure Dff. DP (in of H2O)
1	2.15	1	1.15	2.3	0.9	1.4	-0.25
2	2.3	2.5	-0.2	2.31	0.9	1.41	-1.61
3	2.22	3.3	-1.08	2.31	0.98	1.33	-2.41
4	2.1	2.8	-0.7	2.4	1	1.4	-2.1
5	2.21	2.99	-0.78	2.51	1.12	1.39	-2.17
6	2.35	3.5	-1.15	2.6	1.3	1.3	-2.45
7	2.48	3.7	-1.22	2.25	1	1.25	-2.47
8	2.3	2.89	-0.59	2.42	1.1	1.32	-1.91

4 Bladed Vertical Axis Vane Type Rotor

α = 350°

Tapping Point	Initial Reading (in of H2O)	α = 350° (in of H2O) (Convex surface)		Initial Reading (in of H2O)	α = 350° (in of H2O) (Concave surface)		Pressure Dff. DP (in of H2O)
1	2.15	1.5	0.65	2.3	0.9	1.4	-0.75
2	2.3	2	0.3	2.31	0.9	1.41	-1.11
3	2.22	1.9	0.32	2.31	0.99	1.32	-1
4	2.1	1.88	0.22	2.4	1	1.4	-1.18
5	2.21	2.1	0.11	2.51	1.12	1.39	-1.28
6	2.35	3.1	-0.75	2.6	1.3	1.3	-2.05
7	2.48	3.54	-1.06	2.25	1	1.25	-2.31
8	2.3	2.82	-0.52	2.42	1.1	1.32	-1.84

5 Bladed Vertical Axis Vane Type Rotor

α = 0°

Tapping Point	Initial Reading (in of H2O)	α = 0° (in of H2O) (Convex surface)		Initial Reading (in of H2O)	α = 0° (in of H2O) (Concave surface)		Pressure Dff. DP (in of H2O)
1	2.7	1.7	1	2.9	1.9	1	0
2	2.8	3.22	-0.42	2.82	1.98	0.84	-1.26
3	2.75	3.75	-1	2.8	1.85	0.95	-1.95
4	2.75	3.4	-0.65	2.9	2.1	0.8	-1.45
5	2.79	3.28	-0.49	3.01	2.1	0.91	-1.4
6	2.9	3.51	-0.61	2.85	1.92	0.93	-1.54
7	3	4	-1	3.05	2.1	0.95	-1.95
8	2.89	3.6	-0.71	3.1	2.1	1	-1.71

5 Bladed Vertical Axis Vane Type Rotor

α = 10°

Tapping Point	Initial Reading (in of H2O)	α = 10° (in of H2O) (Convex surface)		Initial Reading (in of H2O)	α = 10° (in of H2O) (Concave surface)		Pressure Dff. DP (in of H2O)
1	2.7	1.8	0.9	2.9	1.9	1	-0.1
2	2.8	3.5	-0.7	2.82	2	0.82	-1.52
3	2.75	4.5	-1.75	2.8	1.9	0.9	-2.65
4	2.75	4	-1.25	2.9	2.1	0.8	-2.05
5	2.79	3.61	-0.82	3.01	2.15	0.86	-1.68
6	2.9	3.6	-0.7	2.85	2	0.85	-1.55
7	3	3.75	-0.75	3.05	2.1	0.95	-1.7
8	2.89	3.4	-0.51	3.1	2.1	1	-1.51

5 Bladed Vertical Axis Vane Type Rotor

α = 20°

Tapping Point	Initial Reading (in of H2O)	α = 20° (in of H2O) (Convex surface)		Initial Reading (in of H2O)	α = 20° (in of H2O) (Concave surface)		Pressure Dff. DP (in of H2O)
1	2.7	1.9	0.8	2.9	2	0.9	-0.1
2	2.8	3.5	-0.7	2.82	2.1	0.72	-1.42
3	2.75	4.5	-1.75	2.8	1.94	0.86	-2.61
4	2.75	4	-1.25	2.9	2.2	0.7	-1.95
5	2.79	3.5	-0.71	3.01	2.22	0.79	-1.5
6	2.9	3.3	-0.4	2.85	2.04	0.81	-1.21
7	3	3.4	-0.4	3.05	2.18	0.87	-1.27
8	2.89	3.2	-0.31	3.1	2.1	1	-1.31

5 Bladed Vertical Axis Vane Type Rotor

α = 30°

Tapping Point	Initial Reading (in of H2O)	α = 30° (in of H2O) (Convex surface)		Initial Reading (in of H2O)	α = 30° (in of H2O) (Concave surface)		Pressure Dff. DP (in of H2O)
1	2.7	1.75	0.95	2.9	2.3	0.6	0.35
2	2.8	3	-0.2	2.82	2.4	0.42	-0.62
3	2.75	3.2	-0.45	2.8	2.28	0.52	-0.97
4	2.75	3.1	-0.35	2.9	2.4	0.5	-0.85
5	2.79	3.1	-0.31	3.01	2.5	0.51	-0.82
6	2.9	3.16	-0.26	2.85	2.3	0.55	-0.81
7	3	3.3	-0.3	3.05	2.45	0.6	-0.9
8	2.89	3.1	-0.21	3.1	2.35	0.75	-0.96

5 Bladed Vertical Axis Vane Type Rotor

α = 40°

Tapping Point	Initial Reading (in of H2O)	α = 40° (in of H2O) (Convex surface)		Initial Reading (in of H2O)	α = 40° (in of H2O) (Concave surface)		Pressure Dff. DP (in of H2O)
1	2.7	2.02	0.68	2.9	2.6	0.3	0.38
2	2.8	3.3	-0.5	2.82	2.6	0.22	-0.72
3	2.75	4	-1.25	2.8	2.5	0.3	-1.55
4	2.75	3.4	-0.65	2.9	2.7	0.2	-0.85
5	2.79	3.12	-0.33	3.01	2.75	0.26	-0.59
6	2.9	3.12	-0.22	2.85	2.6	0.25	-0.47
7	3	3.25	-0.25	3.05	2.78	0.27	-0.52
8	2.89	3.1	-0.21	3.1	2.78	0.32	-0.53

5 Bladed Vertical Axis Vane Type Rotor

α = 50°

Tapping Point	Initial Reading (in of H2O)	α = 50° (in of H2O) (Convex surface)		Initial Reading (in of H2O)	α = 50° (in of H2O) (Concave surface)		Pressure Dff. DP (in of H2O)
1	2.7	2.3	0.4	2.9	2.72	0.18	0.22
2	2.8	3.5	-0.7	2.82	2.7	0.12	-0.82
3	2.75	4.05	-1.3	2.8	2.65	0.15	-1.45
4	2.75	3.5	-0.75	2.9	2.8	0.1	-0.85
5	2.79	3.15	-0.36	3.01	2.9	0.11	-0.47
6	2.9	3.1	-0.2	2.85	2.78	0.07	-0.27
7	3	3.22	-0.22	3.05	2.92	0.13	-0.35
8	2.89	3.1	-0.21	3.1	2.98	0.12	-0.33

5 Bladed Vertical Axis Vane Type Rotor
α = 60°

Tapping Point	Initial Reading (in of H2O)	α = 60° (in of H2O) (Convex surface)		Initial Reading (in of H2O)	α = 60° (in of H2O) (Concave surface)		Pressure Dff. DP (in of H2O)
1	2.7	2.3	0.4	2.9	2.82	0.08	0.32
2	2.8	3.2	-0.4	2.82	2.81	0.01	-0.41
3	2.75	3.6	-0.85	2.8	2.8	0	-0.85
4	2.75	3.2	-0.45	2.9	2.9	0	-0.45
5	2.79	3.1	-0.31	3.01	3	0.01	-0.32
6	2.9	3.12	-0.22	2.85	2.88	-0.03	-0.19
7	3	3.2	-0.2	3.05	3.05	0	-0.2
8	2.89	3.1	-0.21	3.1	3.1	0	-0.21

5 Bladed Vertical Axis Vane Type Rotor
α = 70°

Tapping Point	Initial Reading (in of H2O)	α = 70° (in of H2O) (Convex surface)		Initial Reading (in of H2O)	α = 70° (in of H2O) (Concave surface)		Pressure Dff. DP (in of H2O)
1	2.7	2.55	0.15	2.9	3.2	-0.3	0.45
2	2.8	3	-0.2	2.82	3.19	-0.37	0.17
3	2.75	3.65	-0.9	2.8	3.2	-0.4	-0.5
4	2.75	3.4	-0.65	2.9	3.21	-0.31	-0.34
5	2.79	3.12	-0.33	3.01	3.4	-0.39	0.06
6	2.9	3.1	-0.2	2.85	3.25	-0.4	0.2
7	3	3.25	-0.25	3.05	3.35	-0.3	0.05
8	2.89	3.1	-0.21	3.1	3.51	-0.41	0.2

5 Bladed Vertical Axis Vane Type Rotor
α = 80°

Tapping Point	Initial Reading (in of H2O)	α = 80° (in of H2O) (Convex surface)		Initial Reading (in of H2O)	α = 80° (in of H2O) (Concave surface)		Pressure Dff. DP (in of H2O)
1	2.7	2.6	0.1	2.9	3.5	-0.6	0.7
2	2.8	2.92	-0.12	2.82	3.4	-0.58	0.46
3	2.75	3.6	-0.85	2.8	3.45	-0.65	-0.2
4	2.75	3.5	-0.75	2.9	3.42	-0.52	-0.23
5	2.79	3.32	-0.53	3.01	3.68	-0.67	0.14
6	2.9	3.2	-0.3	2.85	3.54	-0.69	0.39
7	3	3.3	-0.3	3.05	3.6	-0.55	0.25
8	2.89	3.1	-0.21	3.1	3.75	-0.65	0.44

5 Bladed Vertical Axis Vane Type Rotor

α = 90°

Tapping Point	Initial Reading (in of H2O)	α = 90° (in of H2O) (Convex surface)		Initial Reading (in of H2O)	α = 90° (in of H2O) (Concave surface)		Pressure Dff. DP (in of H2O)
1	2.7	2.6	0.1	2.9	3.6	-0.7	0.8
2	2.8	2.88	-0.08	2.82	3.4	-0.58	0.5
3	2.75	3.4	-0.65	2.8	3.5	-0.7	0.05
4	2.75	3.3	-0.55	2.9	3.45	-0.55	0
5	2.79	3.3	-0.51	3.01	3.7	-0.69	0.18
6	2.9	3.2	-0.3	2.85	3.6	-0.75	0.45
7	3	3.3	-0.3	3.05	3.6	-0.55	0.25
8	2.89	3.1	-0.21	3.1	3.8	-0.7	0.49

5 Bladed Vertical Axis Vane Type Rotor

α = 100°

Tapping Point	Initial Reading (in of H2O)	α = 100° (in of H2O) (Convex surface)		Initial Reading (in of H2O)	α = 100° (in of H2O) (Concave surface)		Pressure Dff. DP (in of H2O)
1	2.7	2.7	0	2.9	3.5	-0.6	0.6
2	2.8	3.1	-0.3	2.82	3.4	-0.58	0.28
3	2.75	3.5	-0.75	2.8	3.45	-0.65	-0.1
4	2.75	3.2	-0.45	2.9	3.4	-0.5	0.05
5	2.79	3.1	-0.31	3.01	3.53	-0.52	0.21
6	2.9	3.1	-0.2	2.85	3.5	-0.65	0.45
7	3	3.4	-0.4	3.05	3.5	-0.45	0.05
8	2.89	3.2	-0.31	3.1	3.7	-0.6	0.29

5 Bladed Vertical Axis Vane Type Rotor

α = 110°

Tapping Point	Initial Reading (in of H2O)	α = 110° (in of H2O) (Convex surface)		Initial Reading (in of H2O)	α = 110° (in of H2O) (Concave surface)		Pressure Dff. DP (in of H2O)
1	2.7	2.7	0	2.9	3.48	-0.58	0.58
2	2.8	3.1	-0.3	2.82	3.32	-0.5	0.2
3	2.75	3.78	-1.03	2.8	3.38	-0.58	-0.45
4	2.75	3.7	-0.95	2.9	3.36	-0.46	-0.49
5	2.79	3.6	-0.81	3.01	3.52	-0.51	-0.3
6	2.9	3.4	-0.5	2.85	3.4	-0.55	0.05
7	3	3.42	-0.42	3.05	3.48	-0.43	0.01
8	2.89	3.22	-0.33	3.1	3.7	-0.6	0.27

5 Bladed Vertical Axis Vane Type Rotor

α = 120° Velocity= m/s

Tapping Point	Initial Reading (in of H2O)	α = 120° (in of H2O) (Convex surface)		Initial Reading (in of H2O)	α = 120° (in of H2O) (Concave surface)		Pressure Dff. DP (in of H2O)
1	2.7	2.98	-0.28	2.9	3.4	-0.5	0.22
2	2.8	2.98	-0.18	2.82	3.3	-0.48	0.3
3	2.75	3.2	-0.45	2.8	3.3	-0.5	0.05
4	2.75	3.32	-0.57	2.9	3.3	-0.4	-0.17
5	2.79	3.35	-0.56	3.01	3.5	-0.49	-0.07
6	2.9	3.3	-0.4	2.85	3.4	-0.55	0.15
7	3	3.4	-0.4	3.05	3.48	-0.43	0.03
8	2.89	3.2	-0.31	3.1	3.68	-0.58	0.27

5 Bladed Vertical Axis Vane Type Rotor

α = 130°

Tapping Point	Initial Reading (in of H2O)	α = 130° (in of H2O) (Convex surface)		Initial Reading (in of H2O)	α = 130° (in of H2O) (Concave surface)		Pressure Dff. DP (in of H2O)
1	2.7	2.6	0.1	2.9	3.3	-0.4	0.5
2	2.8	3	-0.2	2.82	3.2	-0.38	0.18
3	2.75	3.05	-0.3	2.8	3.2	-0.4	0.1
4	2.75	3	-0.25	2.9	3.22	-0.32	0.07
5	2.79	3	-0.21	3.01	3.5	-0.49	0.28
6	2.9	3.06	-0.16	2.85	3.2	-0.35	0.19
7	3	3.2	-0.2	3.05	3.4	-0.35	0.15
8	2.89	3.1	-0.21	3.1	3.5	-0.4	0.19

5 Bladed Vertical Axis Vane Type Rotor

α = 140°

Tapping Point	Initial Reading (in of H2O)	α = 140° (in of H2O) (Convex surface)		Initial Reading (in of H2O)	α = 140° (in of H2O) (Concave surface)		Pressure Dff. DP (in of H2O)
1	2.7	2.8	-0.1	2.9	3.3	-0.4	0.3
2	2.8	2.98	-0.18	2.82	3.15	-0.33	0.15
3	2.75	3	-0.25	2.8	3.12	-0.32	0.07
4	2.75	3	-0.25	2.9	3.1	-0.2	-0.05
5	2.79	3	-0.21	3.01	3.3	-0.29	0.08
6	2.9	3.02	-0.12	2.85	3.15	-0.3	0.18
7	3	3.2	-0.2	3.05	3.35	-0.3	0.1
8	2.89	3.1	-0.21	3.1	3.42	-0.32	0.11

5 Bladed Vertical Axis Vane Type Rotor
α = 150°

Tapping Point	Initial Reading (in of H2O)	α = 150° (in of H2O) (Convex surface)		Initial Reading (in of H2O)	α = 150° (in of H2O) (Concave surface)		Pressure Dff. DP (in of H2O)
1	2.7	2.8	-0.1	2.9	3.2	-0.3	0.2
2	2.8	2.98	-0.18	2.82	3.1	-0.28	0.1
3	2.75	3	-0.25	2.8	3.1	-0.3	0.05
4	2.75	3	-0.25	2.9	3.15	-0.25	0
5	2.79	3	-0.21	3.01	3.3	-0.29	0.08
6	2.9	3.02	-0.12	2.85	3.12	-0.27	0.15
7	3	3.2	-0.2	3.05	3.3	-0.25	0.05
8	2.89	3.1	-0.21	3.1	3.4	-0.3	0.09

5 Bladed Vertical Axis Vane Type Rotor
α = 160°

Tapping Point	Initial Reading (in of H2O)	α = 160° (in of H2O) (Convex surface)		Initial Reading (in of H2O)	α = 160° (in of H2O) (Concave surface)		Pressure Dff. DP (in of H2O)
1	2.7	2.82	-0.12	2.9	3.18	-0.28	0.16
2	2.8	2.98	-0.18	2.82	3.05	-0.23	0.05
3	2.75	3	-0.25	2.8	3.01	-0.21	-0.04
4	2.75	3	-0.25	2.9	3.1	-0.2	-0.05
5	2.79	3	-0.21	3.01	3.22	-0.21	4.4409E-16
6	2.9	3.02	-0.12	2.85	3.1	-0.25	0.13
7	3	3.2	-0.2	3.05	3.25	-0.2	0
8	2.89	3.08	-0.19	3.1	3.3	-0.2	0.01

5 Bladed Vertical Axis Vane Type Rotor
α = 170°

Tapping Point	Initial Reading (in of H2O)	α = 170° (in of H2O) (Convex surface)		Initial Reading (in of H2O)	α = 170° (in of H2O) (Concave surface)		Pressure Dff. DP (in of H2O)
1	2.7	2.9	-0.2	2.9	3.15	-0.25	0.05
2	2.8	3	-0.2	2.82	3.05	-0.23	0.03
3	2.75	3	-0.25	2.8	3.05	-0.25	0
4	2.75	3	-0.25	2.9	3.12	-0.22	-0.03
5	2.79	3	-0.21	3.01	3.24	-0.23	0.02
6	2.9	3.02	-0.12	2.85	3.1	-0.25	0.13
7	3	3.2	-0.2	3.05	3.28	-0.23	0.03
8	2.89	3.1	-0.21	3.1	3.3	-0.2	-0.01

5 Bladed Vertical Axis Vane Type Rotor
α = 180°

Tapping Point	Initial Reading (in of H2O)	α = 180° (in of H2O) (Convex surface)		Initial Reading (in of H2O)	α = 180° (in of H2O) (Concave surface)		Pressure Dff. DP (in of H2O)
1	2.7	2.95	-0.25	2.9	3.15	-0.25	0
2	2.8	3	-0.2	2.82	3.06	-0.24	0.04
3	2.75	3.08	-0.33	2.8	3.08	-0.28	-0.05
4	2.75	3.01	-0.26	2.9	3.12	-0.22	-0.04
5	2.79	3.08	-0.29	3.01	3.25	-0.24	-0.05
6	2.9	3.1	-0.2	2.85	3.1	-0.25	0.05
7	3	3.2	-0.2	3.05	3.26	-0.21	0.01
8	2.89	3.1	-0.21	3.1	3.3	-0.2	-0.01

5 Bladed Vertical Axis Vane Type Rotor
α = 190°

Tapping Point	Initial Reading (in of H2O)	α = 190° (in of H2O) (Convex surface)		Initial Reading (in of H2O)	α = 190° (in of H2O) (Concave surface)		Pressure Dff. DP (in of H2O)
1	2.7	3	-0.3	2.9	3.12	-0.22	-0.08
2	2.8	3.06	-0.26	2.82	3.05	-0.23	-0.03
3	2.75	3.1	-0.35	2.8	3.04	-0.24	-0.11
4	2.75	3.08	-0.33	2.9	3.12	-0.22	-0.11
5	2.79	3.08	-0.29	3.01	3.25	-0.24	-0.05
6	2.9	3.1	-0.2	2.85	3.1	-0.25	0.05
7	3	3.24	-0.24	3.05	3.25	-0.2	-0.04
8	2.89	3.22	-0.33	3.1	3.3	-0.2	-0.13

5 Bladed Vertical Axis Vane Type Rotor
α = 200°

Tapping Point	Initial Reading (in of H2O)	α = 200° (in of H2O) (Convex surface)		Initial Reading (in of H2O)	α = 200° (in of H2O) (Concave surface)		Pressure Dff. DP (in of H2O)
1	2.7	2.9	-0.2	2.9	3.14	-0.24	0.04
2	2.8	3.12	-0.32	2.82	3.1	-0.28	-0.04
3	2.75	3.12	-0.37	2.8	3.08	-0.28	-0.09
4	2.75	3.1	-0.35	2.9	3.12	-0.22	-0.13
5	2.79	3.12	-0.33	3.01	3.3	-0.29	-0.04
6	2.9	3.2	-0.3	2.85	3.12	-0.27	-0.03
7	3	3.32	-0.32	3.05	3.3	-0.25	-0.07
8	2.89	3.28	-0.39	3.1	3.32	-0.22	-0.17

5 Bladed Vertical Axis Vane Type Rotor

α = 210°

Tapping Point	Initial Reading (in of H2O)	α = 210° (in of H2O) (Convex surface)		Initial Reading (in of H2O)	α = 210° (in of H2O) (Concave surface)		Pressure Dff. DP (in of H2O)
1	2.7	2.8	-0.1	2.9	3.1	-0.2	0.1
2	2.8	2.9	-0.1	2.82	3.02	-0.2	0.1
3	2.75	3	-0.25	2.8	3.02	-0.22	-0.03
4	2.75	2.98	-0.23	2.9	3.12	-0.22	-0.01
5	2.79	2.98	-0.19	3.01	3.26	-0.25	0.06
6	2.9	3.04	-0.14	2.85	3.1	-0.25	0.11
7	3	3.48	-0.48	3.05	3.3	-0.25	-0.23
8	2.89	3.62	-0.73	3.1	3.34	-0.24	-0.49

5 Bladed Vertical Axis Vane Type Rotor

α = 220°

Tapping Point	Initial Reading (in of H2O)	α = 220° (in of H2O) (Convex surface)		Initial Reading (in of H2O)	α = 220° (in of H2O) (Concave surface)		Pressure Dff. DP (in of H2O)
1	2.7	2.8	-0.1	2.9	3.1	-0.2	0.1
2	2.8	2.7	0.1	2.82	3.01	-0.19	0.29
3	2.75	2.95	-0.2	2.8	3	-0.2	0
4	2.75	2.8	-0.05	2.9	3.1	-0.2	0.15
5	2.79	2.78	0.01	3.01	3.22	-0.21	0.22
6	2.9	2.9	0	2.85	3.1	-0.25	0.25
7	3	3.1	-0.1	3.05	3.28	-0.23	0.13
8	2.89	3.12	-0.23	3.1	3.34	-0.24	0.01

5 Bladed Vertical Axis Vane Type Rotor

α = 230°

Tapping Point	Initial Reading (in of H2O)	α = 230° (in of H2O) (Convex surface)		Initial Reading (in of H2O)	α = 230° (in of H2O) (Concave surface)		Pressure Dff. DP (in of H2O)
1	2.7	2.6	0.1	2.9	3.1	-0.2	0.3
2	2.8	2.5	0.3	2.82	3	-0.18	0.48
3	2.75	2.88	-0.13	2.8	3	-0.2	0.07
4	2.75	2.78	-0.03	2.9	3.1	-0.2	0.17
5	2.79	2.68	0.11	3.01	3.2	-0.19	0.3
6	2.9	2.78	0.12	2.85	3.1	-0.25	0.37
7	3	3	0	3.05	3.28	-0.23	0.23
8	2.89	2.69	0.2	3.1	3.32	-0.22	0.42

5 Bladed Vertical Axis Vane Type Rotor

α = 240°

Tapping Point	Initial Reading (in of H2O)	α = 240° (in of H2O) (Convex surface)		Initial Reading (in of H2O)	α = 240° (in of H2O) (Concave surface)		Pressure Dff. DP (in of H2O)
1	2.7	2.3	0.4	2.9	3.1	-0.2	0.6
2	2.8	2.7	0.1	2.82	3.02	-0.2	0.3
3	2.75	2.75	0	2.8	3.02	-0.22	0.22
4	2.75	2.7	0.05	2.9	3.1	-0.2	0.25
5	2.79	2.68	0.11	3.01	3.26	-0.25	0.36
6	2.9	2.72	0.18	2.85	3.1	-0.25	0.43
7	3	3	0	3.05	3.28	-0.23	0.23
8	2.89	2.2	0.69	3.1	3.34	-0.24	0.93

5 Bladed Vertical Axis Vane Type Rotor

α = 250°

Tapping Point	Initial Reading (in of H2O)	α = 250° (in of H2O) (Convex surface)		Initial Reading (in of H2O)	α = 250° (in of H2O) (Concave surface)		Pressure Dff. DP (in of H2O)
1	2.7	2.6	0.1	2.9	3.2	-0.3	0.4
2	2.8	2.7	0.1	2.82	3.1	-0.28	0.38
3	2.75	2.6	0.15	2.8	3.1	-0.3	0.45
4	2.75	2.5	0.25	2.9	3.15	-0.25	0.5
5	2.79	2.45	0.34	3.01	3.3	-0.29	0.63
6	2.9	2.55	0.35	2.85	3.15	-0.3	0.65
7	3	2.5	0.5	3.05	3.3	-0.25	0.75
8	2.89	1.9	0.99	3.1	3.4	-0.3	1.29

5 Bladed Vertical Axis Vane Type Rotor

α = 260°

Tapping Point	Initial Reading (in of H2O)	α = 260° (in of H2O) (Convex surface)		Initial Reading (in of H2O)	α = 260° (in of H2O) (Concave surface)		Pressure Dff. DP (in of H2O)
1	2.7	2.6	0.1	2.9	3.2	-0.3	0.4
2	2.8	2.6	0.2	2.82	3.12	-0.3	0.5
3	2.75	2.58	0.17	2.8	3.1	-0.3	0.47
4	2.75	2.65	0.1	2.9	3.18	-0.28	0.38
5	2.79	2.6	0.19	3.01	3.3	-0.29	0.48
6	2.9	2.48	0.42	2.85	3.2	-0.35	0.77
7	3	2.3	0.7	3.05	3.32	-0.27	0.97
8	2.89	1.8	1.09	3.1	3.45	-0.35	1.44

5 Bladed Vertical Axis Vane Type Rotor
α = 270°

Tapping Point	Initial Reading (in of H2O)	α = 270° (in of H2O) (Convex surface)		Initial Reading (in of H2O)	α = 270° (in of H2O) (Concave surface)		Pressure Dff. DP (in of H2O)
1	2.7	2.5	0.2	2.9	3.2	-0.3	0.5
2	2.8	2.7	0.1	2.82	3.15	-0.33	0.43
3	2.75	2.6	0.15	2.8	3.15	-0.35	0.5
4	2.75	2.6	0.15	2.9	3.2	-0.3	0.45
5	2.79	2.4	0.39	3.01	3.4	-0.39	0.78
6	2.9	2.2	0.7	2.85	3.25	-0.4	1.1
7	3	2.05	0.95	3.05	3.32	-0.27	1.22
8	2.89	1.98	0.91	3.1	3.5	-0.4	1.31

5 Bladed Vertical Axis Vane Type Rotor
α = 280°

Tapping Point	Initial Reading (in of H2O)	α = 280° (in of H2O) (Convex surface)		Initial Reading (in of H2O)	α = 280° (in of H2O) (Concave surface)		Pressure Dff. DP (in of H2O)
1	2.7	2.85	-0.15	2.9	3.3	-0.4	0.25
2	2.8	2.85	-0.05	2.82	3.2	-0.38	0.33
3	2.75	2.65	0.1	2.8	3.25	-0.45	0.55
4	2.75	2.5	0.25	2.9	3.26	-0.36	0.61
5	2.79	2.2	0.59	3.01	3.46	-0.45	1.04
6	2.9	1.95	0.95	2.85	3.3	-0.45	1.4
7	3	2	1	3.05	3.4	-0.35	1.35
8	2.89	2.1	0.79	3.1	3.6	-0.5	1.29

5 Bladed Vertical Axis Vane Type Rotor
α = 290°

Tapping Point	Initial Reading (in of H2O)	α = 290° (in of H2O) (Convex surface)		Initial Reading (in of H2O)	α = 290° (in of H2O) (Concave surface)		Pressure Dff. DP (in of H2O)
1	2.7	3.15	-0.45	2.9	2.7	0.2	-0.65
2	2.8	2.88	-0.08	2.82	2.62	0.2	-0.28
3	2.75	2.5	0.25	2.8	2.5	0.3	-0.05
4	2.75	2.3	0.45	2.9	2.8	0.1	0.35
5	2.79	1.84	0.95	3.01	2.9	0.11	0.84
6	2.9	1.72	1.18	2.85	2.8	0.05	1.13
7	3	2.2	0.8	3.05	3	0.05	0.75
8	2.89	2.8	0.09	3.1	3.12	-0.02	0.11

5 Bladed Vertical Axis Vane Type Rotor

α = 300°

Tapping Points	Initial Reading (in of H2O)	α = 300° (in of H2O) (Convex surface)		Initial Reading (in of H2O)	α = 300° (in of H2O) (Concave surface)		Pressure Dff. DP (in of H2O)
1	2.7	3.02	-0.32	2.9	2.6	0.3	-0.62
2	2.8	2.7	0.1	2.82	2.6	0.22	-0.12
3	2.75	2.3	0.45	2.8	2.4	0.4	0.05
4	2.75	2	0.75	2.9	2.6	0.3	0.45
5	2.79	1.7	1.09	3.01	2.6	0.41	0.68
6	2.9	1.9	1	2.85	2.5	0.35	0.65
7	3	2.65	0.35	3.05	2.6	0.45	-0.1
8	2.89	3.38	-0.49	3.1	2.65	0.45	-0.94

5 Bladed Vertical Axis Vane Type Rotor

α = 310°

Tapping Point	Initial Reading (in of H2O)	α = 310° (in of H2O) (Convex surface)		Initial Reading (in of H2O)	α = 310° (in of H2O) (Concave surface)		Pressure Dff. DP (in of H2O)
1	2.7	2.8	-0.1	2.9	2.2	0.7	-0.8
2	2.8	2.6	0.2	2.82	2.2	0.62	-0.42
3	2.75	2.25	0.5	2.8	2.1	0.7	-0.2
4	2.75	1.9	0.85	2.9	2.3	0.6	0.25
5	2.79	1.68	1.11	3.01	2.3	0.71	0.4
6	2.9	2	0.9	2.85	2.1	0.75	0.15
7	3	2.8	0.2	3.05	2.3	0.75	-0.55
8	2.89	3.3	-0.41	3.1	2.32	0.78	-1.19

5 Bladed Vertical Axis Vane Type Rotor

α = 320°

Tapping Point	Initial Reading (in of H2O)	α = 320° (in of H2O) (Convex surface)		Initial Reading (in of H2O)	α = 320° (in of H2O) (Concave surface)		Pressure Dff. DP (in of H2O)
1	2.7	2.8	-0.1	2.9	2.2	0.7	-0.8
2	2.8	2.6	0.2	2.82	2.2	0.62	-0.42
3	2.75	2.25	0.5	2.8	2.1	0.7	-0.2
4	2.75	1.9	0.85	2.9	2.3	0.6	0.25
5	2.79	1.68	1.11	3.01	2.3	0.71	0.4
6	2.9	2	0.9	2.85	2.1	0.75	0.15
7	3	2.8	0.2	3.05	2.3	0.75	-0.55
8	2.89	3.3	-0.41	3.1	2.32	0.78	-1.19

5 Bladed Vertical Axis Vane Type Rotor
α = 330°

Tapping Point	Initial Reading (in of H2O)	α = 330° (in of H2O) (Convex surface)		Initial Reading (in of H2O)	α = 330° (in of H2O) (Concave surface)		Pressure Dff. DP (in of H2O)
1	2.7	2.9	-0.2	2.9	1.9	1	-1.2
2	2.8	3	-0.2	2.82	2	0.82	-1.02
3	2.75	2.52	0.23	2.8	1.88	0.92	-0.69
4	2.75	1.8	0.95	2.9	2.1	0.8	0.15
5	2.79	1.85	0.94	3.01	2.12	0.89	0.05
6	2.9	2.6	0.3	2.85	1.95	0.9	-0.6
7	3	3.4	-0.4	3.05	2.1	0.95	-1.35
8	2.89	3.5	-0.61	3.1	2.1	1	-1.61

5 Bladed Vertical Axis Vane Type Rotor
α = 340°

Tapping Points	Initial Reading (in of H2O)	α = 340° (in of H2O) (Convex surface)		Initial Reading (in of H2O)	α = 340° (in of H2O) (Concave surface)		Pressure Dff. DP (in of H2O)
1	2.7	2.7	0	2.9	1.9	1	-1
2	2.8	3.12	-0.32	2.82	1.95	0.87	-1.19
3	2.75	3.12	-0.37	2.8	1.84	0.96	-1.33
4	2.75	2	0.75	2.9	2.1	0.8	-0.05
5	2.79	1.88	0.91	3.01	2.12	0.89	0.02
6	2.9	2.75	0.15	2.85	1.9	0.95	-0.8
7	3	3.6	-0.6	3.05	2.1	0.95	-1.55
8	2.89	3.4	-0.51	3.1	2.1	1	-1.51

5 Bladed Vertical Axis Vane Type Rotor
α = 350°

Tapping Point	Initial Reading (in of H2O)	α = 350° (in of H2O) (Convex surface)		Initial Reading (in of H2O)	α = 350° (in of H2O) (Concave surface)		Pressure Dff. DP (in of H2O)
1	2.7	2	0.7	2.9	1.9	1	-0.3
2	2.8	3.1	-0.3	2.82	1.95	0.87	-1.17
3	2.75	3.1	-0.35	2.8	1.8	1	-1.35
4	2.75	2.75	0	2.9	2.06	0.84	-0.84
5	2.79	2.8	-0.01	3.01	2.1	0.91	-0.92
6	2.9	3.08	-0.18	2.85	1.9	0.95	-1.13
7	3	3.7	-0.7	3.05	2.1	0.95	-1.65
8	2.89	3.6	-0.71	3.1	2.1	1	-1.71

6 Bladed Vertical Axis Vane Type Rotor

α = 0°

Tapping Point	Initial Reading (in of H2O)	α = 0° (in of H2O) (Convex surface)		Initial Reading (in of H2O)	α = 0° (in of H2O) (Concave surface)		Pressure Dff. DP (in of H2O)
1	2.7	1.7	1	2.9	2.05	0.85	0.15
2	2.8	3.66	-0.86	2.82	2.04	0.78	-1.64
3	2.75	4.62	-1.87	2.8	1.9	0.9	-2.77
4	2.75	4	-1.25	2.9	2.1	0.8	-2.05
5	2.79	3.5	-0.71	3.01	2.2	0.81	-1.52
6	2.9	3.51	-0.61	2.85	2	0.85	-1.46
7	3	3.7	-0.7	3.05	2.15	0.9	-1.6
8	2.89	3.4	-0.51	3.1	2.15	0.95	-1.46

6 Bladed Vertical Axis Vane Type Rotor

α = 10°

Tapping Point	Initial Reading (in of H2O)	α = 10° (in of H2O) (Convex surface)		Initial Reading (in of H2O)	α = 10° (in of H2O) (Concave surface)		Pressure Dff. DP (in of H2O)
1	2.7	1.7	1	2.9	1.88	1.02	-0.02
2	2.8	3.8	-1	2.82	1.94	0.88	-1.88
3	2.75	4.9	-2.15	2.8	1.8	1	-3.15
4	2.75	4.28	-1.53	2.9	2.05	0.85	-2.38
5	2.79	3.65	-0.86	3.01	2.14	0.87	-1.73
6	2.9	3.5	-0.6	2.85	1.88	0.97	-1.57
7	3	3.5	-0.5	3.05	2.1	0.95	-1.45
8	2.89	3.3	-0.41	3.1	2.05	1.05	-1.46

6 Bladed Vertical Axis Vane Type Rotor

α = 20°

Tapping Point	Initial Reading (in of H2O)	α = 20° (in of H2O) (Convex surface)		Initial Reading (in of H2O)	α = 20° (in of H2O) (Concave surface)		Pressure Dff. DP (in of H2O)
1	2.7	1.92	0.78	2.9	1.88	1.02	-0.24
2	2.8	3.55	-0.75	2.82	1.92	0.9	-1.65
3	2.75	4.4	-1.65	2.8	1.78	1.02	-2.67
4	2.75	3.98	-1.23	2.9	2.02	0.88	-2.11
5	2.79	3.45	-0.66	3.01	2.1	0.91	-1.57
6	2.9	3.15	-0.25	2.85	1.88	0.97	-1.22
7	3	3.2	-0.2	3.05	2.05	1	-1.2
8	2.89	3.1	-0.21	3.1	2.01	1.09	-1.3

6 Bladed Vertical Axis Vane Type Rotor
α = 30°

Tapping Point	Initial Reading (in of H2O)	α = 30° (in of H2O) (Convex surface)		Initial Reading (in of H2O)	α = 30° (in of H2O) (Concave surface)		Pressure Dff. DP (in of H2O)
1	2.7	1.9	0.8	2.9	1.85	1.05	-0.25
2	2.8	3.48	-0.68	2.82	1.9	0.92	-1.6
3	2.75	4.2	-1.45	2.8	1.76	1.04	-2.49
4	2.75	3.8	-1.05	2.9	2.02	0.88	-1.93
5	2.79	3.4	-0.61	3.01	2	1.01	-1.62
6	2.9	3.12	-0.22	2.85	1.88	0.97	-1.19
7	3	3.2	-0.2	3.05	2.04	1.01	-1.21
8	2.89	3.1	-0.21	3.1	2	1.1	-1.31

6 Bladed Vertical Axis Vane Type Rotor
α = 40°

Tapping Point	Initial Reading (in of H2O)	α = 40° (in of H2O) (Convex surface)		Initial Reading (in of H2O)	α = 40° (in of H2O) (Concave surface)		Pressure Dff. DP (in of H2O)
1	2.7	1.9	0.8	2.9	1.82	1.08	-0.28
2	2.8	3.22	-0.42	2.82	1.9	0.92	-1.34
3	2.75	4.15	-1.4	2.8	1.75	1.05	-2.45
4	2.75	3.85	-1.1	2.9	2.02	0.88	-1.98
5	2.79	3.55	-0.76	3.01	2.1	0.91	-1.67
6	2.9	3.28	-0.38	2.85	1.85	1	-1.38
7	3	3.3	-0.3	3.05	2.04	1.01	-1.31
8	2.89	3.1	-0.21	3.1	1.98	1.12	-1.33

6 Bladed Vertical Axis Vane Type Rotor
α = 50°

Tapping Point	Initial Reading (in of H2O)	α = 50° (in of H2O) (Convex surface)		Initial Reading (in of H2O)	α = 50° (in of H2O) (Concave surface)		Pressure Dff. DP (in of H2O)
1	2.7	2.1	0.6	2.9	1.85	1.05	-0.45
2	2.8	3.15	-0.35	2.82	1.95	0.87	-1.22
3	2.75	3.92	-1.17	2.8	1.8	1	-2.17
4	2.75	3.7	-0.95	2.9	2.05	0.85	-1.8
5	2.79	3.52	-0.73	3.01	2.15	0.86	-1.59
6	2.9	3.28	-0.38	2.85	1.9	0.95	-1.33
7	3	3.25	-0.25	3.05	2.1	0.95	-1.2
8	2.89	3.08	-0.19	3.1	2.05	1.05	-1.24

6 Bladed Vertical Axis Vane Type Rotor
$\alpha = 60°$

Tapping Point	Initial Reading (in of H2O)	α = 60° (in of H2O) (Convex surface)		Initial Reading (in of H2O)	α = 60° (in of H2O) (Concave surface)		Pressure Dff. DP (in of H2O)
1	2.7	2.1	0.6	2.9	1.98	0.92	-0.32
2	2.8	3.1	-0.3	2.82	2.1	0.72	-1.02
3	2.75	3.72	-0.97	2.8	1.92	0.88	-1.85
4	2.75	3.52	-0.77	2.9	2.2	0.7	-1.47
5	2.79	3.45	-0.66	3.01	2.3	0.71	-1.37
6	2.9	3.3	-0.4	2.85	2.05	0.8	-1.2
7	3	3.3	-0.3	3.05	2.22	0.83	-1.13
8	2.89	3.1	-0.21	3.1	2.2	0.9	-1.11

6 Bladed Vertical Axis Vane Type Rotor
$\alpha = 70°$

Tapping Point	Initial Reading (in of H2O)	α = 70° (in of H2O) (Convex surface)		Initial Reading (in of H2O)	α = 70° (in of H2O) (Concave surface)		Pressure Dff. DP (in of H2O)
1	2.7	1.98	0.72	2.9	2.2	0.7	0.02
2	2.8	3.12	-0.32	2.82	2.48	0.34	-0.66
3	2.75	3.82	-1.07	2.8	2.2	0.6	-1.67
4	2.75	3.02	-0.27	2.9	2.5	0.4	-0.67
5	2.79	3.5	-0.71	3.01	2.6	0.41	-1.12
6	2.9	3.4	-0.5	2.85	2.4	0.45	-0.95
7	3	3.4	-0.4	3.05	2.62	0.43	-0.83
8	2.89	3.18	-0.29	3.1	2.62	0.48	-0.77

6 Bladed Vertical Axis Vane Type Rotor
$\alpha = 80°$

Tapping Point	Initial Reading (in of H2O)	α = 80° (in of H2O) (Convex surface)		Initial Reading (in of H2O)	α = 80° (in of H2O) (Concave surface)		Pressure Dff. DP (in of H2O)
1	2.7	2.02	0.68	2.9	2.71	0.19	0.49
2	2.8	3.1	-0.3	2.82	2.72	0.1	-0.4
3	2.75	3.7	-0.95	2.8	2.65	0.15	-1.1
4	2.75	3.5	-0.75	2.9	2.8	0.1	-0.85
5	2.79	3.5	-0.71	3.01	2.98	0.03	-0.74
6	2.9	3.4	-0.5	2.85	2.88	-0.03	-0.47
7	3	3.4	-0.4	3.05	3.1	-0.05	-0.35
8	2.89	3.18	-0.29	3.1	3.1	0	-0.29

6 Bladed Vertical Axis Vane Type Rotor

α = 90°

Tapping Point	Initial Reading (in of H2O)	α = 90° (in of H2O) (Convex surface)		Initial Reading (in of H2O)	α = 90° (in of H2O) (Concave surface)		Pressure Dff. DP (in of H2O)
1	2.7	2.1	0.6	2.9	2.82	0.08	0.52
2	2.8	3	-0.2	2.82	2.81	0.01	-0.21
3	2.75	3.55	-0.8	2.8	2.78	0.02	-0.82
4	2.75	3.42	-0.67	2.9	2.9	0	-0.67
5	2.79	3.42	-0.63	3.01	3.01	0	-0.63
6	2.9	3.4	-0.5	2.85	2.9	-0.05	-0.45
7	3	3.4	-0.4	3.05	3.1	-0.05	-0.35
8	2.89	3.18	-0.29	3.1	3.14	-0.04	-0.25

6 Bladed Vertical Axis Vane Type Rotor

α = 100°

Tapping Point	Initial Reading (in of H2O)	α = 100° (in of H2O) (Convex surface)		Initial Reading (in of H2O)	α = 100° (in of H2O) (Concave surface)		Pressure Dff. DP (in of H2O)
1	2.7	2.5	0.2	2.9	2.85	0.05	0.15
2	2.8	2.95	-0.15	2.82	2.8	0.02	-0.17
3	2.75	3.3	-0.55	2.8	2.88	-0.08	-0.47
4	2.75	3.25	-0.5	2.9	2.9	0	-0.5
5	2.79	3.18	-0.39	3.01	3	0.01	-0.4
6	2.9	3.15	-0.25	2.85	2.88	-0.03	-0.22
7	3	3.25	-0.25	3.05	3.05	0	-0.25
8	2.89	3.1	-0.21	3.1	3.1	0	-0.21

6 Bladed Vertical Axis Vane Type Rotor

α = 110°

Tapping Point	Initial Reading (in of H2O)	α = 110° (in of H2O) (Convex surface)		Initial Reading (in of H2O)	α = 110° (in of H2O) (Concave surface)		Pressure Dff. DP (in of H2O)
1	2.7	2.5	0.2	2.9	3.2	-0.3	0.5
2	2.8	3	-0.2	2.82	3.15	-0.33	0.13
3	2.75	3.1	-0.35	2.8	3.18	-0.38	0.03
4	2.75	3.1	-0.35	2.9	3.2	-0.3	-0.05
5	2.79	3	-0.21	3.01	3.4	-0.39	0.18
6	2.9	3.02	-0.12	2.85	3.3	-0.45	0.33
7	3	3.2	-0.2	3.05	3.4	-0.35	0.15
8	2.89	3.16	-0.27	3.1	3.52	-0.42	0.15

6 Bladed Vertical Axis Vane Type Rotor
α = 120°

Tapping Point	Initial Reading (in of H2O)	α = 120° (in of H2O) (Convex surface)		Initial Reading (in of H2O)	α = 120° (in of H2O) (Concave surface)		Pressure Dff. DP (in of H2O)
1	2.7	2.5	0.2	2.9	3.5	-0.6	0.8
2	2.8	2.98	-0.18	2.82	3.45	-0.63	0.45
3	2.75	3	-0.25	2.8	3.51	-0.71	0.46
4	2.75	2.99	-0.24	2.9	3.5	-0.6	0.36
5	2.79	2.98	-0.19	3.01	3.7	-0.69	0.5
6	2.9	3	-0.1	2.85	3.65	-0.8	0.7
7	3	3.18	-0.18	3.05	3.6	-0.55	0.37
8	2.89	3.08	-0.19	3.1	3.9	-0.8	0.61

6 Bladed Vertical Axis Vane Type Rotor
α = 130°

Tapping Point	Initial Reading (in of H2O)	α = 130° (in of H2O) (Convex surface)		Initial Reading (in of H2O)	α = 130° (in of H2O) (Concave surface)		Pressure Dff. DP (in of H2O)
1	2.7	2.48	0.22	2.9	3.6	-0.7	0.92
2	2.8	2.96	-0.16	2.82	3.52	-0.7	0.54
3	2.75	3.1	-0.35	2.8	3.65	-0.85	0.5
4	2.75	3.05	-0.3	2.9	3.6	-0.7	0.4
5	2.79	3	-0.21	3.01	3.8	-0.79	0.58
6	2.9	3	-0.1	2.85	3.8	-0.95	0.85
7	3	3.19	-0.19	3.05	3.7	-0.65	0.46
8	2.89	3.08	-0.19	3.1	3.9	-0.8	0.61

6 Bladed Vertical Axis Vane Type Rotor
α = 140°

Tapping Point	Initial Reading (in of H2O)	α = 140° (in of H2O) (Convex surface)		Initial Reading (in of H2O)	α = 140° (in of H2O) (Concave surface)		Pressure Dff. DP (in of H2O)
1	2.7	2.5	0.2	2.9	3.6	-0.7	0.9
2	2.8	2.9	-0.1	2.82	3.5	-0.68	0.58
3	2.75	3.2	-0.45	2.8	3.62	-0.82	0.37
4	2.75	3.1	-0.35	2.9	3.6	-0.7	0.35
5	2.79	3.08	-0.29	3.01	3.8	-0.79	0.5
6	2.9	3.05	-0.15	2.85	3.8	-0.95	0.8
7	3	3.19	-0.19	3.05	3.7	-0.65	0.46
8	2.89	3.08	-0.19	3.1	3.9	-0.8	0.61

6 Bladed Vertical Axis Vane Type Rotor
α = 150°

Tapping Point	Initial Reading (in of H2O)	α = 150° (in of H2O) (Convex surface)		Initial Reading (in of H2O)	α = 150° (in of H2O) (Concave surface)		Pressure Dff. DP (in of H2O)
1	2.7	2.5	0.2	2.9	3.5	-0.6	0.8
2	2.8	2.98	-0.18	2.82	3.35	-0.53	0.35
3	2.75	3.2	-0.45	2.8	3.41	-0.61	0.16
4	2.75	3.1	-0.35	2.9	3.4	-0.5	0.15
5	2.79	3.05	-0.26	3.01	3.6	-0.59	0.33
6	2.9	3.02	-0.12	2.85	3.5	-0.65	0.53
7	3	3.2	-0.2	3.05	3.52	-0.47	0.27
8	2.89	3.08	-0.19	3.1	3.8	-0.7	0.51

6 Bladed Vertical Axis Vane Type Rotor
α = 160°

Tapping Point	Initial Reading (in of H2O)	α = 160° (in of H2O) (Convex surface)		Initial Reading (in of H2O)	α = 160° (in of H2O) (Concave surface)		Pressure Dff. DP (in of H2O)
1	2.7	2.6	0.1	2.9	3.4	-0.5	0.6
2	2.8	2.98	-0.18	2.82	3.3	-0.48	0.3
3	2.75	3	-0.25	2.8	3.38	-0.58	0.33
4	2.75	3	-0.25	2.9	3.35	-0.45	0.2
5	2.79	3	-0.21	3.01	3.5	-0.49	0.28
6	2.9	3.02	-0.12	2.85	3.45	-0.6	0.48
7	3	3.2	-0.2	3.05	3.5	-0.45	0.25
8	2.89	3.1	-0.21	3.1	3.72	-0.62	0.41

6 Bladed Vertical Axis Vane Type Rotor
α = 170°

Tapping Point	Initial Reading (in of H2O)	α = 170° (in of H2O) (Convex surface)		Initial Reading (in of H2O)	α = 170° (in of H2O) (Concave surface)		Pressure Dff. DP (in of H2O)
1	2.7	2.6	0.1	2.9	3.35	-0.45	0.55
2	2.8	3	-0.2	2.82	3.2	-0.38	0.18
3	2.75	3	-0.25	2.8	3.28	-0.48	0.23
4	2.75	3	-0.25	2.9	3.3	-0.4	0.15
5	2.79	3	-0.21	3.01	3.45	-0.44	0.23
6	2.9	3	-0.1	2.85	3.35	-0.5	0.4
7	3	3.2	-0.2	3.05	3.45	-0.4	0.2
8	2.89	3.1	-0.21	3.1	3.65	-0.55	0.34

6 Bladed Vertical Axis Vane Type Rotor
α = 180°

Tapping Point	Initial Reading (in of H2O)	α = 180° (in of H2O) (Convex surface)		Initial Reading (in of H2O)	α = 180° (in of H2O) (Concave surface)		Pressure Dff. DP (in of H2O)
1	2.7	2.6	0.1	2.9	3.28	-0.38	0.48
2	2.8	2.99	-0.19	2.82	3.15	-0.33	0.14
3	2.75	2.98	-0.23	2.8	3.16	-0.36	0.13
4	2.75	2.99	-0.24	2.9	3.2	-0.3	0.06
5	2.79	2.99	-0.2	3.01	3.35	-0.34	0.14
6	2.9	3	-0.1	2.85	3.25	-0.4	0.3
7	3	3.16	-0.16	3.05	3.4	-0.35	0.19
8	2.89	3.05	-0.16	3.1	3.5	-0.4	0.24

6 Bladed Vertical Axis Vane Type Rotor
α = 190°

Tapping Point	Initial Reading (in of H2O)	α = 190° (in of H2O) (Convex surface)		Initial Reading (in of H2O)	α = 190° (in of H2O) (Concave surface)		Pressure Dff. DP (in of H2O)
1	2.7	2.68	0.02	2.9	3.15	-0.25	0.27
2	2.8	3	-0.2	2.82	3.05	-0.23	0.03
3	2.75	2.98	-0.23	2.8	3.05	-0.25	0.02
4	2.75	2.99	-0.24	2.9	3.15	-0.25	0.01
5	2.79	3	-0.21	3.01	3.3	-0.29	0.08
6	2.9	3	-0.1	2.85	3.2	-0.35	0.25
7	3	3.16	-0.16	3.05	3.32	-0.27	0.11
8	2.89	3.02	-0.13	3.1	3.4	-0.3	0.17

6 Bladed Vertical Axis Vane Type Rotor
α = 200°

Tapping Point	Initial Reading (in of H2O)	α = 200° (in of H2O) (Convex surface)		Initial Reading (in of H2O)	α = 200° (in of H2O) (Concave surface)		Pressure Dff. DP (in of H2O)
1	2.7	2.8	-0.1	2.9	3.1	-0.2	0.1
2	2.8	2.98	-0.18	2.82	3	-0.18	0
3	2.75	2.98	-0.23	2.8	3.01	-0.21	-0.02
4	2.75	3	-0.25	2.9	3.12	-0.22	-0.03
5	2.79	3	-0.21	3.01	3.28	-0.27	0.06
6	2.9	3	-0.1	2.85	3.18	-0.33	0.23
7	3	3.18	-0.18	3.05	3.3	-0.25	0.07
8	2.89	3.08	-0.19	3.1	3.4	-0.3	0.11

6 Bladed Vertical Axis Vane Type Rotor
α = 210°

Tapping Point	Initial Reading (in of H2O)	α = 210° (in of H2O) (Convex surface)		Initial Reading (in of H2O)	α = 210° (in of H2O) (Concave surface)		Pressure Dff. DP (in of H2O)
1	2.7	2.7	0	2.9	3.1	-0.2	0.2
2	2.8	3.1	-0.3	2.82	3	-0.18	-0.12
3	2.75	3.2	-0.45	2.8	3.01	-0.21	-0.24
4	2.75	3.1	-0.35	2.9	3.1	-0.2	-0.15
5	2.79	3.1	-0.31	3.01	3.25	-0.24	-0.07
6	2.9	3.12	-0.22	2.85	3.12	-0.27	0.05
7	3	3.4	-0.4	3.05	3.3	-0.25	-0.15
8	2.89	3.5	-0.61	3.1	3.35	-0.25	-0.36

6 Bladed Vertical Axis Vane Type Rotor
α = 220°

Tapping Point	Initial Reading (in of H2O)	α = 220° (in of H2O) (Convex surface)		Initial Reading (in of H2O)	α = 220° (in of H2O) (Concave surface)		Pressure Dff. DP (in of H2O)
1	2.7	2.66	0.04	2.9	3.1	-0.2	0.24
2	2.8	2.78	0.02	2.82	3	-0.18	0.2
3	2.75	3.01	-0.26	2.8	3.01	-0.21	-0.05
4	2.75	2.9	-0.15	2.9	3.1	-0.2	0.05
5	2.79	2.85	-0.06	3.01	3.25	-0.24	0.18
6	2.9	2.95	-0.05	2.85	3.1	-0.25	0.2
7	3	3.34	-0.34	3.05	3.1	-0.05	-0.29
8	2.89	3.3	-0.41	3.1	3.3	-0.2	-0.21

6 Bladed Vertical Axis Vane Type Rotor
α = 230°

Tapping Point	Initial Reading (in of H2O)	α = 230° (in of H2O) (Convex surface)		Initial Reading (in of H2O)	α = 230° (in of H2O) (Concave surface)		Pressure Dff. DP (in of H2O)
1	2.7	2.5	0.2	2.9	3.1	-0.2	0.4
2	2.8	2.45	0.35	2.82	3	-0.18	0.53
3	2.75	2.8	-0.05	2.8	3	-0.2	0.15
4	2.75	2.8	-0.05	2.9	3.1	-0.2	0.15
5	2.79	2.6	0.19	3.01	3.2	-0.19	0.38
6	2.9	2.7	0.2	2.85	3.1	-0.25	0.45
7	3	3	0	3.05	3.3	-0.25	0.25
8	2.89	2.78	0.11	3.1	3.35	-0.25	0.36

6 Bladed Vertical Axis Vane Type Rotor

α = 240°

Tapping Points	Initial Reading (in of H2O)	α = 240° (in of H2O) (Convex surface)		Initial Reading (in of H2O)	α = 240° (in of H2O) (Concave surface)		Pressure Dff. DP (in of H2O)
1	2.7	2.46	0.24	2.9	3.1	-0.2	0.44
2	2.8	2.36	0.44	2.82	3	-0.18	0.62
3	2.75	2.6	0.15	2.8	2.98	-0.18	0.33
4	2.75	2.62	0.13	2.9	3.1	-0.2	0.33
5	2.79	2.5	0.29	3.01	3.2	-0.19	0.48
6	2.9	2.6	0.3	2.85	3.08	-0.23	0.53
7	3	2.8	0.2	3.05	3.26	-0.21	0.41
8	2.89	2.2	0.69	3.1	3.3	-0.2	0.89

6 Bladed Vertical Axis Vane Type Rotor

α = 250°

Tapping Point	Initial Reading (in of H2O)	α = 250° (in of H2O) (Convex surface)		Initial Reading (in of H2O)	α = 250° (in of H2O) (Concave surface)		Pressure Dff. DP (in of H2O)
1	2.7	2.55	0.15	2.9	3.1	-0.2	0.35
2	2.8	2.65	0.15	2.82	3	-0.18	0.33
3	2.75	2.48	0.27	2.8	3	-0.2	0.47
4	2.75	2.45	0.3	2.9	3.1	-0.2	0.5
5	2.79	2.4	0.39	3.01	3.2	-0.19	0.58
6	2.9	2.5	0.4	2.85	3.1	-0.25	0.65
7	3	2.4	0.6	3.05	3.3	-0.25	0.85
8	2.89	1.8	1.09	3.1	3.34	-0.24	1.33

6 Bladed Vertical Axis Vane Type Rotor

α = 260°

Tapping Point	Initial Reading (in of H2O)	α = 260° (in of H2O) (Convex surface)		Initial Reading (in of H2O)	α = 260° (in of H2O) (Concave surface)		Pressure Dff. DP (in of H2O)
1	2.7	2.48	0.22	2.9	3.08	-0.18	0.4
2	2.8	2.42	0.38	2.82	3	-0.18	0.56
3	2.75	2.2	0.55	2.8	3	-0.2	0.75
4	2.75	2.3	0.45	2.9	3.1	-0.2	0.65
5	2.79	2.32	0.47	3.01	3.22	-0.21	0.68
6	2.9	2.3	0.6	2.85	3.08	-0.23	0.83
7	3	2.15	0.85	3.05	3.28	-0.23	1.08
8	2.89	1.78	1.11	3.1	3.32	-0.22	1.33

6 Bladed Vertical Axis Vane Type Rotor
α = 270°

Tapping Point	Initial Reading (in of H2O)	α = 270° (in of H2O) (Convex surface)		Initial Reading (in of H2O)	α = 270° (in of H2O) (Concave surface)		Pressure Dff. DP (in of H2O)
1	2.7	2.6	0.1	2.9	3.1	-0.2	0.3
2	2.8	2.4	0.4	2.82	3	-0.18	0.58
3	2.75	2.12	0.63	2.8	3	-0.2	0.83
4	2.75	2.2	0.55	2.9	3.1	-0.2	0.75
5	2.79	2.15	0.64	3.01	3.2	-0.19	0.83
6	2.9	2	0.9	2.85	3.08	-0.23	1.13
7	3	2	1	3.05	3.2	-0.15	1.15
8	2.89	1.9	0.99	3.1	3.31	-0.21	1.2

6 Bladed Vertical Axis Vane Type Rotor
α = 280°

Tapping Point	Initial Reading (in of H2O)	α = 280° (in of H2O) (Convex surface)		Initial Reading (in of H2O)	α = 280° (in of H2O) (Concave surface)		Pressure Dff. DP (in of H2O)
1	2.7	2.9	-0.2	2.9	3.1	-0.2	4.44089E-16
2	2.8	2.4	0.4	2.82	3	-0.18	0.58
3	2.75	2.1	0.65	2.8	3.01	-0.21	0.86
4	2.75	2.05	0.7	2.9	3.1	-0.2	0.9
5	2.79	1.9	0.89	3.01	3.2	-0.19	1.08
6	2.9	1.78	1.12	2.85	3.1	-0.25	1.37
7	3	2.02	0.98	3.05	3.2	-0.15	1.13
8	2.89	2.34	0.55	3.1	3.3	-0.2	0.75

6 Bladed Vertical Axis Vane Type Rotor
α = 290°

Tapping Point	Initial Reading (in of H2O)	α = 290° (in of H2O) (Convex surface)		Initial Reading (in of H2O)	α = 290° (in of H2O) (Concave surface)		Pressure Dff. DP (in of H2O)
1	2.7	2.9	-0.2	2.9	3.1	-0.2	4.44089E-16
2	2.8	2.42	0.38	2.82	3	-0.18	0.56
3	2.75	2.1	0.65	2.8	3.01	-0.21	0.86
4	2.75	1.99	0.76	2.9	3.1	-0.2	0.96
5	2.79	1.78	1.01	3.01	3.2	-0.19	1.2
6	2.9	1.7	1.2	2.85	3.1	-0.25	1.45
7	3	2.26	0.74	3.05	3.28	-0.23	0.97
8	2.89	2.8	0.09	3.1	3.31	-0.21	0.3

6 Bladed Vertical Axis Vane Type Rotor
α = 300°

Tapping Point	Initial Reading (in of H2O)	α = 300° (in of H2O) (Convex surface)		Initial Reading (in of H2O)	α = 300° (in of H2O) (Concave surface)		Pressure Dff. DP (in of H2O)
1	2.7	2.9	-0.2	2.9	3.1	-0.2	4.44089E-16
2	2.8	2.48	0.32	2.82	3	-0.18	0.5
3	2.75	2.12	0.63	2.8	3	-0.2	0.83
4	2.75	1.9	0.85	2.9	3.1	-0.2	1.05
5	2.79	1.68	1.11	3.01	3.2	-0.19	1.3
6	2.9	1.8	1.1	2.85	3.08	-0.23	1.33
7	3	2.05	0.95	3.05	3.25	-0.2	1.15
8	2.89	3.16	-0.27	3.1	3.3	-0.2	-0.07

6 Bladed Vertical Axis Vane Type Rotor
α = 310°

Tapping Point	Initial Reading (in of H2O)	α = 310° (in of H2O) (Convex surface)		Initial Reading (in of H2O)	α = 310° (in of H2O) (Concave surface)		Pressure Dff. DP (in of H2O)
1	2.7	3	-0.3	2.9	3.1	-0.2	-0.1
2	2.8	2.85	-0.05	2.82	3	-0.18	0.13
3	2.75	2.48	0.27	2.8	3	-0.2	0.47
4	2.75	2	0.75	2.9	3.1	-0.2	0.95
5	2.79	1.65	1.14	3.01	3.2	-0.19	1.33
6	2.9	2	0.9	2.85	3.08	-0.23	1.13
7	3	2.9	0.1	3.05	3.26	-0.21	0.31
8	2.89	3.5	-0.61	3.1	3.3	-0.2	-0.41

6 Bladed Vertical Axis Vane Type Rotor
α = 320°

Tapping Point	Initial Reading (in of H2O)	α = 320° (in of H2O) (Convex surface)		Initial Reading (in of H2O)	α = 320° (in of H2O) (Concave surface)		Pressure Dff. DP (in of H2O)
1	2.7	3	-0.3	2.9	3.1	-0.2	-0.1
2	2.8	3.15	-0.35	2.82	3.04	-0.22	-0.13
3	2.75	2.8	-0.05	2.8	3.04	-0.24	0.19
4	2.75	2.04	0.71	2.9	3.1	-0.2	0.91
5	2.79	1.62	1.17	3.01	3.25	-0.24	1.41
6	2.9	2.15	0.75	2.85	3.12	-0.27	1.02
7	3	3.12	-0.12	3.05	3.3	-0.25	0.13
8	2.89	3.62	-0.73	3.1	3.38	-0.28	-0.45

6 Bladed Vertical Axis Vane Type Rotor
α = 330°

Tapping Point	Initial Reading (in of H2O)	α = 330° (in of H2O) (Convex surface)		Initial Reading (in of H2O)	α = 330° (in of H2O) (Concave surface)		Pressure Dff. DP (in of H2O)
1	2.7	2.8	-0.1	2.9	3.2	-0.3	0.2
2	2.8	3.2	-0.4	2.82	3.18	-0.36	-0.04
3	2.75	3.18	-0.43	2.8	3.2	-0.4	-0.03
4	2.75	2.2	0.55	2.9	3.2	-0.3	0.85
5	2.79	1.62	1.17	3.01	3.38	-0.37	1.54
6	2.9	2.4	0.5	2.85	3.28	-0.43	0.93
7	3	3.4	-0.4	3.05	3.4	-0.35	-0.05
8	2.89	3.6	-0.71	3.1	3.58	-0.48	-0.23

6 Bladed Vertical Axis Vane Type Rotor
α = 340°

Tapping Point	Initial Reading (in of H2O)	α = 340° (in of H2O) (Convex surface)		Initial Reading (in of H2O)	α = 340° (in of H2O) (Concave surface)		Pressure Dff. DP (in of H2O)
1	2.7	1.8	0.9	2.9	2.9	0	0.9
2	2.8	2.9	-0.1	2.82	2.78	0.04	-0.14
3	2.75	2.92	-0.17	2.8	2.6	0.2	-0.37
4	2.75	2.68	0.07	2.9	2.78	0.12	-0.05
5	2.79	2.68	0.11	3.01	2.85	0.16	-0.05
6	2.9	2.82	0.08	2.85	2.6	0.25	-0.17
7	3	3.7	-0.7	3.05	2.8	0.25	-0.95
8	2.89	3.8	-0.91	3.1	2.85	0.25	-1.16

6 Bladed Vertical Axis Vane Type Rotor
α = 350°

Tapping Point	Initial Reading (in of H2O)	α = 350° (in of H2O) (Convex surface)		Initial Reading (in of H2O)	α = 350° (in of H2O) (Concave surface)		Pressure Dff. DP (in of H2O)
1	2.7	1.68	1.02	2.9	2.62	0.28	0.74
2	2.8	3.3	-0.5	2.82	2.57	0.25	-0.75
3	2.75	3.7	-0.95	2.8	2.4	0.4	-1.35
4	2.75	3.3	-0.55	2.9	2.6	0.3	-0.85
5	2.79	3.1	-0.31	3.01	2.7	0.31	-0.62
6	2.9	3.3	-0.4	2.85	2.5	0.35	-0.75
7	3	3.82	-0.82	3.05	2.65	0.4	-1.22
8	2.89	3.7	-0.81	3.1	2.7	0.4	-1.21